DOMAIN-SPECIFIC INTERACTIONS OF BPM1 WITH DMS3 AND RDM1 IN RNADIRECTED DNA METHYLATION

Jagić, Mateja

University of Zagreb

Faculty of Science
Department of Biology

Mateja Jagić

DOMAIN-SPECIFIC INTERACTIONS OF BPM1 WITH DMS3 AND RDM1 IN RNA-DIRECTED DNA METHYLATION

DOCTORAL DISSERTATION

Zagreb, 2023

University of Zagreb

Faculty of Science
Department of Biology

Mateja Jagić

DOMAIN-SPECIFIC INTERACTIONS OF BPM1 WITH DMS3 AND RDM1 IN RNA-DIRECTED DNA METHYLATION

DOCTORAL DISSERTATION

Supervisor:
Dr. Dunja Leljak-Levanić, Prof.

Zagreb, 2023

Sveučilište u Zagrebu

Prirodoslovno-matematički fakultet
Biološki odsjek

Mateja Jagić

INTERAKCIJE DOMENA PROTEINA BPM1 S PROTEINIMA DMS3 I RDM1 U RNA-POSREDOVANOJ METILACIJI DNA

DOKTORSKI RAD

Mentor:
Prof. dr. sc. Dunja Leljak-Levanić

Zagreb, 2023

This doctoral thesis was prepared in the Division of Molecular Biology, Department of Biology, Faculty of Science, University of Zagreb under the supervision of Dr. Dunja Leljak-Levanić, Prof. The thesis was prepared as part of the University postgraduate program of Biology at the Department of Biology, Faculty of Science, University of Zagreb. The doctoral thesis was prepared within the Croatian Science Foundation scientific research project "MATH-BTB proteins as switches between transcription and RNA-directed DNA methylation during plant development" (IP-2016-06-6229) led by Dr. Dunja Leljak-Levanić, Prof.

Ovaj je doktorski rad izrađen u Zavodu za molekularnu biologiju Biološkog odsjeka Prirodoslovno-matematičkog fakulteta Sveučilišta u Zagrebu, pod vodstvom prof. dr. sc. Dunje Leljak-Levanić, u sklopu Sveučilišnog poslijediplomskog doktorskog studija Biologije pri Biološkom odsjeku Prirodoslovno-matematičkog fakulteta Sveučilišta u Zagrebu. Doktorski rad izrađen je u sklopu znanstveno-istraživačkog projekta Hrvatske zaklade za znanost „MATH-BTB proteini kao regulatori transkripcije i RNA posredovane metilacije DNA u biljnom razvitku“ (IP-2016-06-6229) voditeljice prof. dr. sc. Dunje Leljak-Levanić.

INFORMATION ABOUT SUPERVISOR

Dr. Dunja Leljak-Levanić, Prof. graduated from the Department of Biology, Faculty of Science, University of Zagreb in 1993 with a degree in Molecular Biology. She obtained her MSc degree in 1997 and her PhD in 2001 in Molecular and Cell Biology, both from the Faculty of Science. Since 1994 she has been working in the Division of Molecular Biology, Department of Biology, Faculty of Science, University of Zagreb. First as a research assistant in the group of Dr. Sibila Jelaska Prof. Emer, then from 2005 to 2014 as an assistant professor, from 2014 to 2021 as an associate professor and in 2021 she became a full professor, which remains her current position in the Division. She teaches four classes in the undergraduate and graduate programs in molecular biology, and three classes in the doctoral program in biology.

Dunja Leljak-Levanić's primary scientific interests are plant reproductive biology, embryogenesis and DNA methylation, and the correlation between the above and plant response to stress. She developed her scientific career through a series of foreign scientific trainings in the period from 2000 to 2009 and participation in numerous congresses. She has co-authored 34 original scientific papers, five book chapters, and one patent, and has been cited 687 times, with an h-index of 14 according to Google Scholar. She supervised five doctoral theses (including this) and 13 master's and bachelor's theses. As an active researcher, she participated in numerous projects and was the principal investigator of three successfully completed grants (a project of the Alexander von Humboldt Foundation project, a project of the foundation of the Croatian Academy of Sciences and Arts, and a project of the Croatian Science Foundation).

ZAHVALE

Posebno hvala mojoj mentorici, profesorici Dunji Leljak-Levanić, na povjerenju, savjetima i pomoći kako prilikom mog rada u laboratoriju, tako i prilikom pisanja ove disertacije.

Veliko hvala i profesorici Nataši Bauer na susretljivosti i pomoći pri radu te svim korisnim savjetima.

Ogromno hvala mojim curama iz laboratorija: Andreji Škiljaici, Luciji Markulin, Tamari Vuk, Mirti Tokić i Sandri Vitko na beskrajnoj potpori, konstruktivnim savjetima i nadasve prijateljskoj atmosferi. Svaka je na poseban način pridonijela izradi ovog doktorskog rada.

Hvala profesoru Nenadu Malenici na pomoći oko križanja i dobivanja reporterskih linija uročnjaka.

Hvala Karlu Miškecu, čiji je diplomski rad bio temelj kasnijih analiza proteinske kopurifikacije.

Zahvaljujem se i svim ostalim kolegama sa Zavoda za molekularnu biologiju na suradnji, savjetima i kolegijalnosti, a posebno Ani-Mariji Boljkovac na održavanju laboratorija i brizi da uvijek ima spremnih kemikalija i medija, te Marici Vuk na pomoći oko brojnih administrativnih problema.

Hvala profesoru Igoru Weberu te Marku Šoštaru i Luciji Horvat s Instituta Ruđer Bošković na pomoći oko konfokalne mikroskopije i provedbe FRET-FLIM analize.

Hvala Genadiju Razdorovu i Siniši Habazinu iz Genosa na provedbi tekućinske kromatografije i spektrometrije masa te pomoći s analizom dobivenih podataka.

Hvala od srca mojim roditeljima Vesni (Mariji) i Josipu na razumijevanju i podršci tijekom mog beskrajnog školovanja. Nije im uvijek bilo lako. I naposljetku, hvala cijeloj mojoj obitelji i mojim prijateljima koji su uvijek bili tu kad sam ih trebala.

University of Zagreb
Faculty of Science
Department of Biology

Doctoral thesis

DOMAIN-SPECIFIC INTERACTIONS OF BPM1 WITH DMS3 AND RDM1 IN RNA-DIRECTED DNA METHYLATION

MATEJA JAGIĆ

Division of Molecular Biology, Faculty of Science,
Horvatovac 102a, 10000 Zagreb

BPM1 protein belongs to the MATH-BTB protein family, characterized as adaptors of CUL3-dependent E3 ubiquitin ligase complex responsible for recognizing and directing substrates for proteasomal degradation. An initial mass spectrometry experiment identified a key component of the RdDM, the DMS3 protein, as a potential BPM1 partner. Since RdDM is the major epigenetic mechanism responsible for *de novo* DNA methylation in plants, the goal of this work was to further investigate the role of BPM1 in RdDM. By mass spectrometry, along DMS3, another component of RdDM, the RDM1, was determined in complex with BPM1. Their direct interactions with BPM1 were confirmed by Y2H, pull-down, microthermophoresis and FRET-FLIM. Colocalization of BPM1, DMS3, and RDM1 was observed in the nucleus, indicating the site of their common function. The reduced activity of the RdDM-controlled *FWA* gene promoter in the BPM1-overexpressing line together with protein-protein interaction data strongly suggest a role for BPM1 in controlling gene expression as part of RdDM.

(146 pages, 41 figures, 35 tables, 178 references, original in: English)

Keywords: MATH-BTB, BPM1, RdDM, DDR complex, protein interactions, *Arabidopsis thaliana*

Supervisor: Dr. Dunja Leljak-Levanić, Prof.

Reviewers: Dr. Biljana Balen, Prof.
Dr. Petra Peharec Štefanić, Assoc. Prof.
Dr. Zdravko Lorković, Research Associate

Sveučilište u Zagrebu
Prirodoslovno-matematički fakultet
Biološki odsjek

Doktorski rad

INTERAKCIJE DOMENA PROTEINA BPM1 S PROTEINIMA DMS3 I RDM1 U RNA-POSREDOVANOJ METILACIJI DNA

MATEJA JAGIĆ

Zavod za molekularnu biologiju Prirodoslovno-matematičkog fakulteta,
Horvatovac 102a, 10000 Zagreb

Protein BPM1 pripada porodici proteina MATH-BTB koji su opisani kao adapteri u CUL3-ovisnom kompleksu ubikvitinskih ligaza E3 odgovornih za prepoznavanje i usmjeravanje supstrata na proteasomalnu razgradnju. U preliminarnom eksperimentu spektrometrije masa kao potencijalni partner proteina BPM1 utvrđena je važna komponenta mehanizma RdDM, protein DMS3. Budući da je RdDM glavni epigenetski mehanizam odgovoran za metilaciju DNA *de novo* u biljkama, cilj ovog rada bio je detaljnije razjasniti ulogu BPM1 u sklopu RdDM-a. Spektrometrijom masa u kompleksu s proteinom BPM1 uz DMS3, utvrđena je i druga komponenta RdDM-a, protein RDM1. Njihove izravne interakcije s BPM1 potvrđene su metodama sustava dvaju kvašćevih hibrida, proteinske kopurifikacije, mikrotermoforeze te metodom FRET-FLIM. Kolokalizacija proteina BPM1, DMS3 i RDM1 utvrđena je u jezgri što ukazuje na mjesto njihove zajedničke funkcije. Smanjena aktivnost promotora gena *FWA* kontroliranog RdDM-om u liniji s prekomjernom ekspresijom gena *BPM1* zajedno s rezultatima proteinskih interakcija snažno upućuju na ulogu proteina BPM1 u kontroli genske ekspresije u sklopu mehanizma RdDM.

(146 stranica, 41 slika, 35 tablica, 178 literaturnih navoda, jezik izvornika: engleski)

Ključne riječi: MATH-BTB, BPM1, RdDM, kompleks DDR, interakcije proteina, *Arabidopsis thaliana*

Mentor: dr. sc. Dunja Leljak-Levanić, prof.

Ocjenjivači: dr. sc. Biljana Balen, prof.
dr. sc. Petra Peharec Štefanić, izv. prof.
dr. sc. Zdravko Lorković, znanstveni savjetnik

CONTENTS

1. INTRODUCTION

A small family of six *BPM* genes (*BPM1-6*) is described in *Arabidopsis thaliana,* encoding for at least 16 different BPM protein isoforms due to the alternative splicing (Škiljaica et al., 2020). BPM proteins belong to the MATH-BTB protein family and are members of the BTB protein superfamily. The main element of the superfamily is the BTB (Bric a brac, Tramtrack and Broad Complex) domain, also known as the POZ (Pox virus and Zinc finger) domain. The BTB domain is a protein-protein interaction motif with variety of functional roles, including transcription repression (Melnick et al., 2000), cytoskeleton regulation (Bauer et al., 2019; Juranić et al., 2012), tetramerization and gating of ion channels (Smaldone et al., 2016), and protein ubiquitination and degradation (Gingerich et al., 2005; Pintard et al., 2003). The BTB domain can both self-associate and interact with non-BTB proteins, thus forming homo- and heterodimers, respectively (Stogios et al., 2005). In several BTB protein families, which are best known for their role in protein ubiquitination and degradation, there is also a carboxy-terminal BACK (BTB and C-terminal Kelch) domain mainly considered to play a role in the orientation of targeted substrates (Stogios et al., 2005; Stogios & Privé, 2004). Unlike other BTB protein families, the BTB domain of MATH-BTB proteins is found C-terminally to the partner, MATH (Meprin and TRAF-homology) domain (Stogios et al., 2005). MATH-BTB proteins partake in numerous developmental processes in plants and animals; they are known as key regulators of the cell cycle and, among other roles, are involved in mitotic spindle assembly, correct chromosome segregation and correct nuclei separation (Juranić et al., 2012; Pintard et al., 2003). The most prevalent and best-studied mode of function of MATH-BTB proteins is in proteasomal degradation where they act as substrate-specific adaptors of E3 ubiquitin ligase complexes — CULLIN 3 (CUL3)-based REALLY INTERESTING NEW GENE (RING) E3 ligases or CRL3 (Gingerich et al., 2007; Pintard et al., 2003). In this process, the C-terminal BTB domain is known to bind a CUL3 scaffold protein, while the N-terminal MATH domain selects and targets among a highly diverse collection of substrate proteins to promote their specific ubiquitination and subsequent degradation on 26S proteasome. In *Arabidopsis,* some of the known transcription factors (TF) degraded by the MATH-BTB-mediated pathway are members of Apetala2/ethylene responsive family of TFs (Chen et al., 2013; Morimoto et al., 2017; Phukan et al., 2017; Weber & Hellmann, 2009), a class I homeobox-leucine zipper TFs (Lechner et al., 2011), R2R3 MYB family of TFs (Beathard et al., 2021; Chen et al., 2015) and bHLH TF family (Chico et al., 2020). In addition, protein phosphatases type 2C are also described as substrates of

MATH-BTB proteins (Julian et al., 2019). Consequently, MATH-BTB proteins play important roles in plant flowering, seed development and abiotic stress responses in *Arabidopsis*.

However, there is some evidence of distinct roles of MATH-BTB proteins that are independent of the CUL3 mechanism. In *Caenorhabditis elegans*, the female germline-specific MATH-BTB protein MATERNAL EFFECT LETHAL 26 (MEL-26) which regulates the microtubule cytoskeleton by degrading the katanin-like protein MEI-1 (Pintard et al., 2003), additionally regulates cytokinesis in a CUL3-independent manner through interaction with actin-binding protein POD-1 (Luke-Glaser et al., 2005). Indications of similar roles in plants are described for wheat TaMAB2 and maize ZmMAB1 protein, both involved in cytoskeletal regulation during plant reproduction (Bauer et al., 2019; Juranić et al., 2012). Another protein with indications of a novel, CUL3-independent role is a member of the *Arabidopsis* MATH-BTB protein family, BPM1. BPM1 protein localizes in the cell cytoplasm but also in the nucleus and nucleolus, as mediated by its C-terminal nuclear localization signal (Kekez et al., 2016; Leljak Levanić et al., 2012). In the cytoplasm and nucleus, BPM1 might assemble with CRL3 and TFs, thereby mediating the degradation of targeted TFs on 26S proteasome (Lechner et al., 2011; Weber & Hellmann, 2009). Abundant BPM1 agglomerates in the nucleolus, the sub-compartment where the lowest level of colocalization with CUL3 is recorded, indicate a potential CUL3-independent and as of yet the unidentified function of BPM1 protein (Leljak Levanić et al., 2012).

In the comparative mass spectrometry proteomics assay focused on wheat MATH-BTB protein TaMAB2 (Bauer et al., 2019), in which *Arabidopsis* proteins BPM1 and seryl-tRNA synthetase (SerRS; Kekez et al., 2016) served as controls for the elimination of unspecific interactions and false positives, DMS3 protein, an important component of RNA-directed DNA methylation (RdDM) pathway, has been identified in the complex with BPM1. Interestingly, none of the expected components of the E3 ligase complex, such as CUL3a and CUL3b, were detected in the assay. The finding of DMS3 as a potential BPM1 interactor, together with abundant BPM1 accumulation in the nucleolus (Leljak Levanić et al., 2012), a cell sub-compartment with hints of an additional, non-conventional role in the processing of small interfering RNAs (siRNAs) that direct cytosine methylation (Pontes et al., 2006), indicated a possible role of BPM1 in RNA-directed DNA methylation (RdDM) pathway.

RdDM is the main epigenetic mechanism responsible for *de novo* DNA methylation in plants (Aufsatz et al., 2002). RdDM is mediated by a specialized transcription mechanism composed of

two RNA polymerase II (POL II)–related RNA polymerases, POL IV and POL V, that function independently, and various associated proteins (Matzke et al., 2015). While POL IV transcripts serve as siRNA precursors, POL V generates transcripts at siRNA-targeted loci with the assistance of a putative chromatin-remodeling complex termed DDR. The DDR consists of three proteins: DEFECTIVE IN RNA-DIRECTED DNA METHYLATION 1 (DRD1), DEFECTIVE IN MERISTEM SILENCING 3 (DMS3) and RNA-DIRECTED DNA METHYLATION 1 (RDM1), and is crucial in the positioning of the RdDM machinery (Wierzbicki et al., 2012; Wongpalee et al., 2019; Zhong et al., 2012). The RDM1 additionally acts as a bridging protein for DNA methyltransferase DOMAINS REARRANGED METHYLTRANSFERASE 2 (DRM2), thus recruiting the effector complex of RdDM and resulting in *de novo* cytosine methylation at target sites (Gao et al., 2010; Wierzbicki et al., 2012). Whilst DRD1 and RDM1 associate with proteins outside the DDR complex (Gao et al., 2010; Law et al., 2010), the only known function of DMS3 is stabilizing interactions between the DRD1 and RDM1 (Zhong et al., 2019).

Two hypotheses were proposed in this thesis based on the literature review and preliminary results. First, BPM proteins, along with other associated proteins of the MATH-BTB protein family, have a wide range of protein partners and, apart from targeting TFs for degradation, have a novel fundamental role. Following is the hypothesis that BPM1 protein interacts with important components of the RdDM methylation pathway.

The aim of this study was to identify potentially new protein interaction partners of BPM1 protein with a focus to those that might be involved in the RdDM pathway. The selection of potential interaction partners of BPM1 was conducted using tandem affinity purification combined with mass spectrometry (TAP-MS). Furthermore, detailed domain-specific interaction studies were performed to determine if those interactions are direct or indirect and if the role of BPM1 protein in identified interactions is mediated by proteasomal degradation of its targets. Analysis of the binding potential of BPM1 protein and its truncated versions missing one or two protein domains for selected targets were performed using yeast-two hybrid assays, pull-down, microscale thermophoresis, and *in planta* by fluorescence-lifetime imaging microscopy. Additionally, subcellular localization and colocalization of BPM1 and its domain-omitted variants and individual interaction partners was investigated to obtain insights into the influence of specific protein domain or certain interactor on BPM1's subcellular localization. Finally, the influence of BPM1 on the promoter activity of the RdDM-controlled gene *FWA* was inspected.

2. LITERATURE REVIEW

2.1. Ubiquitin-dependent protein degradation

Removal of unnecessary, redundant, damaged, or misfolded proteins is necessary for the normal functioning of every eukaryotic cell. Two major pathways responsible for protein degradation are ubiquitin-proteasome system (UPS) and autophagy-lysosome system (Marshall & Vierstra, 2019). While UPS is mainly involved in the removal of short-lived regulatory proteins and soluble misfolded proteins (Finley, 2009; Samant et al., 2018), larger protein complexes, insoluble protein aggregates, but also entire organelles and pathogens are eliminated by autophagy (Gatica et al., 2018; Reggiori & Klionsky, 2013). Since proteolysis is irreversible, selective degradation is of great importance for protein homeostasis maintenance because degradation of wrong proteins may impair cell functionality and viability, the same as the accumulation of useless or harmful proteins. The ubiquitination of substrate proteins is therefore an essential part of every eukaryotic cell functionality (Genschik et al., 2013; Ronai, 2016). Ubiquitin is a small, highly conserved protein comprised of only 76 amino acids (Mw = 8.6 kDa) found in almost every eukaryotic cell, as its name implies ('ubiquitously'). For ubiquitin to be activated, adenylation of its C-terminus is needed. This ATP-dependent process is catalyzed by ubiquitin-activating enzyme E1 (Haas et al., 1982; Passmore & Barford, 2004). Activated ubiquitin is further transferred to the ubiquitin-conjugating enzyme E2 via a transthiolation reaction (Haas et al., 1982; Hershko & Ciechanover, 1998). As a mediator between E2 enzyme and targeted substrate, ubiquitin ligase E3 facilitates transfer of the ubiquitin usually onto the ε-amino group of lysine in the target protein, forming a covalent isopeptide bond between the ubiquitin and the substrate (Kerscher et al., 2006; Stewart et al., 2016). Whereas monoubiquitination is mainly associated with intracellular localization, trafficking, and regulation of protein complex formation, polyubiquitination has a role in protein signaling and turnover via proteasomal degradation (Finley, 2009; Khaminets et al., 2016).

There are only a few known E1 and slightly more E2 enzymes, but numerous proteins from different protein families serve as E3 ligases (Hershko & Ciechanover, 1998). This myriad of different E3 ligases leads to the specificity of substrate targeting. All known E3 ubiquitin ligases are divided into four distinct types regarding their structure and function as reviewed in Yang et al. (2021):

- HECT E3 ligases – contain a HECT (homologous to the E6AP carboxyl terminus) domain that is responsible for ubiquitin charged E2 enzyme binding. Ubiquitination proceeds in two steps: ubiquitin is first transferred to the active site of the E3 ligase, and then transferred from the E3 to the substrate. This is one of the largest E3 ligase families whose members are divided into three groups: Nedd4 family which consists of 9 members, the HERC family consisting of 6 members, and other HECTs with various domains to which 13 members belong (**Figure 1 A**, Rotin & Kumar, 2009).
- RING-finger E3 ligases – dominant and the most studied family of E3 ligases whose structure is based on RING domain. Here, the RING domain binds E2 enzyme and mediates direct transfer of the ubiquitin from the E2 to the substrate. RING-finger type of E3 ligases comprises of two big families: monomeric RING-finger with additional ability of autoubiquitination, and multi-subunit E3 ligases. To multi-subunit E3 ligases belong cullin-RING ligases (CRLs, Bulatov & Ciulli, 2015), anaphase promoting complex/cyclosome (APC/C, Primorac & Musacchio, 2013) and the largest ligase complex SCF (Skp1-cullin-F-box, Xie et al., 2019) E3 ligases (**Figure 1 B**).
- U-box E3 ligases – contain a conserved U-box domain by which ubiquitin-loaded E2 is bound to the E3 ligase leading to direct transfer of the ubiquitin to the substrate protein. This E3 ligase family is relatively small and shares some structural similarities with RING-finger type of E3 ligases (**Figure 1 C**, Hatakeyama & Nakayama, 2003)
- RBR E3 ligases – last discovered E3 ligase family whose conserved catalytic region includes three distinct domains, a RING1 and RING2 domains divided by central in-between-RINGs (IBR). Mechanism of ubiquitination undergoes in two steps. First, RING1 domain binds ubiquitin-activated E2 facilitating transfer of ubiquitin to the catalytic site in RING2 domain, and then the ubiquitin is transferred to the substrate. Although they possess some characteristics of HECT and RING-finger types of E3 ligases, the reaction mechanism significantly differs from both (**Figure 1 D**, Smit et al., 2014).

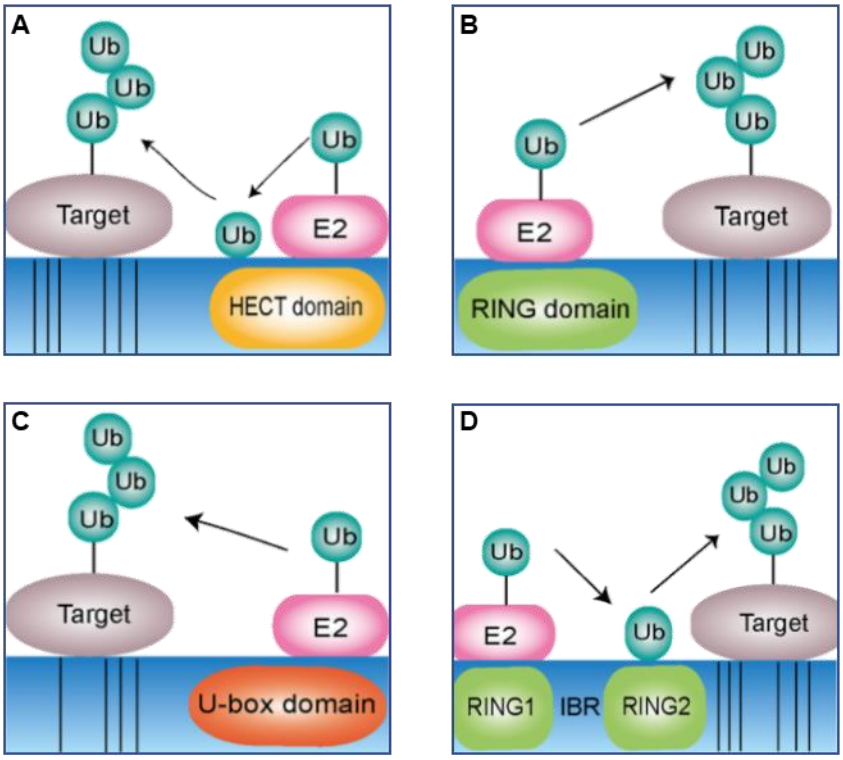

Figure 1 Four different types of E3 ubiquitin ligases regarding their catalytic domain. **A**) The HECT E3 ligase ubiquitination occurs via two-step reaction: first, E2-ubiquitin complex binds to the C-terminal HECT domain and ubiquitin is transferred to the catalytic site of the HECT domain, and second, ubiquitin is further transferred to the substrate. **B**) The RING E3 ligase structure is based on the N-terminal RING domain which mediates direct transfer of the ubiquitin from the E2-ubiquitin complex to the substrate. **C**) The U-box E3 ligases contain a conserved C-terminal U-box domain that mediates direct transfer from the ubiquitin-activated E2 to the substrate protein. **D**) The RBR E3 ligases catalytic region includes two RING domains (RING1 and RING2) separated by IBR domain and the ubiquitination proceeds in two steps: RING1 binds E2-ubiquitin complex and facilitates transfer of the ubiquitin from E2 to the catalytic site in RING2, then ubiquitin is transferred from the RING2 to the substrate. Illustration from Yang et al. (2021).

Once substrate protein is polyubiquitinated by one of the E3 ligases, it is usually targeted for degradation on 26S proteasome. The 26S proteasome is a multi-subunit protease found in all eukaryotic cells and consists of two main subcomplexes: 20S proteolytic core and 19S regulatory complex (Tanaka, 2009). Polyubiquitin tag is first recognized by the 19S complex, which is composed of the lid subcomplex and the base consisting of six ATPases and two non-ATPase subunits. Substrates are de-ubiquitylated and unfolded by 19S complex, and the energy produced by ATP hydrolysis is used to translocate unfolded polypeptide chains into the core of the 20S complex. Here, ubiquitin molecules are released, while substrate is degraded by proteolysis into small peptides that are mostly 2-10 amino acids long (Collins & Tansey, 2006; Kisselev et al., 1999; Lee et al., 2001). Ubiquitin molecules can be further reused in new ubiquitination processes,

while nearly all peptides are digested into amino acids that can be further used for polypeptide synthesis.

2.2. CUL3-RING E3 ubiquitin ligases

Cullin–RING ligases (CRLs) are an important class of multi-subunit ubiquitin E3 ligases built on a cullin scaffold. The cullin protein family is evolutionarily conserved and the number of cullin or cullin-like proteins varies between different eukaryotic organisms (Sarikas et al., 2011). For example, the mammalian genome encodes seven canonical cullin proteins (Cul1, Cul2, Cul3, Cul4A, Cul4B, Cul5, and Cul7), *Caenorhabditis elegans* has six (Cul1-6) and *Drosophila melanogaster* has five (Cul1-5), while in yeasts only three cullin proteins are present (Cul1 and Cul3, and Cul8 in *Saccharomyces cerevisiae*, or Cul4 in *Schizosaccharomyces pombe*). The *Arabidopsis thaliana* genome encodes six cullin-like proteins (CUL1, CUL2, CUL3A, CUL3B, CUL4, and APC2), all characterized by a conserved cullin region of approximately 200 amino acids in length (Choi et al., 2014). The CRL assembly and catalytic mechanism is the same for all cullin proteins. The C-terminal domain of a cullin serves as an anchor for the RING domain-containing protein (either RING BOX-1, abbreviated RBX1, or RBX2), thus forming the catalytic core of the complex. RBX1 has been shown to anchor all cullins except CUL5, which is anchored by RBX2 (Choi et al., 2014; Duda et al., 2012; Kamura et al., 2004). The N-terminal domain of a cullin serves to bind adaptor proteins, which in turn bind substrate receptors and link them to the cullin. The substrate receptors recognize and bind substrate proteins, whereas RBX1 or RBX2 in the catalytic core recruits the E2 enzyme and facilitates the direct transfer of ubiquitin from the E2 to the substrate, to make it a target for proteasomal degradation (Nguyen et al., 2017). Each member of the cullin family has its own set of specific adaptor proteins through which numerous substrate receptors can be recruited, resulting in a wide variety of proteins that can be targeted for ubiquitination. Therefore, as key regulators of posttranslational protein regulation, CRLs are involved in the regulation of numerous eukaryotic physiological functions and developmental processes (Petroski & Deshaies, 2005; Sarikas et al., 2011).

The peculiarity of the ubiquitin E3 ligase complex assembled on CUL3, the Cullin3-RING E3 ligase (CRL3), is that the substrate receptor and the adaptor are the same protein – the BTB domain protein. Here, the BTB domain is the one with the CUL3 binding site, while an independent additional protein–protein interaction domain binds specific substrate proteins (Genschik et al.,

2013). More about BTB proteins will be discussed in the next chapter, but here it is important to emphasize that not all BTB proteins serve as CRL3 substrate adaptors, only those that contain a conserved helical structure positioned C-terminal to the BTB domain. This structure is referred to as the 3-box (CUL3-Interacting box) and forms a hydrophobic groove that serves to bind the 22 amino acids long N-terminal extension of CUL3 (Canning et al., 2013; Zhuang et al., 2009). Since BTB proteins form dimers, a dimeric CRL3 complex can be formed, which is a characteristic feature of the CRL3 family (Nguyen et al., 2017). Therefore, the CRL3 complex consists of two substrate-binding sites (BTB dimer) and two catalytic cores (CUL3-RBX1 bind to each BTB domain) that can act independently and target two substrates (each half of the CRL3 dimer ubiquitinates one substrate) or dimeric CRL3 can target the same protein with both halves (Zimmerman et al., 2010). This dimerization has been associated with increased ubiquitination efficiency (Errington et al., 2012).

In plants, two cullin-like proteins, CUL3A and CUL3B, which are functionally redundant, form CRL3. While loss of function of one of the cullins has only weak effects on plant development (*cul3a* or *cul3b* null mutants), homozygous *cul3a cul3b* double mutants show an embryo lethal phenotype (Figueroa et al., 2005). Furthermore, *cul3*$^{\text{hypomorph}}$ (*cul3*$^{\text{hyp}}$) double mutant, which has a partially functional CUL3a, but a nonfunctional CUL3b, demonstrates the importance of CUL3 for normal post-embryonic plant development particularly root and shoot growth, and cotyledon development (Thomann et al., 2009). CRL3 ligases are involved in phytohormone regulation, pathogen response and in red and blue light signal transduction pathways (Choi et al., 2014). Interestingly, the blue light receptor PHOTOTROPIN 1 (PHOT1) is mono/multiubiquitinated by CRL3 at weak blue light intensity, possibly stimulating the internalization of the protein rather than destabilizing it, whereas PHOT1 is both mono/multiubiquitinated and polyubiquitinated at strong blue light intensity, the latter being destined for 26S proteasomal degradation (Roberts et al., 2011). PHOT1 ubiquitination by CRL3 is mediated by NON-PHOTOTROPHIC HYPOCOTYL 3 (NPH3), a substrate adaptor protein with N-terminal BTB domain. As stated in Choi et al. (2014), it is important to point out that this discovery links the protein ubiquitination by CRL3 ligases to the protein activity regulation and not just to the degradation of targeted proteins.

2.3. BTB proteins as mediators of cullin3-dependent protein degradation

One of the main features of CRL3 complexes, in addition to CUL3, are the members of a diverse BTB protein superfamily named after the evolutionarily conserved protein-protein interaction motif – the BTB/POZ domain. The BTB proteins are found in viruses (poxvirus and mimivirus families), where they affect the ubiquitin protein modification pathway and alter host immune responses and cellular signaling to ensure virus survival (Gao et al., 2019; Wilton et al., 2008), and in all eukaryotes where they are involved in a variety of cellular functions, from transcriptional regulation and chromatin remodeling to protein degradation and cytoskeletal regulation (Chaharbakhshi & Jemc, 2016). The specificity of their function is determined by additional partner domains in the protein and by the wide range of interaction partners (Chaharbakhshi & Jemc, 2016). Although some BTB proteins contain only BTB domain (such as Skp1 and ElonginC), there are over twenty different domains associated with the BTB domain in proteins (Perez-Torrado et al., 2006). Among the many BTB protein families, the most common are the BTB-zinc finger (BTB-ZF), BTB-BACK-Kelch, voltage-gated potassium channel T1, MATH-BTB, BTB-NPH3, and BTB-BACK-PHR families, in which the BTB domain usually occurs in a single copy and is associated with one or two additional domains (Stogios et al., 2005). It is suggested that the domain undergoes a domain shuffling followed by lineage-specific expansion during speciation events and that diversification of BTB proteins followed divergence of the major lineages of the eukaryotic crown group (Lespinet et al., 2002; Stogios et al., 2005). Interestingly, there were organism-specific expansions and contractions of BTB protein families. For example, BTB-NPH3 proteins are found only in *Arabidopsis* and related plants, while there is no evidence for BTB-Kelch or BTB-ZF proteins in *Arabidopsis* (Perez-Torrado et al., 2006). Similarly, there are no BTB-Kelch or BTB-ZF proteins in *Caenorhabditis elegans*, while there are an unexpectedly large number of MATH-BTB proteins (Perez-Torrado et al., 2006). Moreover, they are not found in prokaryotes, except in the endosymbiotic bacteria of the amoeba family Parachlamydiaceae (Domman et al., 2014; Perez-Torrado et al., 2006). The origin of BTB-containing genes in these bacteria is probably in amoeba host cells (Perez-Torrado et al., 2006).

The sequence of the BTB domain is generally highly variable among different BTB proteins, but the secondary structure and the resulting core BTB fold, which consists of approximately 95 amino acids forming five α-helices and three β-sheets, is well conserved (for a detailed structure, see Stogios et al., 2005). Majority of BTB domains from the most common BTB protein families,

such as BTB-zinc finger, BTB-BACK-Kelch and MATH-BTB, contain the so-called 'long form' of the BTB domain with a size of about 120 amino acids N-terminal to the BTB core region (Stogios et al., 2005). The amino acid residues exposed at the surface of the BTB fold are highly variable between the different protein families, reflecting the large number of diverse protein-protein interactions among studied BTB proteins in the form of homodimers and heterodimers (Stogios et al., 2005). The protein architecture of the different families generally consists of a single N-terminal BTB domain, a middle linker region, and a characteristic C-terminal domain (Stogios et al., 2005). In some BTB protein families best known to be involved in protein ubiquitination and degradation, adjacent to the C-terminus of the BTB domain is the BACK domain, which is predicted to contain only α-helices (Stogios et al., 2005; Stogios & Privé, 2004). The BACK domain is thought to play a major role in protein oligomerization and orientation of targeted substrates, resulting in large dynamic assemblies that associate and dissociate rapidly depending on concentration (Errington et al., 2012; Stogios & Privé, 2004). The BACK domain is predominantly found in the BTB-BACK-Kelch and BTB-BACK-PHR families, but also in many MATH-BTB proteins. Additionally, bioinformatics search within 183 human BTB proteins predicted the existence of 3-box motif C-terminal to the BTB domain, probably within the BACK domain, in all MATH-BTB and BTB-Kelch proteins (Zhuang et al., 2009).

2.4. MATH-BTB protein family

Unlike most BTB protein families, the BTB domain of MATH-BTB proteins is located C-terminal to its partner, the MATH domain (Stogios et al., 2005). The MATH domain generally represents a 180 amino acids long conserved region that is homologues to the meprins, a mammalian extracellular metalloendopeptidases, and to the intracellular TUMOR NECROSIS FACTOR (TNF) receptor associated factors (TRAFs, Sunnerhagen et al., 2002). This region is highly similar to the TRAF-C domain of TNF and is predicted to form eight anti-parallel β-sheets (Sunnerhagen et al., 2002; Zapata et al., 2001). The MATH-BTB protein family is common in both animals and plants where they are involved in numerous developmental processes. They are known to be key regulators of the cell cycle and are involved in mitotic spindle assembly, correct chromosome segregation, and correct nuclei separation, among other processes (Juranić et al., 2012; Pintard et al., 2003). The most widespread and well-studied role of the MATH-BTB proteins is proteasomal degradation, in which they act as substrate-specific adaptors of CRL3 complexes

(Gingerich et al., 2007; Pintard et al., 2003). In this process, the C-terminal BTB domain is known to bind a CUL3 scaffold protein, while the N-terminal MATH domain targets a variety of substrate proteins such as transcription factors (TFs) to promote their ubiquitination and subsequent degradation by the 26S proteasome (**Figure 2**). The first described MATH-BTB protein with a role in ubiquitination mediated by CRL3 E3 ligases is MEL-26 from *C. elegans* (Pintard et al., 2003). The MEL-26 is involved in proteasomal degradation of MEI-1, a katanin-like protein required for meiotic spindle formation and is therefore directly associated with microtubule cytoskeleton regulation in meiosis-to-mitosis transition. Additionally, MEL-26 is involved in cytokinesis promotion by interaction with the actin binding protein POD-1 in a manner that is independent of the CUL3 (Luke-Glaser et al., 2005). This was the first evidence of a CUL3-independent interaction of MATH-BTB proteins, and the first insight of a potential MATH-BTB dual role in the coordination of close physiological functions by two distinct functions, both in early embryogenesis: first, by degrading MEI-1 it allows normal assembly of the mitotic spindle, and second, by inducing cortical concentrations of POD-1 potentiating the onset of cytokinesis (Luke-Glaser et al., 2005).

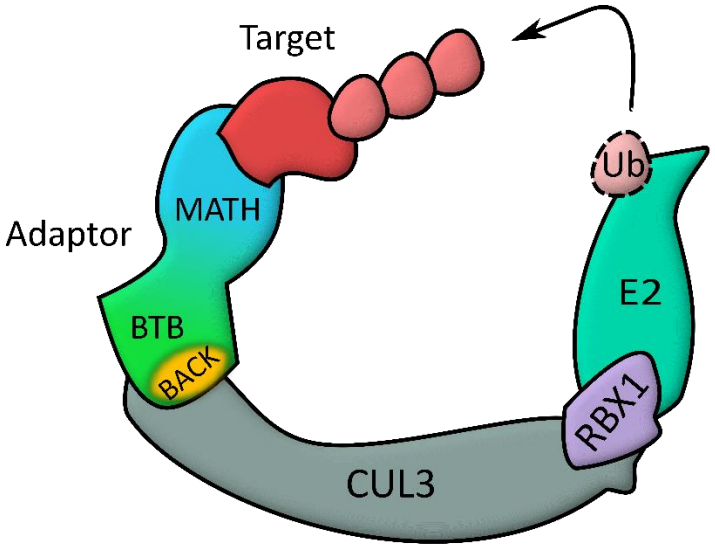

Figure 2 MATH-BTB-CUL3-RING E3 ligase ($CRL3^{MATH\text{-}BTB}$) complex. The $CRL3^{MATH\text{-}BTB}$ complex is formed around the CUL3 scaffold protein. The C-terminal domain of CUL3 serves as an anchor for the RBX1 protein, which binds the ubiquitin-activated E2 enzyme, forming the catalytic core of the complex. The N-terminal region of CUL3 binds the C-terminal BTB domain of the substrate adaptor MATH-BTB protein. This interaction is facilitated by a proximal hydrophobic groove at the interface between the BTB domain and the 3-box-containing BACK domain. The N-terminal MATH domain of the substrate adaptor binds target proteins intended for ubiquitination. The RBX1 protein in the catalytic core of the complex mediates the direct transfer of ubiquitin from E2 to the target protein. Generated in Inkscape vector graphics editor.

Phylogenetic analyzes have been performed for some plant MATH-BTB proteins and have shown that plant MATH-BTB genes cluster into two separate clades: the core clade, which typically includes four to six MATH-BTB proteins from each of the nine land plant species analyzed, and the expanded grass-specific clade (Gingerich et al., 2007; Juranić & Dresselhaus, 2014). Based on the significant sequence conservation of MATH-BTB proteins and their constitutive expression, core clade genes have been hypothesized to regulate evolutionarily ancient pathways in plant development or physiology (Wicker & Keller, 2007), while grass-specific expansion may be caused by rapid diversification of their physiological substrates (Gingerich et al., 2007). Accordingly, there are many MATH-BTB proteins in grasses. For example, rice (*Oryza sativa*) genome encodes for at least 69 MATH-BTB proteins (Gingerich et al., 2007), maize (*Zea mays*) genome for 31 (Juranić & Dresselhaus, 2014), and wheat (*Triticum aestivum*) genome for 46 (Bauer et al., 2019). In contrast, there are only six MATH-BTB genes in *Arabidopsis thaliana* genome (Gingerich et al., 2005), seven in banana (*Musa acuminate*) genome (Juranić & Dresselhaus, 2014), and five in grapevine (*Vitis vinifera*) genome (Juranić & Dresselhaus, 2014).

Despite the large number of genes and proteins, only a few plant MATH-BTB proteins have been functionally characterized, with their role in CUL3-dependent protein degradation largely confirmed. These are *Z. mays* MAB1 (ZmMAB1), *T. aestivum* MAB2 (TaMAB2), and the best studied BPM proteins from *A. thaliana*. Juranić et al. (2012) show that ZmMAB1 forms homodimers and interacts with CUL3a in the cytoplasm. Furthermore, they point to katanin as a potential target for CUL3 ubiquitination mediated by ZmMAB1, which, together with the expression of *ZmMAB1* during male and female meiosis, during the transition from meiosis to mitosis, and in early embryogenesis, suggests a similarity of ZmMAB1 to the MEL-26 role in *C. elegans*. In Bauer et al. (2019), the TaMAB2, a protein transiently expressed in the zygote and during the early embryogenesis (Leljak-Levanić et al., 2013), is characterized. In this paper, the interaction of TaMAB2 and CUL3 is confirmed and colocalization pattern with microtubules is shown. Furthermore, tandem affinity purification of TaMAB2 interactors pointed to the cytoskeletal proteins like tubulin and actin, and eukaryotic translation initiation factors as potential targets of TaMAB2. Unlike the studied MATH-BTB proteins of the grass family, where their role was almost exclusively established in early embryogenesis, the described roles of *Arabidopsis* MATH-BTB proteins are mainly related to plant flowering (Chen et al., 2015), seed development

(Chen et al., 2013; Julian et al., 2019) and stress responses (Beathard et al., 2021; Chico et al., 2020; Julian et al., 2019; Lechner et al., 2011; Morimoto et al., 2017; Weber & Hellmann, 2009).

2.4.1. MATH-BTB proteins in *Arabidopsis thaliana*

The *Arabidopsis thaliana* genome contains six genes (*BPM1-6*) encoding at least 16 MATH-BTB protein isoforms (Škiljaica et al., 2020). The best studied role of BPM proteins is recognizing and binding substrates, predominantly transcription factors, and targeting them for degradation. Some of the known substrates of $CRL3^{BPM}$-mediated protein degradation are members of the Homeodomain Leucine Zipper class I/Homeobox (Hd-Zip/HB) TF family (HB6, but also HB5 and HB16, Lechner et al., 2011), APETALA 2/ethylene response factor (AP2/ERF) TF family members ERF4 (ETHYLENE RESPONSE FACTOR 4, Chen et al., 2013), RAV1 (RELATED TO ABI3/VP1, Chen et al., 2013), RAP2.4 (RELATED TO AP2 4, Weber & Hellmann, 2009), WRI1 (WRINKLED 1, Chen et al., 2013; Ma et al., 2015) and DREB2A (DEHYDRATION-RESPONSIVE ELEMENT BINDING PROTEIN 2A, Morimoto et al., 2017), members of the R2R3 myeloblastosis (MYB) TF family (MYB56, MYB1, MYB25 and MYB109; Beathard et al., 2021; Chen et al., 2015), and the basic Helix-Loop-Helix (bHLH) TF family (MYC2, MYC3 and MYC4, Chico et al., 2020). So far, the only identified $CRL3^{BPM}$ targets that are not TFs are members of the clade A protein phosphatases type 2C (PP2Cs): PP2CA, ABA INSENSITIVE 1 (ABI1) and ABI2, and HYPERSENSITIVE TO ABA 1 (HAB1, Julian et al., 2019). In addition, a few lines with downregulation of multiple BPMs have been generated, all showing developmental alterations (Chen et al., 2013; Lechner et al., 2011; Morimoto et al., 2017), and there are no viable BPM knock-out mutants, probably due to the lethality of the BPMs absence.

In BPM-mediated CUL3-dependent ubiquitination, BTB domain binds CUL3 while MATH domain targets specific substrates (Chen et al., 2013; Lechner et al., 2011; Weber et al., 2005). As far as is known, all BPM substrates contain at least one of two motifs that are recognized by the MATH domain (Mooney et al., 2019; Morimoto et al., 2017; Zhuang et al., 2009). These motifs are a Speckled-type POZ (SPOP)-Binding Consensus (SBC) motif comprised of five amino acids in defined order ϕ-π-S-S/T-S/T (ϕ = nonpolar, π = polar, S = serine, T = threonine), and PEST motif that is enriched in proline (P), glutamate (E), serine (S) and threonine (T). C-terminal to the CUL3-binding BTB domain of all BPM proteins, apart from the three BPM2 splicing variants (BPM2.2, BPM2.3 and BPM2.4), lays a BACK domain (Škiljaica, 2022). Inside the BACK domain probably lays a 3-box motif that further contributes to CUL3-binding.

2.5. Epigenetics and DNA methylation

The term epigenetics has been coined in the middle of the last century when Waddington (2012) recognized that there must be some link between genotype and phenotype. Since then, the understanding of epigenetics has changed a lot, and today we know that the term epigenetics refers to chemical and structural changes in chromatin that lead to hereditary changes in gene function and are not caused by alterations in the DNA sequence (Felsenfeld, 2014). It mainly involves histone modifications (histone acetylation and methylation) and DNA methylation. While histone modifications are an important part of a chromatin architecture regulation and transcription machinery, thus consequentially affecting phenotype, their role in the process is not yet fully clarified (Cui et al., 2018; Felsenfeld, 2014). On the other hand, DNA methylation is known to play a crucial role in the early eukaryote development (Deichmann, 2016). It is necessary for genome stability, transposable elements (TE) silencing and genomic imprinting (Bartels et al., 2018). DNA methylation is established by the addition of a methyl group to the cytosine, resulting in 5-methylcytosine. This reaction is catalyzed by a family of methyltransferases that transfer the methyl group from S-adenosylmethionine to the fifth carbon atom of cytosine (Moore et al., 2013). In plants, where dynamic changes of DNA methylation are involved in development, growth and stress response, DNA methylation occurs in three sequence contexts: CG, CHG and CHH (H = A, C or T). While symmetric CG and CHG methylation is mainly maintained by DNA methyltransferases DNA METHYLTRANSFERASE1 (MET1) and CHROMOMETHYLASE3 (CMT3), respectively (Han et al., 2019; Kankel et al., 2003; Lindroth et al., 2001), asymmetric CHH methylation requires *de novo* methylation in every cell cycle (**Figure 3**). CHH methylation is maintained by DOMAINS REARRANGED METHYLTRANSFERASE 2 (DRM2) or CMT2, depending on the genomic region. The DRM2 is methyltransferase active in the process of RdDM, thus it maintains CHH methylation at RdDM target regions, which are preferentially intergenic regions and plant genes located primarily in euchromatin, especially if the regions contain evolutionarily young or short transposons (Huettel et al., 2006; Liu et al., 2014; Zhang et al., 2018). By contrast, CMT2 catalyzes CHH methylation at histone H1-containing heterochromatin, independently of the RdDM (Zemach et al., 2013; Zhang et al., 2018).

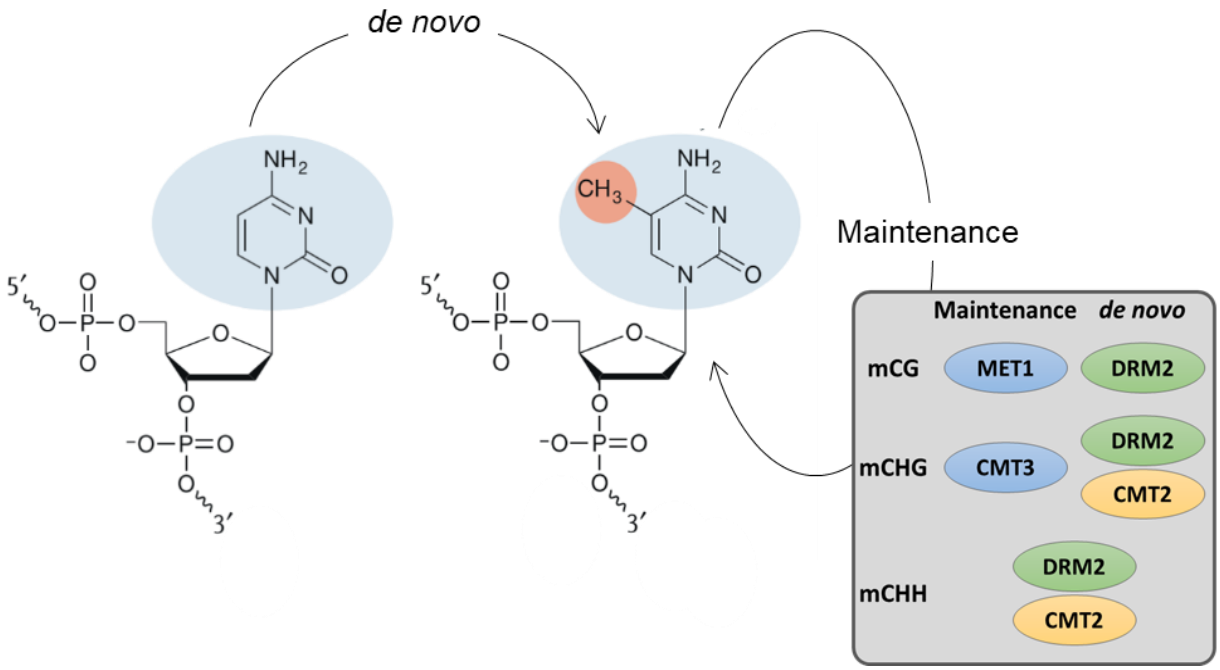

Figure 3 Maintenance and *de novo* DNA methylation in plants. DNA methylation is established by the addition of a methyl group to the 5-carbon of the cytosine, resulting in 5-methylcytosine. Depending on the sequence context, the reaction is catalyzed by different methyltransferases. Following DNA replication, methylation in the symmetric CG context is maintained by MET1, while CHG (H = A, T or C) methylation is maintained by CMT3. Asymmetric CHH context is always methylated *de novo* by DRM2 through the RdDM or by CMT2. Methylation in symmetric contexts can also occur *de novo* in a process that involves DRM2 or CMT2 methyltransferases. Adapted from Zhang et al. (2018).

2.6. RNA-directed DNA methylation

The main epigenetic mechanism responsible for *de novo* DNA methylation in plants is RdDM, the mechanism guided by siRNAs (Aufsatz et al., 2002; Wierzbicki et al., 2012). The backbone of the RdDM consists of two RNA polymerases, POL IV and POL V, and various associated proteins, but the exact mechanism is not fully understood (Matzke et al., 2015). In nucleus, the RNA-DEPENDENT RNA POLYMERASE 2 (RDR2) converts single-stranded RNA transcripts of POL IV to double-stranded RNAs (dsRNAs) that are then cut by DICER-LIKE 3 (DCL3) protein into 24-nucleotide (24-nt) siRNAs. siRNAs are further methylated at their 3'-end by HUA ENCHANCER1 (HEN1) and loaded onto ARGONAUTE (AGO) proteins 4, mainly AGO4 forming AGO-siRNA complex (**Figure 4 A**, Huang et al., 2009; Pontes et al., 2006; Wierzbicki et al., 2012).

Independent of POL IV activity and siRNA biogenesis, POL V produces long non-coding RNAs (lncRNAs) using specific genomic loci as templates (Böhmdorfer et al., 2016; Wierzbicki et al., 2008). Correct positioning of the POL V machinery at accurate loci is crucial for targeted methylation of specific genome loci. The process is mediated by SUPPRESSOR OF VARIEGATION 3-9 HOMOLOG PROTEIN 2 (SUVH2) and SUVH9, which recognize previously methylated cytosines through their SET and RING finger-associated (SRA) domains. SUVH2 and SUVH9 associate with a chromatin-remodeling DDR complex, consistent of three proteins: DRD1, DMS3 and RDM1, (Wongpalee et al., 2019; Zhong et al., 2012), thus promoting Pol V recruitment to the specific RdDM loci that are meant to be methylated (Johnson et al., 2014; Liu et al., 2014). It is important to point out that tethering of SUVH9 by a zinc-finger tag to unmethylated DNA is sufficient to recruit POL V and stimulate DNA methylation (Johnson et al., 2014). The lncRNAs produced by POL V serve as "scaffolds" for binding of AGO4-siRNA complex through RNA-RNA base pairing. While DMS3 has a role exclusively in the DDR complex, RDM1 additionally acts as a bridging protein between AGO4 and DNA methyltransferase DRM2, thus recruiting the effector complex of RdDM to the specific genomic loci, resulting in *de novo* cytosine methylation at target sites (**Figure 4 B**, Gao et al., 2010; Wierzbicki et al., 2012).

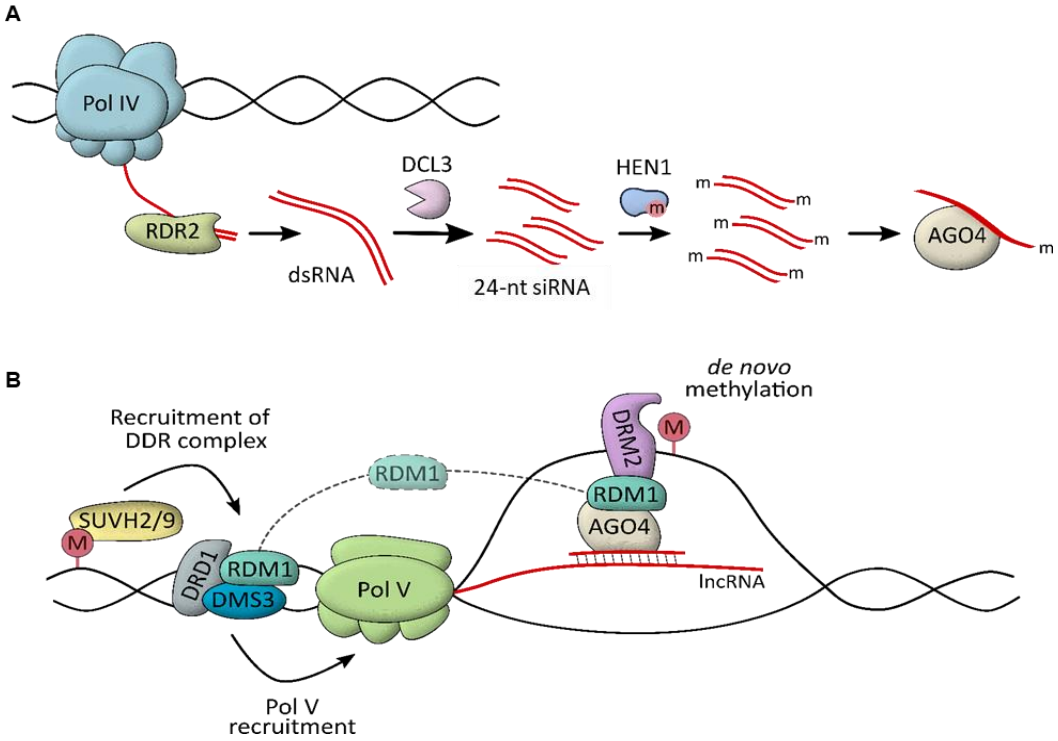

Figure 4. RNA-directed DNA methylation machinery.

Figure 4 - continued

A) POL IV-dependent siRNA biogenesis: POL IV produces non-coding ssRNAs that are used by RDR2 to synthetize dsRNA. dsRNA is then processed by DCL3 into 24-nt siRNAs that are methylated at their 3'-end by HEN1 and loaded onto AGO4. **B**) POL V-mediated DNA methylation: positioning of POL V is mediated by the adapter proteins SUVH2 and SUVH9, which bind previously methylated DNA regions and associate with the DDR complex (DRD1, DMS3 and RDM1). The DDR complex recruits POL V and promotes its production of lncRNAs. The AGO4-siRNA complex binds complementary lncRNA and associates with RDM1, which in turn recruits DRM2 to catalyze *de novo* DNA methylation at homologous genomic sites. Generated in Inkscape vector graphics editor.

In addition to the canonical POL IV–RDR2–DCL3 pathway, there is a non-canonical RdDM pathway dependent on POL II instead of POL IV and RDR6 instead of RDR2. The RDR6 generates dsRNA on POL II transcript. The dsRNA is further processed by DCL2 and DCL4 into 21-nt or 22-nt siRNAs that are loaded onto AGO6, or by DCL3 into 24-nt siRNAs that are loaded onto AGO4 (Zhang et al., 2018; Zheng et al., 2009). The AGO-siRNA complex, just as in canonical RdDM, facilitates POL V mediated DNA methylation. Interestingly, although it was shown that AGO4 and AGO6 are redundant, they differ in their subnuclear colocalization with RNA polymerases involved in RdDM: AGO4 colocalizes with POL V in perinucleolar foci, whereas AGO4 and POL II, as well as AGO6 and POL V display strong colocalization in nucleoplasm (Duan et al., 2015). Non-canonical RdDM occurs at intergenic low-copy-number loci and at some regions of transcriptionally active transposons (Nuthikattu et al., 2013; Zheng et al., 2009).

2.6.1. DDR complex

The chromatin remodeling DDR complex is essential for correct positioning of the POL V and, therefore, the rest of RdDM machinery consists of three proteins: a putative SNF2-containing chromatin remodeling protein DRD1 (Kanno et al., 2004), a structural maintenance of chromosomes (SMC) hinge domain-containing protein DMS3 (Kanno et al., 2008) and a small plant-specific protein RDM1 with a conserved DUF1950 domain (Sasaki et al., 2014). Recruitment of the DDR complex to the specific DNA sites is mediated by SUVH2 and SUVH9 through their binding with the DMS3 component of the complex (Liu et al., 2014). The precise stoichiometric balance of the three DDR components DRD1, DMS3 and RDM1 in the ratio 1:4:2 is necessary for the proper function of the DDR complex (Wongpalee et al., 2019). Wongpalee et al. (2019) applied cryogenic electron microscopy to resolve the DDR complex structure and formation. First step in the formation of the DDR complex is formation of the DMS3-RDM1 complex. The core of the DMS3-RDM1 complex is RDM1 homodimer formed by the hydrophobic RDM1 interactions.

Surrounding the core are two DMS3 dimers, each bound to the exposed side of a RDM1 monomer by numerous mutual interactions involving the hinge and the coiled-coil (CC) domains of DMS3. Additionally, the two DMS3 dimers bridge to each other across the RDM1 core by the two flexible CC domains. The DMS3 homodimerization is mediated by their hinge domains and has proved to be crucial for the stability of the DR complex. There is a striking difference between the DMS3 monomers inside each DMS3 dimer regarding the CC domain: the CC domain of one DMS3 protein interacts with the hydrophobic pockets of the RDM1, while the CC domain of the other DMS3 remains free and disordered. One free CC domain of one DMS3 protein recruits DRD1 by its N-terminal domain and assembles the full DDR complex. Here, the RDM1 dimer also plays an important role since DRD1 is additionally bound into its surface hydrophobic cleft. Moreover, the proper levels of DMS3 proved to be crucial for the correct assembly and stability of the DDR complex, and optimal concentrations are maintained by the degradation of DMS3 through the APC/C mediated process (Zhong et al., 2019). Considering that DRD1 also interacts with POL V (Law et al., 2010), two hypotheses of the POL V recruitment were proposed (Wongpalee et al., 2019): either the POL V is recruited to the fully assembled DDR complex, or a performed DRD1-POL V complex is bound to the stable DR complex (**Figure 5**).

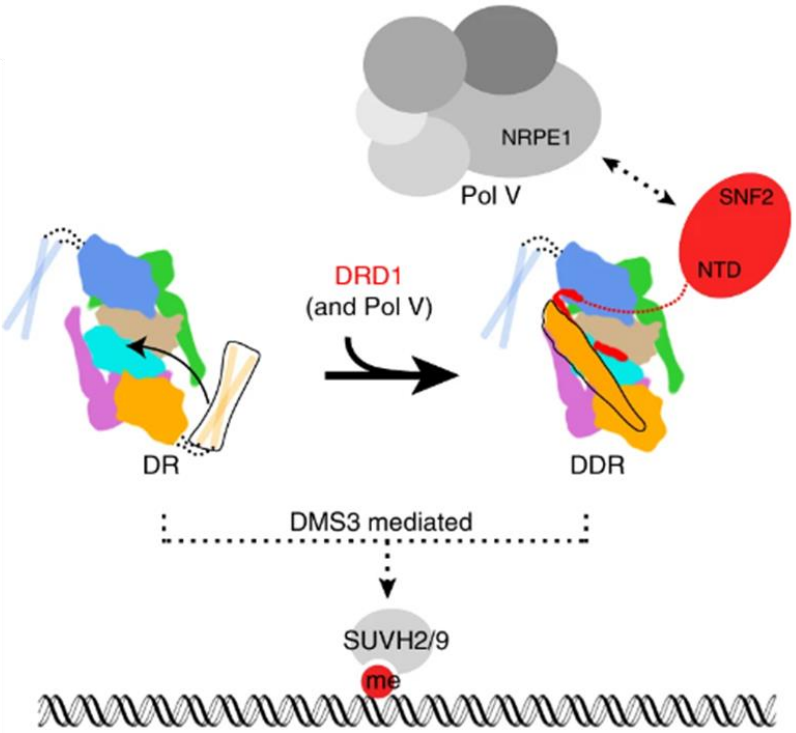

Figure 5 Proposed mechanism of DDR-mediated POL V recruitment.

Figure 5 - continued

The full DDR complex is formed after binding of peptide 7 of the N-terminal domain (NTD) of DRD1 to the DR complex. This results in a conformational change in one of the DMS3 dimers from the "open" to the "closed" state. Chromatin targeting is mediated by the interaction of DMS3 and SUVH2 or SUVH9. The POL V is recruited through its largest subunit NRPE1, either by interaction with DRD1 in the DDR complex or simultaneously with DRD1 as a preformed DRD1-POL V complex. Illustration from Wongpalee et al. (2019)**.**

Outside of the DDR complex, RDM1 associates with AGO4 and DRM2 facilitating *de novo* DNA methylation. RDM1 is also able to bind CHH-methylated ssDNA and to interact with POL II, indicating a potential role of the RDM1 in the non-canonical RdDM (Gao et al., 2010). In contrast, the only interaction of DRD1 outside the DDR complex is with POL V-specific subunits (mainly NRPE1), but no interactions with the subunits specific to POL II or IV exist (Law et al., 2010).

The DMS3, apart from the DDR complex formation, associates with methylated DNA-binding proteins SUVH2 and SUVH9 thus recruiting the DDR complex to the DNA methylated sites (Johnson et al., 2014; Liu et al., 2014). Additionally, DMS3 interacts with MICRORCHIDIA6 (MORC6), the GHKL (Gyrase, Hsp90, Histidine Kinase, MutL) ATPase, in an interaction that might provide the missing ATPase function for DMS3, thus facilitating the chromatin structure modification and POL V transcription at RdDM loci (Liu et al., 2014; Lorković et al., 2012; Matzke et al., 2015).

3. MATERIALS AND METHODS

3.1. Materials

3.1.1. Plant material and growth conditions

3.1.1.1. *Arabidopsis thaliana* (L.) Heynh.

Arabidopsis thaliana (L.) Heynh. ecotype Columbia wild type (WT) and transgenic lines in the same background were used in this study. Line overexpressing EGFP-tagged BPM1, designated as oeBPM1-EGFP, is described as line L104 in Škiljaica et al. (2020). Line overexpressing TAP-tagged BPM1, designated as oeBPM1-TAP, and line overexpressing EGFP-tagged DMS3, designated as oeEGFP-DMS3, are described in Jagić et al. (2022). Furthermore, line amiR-bpm with downregulation of *BPM 1, 4, 5* and *6* (Lechner et al., 2011) and line *dms3-1* with point mutation at the position 339 of DMS3 (glycine to glutamic acid substitution) leading to failure in formation of an active dimer (Kanno et al., 2008) were used. Plants were cultivated on solid MS medium (Murashige & Skoog, 1962, **Appendix A Table A1-1**) or in liquid growth media (GM, Gilkerson et al., 2009). Details on *A. thaliana* cultivation and growing conditions are given in section 3.2.1

Prior any experiments, plant lines were verified on solid MS medium supplemented with appropriate selection agent: 30 ng/mL of hygromycin B (Sigma-Aldrich, Merck KGaA) for oeBPM1-TAP and *dms3-1*, and 60 ng/mL glufosinate-ammonium (Supelco®) for oeBPM1-EGFP, amiR-bpm and oeEGFP-DMS3.

3.1.1.2. Tobacco BY-2 suspension cells

Tobacco BY-2 (PC-1181 *Nicotiana tabacum* L. cv. Bright Yellow-2) cells were purchased from Leibniz Institute DSMZ-German Collection of Microorganisms and Cell Cultures GmbH (http://www.dsmz.de) in the form of callus. BY-2 cell suspension was obtained by shaking (100 rpm) a loose callus in a liquid MS-BY2 medium (**Appendix A Table A1-2**) supplemented with synthetic auxin 2,4-D and kept in the dark at 24 °C with shaking at 100 rpm. After weekly subculturing and refining, an actively growing suspension composed of individual cells was achieved.

3.1.1.3. *Nicotiana benthamiana* Domin

Seeds of *Nicotiana benthamiana* were sown in a mixture of white peat and perlite (Steckmedium KLASMANN, Klasmann-Deilmann GmbH), followed by stratification at 4 °C for 2-3 days. After germination, plants were grown in a long-day conditions (16 h light/8 h dark, 100 µmol/m^2/s, 24 °C) with 50% relative humidity.

3.1.2. Yeast, *Saccharomyces cerevisiae* host strain

For yeast two-hybrid screens, the yeast host HF7c [*MATa, ura3-52, his3-200, ade2-101, lys2-801, trp1-901, leu2-3, 112, gal4-542, gal80-538, LYS2::GAL1$_{UAS}$-GAL1$_{TATA}$-HIS3, URA3::GAL4$_{17mers(x3)}$-CYC1$_{TATA}$-lacZ*] was used. The HF7c strain contains two reporter genes, *HIS3* and *lacZ*, integrated into the genome and transcribed solely upon interaction between two hybrid proteins synthesized from externally introduced vectors (one carrying GAL4 activation domain, and the other carrying DNA-binding domain, Feilotter et al., 1994). Used vectors will be later described in more detail (sections 3.1.4.1 and 3.2.5.1). In HF7c, the promoter of the *HIS3* gene, whose protein product participates in histidine biosynthesis, has been replaced with the GAL1 promoter, while *lacZ* is under control of the conserved 17-mer consensus sequence of the UAS ($UAS_{G\ 17\text{-}mer\ (x3)}$) and the extremely weak minimal promoter of the yeast cytochrome C1 (*CYC1*) gene (Feilotter et al., 1994). Both promoters are activated by GAL4 transcription factor. Yeasts were grown on a solid YPD medium (**Appendix A Table A2-1**) at 30 °C. Selection of co-transformed yeasts was carried on minimal SD medium without leucine and tryptophan (SD/-Leu/-Trp medium, **Appendix A Table A2-2**), and interaction screening (histidine prototrophy assay) was carried out on minimal SD medium additionally lacking histidine and supplemented with 3-AT to suppress leaky *HIS3* expression (SD/-His/-Leu/-Trp + 3-AT, **Appendix A Table A2-2**).

3.1.3. Bacteria strains

3.1.3.1. *Escherichia coli* strains

Escherichia coli NEB5-alpha competent cells (New England Biolabs; chemically competent cells #C2987I), XL10-Gold Ultracompetent Cells (Stratagene), XL1-Blue Competent Cells (Agilent) and HST04 (Stellar™ Competent Cells, Clontech Laboratories, Inc. Takara Bio, #636763) were used for cloning. BL21 (DE3) (New England BioLabs) and Rosetta™ (DE3) Competent Cells (Novagen MSDS) were used for protein overexpression. All *E. coli* strains were

grown on solid or in liquid LB medium (**Appendix A Table A3-1**) at 37 °C. Rosetta™ (DE3) host strain is BL21 derivate designed to enhance the expression of eukaryotic proteins that contain codons rarely used in *E. coli* (AUA, AGG, AGA, CUA, CCC, and GGA) and thus carry the pRARE plasmid with chloramphenicol resistance (Novy et al., 2001).

3.1.3.2. *Agrobacterium tumefaciens* strain

Agrobacterium tumefaciens electrocompetent cells GV3101 (pMP90) (Gold Biotechnology®) were used for agroinfiltration of electroporated plasmids into *Nicotiana benthamiana* epidermal leaves cells and for floral dip transformation of *Arabidopsis thaliana*. The GV3101 strain has a C58 chromosomal background with rifampicin resistance and the Ti plasmid pmp90 (pTiC58DT-DNA) with gentamicin resistance (Koncz & Schell, 1986). Bacteria were grown on solid or in liquid LB medium (**Appendix A Table A3-1**) supplemented with required antibiotics at 28 °C **(Appendix A Table A3-2)**.

3.1.4. Plasmid constructs

3.1.4.1. Plasmid constructs used for protein interaction assays

For yeast two-hybrid assays, the Matchmaker cloning vectors pGAD424 and pGBT9 (Clontech Laboratories, Inc. Takara Bio) were used. pGAD424 encodes for a hybrid protein with N-terminal GAL4 activation domain (AD), while pGBT9 encodes for a hybrid protein with N-terminal GAL4 DNA binding domain (BD). pGAD424:BPM1 and pGBT9:BPM1 constructs, encoding for hybrid proteins AD-BPM1 and BD-BPM1, respectively, are described in Jagić et al. (2022). pGAD424 and pGBT9 each carrying hybrid *DMS3* or *RDM1* (pGAD424:DMS3 encoding for AD-DMS3, pGBT9:DMS3 for BD-DMS3, pGAD424:RDM1 encoding for AD-RDM1 and pGBT9:RDM1 for BD-RDM1) were provided by the courtesy of prof. Zdravko Lorković and the details on cloning are reported in Lorković et al. (2012). Bacterial and yeast selection regarding used vectors is summarized in **Appendix B Table B1-1**.

For protein expression in *E. coli*, pGEX-4T-1 (Amersham) plasmid carrying *GST-BPM1* that is designated as pGEX-4T-1:BPM1, pET28a (Novagen) carrying *HIS-RDM1* designated as pET28a:RDM1 (Jagić et al., 2022) and *HIS-DMS3* designated as pET28a:DMS3 (Lorković et al., 2012) were used. Additionally, pGEX-4T-1:BPM1ΔMATH, pGEX-4T-1:BPM1ΔBTB and pGEX-

4T-1:BPM1ΔBACK from which *GST-BTB-BACK$_{BPM1}$*, *GST-MATH-BACK$_{BPM1}$* and *GST-MATH-BTB$_{BPM1}$* were expressed, respectively, are described in Miškec (2019).

3.1.4.2. Plasmid constructs used for localization and colocalization studies

For overexpression of fluorescently tagged BPM1 in BY-2 and *N. benthamiana* epidermal cells, coding DNA sequence (CDS) of *BPM1* was cloned into Gateway destination vectors: pB7WGF2 to obtain pB7WGF2:BPM1 encoding for EGFP-BPM1, pB7FWG2 to obtain pB7FWG2:BPM1 encoding for BPM1-EGFP and pB7WGR2 to obtain pB7WGR2:BPM1 encoding for mRFP1-BPM1 (Leljak Levanić et al., 2012). For overexpression of fluorescently tagged DMS3, destination vectors pB7WGF2 to obtain pB7WGF2:DMS3 encoding for EGFP-DMS3 and pB7WGR2 to obtain pB7WGR2:DMS3 encoding for mRFP1-DMS3 (Jagić et al., 2022) were used. For overexpression of fluorescently tagged RDM1, destination vectors pB7WGF2 to obtain pB7WGF2:RDM1 encoding for EGFP-RDM1 and pH7WGR2 to obtain pH7WGR2:RDM1 encoding for mRFP1-RDM1 (Jagić et al., 2022) were used. All mentioned plasmid constructs were also used for Förster's resonance energy transfer - fluorescence lifetime imaging microscopy (FRET-FLIM) analysis.

To observe BPM1 homodimer formation and localization in living cells via bimolecular fluorescence complementation (BiFC), plasmid vectors pSPYNE:BPM1 and pSPYCE:BPM1 encoding for N-terminal or C-terminal fragment of YFP (Walter et al., 2004) fused to BPM1, were used. Mentioned plasmids were generated as a part of Rendulić's master thesis (2018).

Bacterial selection regarding used vectors is summarized in **Appendix B Table B1-2**.

3.1.4.3. Plasmid vector used for analysis of promoter activity

To analyze influence of RdDM and of BPM proteins on promoter activity of *FWA*, a well-studied RdDM regulated gene (Soppe et al., 2000), the binary vector pCambia1301 (Abcam) carrying the *gusA* reporter gene encoding a new β-glucuronidase (GUS) enzyme (Russell & Klaenhammer, 2001) was used to generate pCambia1301 with *pFWA::GUS* expression cassette (cloning details are described in section 3.2.5.2). Vector contains a gene for kanamycin resistance in bacteria and hygromycin B resistance for plant selection.

3.1.5. Primer sequences

All primers used in this study were ordered from Macrogen Europe and diluted in deionized water to achieve a 100 μM stock solution and diluted to 10 μM working solution before use. The stocks and working solutions were stored at -20 °C. Oligonucleotide sequences used in this work are listed in **Appendix C**.

3.2. Methods

3.2.1. *Arabidopsis thaliana* cultivation, growth conditions and treatments

Arabidopsis seeds were surface sterilized by incubation in 1 mL of 70% ethanol for 1 min, followed by 10 min incubation with constant rotation on Dynal sample mixer, model MXICI (Invitrogen™) in 1 mL water solution containing 1% NaOCl (Izosan® G; Pliva) and 0.1% Mucasol™ (Sigma-Aldrich, Merck KGaA) and rinsed five times in 1 mL of sterile distilled water. The sterile seeds were then plated on solid MS or liquid GM medium and stratified for two days at 4 °C.

To examine BPM1 protein stability, 2 mg of WT, oeBPM1-EGFP and oeBPM1-TAP seeds were sterilized, plated, stratified and further grown in liquid GM for 7 days at 24 °C in a growth chamber with long-day conditions (16 h light/8 h dark, 100 μmol/m^2/s). On the 7th day, WT and oeBPM1-EGFP seedlings were incubated with 0.2 g/L of cycloheximide (CHX) for 1 or 3 h at 24 °C or 37 °C under standard light conditions. Protocol for CHX treatment is given in Gilkerson et al. (2015). As a control, some seedlings were only subjected to elevated temperature (37 °C) for the 1, 3 and 6 h periods but without CHX addition. After treatment, seedlings were sampled, frozen in liquid nitrogen and homogenized (section 3.2.2). Ten seedlings per line and treatment were used for RNA isolation (section 3.2.3.1) followed by relative expression analysis (section 3.2.3.2), and 20 seedlings per line and treatment were used for protein extraction (section 3.2.4.1) and immunoblotting (sections 3.2.4.4).

Additionally, BPM1 protein stability in line oeBPM1-TAP at 37 °C was tested. Seven days old seedlings of WT and line oeBPM1-TAP were subjected to 37 °C for 3 h, without CHX and further processed as described above.

For TAP-MS, approximately 100 sterilized seeds per line, lines oeBPM1-TAP and oeBPM1-EGFP, were plated on solid MS medium, stratified and grown for 12 days at 24 °C in long-day

conditions. On the 12th day seedlings were treated for 3 h at 37 °C under standard light conditions (100 μmol/m^2/s).

For agrobacterial transformation (floral dip), sterilized, plated and stratified WT seeds were first transferred to Plant growth chamber RK-500 CH (Kambič) with short-day conditions (8 h light/16 h dark, 70 μmol/m^2/s, 24 °C) for two weeks, then transferred to a mixture of white peat and perlite (Steckmedium KLASMANN, Klasmann-Deilmann GmbH) and kept for one additional week in short day conditions. Afterwards, they were transferred to a chamber with long-day conditions until flowering. To obtain more flower buds per plant, the primary inflorescences were cut off, thus relieving apical dominance, and encouraging the synchronized appearance of several secondary inflorescences.

After floral dip transformation, seeds were collected and selected on hygromycin B supplemented solid MS medium. Before plating, seeds were surface sterilized as mentioned above. Selection was carried out following rapid and robust method by Harrison et al. (2006). Platted seeds were first stratified for 2 days at 4 °C, then kept under the standard light conditions for 4-6 h, following 48 h in the dark and 24 h under lights. Transformants (T1) had long hypocotyls (0.8-1.0 cm) while non-resistant seedlings had shorter hypocotyls (0.2-0.4 cm). Transformant seedlings were planted in a mixture of white peat and perlite (Steckmedium KLASMANN, Klasmann-Deilmann GmbH) and grown till maturity in long-day conditions, the presence of a transgene was verified by PCR (section 3.2.3.7). T1 transgenics were designated as pFWA::GUS lines.

3.2.2. Plant tissue homogenization

All plant tissues were frozen in liquid nitrogen prior homogenization. Frozen *Arabidopsis* seedlings used for RNA isolation (section 3.2.3.1) and protein extraction (section 3.2.4.1), and frozen seedlings and leaves for DNA isolation (sections 3.2.3.5 and 3.2.3.6) were homogenized in two repeats for 8 s in GC 19163 Silver Mix 90 Mixer Machine (GC EUROPE N.V., C.M.F. SRL) at frequency of 4300 oscillations per min using SiLibeads Typ S 1.0-1.3 mm.

Frozen seedlings used for TAP were homogenized using mortar and pestle while still frozen and were immediately transferred to prechilled 15 mL Falcon tube and further processed as described in section 3.2.7.

3.2.3. Nucleic acid isolation and analysis

3.2.3.1. RNA isolation from *Arabidopsis thaliana* seedlings

For BPM1 stability analysis (section 3.2.1), approximately 10 seedlings for each line and treatment were sampled and used for RNA isolation. Collected seedlings were immediately frozen in liquid nitrogen and homogenized as described in section 3.2.2. RNA was extracted from the samples using MagJET Plant RNA Isolation kit (Thermo Fisher Scientific), following manufacturer's instructions for manual RNA purification. Lysis Buffer from the kit was supplemented with dithiothreitol (DTT, 1,4-Dithiothreitol, Carl Roth) to final concentration of 40 mM and polyvinylpyrrolidone (PVP40, Sigma-Aldrich, Merck KGaA) at a 2% (w/v) of final concentration. RNA purity and concentrations were determined using NanoDrop™ 1000 (ND-1000) Spectrophotometer (Thermo Fisher Scientific).

3.2.3.2. cDNA synthesis and quantitative Real-Time PCR

Approximately 720 ng of isolated RNA was used for reverse transcription (RT) reaction in total volume of 20 µL using 200 units of RevertAid H Minus Reverse Transcriptase and 1x Reaction Buffer (Thermo Fisher Scientific), 20 units of RNase inhibitor (RiboLock, Thermo Fisher Scientific), 0.5 mM dNTPs (Sigma-Aldrich, Merck KGaA) and 5 µM Oligo$(dT)_{18}$ primer (Thermo Fisher Scientific). RT reaction mix containing only RNA, Oligo$(dT)_{18}$ primer and dNTPs was incubated for 5 min at 65 °C, then the rest of the components (RevertAid H Minus Reverse Transcriptase, Reaction Buffer and RNase inhibitor) were added and incubated for 45 min at 42 °C. Reaction was terminated by heating at 70 °C for 15 min.

Quality of complementary DNA (cDNA) and check for genomic DNA (gDNA) contamination was performed using ACT3_fw and ACT3_rev primers (**Appendix C Table C1-1**) and EmeraldAmp® MAX PCR Master Mix (Takara Bio, Inc) according to manufacturer's instructions. ACT3 primer set is used for amplifying part of the *ACT3* gene with the ability to distinguish cDNA (638 bp amplicon) from gDNA (732 bp amplicon). PCR reaction was performed in total volume of 25 µL, initial denaturation step was performed at 98 °C for 3 min, followed by 35 cycles of denaturation at 98 °C for 10 s, annealing at 60 °C for 30 s and elongation at 72 °C for 1 min/kb, and a final elongation step at 72 °C for 7 min. Reaction products were analyzed by agarose gel electrophoresis (section 3.2.3.8).

For quantitative Real-Time PCR (qRT-PCR), cDNA was diluted two times and mixed with GoTaq qPCR Master mix (Promega) and BPM1-specific 130 nM primers OEBPM1Fw and OEBPM1R (**Appendix C Table C1-2**) which amplify both, transgenic and endogenous *BPM1*. GoTaq qPCR system contains fluorescent BRYT Green® Dye that is used to monitor double stranded DNA synthesis. Reactions were performed in total volume of 15 µL in an optical 96-well plate using an Applied Biosystems 7500 Fast Real-Time PCR system according to the manufacturer's instructions. The thermal profile was as follows: 50 °C for 20 s, 95 °C for 10 min, 40 cycles of 95 °C for 10 s, and 58 °C for 60 s. Reference gene *RHIP1* (primer sequences are listed in **Appendix C Table C1-2**) was used for expression normalization (Škiljaica et al., 2022). The presence of a single amplicon was confirmed as a single peak in the melting curve obtained after amplification using the following parameters: 20–95 °C with ramp speed of 0.3 °C/min. Quantification cycle (Cq) values and primer efficiencies were calculated from raw amplification data in the exponential phase of each individual amplification plot using LinRegPCR software (Ramakers et al., 2003). The mean value of two replicates was normalized to expression of *RHIP1* and results were analyzed with ΔΔCt method (Pfaffl et al., 2004; Vandesompele et al., 2002).

3.2.3.3. Colony PCR for transformant screening

Prior plasmid DNA isolation (NEB5-alpha, XL10-Gold, XL1-Blue or HST04 cells) or protein expression (BL21 or Rosetta^{TM} cells), single *E. coli* colonies were picked and cultured overnight at 37 °C in 3 mL of liquid LB medium supplemented with the appropriate antibiotics (information regarding bacterial selections are written in **Appendix B Table B1-1** and **Table B1-2**). To screen for transformants, 100 µL of overnight bacterial cultures were transferred into 1.5 mL microcentrifuge tubes and centrifuged for 2 min at 14 000 rpm. Supernatant was discarded and pellets were resuspended in 100 µL of sterile distilled water. The resuspended bacteria were denatured at 95 °C for 5 min. The denatured bacterial suspensions (2 µL) were used as templates for PCR. PCR was performed in total volume of 25 µL using EmeraldAmp® MAX PCR Master Mix (Takara Bio, Inc) according to manufacturer's instructions. Initial denaturation step was performed at 98 °C for 3 min, followed by 40 cycles of denaturation at 98 °C for 10 s, annealing at 54 °C to 58 °C for 30 s regarding to the transgene being tested, elongation at 72 °C for 1 min/kb and a final elongation step at 72 °C for 7 min. PCR reactions were analyzed on agarose gel (section

3.2.3.8). Primers, annealing temperature and expected amplicon length are given in **Table 1** and **Appendix C Table C2-1**.

Prior to the agroinfiltration, single *A. tumefaciens* (strain GV3101) colonies were picked and cultured overnight at 28 °C in 5 mL of liquid LB medium supplemented with 50 ng/mL rifampicin, 50 ng/mL gentamicin and 100 ng/mL spectinomycin. To verify transformants, 100 µL of overnight agrobacterial cultures were transferred into 1.5 mL microcentrifuge tubes and centrifuged for 2 min at 14 000 rpm. Supernatant was discarded and pellets were resuspended in 100 µL of sterile distilled water. The resuspended agrobacteria were denatured at 95 °C for 10 min and colony PCR was performed as described for *E. coli* bacteria above with primer set and PCR conditions given in **Table 1**.

Table 1 Colony PCR inserts checkup. Insert, primer set, annealing temperature (T_a) and amplicon length are indicated. Colony PCR was performed using EmeraldAmp® MAX PCR Master Mix (Takara Bio, Inc) according to manufacturer's instructions.

Insert	**Primer set**	**T_a / °C**	**Amplicon length / bp**
BPM1	attB1BPM1fw and BPM1-STOPattB2rev	58	1274
BTB-BACK$_{BPM1}$			869
MATH-BACK$_{BPM1}$			920
MATH-BTB$_{BPM1}$			1082
MATH$_{BPM1}$			725
BTB$_{BPM1}$			677
BACK$_{BPM1}$			510
DMS3	DMS3_BiFC_IFf and DMS3_BiFC_IFrev	58	1292
RDM1	InF_RDM1_fw and InF_RDM1_rev	58	534
35S::GUS	M13-rev and pCAMBIA-GUSup	56	1093
Δ35S			321
GUS	GUS-dn and GUS-up2	54	764
PFWA	M13-rev and Fwa-InF up	56	1087

3.2.3.4. Plasmid DNA isolation from *Escherichia coli*

For plasmid DNA isolation from *E. coli*, 2 mL of verified overnight culture (section 3.2.3.3) was used for plasmid DNA isolation by Wizard® Plus SV Minipreps DNA Purification System (Promega) following manufacturers' instructions. To gain better yield of plasmid DNA, elution

step was slightly modified: 50 µL of Nuclease-Free Water was added to the Spin Column, incubated for 15 min at 37 °C and then centrifuged at 14 000 rpm for 1 min. The described elution step was repeated once more and eluted plasmid DNA concentrations were determined using ND-1000 Spectrophotometer.

Before further use, all plasmids were verified by sequencing at Macrogen Europe using universal or pre-ordered primers. Cloned DNA sequence and reading frame of a fused transcript were carefully examined for point or frameshift mutations and only correct clones were further used. Primers used for sequencing of specific plasmid constructs are listed in **Appendix C Table C3-1**.

3.2.3.5. DNA isolation from *Arabidopsis thaliana* seedlings

DNA from *A. thaliana* seedlings, used for promoter region amplification (section 3.2.5.2) followed by promoter activity analysis (section 3.2.10), was isolated by modified cetyltrimethylammonium bromide (CTAB) method. Hundred milligrams of WT seedlings were collected and homogenized as described in section 3.2.2. To the homogenized tissue, 500 µL of pre-warmed (65 °C) extraction buffer (100 mM Tris-HCl pH 7.5, 1.4 M NaCl, 20 mM EDTA pH 8.0, 2% CTAB and 20 mM 2-Mercaptoethanol) was added. After 30 min incubation at 65 °C sample was pelleted for 5 min at 16 000 × g at room temperature. Supernatant was transferred into new 1.5 mL microcentrifuge tube and mixed with the same volume of the chloroform:isoamyl solution (24:1). Sample was further incubated for 10 min, then centrifuged for 10 min at 14 000 × g. Upper aqueous phase was transferred to new microcentrifuge tube (1.5 mL) and mixed with double volume of precipitation buffer (50 mM Tris-HCl pH 7.5, 10 mM EDTA pH 8.0 and 1% CTAB). Mixture was incubated for 60 min at room temperature and afterwards, nucleic acids were pelleted at 14 000 × g for 10 min. Supernatant was removed and pellet was resuspended in 600 µL of RNase buffer containing 1.5 M NaCl and 10 ng/mL PureLink™ RNase A (Cat. No. 10618703, Invitrogen™) and incubated for 30 min at 55 °C. After incubation, solution was transferred into 2 mL microcentrifuge tube, mixed with 1200 µL of cold 96% ethanol and left to precipitate at room temperature overnight.

The next day, sample was pelleted at 14 000 × g for 10 min, supernatant was removed and precipitate was resuspended in 500 µL of cold 70% ethanol. Sample was again pelleted for 5 min at 7 000 × g, supernatant was discarded and pellet was dried at 37 °C. Dry pellet was dissolved in 100 µL of deionized water.

3.2.3.6. Quick DNA isolation from *Arabidopsis thaliana* leaves

To determine whether T-DNA insertion was successful in hygromycin-resistant pFWA::GUS plants (section 3.2.6.6) and that the insert was still present in pFWA::GUS crossed plants (described later in 3.2.10.1), quick DNA isolation was performed. One leaf per plant was collected and homogenized as described in section 3.2.2. Hundred microliters of DNA extraction buffer (200 mM Tris-HCl pH 7.5, 250 mM NaCl, 25 mM EDTA pH 8.0 and 0.5% SDS) was added to the leaf powder, mixture was severely vortexed and tissue debris was pelleted by centrifugation at 16 000 × g for 5 min at room temperature. Double volume of 96% ethanol was added to the clear supernatant, solution was vortexed and DNA was pelleted at 16 000 × g for 10 min. Pellet was dried for 20 min at room temperature and thereupon DNA was dissolved in TE buffer (10 mM Tris-HCl pH 7.5, 1 mM EDTA pH 8.0), vortexed and solution was centrifuged for 5 min at 16 000 × g. Isolated DNA was kept on 4 °C till use for T-DNA genotyping.

3.2.3.7. *Arabidopsis thaliana* T-DNA genotyping

Two microliters of each DNA sample obtained in the previous section were used as templates for PCR genotyping. PCR was performed in total volume of 25 μL using GUSup2 and GUSdn primers (**Appendix C Table C2-1**) and EmeraldAmp® MAX PCR Master Mix (Takara Bio, Inc) according to manufacturer's instructions. Initial denaturation step was performed at 98 °C for 3 min, followed by 40 cycles of denaturation at 98 °C for 10 s, annealing at 54 °C for 30 s, elongation at 72 °C for 1 min/kb and a final elongation step at 72 °C for 7 min. PCR reactions were analyzed on agarose gel. As a control of isolated DNA, PCR reactions with the same templates were performed using ACT3_fw and ACT3_rev primers (**Appendix C Table C1-1**) under the same conditions with the change in annealing temperature to 60 °C. Additionally, *dms3-1* × pFWA::GUS crossing progeny (section 3.2.10.1) was tested for presence of the kanamycin resistance gene using Kan_FW and Kan_REV primers (**Appendix C Table C2-1**) thus indirectly confirming the presence of *dms3-1* mutant allele.

3.2.3.8. Agarose gel electrophoresis

To separate DNA fragments, whether to check for the quality of cDNA (section 3.2.3.2), screen for transformants (section 3.2.3.3) or for T-DNA genotyping (section 3.2.3.7), DNA samples were loaded on 1% agarose gel and 20 min electrophoresis at 100 V in TAE buffer (40 mM Tris-HCl

pH 8.3, 1 mM EDTA) was carried out in RunOne™ System (Embi Tec). DNA fragments were stained for 5 min in ethidium bromide solution prepared in TAE buffer (10 ng/L) and visualized under the 100% UV light strength using Kodak EDAS 290 Photo Cabinet and 2 s exposition.

If DNA fragment separation was performed in order to purify precise-sized linearized DNA fragments used for cloning reactions (section 3.2.5), 0.8% agarose gel was used and fragments were separated at 50 V electrophoresis for 40 min, briefly stained in ethidium bromide solution for 2-3 min, visualized under 70% UV light strength and excised from the gel with scalpel.

3.2.3.9. Purification of DNA fragments from gel or PCR reaction

Purification of linearized vectors and amplified inserts from gel used for cloning (section 3.2.3.8) or directly from PCR reaction solution used for Biolistic transformation (section 3.2.6.4) was performed using NucleoSpin® Gel and PCR Clean-up kit (Macherey-Nagel) according to manufacturer's guidelines.

3.2.4. Protein extraction and analysis

3.2.4.1. Protein extraction from *Arabidopsis thaliana* seedlings and protein quantification

For BPM1 stability assay (section 3.2.1) approximately 20 seedlings per line and treatment were sampled parallel with sampling for RNA isolation, and were homogenized as described in section 3.2.2. After homogenization, 200 µL of protein extraction buffer containing 100 mM Tris-HCl pH 6.8, 8% SDS, 40% glycerol, bromophenol blue and 3% (v/v) 2-Mercaptoethanol, preheated to 60 °C was added to the tissue powder, and the samples were denatured for 10 min at 95 °C. The soluble protein fraction was obtained by centrifugation at 16 000 × g for 20 min at 4 °C and protein extract was transferred to clean prechilled Eppendorf tube (1.5 mL) and kept on ice. For relative protein quantification, 20 µL of each protein extract was loaded onto polyacrylamide gel, proteins were separated using sodium dodecyl sulfate – polyacrylamide gel electrophoresis (SDS-PAGE) and stained with Coomassie Brilliant Blue (CBB) R-250 (section 3.2.4.3). Protein bends were then quantified using ImageJ v.1.51 (section 3.2.4.5).

To analyze endogenous DMS3 protein levels, 11-days old seedlings (70 mg), WT and oeBPM1-EGFP line were homogenized in liquid nitrogen (section 3.2.2) and proteins were extracted in 250 µL extraction buffer PEB50 (**Appendix D Table D1-1**). Crude protein extracts were incubated for 20 min on ice with periodical vortexing and centrifuged for 20 min at 4 °C and

16 000 × g. Relative soluble protein concentrations were quantified on ND-1000 Spectrophotometer using default general reference settings (1 Abs = 1 mg/mL). Equal amounts of protein were mixed with Sample loading buffer (SLB, for composition see **Appendix D Table D1-2**) and denatured for 10 min at 80 °C.

3.2.4.2. Protein purification from *Escherichia coli*

For pull-down and microscale thermophoresis analysis, protein purification from expression *E. coli* strains (BL21 and Rosetta™, section 3.1.3.1) was performed. Rosetta™ (DE3) cells were transformed with pGEX-4T1:BPM1, pGEX-4T1:BPM1ΔBTB, pET28a:DMS3 or pET28a:RDM1 plasmids, while BL21 (DE3) cells were transformed with pGEX-4T1:BPM1ΔMATH or pGEX-4T1:BPM1ΔBACK (for construct description see sections 3.1.4.1 and 3.2.5.1). Selection was carried out on LB plates containing appropriate antibiotics: ampicillin for pGEX-4T1 constructs or kanamycin for pET28a constructs, with the addition of chloramphenicol when Rosetta™ (DE3) cells were used (for antibiotic concentrations see **Appendix A Table A3-2**).

Overnight cultures of bacteria carrying plasmid constructs of BPM1 or its deletion variants fused with GST, or His-tagged RDM1 or DMS3 were grown at 37 °C in the presence of appropriate antibiotics, diluted in 4 × YT (**Appendix A, Table A3-3**) medium and grown until OD_{600} reached value between 0.6 and 1.0. Protein synthesis was induced with 0.3 mM IPTG and suspensions were incubated at 15 °C overnight. Rosetta™ (DE3) cells, transformed with empty pGEX-4T1 plasmid, served to synthesize GST alone protein that was later used as negative control in pull-down assay. Cells expressing GST-tagged proteins were collected and resuspended in 20 mL of PBS containing 0.1% Triton X-100, 1 mg/mL Lysozyme and 1 mM PMSF, incubated for 30 min at room temperature and sonicated six times for 40 s with Bioblock Scientific Vibracell. Sonicated cells were pelleted by centrifugation at 20 000 × g for 20 min at 4 °C, protein extracts (supernatant) were filtered through Minisart® Syringe Filters, Pore Size 0.45 µm (Sartorius) and mixed with 150 µL (for GST-BTB-$BACK_{BPM1}$) or 500 µL (for GST-BPM1 and GST-MATH-$BACK_{BPM1}$) of prewashed Glutathione Sepharose 4B beads (Cytiva 17-0756-01, GE Healthcare) and incubated overnight at 4 °C with gentle shaking. Collected beads were washed first with PBS containing 0.05% Tween 20, then with PBS containing 0.5 M NaCl and four times with pure PBS buffer. Beads with bound protein (GST-BPM1, GST-BTB-$BACK_{BPM1}$ or GST-MATH-$BACK_{BPM1}$) were stored in 200 µL of PBS buffer at 4 °C.

Cells expressing His-tagged DMS3 or RDM1 protein were collected and resuspended in 20 mL of lysis buffer containing 50 mM Tris-HCl, pH 8.0, 300 mM NaCl, 1 mM 2-Mercaptoethanol, 10 mM Imidazole, 0.5% Triton X-100, 1 mg/mL Lysozyme and 1 mM PMSF, incubated for 30 min at room temperature and sonicated six times for 40 s with Bioblock Scientific Vibracell. After sonication cells were centrifuged at 20 000 × g for 20 min at 4 °C, protein extracts in supernatant were filtered through Minisart® Syringe Filters, Pore Size 0.45 µm (Sartorius) and incubated with prewashed Ni-NTA agarose beads (QIAGEN, GmBH), 350 µL for DMS3 or 200 µL for RDM1, and incubated overnight at 4 °C with gentle shaking. Collected beads were washed first with 50 mM Tris-HCl, pH 8.0 containing 1 M NaCl, 1 mM 2-Mercaptoethanol, and 20 mM imidazole, then twice with 50 mM Tris-HCl, pH 8.0 containing 500 mM NaCl, 1 mM 2-Mercaptoethanol, and 10 mM imidazole and finally with 50 mM Tris-HCl, pH 8.0 containing 50 mM NaCl, 1 mM 2-Mercaptoethanol and 10 mM imidazole. After fourth wash, beads were transferred on 35 µm pore size filter column (Mobicol M2135, MoBiTec), washed three more times with last washing buffer and eluted twice with 50 mM Tris-HCl, pH 8.0, 50 mM NaCl and 500 mM imidazole and once with 2 M imidazole. Eluted proteins were concentrated in parallel with buffer exchange into PBS using Amicon® Ultra-4 Centrifugal Filter Devices (MilliporeSigma, Merck KGaA). Purified and desalted His-tagged DMS3 and RDM1proteins were stored at 4 °C.

3.2.4.3. SDS-PAGE and polyacrylamide gel staining

Protein extracts were loaded on polyacrylamide gel (4% stacking gel and 12% resolving gel, for composition see **Appendix D Table D1-3**) and proteins were resolved using SDS-PAGE in Tris-Glycine-SDS buffer (TG-SDS: 3 g/L Tris, 14.4 g/L glycine, 1 g/L SDS, pH 8.3). If SDS-PAGE was performed to quantify protein amounts, 20 µL of protein extracts were loaded on polyacrylamide gel. If SDS-PAGE was performed to analyze and compare protein levels in plants (section 3.2.4.4), equal protein amounts were loaded in duplicates. The amount of proteins was adjusted based on the sample with the lowest value obtained by quantification (section 3.2.4.5), and the maximum volume loaded was 20 µL (for this sample). PageRuler Prestained Protein Ladder 10-180 kDa (Thermo Fisher Scientific) was used for size standards. SDS-PAGE was carried out in Electrophoresis Unit MINI Vertical (Carl Roth) for 30 min at 90 V and 120 min at 200 V using Consort EV243 Power Supply (Sigma-Aldrich, Merck KGaA). After electrophoresis, proteins were

either stained with CBB R-250 or electroblotted on a polyvinylidene difluoride (PVDF) membrane (section 3.2.4.4).

For protein staining, CBB R-250 at final concentration of 0.1% (w/v) was dissolved in 45% (v/v) methanol and 10% (v/v) acetic acid mixture and gels were incubated in the solution for around 10 min with occasional heating in the microwave. Gels were distained by shaking in hot distilled water for approximately 30 min till protein bands were visible.

3.2.4.4. Western blot analysis and PVDF membrane staining

After SDS-PAGE, gels were preequilibrated in transfer buffer (3.39 g/L Tris-HCl, 14.4 g/L glycine, 20% (v/v) methanol, pH 8.3) and electroblotted on a PVDF membrane (Transfer Membranes, Immobilon®-P) pretreated in 100% methanol and washed twice in deionized water. Transfer was carried out in Trans-Blot Cell (Bio-Rad Laboratories, Inc.) according to Trans-Blot Electrophoretic Transfer Cell Instruction Manual (Bio-Rad Laboratories, Inc.), in transfer buffer at 200 mA for 2 h or at 12 V overnight. Membranes were briefly washed in phosphate buffered saline (PBS, 137 mM NaCl, 2.7 mM KCl, 10 mM Na_2HPO_4, 1.8 mM KH_2PO_4, pH 7.3) and blocked overnight at 4 °C in 2% non-fat milk dissolved in PBS (blocking solution). Depending on the proteins to be detected, different antibodies were used as described in paragraphs bellow.

For BPM1 stability assay, immunodetection of the fusion BPM1-EGFP and BPM1-TAP proteins was performed. To detect BPM1-EGFP, membranes were incubated with primary Anti-GFP antibody (Cat. No.11814460001, Roche, dilution 1:1000) for 3 h, washed three times with PBS and incubated for 2 h in secondary Anti-Mouse IgG (whole molecule)-Peroxidase antibody produced in goat (Cat. No. A4416, Sigma-Aldrich, Merck KGaA, dilution 1:5000). For BPM1-TAP detection membranes were incubated for 2 h in Peroxidase Anti-Peroxidase (PAP) Soluble Complex antibody produced in rabbit (Cat. No. P1291, Sigma-Aldrich, Merck KGaA, dilution 1:2000). PAP antibody soluble complex detects Protein A in the TAP tag and since the horseradish peroxidase (HRP) in the complex is not covalently coupled to the antibody, the soluble complex retains its enzyme and antibody reactivity enabling immediate detection. All antibody dilutions were prepared in blocking solution and incubations were carried out at room temperature.

To analyze endogenous DMS3 protein levels, the blot was incubated with primary anti-DMS3 antibody (Zhong et al., 2019) diluted in ratio 1:500 in PBS at 4 °C overnight, washed two times

with PBS and incubated with secondary Goat Anti-Rabbit IgG Antibody, HRP-conjugate (Merck Millipore, dilution 1:6000), prepared in blocking solution at room temperature for 2 h.

To analyze pull-down (section 3.2.9.2), the membrane was incubated with primary Anti-His_6 from mouse IgG1 antibody (Cat. No. 11922416001, Roche, dilution 1:1000) at 4 °C overnight. After incubation, membrane was washed three times in PBS and incubated with secondary Anti-Mouse IgG (whole molecule)-Peroxidase antibody produced in goat (Cat. No. A4416, Sigma-Aldrich, Merck KGaA, dilution 1:5000) at room temperature for 2 h. Both antibody dilutions were prepared in blocking solution.

Membranes with bound antibodies were washed three times in PBS buffer and signals were detected using 500 µL of chemiluminescent HRP detection reagent Luminata Forte Western HRP substrate (Millipore, Merck) per membrane, followed by exposure to autoradiographic films (Hyperfilm, Amersham Pharmacia Biotech) for 20 min. The films were developed using 15% developer (Heraeus Kulzer GmBH) and 15% fixer (Heraeus Kulzer GmBH) solutions, respectively. Alternatively, detection was performed using 500 µL of Solution A mixed with 500 µL of Solution B from ECL™ Prime Western Blotting System (Cytiva Amersham™) and UVItec Alliance 4.7 for Fluorescence and Chemiluminescence Systems (UVItec Ltd.) following manufacturer's instructions.

After detection, the membranes were stained with 0.1% (w/v) CBB R-250 prepared in 50% (v/v) methanol and 7% (v/v) acetic acid, and distained first for 5 min in 50% methanol and 7% acetic acid then briefly in 90% methanol and 10% acetic acid. Finally, membranes were washed in distilled water and dried on towel paper.

3.2.4.5. Protein quantification using ImageJ

Relative quantification of protein levels was done in public domain Java image processing software ImageJ v.1.51 (https://imagej.nih.gov/ij/). The stained polyacrylamide gels or PVDF membranes were scanned in high resolution. Scanned images were first converted to 8-bit, then region of interest (ROI) was selected in the first lane and densitometry was performed following procedure described on https://www.sybil-fp7.eu/node/95.

Same procedure was used to quantify intensities of detected protein bands on autoradiographic films or images taken with UVItec. Band intensities were normalized to CBB stained bands on membrane.

3.2.5. Cloning procedures

3.2.5.1. Generation of domain-omitted BPM1 plasmid constructs

To investigate the role of particular domains of BPM1 protein in localization and interaction experiments, vectors containing domain-omitted BPM1 CDS were generated using previously described pGAD424:BPM1, pGBT9:BPM1 and pB7WGF2:BPM1 (section 3.1.4.1 and 3.1.4.2) as backbones. Domain delineations were specified according to the NCBI's conserved domain database where MATH domain covers amino acids from N33 to V167, BTB domain from L193 to E310 and BACK domain from V312 to R375 (**Figure 6 A**).

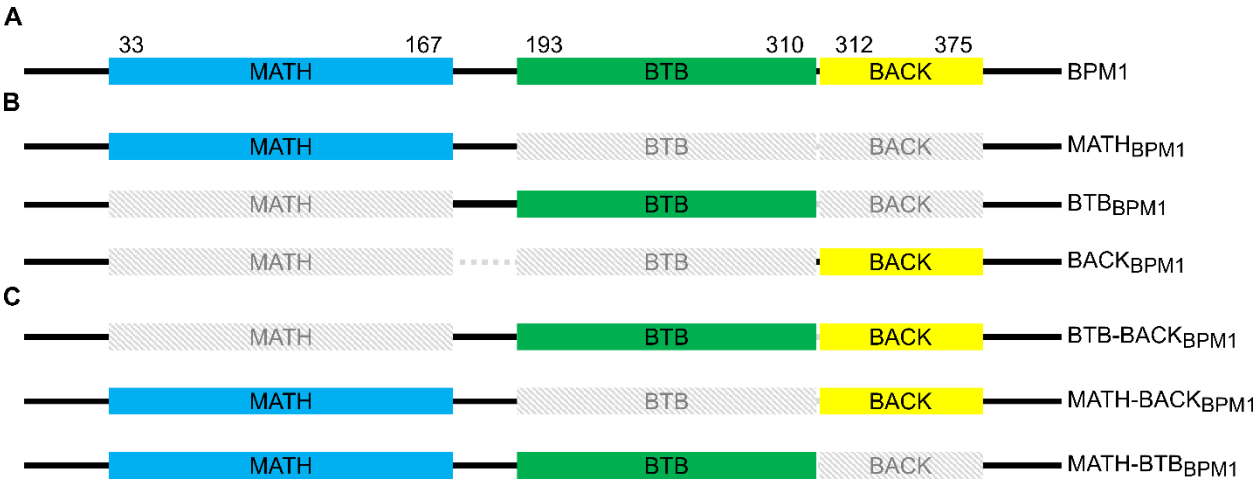

Figure 6 Schematic representation of the BPM1 protein and BPM1 domain-omitted constructs functionally tested in this study. BPM1 protein contains three domains: N-terminal MATH domain (blue), and C-terminal BTB (green) and BACK (yellow) domains (**A**). Double-domain deletion constructs of BPM1 with only one protein domain (MATH, BTB or BACK) remaining (**B**). Truncated versions of BPM1 with deletion of MATH, BTB or BACK domain (**C**).

Q5 Site-Directed Mutagenesis kit (New England Biolabs) and suitable primers for deletion of MATH (MATHdel_fw and MATHdel_rev), BTB (BTBdel_fw and BTBdel_rev) or BACK (BACKdel_fw and BACKdel_rev) domain of BPM1 (for primer sequences see **Appendix C Table C4-1**) were used to generate pGAD424:BPM1ΔMATH encoding for *AD-BTB-BACK$_{BPM1}$*, pGBT9:BPM1ΔMATH encoding for *BD-BTB-BACK$_{BPM1}$*, pB7WGF2:BPM1ΔMATH encoding for *EGFP-BTB-BACK$_{BPM1}$*, pGBT9:BPM1ΔBTB encoding for *BD-MATH-BACK$_{BPM1}$*, pGAD424:BPM1ΔBACK encoding for *AD-MATH-BTB$_{BPM1}$*, pGBT9:BPM1ΔBACK encoding for *BD-MATH-BTB$_{BPM1}$* and pB7WGF2:BPM1ΔBACK encoding for *EGFP-MATH-BTB$_{BPM1}$*. Site directed mutagenesis was performed according to manufacturer's instructions. The first step

was exponential amplification of plasmid missing one of the BPM1's domain. Specific conditions regarding annealing temperature (T_a) and elongation time (t_e) for each cloning reaction are summarized in **Table 2**. After exponential amplification of plasmid, the amplified material is added directly to the unique Kinase-Ligase-DpnI (KLD) enzyme mix for 5 min at room temperature to catalyze plasmid circularization and template removal.

Table 2 Q5 Site-Directed Mutagenesis PCR condition for generation of domain-omitted BPM1 plasmid constructs: pGAD424:BPM1ΔMATH, pGBT9:BPM1ΔMATH, pB7WGF2:BPM1ΔMATH, pGBT9:BPM1ΔBTB, pGAD424:BPM1ΔBACK, pGBT9:BPM1ΔBACK and pB7WGF2:BPM1ΔBACK.

Domain-omitted BPM1 vector*	**T_a / °C**	**t_e / min**
PGAD424:BPM1ΔMATH	71	3.5
PGBT9:BPM1ΔMATH	71	3
PB7WGF2:BPM1ΔMATH	71	6
PGBT9:BPM1ΔBTB	70	3.5
PGAD424:BPM1ΔBACK	69	3.5
PGBT9:BPM1ΔBACK	70	3.5
PB7WGF2:BPM1ΔBACK	69	6

*Plasmid constructs: pGAD424:BPM1ΔBTB and pB7WGF2:BPM1ΔBTB were generated by different methods as follows in the paragraphs bellow.

To generate pGAD424:BPM1ΔBTB from which *AD-MATH-BACK$_{BPM1}$* was expressed, BPM1ΔBTB insert was cut from pGBT9:BPM1ΔBTB using FastDigest BamHI restriction enzyme (Thermo Fisher Scientific). Vector pGAD424:BPM1 was linearized, and BPM1 insert was cut out, using BamHI restriction enzyme. Restriction reaction was performed at 37 °C for 50 min and reaction was inactivated at 80 °C for 5 min. Linearized vector (pGAD424) was purified (section 3.2.3.9) and dephosphorylated using Alkaline Phosphatase from northern shrimps (Roche). Dephosphorylation was performed for 10 min at 37 °C and phosphatase was inactivated by incubation for 5 min at 70 °C. Dephosphorylated vector (pGAD424) and excised insert (BPM1ΔBTB), both with BamHI sticky ends, were purified from gel (section 3.2.3.9). One Weiss unit of T4 ligase (Thermo Fisher Scientific) was used to ligate BPM1ΔBTB insert (500 ng) and dephosphorylated pGAD424 vector (100 ng). Reaction mixture was incubated for 18 h at 22 °C, and T4 ligase was inactivated by incubation at 65 °C for 10 min afterwards.

To generate pB7WGF2:BPM1ΔBTB, from which *EGFP-MATH-BACK*$_{BPM1}$ was expressed, In-Fusion® HD Cloning Kit (Takara Bio, Inc) was used. Vector pB7WGF2 was linearized using Q5 Hot Start High-Fidelity DNA polymerase (New England Biolabs) and primers STOPattB2 and EGFPrev_sdm (**Appendix C Table C4-2**). PCR reaction was carried out according to manufacturer's guidelines with annealing temperature set to 71 °C and elongation time of 4 min. Insert BPM1ΔBTB was amplified from pGBT9:BPM1ΔBTB using CloneAmp™ DNA polymerase (Takara Bio, Inc) and primer set InF_BPM1_fw and InF_BPM1_rev (**Appendix C Table C4-2**) according to manufacturer's instructions. Linearized vector and amplified insert were both purified from agarose gel (section 3.2.3.9). In-Fusion cloning reaction was performed using 20 ng of insert (BPM1ΔBTB) and 50 ng of linearized vector (pB7WGF2) following manufacturer's instructions.

Single-domain constructs used only for yeast two-hybrid (Y2H) experiments were generated using the previously described pGAD424:BPM1 and pGBT9:BPM1 or their domain-omitted versions (pGAD424:BPM1ΔMATH, pGBT9:BPM1ΔMATH, pGAD424:BPM1ΔBTB, pGBT9:BPM1ΔBTB) and different primer combinations with Q5 Site-Directed Mutagenesis kit. To generate pGAD424:BPM1ΔBTBΔBACK or pGBT9:BPM1ΔBTBΔBACK from which *AD-MATH*$_{BPM1}$ or *BD-MATH*$_{BPM1}$ were expressed, pGAD424:BPM1 or pGBT9:BPM1 were used as backbones for PCR amplification with BACKdel_fw and BTBdel_rev primers. To generate pGAD424:BPM1ΔMATHΔBACK or pGBT9:BPM1ΔMATHΔBACK from which *AD-BTB*$_{BPM1}$ or *BD-BTB*$_{BPM1}$ were expressed, pGAD424:BPM1ΔMATH or pGBT9:BPM1ΔMATH were used as backbones for PCR amplification with BACKdel_fw and BACKdel_rev primers. To generate pGAD424:BPM1ΔMATHΔBTB or pGBT9:BPM1ΔMATHΔBTB from which *AD-BACK*$_{BPM1}$ or *BD-BACK*$_{BPM1}$ were expressed, pGAD424:BPM1ΔBTB or pGBT9:BPM1ΔBTB were used as backbones for PCR amplification with MATHdel_fw and MATHdel_rev primers. Details on backbone and primers (**Appendix C Table C4-1**) used, together with the annealing temperatures (T_a) and elongation time (t_e) are summarized in **Table 3**. KLD reaction was performed first 5 min at 37 °C and for another 5 min at room temperature. Full-length BPM1 protein and BPM1 deletion mutants are schematically shown in **Figure 6**.

Table 3 Q5 Site-Directed Mutagenesis PCR condition for generation of single-domain constructs of pGAD424:BPM1 and pGBT9:BPM1 used in Y2H analysis

Single-domain BPM1 vector	T_a / °C	t_e / min
PGAD424:BPM1ΔBTBΔBACK	69	3.5
PGBT9:BPM1ΔBTBΔBACK		
PGAD424:BPM1ΔMATHΔBACK	69	3.5
PGBT9:BPM1ΔMATHΔBACK		
PGAD424:BPM1ΔMATHΔBTB	71	3.5
PGBT9:BPM1ΔMATHΔBTB		

To generate plasmids carrying domain-omitted versions of BPM1 protein for BiFC analysis vectors pSPYCE:BPM1 and pSPYNE:BPM1 (Rendulić 2018) were linearized by BamHI restriction (50 min at 37 °C followed by 5 min inactivation at 80 °C) cutting out BPM1 insert along the way. Inserts (BPM1ΔMATH, BPM1ΔBTB and BPM1ΔBACK) were amplified from pGAD424 backbones carrying designated sequences using CloneAmp™ DNA polymerase (Takara Bio, Inc) and primer set BPM1_BIFC_IFf and BPM1_BIFC_IFrev (**Appendix C Table C4-2**) according to manufacturer's instructions. Linearized vector and amplified inserts were purified from gel (section 3.2.3.9). In-Fusion cloning reaction was performed using approximately 20 ng of inserts and 50 ng of linearized vectors following manufacturer's instructions thus generating pSPYCE:BPM1ΔMATH, pSPYCE:BPM1ΔBTB, pSPYCE:BPM1ΔBACK, pSPYNE:BPM1ΔMATH, pSPYNE:BPM1ΔBTB and pSPYNE:BPM1ΔBACK.

3.2.5.2. Generation of *pFWA::GUS* construct for promoter activity analysis

To analyze *FWA* promoter activity, 1 kb sequence directly upstream of the transcription start site was amplified using CloneAmp™ DNA polymerase (Takara Bio, Inc) and primer set Fwa-InF-dn and Fwa-InF-up (**Appendix C Table C4-3**) from WT seedlings DNA. The binary vector pCambia1301 (Abcam) was linearized using pCam1301-InF-dn and pCam1301-InF-up primers (**Appendix C Table C4-3**) and Q5 Hot Start High-Fidelity DNA polymerase (New England Biolabs) thus deleting CaMV 35S promoter and much of the *lacZ*a gene out of the vector. Deletion of *lacZ*a allows blue-white screening of recombinant bacteria. Linearized vector and amplified insert were purified (section 3.2.3.9) and In-Fusion cloning reaction was performed according to

manufacturer's instructions generating pCambia1301 carrying *pFWA::GUS* expression cassette. For negative control (pCambia1301Δ35S), linearized vector missing CaMV 35S promoter and *lacZ*a was recirculated and template was removed by KLD reaction (New England Biolabs).

3.2.6. Transformation procedures

3.2.6.1. Transformation of chemically competent *Escherichia coli* cells

Depending on cloning procedure (section 3.2.5), different transformation mixtures were used. KLD mixture (5 μL) after Q5 Site-Directed Mutagenesis was added to NEB 5-alpha competent *E. coli* cells, In-Fusion mix (2.5 μL) was added to Stellar™ Competent Cells (HST04) and ligation mixture (5 μL) was added to XL10-Gold Ultracompetent Cells. For promoter activity analyses cloning mixture (In-Fusion mix for pCambia1301 carrying *pFWA::GUS* or KLD mixture for pCambia1301 carrying Δ35S) was added to XL1-Blue Competent cells. Competent bacterial cells were thawed on ice, transformation mixture was added to cell suspension and incubated on ice for 30 min. Cells were then transferred to a 42 °C water bath for 30-45 s depending on the competent cell type and tubes used (**Table 4**), cooled down for 2-5 min on ice, subsequently supplemented with 500-950 μL of SOC medium (New England Biolabs) and incubated at 37 °C for 45-50 min with shaking (250 rpm). Finally, transformed bacteria cells were plated on solid LB medium supplemented with appropriate antibiotics (see **Appendix A Table A3-2** for antibiotic concentrations and **Appendix B Table B1-1** and **Table B1-2** for antibiotic resistance according to plasmid transformed) and grown overnight at 37 °C. For blue-white screening of XL1-Blue transformants LB medium was supplemented with kanamycin at 50 ng/mL final concentration, IPTG at 0.5 mM final concentration and X-gal at 32 μg/mL final concentration.

Table 4 Transformation conditions of chemically competent *E. coli* cells dependent on bacterial strain used.

***E. coli* strain**	**Cloning method**	**Tubes used**	**Heat shock duration**
NEB 5-alpha	Q5 Site-Directed Mutagenesis	1.5 mL Eppendorf tube	30 s
Stellar™	In-fusion cloning	Falcon® 14 mL round bottom polystyrene test tube	45 s
XL10-Gold	T4 ligation	1.5 mL Eppendorf tube	45 s
XL1-Blue	Q5 Site-Directed Mutagenesis / In-fusion cloning	Falcon® 14 mL round bottom polystyrene test tube	60 s

For protein overexpression, 50-100 ng of plasmid DNA was added to BL21 (DE3) or Rosetta™ (DE3) competent cells. Competent bacterial cells in 1.5 mL Eppendorf tubes were thawed on ice, plasmid DNA was added to the cells and suspension was incubated on ice for 30 min. Cells were then transferred to a 42 °C water bath for 45 s, cooled down for 90 s on ice then supplemented with 500 µL of SOC medium (New England Biolabs) and incubated at 37 °C for 1 h with shaking (250 rpm). Transformed bacteria cells (100 µL) were plated on solid LB medium supplemented with appropriate antibiotics: kanamycin or ampicillin for added plasmid selection and chloramphenicol for pRARE plasmid preservation in Rosetta™ (DE3) cells (see **Appendix A Table A3-2** for antibiotic concentrations) and grown overnight at 37 °C.

3.2.6.2. Transformation of electrocompetent cells of *Agrobacterium tumefaciens*

Electrocompetent *A. tumefaciens* strain GV3101 (pMP90) cells were thawed on ice and 100-200 ng of plasmid DNA was added to cells. The whole suspension was transferred to a pre-chilled electroporation cuvette and the cuvette was inserted into the MicroPulser™ electroporator (Bio-Rad Laboratories, Inc.). Plasmid DNA was electroporated to cells with the pulse strength of 2.1-2.3 kV that lasted for 5 ms. Immediately after pulsation, suspensions were supplemented with 450 µL of SOC medium (New England Biolabs), transferred back into the 1.5 mL tubes and incubated at 28°C with shaking (350 rpm). After two-hour incubation, cell suspensions (100 µL) were plated on solid LB medium supplemented with appropriate antibiotics: rifampicin (50 ng/mL) and gentamicin (50 ng/mL) to ensure growth of the used agrobacteria strain, and spectinomycin (100 ng/mL) or kanamycin (50 ng/mL) regarding the plasmid used for transformation (**Table 5**). Agrobacteria were grown at 28 °C for two days.

Table 5 Plasmid backbone used for generation of plasmid constructs for electroporation with targeted application and appropriate bacterial selection.

Backbone	Application	Bacterial selection
pB7WGF2	Subcellular localization and colocalization and FRET-FLIM analysis	Spectinomycin
pB7FWG2		
pB7WGR2		
pH7WGR2		
pSPYCE	BiFC	Kanamycin
pSPYNE		
pCambia1301	Promoter analysis (GUS assay)	

3.2.6.3. Transformation of yeast cells

For Y2H assays, the yeast strain HF7c was co-transformed with vectors pGBT9 as bait and pGAD424 as prey, each carrying either *BPM1* or its deletion variants, or *DMS3* or *RDM1* genes, or empty vectors for negative control. Plasmid combinations are written in **Table 6** and plasmid constructs are described in sections 3.1.4.1 and 3.2.5.1. Standard lithium-acetate transformation of yeasts was used according to Agatep et al. (1998). In short, three yeast colonies were transferred and grown overnight in 5 mL of liquid YPD medium. Overnight culture was diluted 20 times in fresh YPD and further grown for 3-4 h at 30 °C to reach OD_{600} of 0.4-0.6. Yeasts were pelleted by centrifugation at 2 000 × g for 3 min, pellet was washed in prechilled sterile deionized water and resuspended in pre-transformation mix containing 240 µL of 50% polyethylene glycol, 36 µL lithium acetate (1 M) and 5 µL of ssDNA (UltraPure™ Herring Sperm DNA Solution, Invitrogen™, Thermo Fisher Scientific, 10 mg/mL, previously boiled at 95 °C for 5 min and chilled on ice) per transformation. Transformation mixture (281 µL) was then added to prepared plasmid combination (200-300 ng per plasmid) according to **Table 6** and incubated for 30 min at 30 °C with shaking (250 rpm). Next, 15 min heat-shock (42 °C) was done, mixture was cooled down on ice for 2 min, pelleted at 3000 × g for 1 min and resuspended in 1 mL of YPD medium. After 1 h incubation with shaking (250 rpm) in YPD at 30 °C, the transformants were plated on SD/-Leu/-Trp medium (**Appendix A Table A2-2**) later designated as "master" plates, wrapped with parafilm, and grown for 3 days at 30 °C. As mentioned above, the HF7c strain contains two reporter genes, *HIS3* and *lacZ*, both used to inspect protein-protein interaction.

Table 6 Plasmid combinations for Y2H protein interaction assays.

Protein interaction analysis		**Plasmid combinations**	
BPM1 – DMS3		pGAD424:BPM1	pGBT9:DMS3
		pGAD424:DMS3	pGBT9:BPM1
BPM1 – RDM1		pGAD424:BPM1	pGBT9:RDM1
		pGAD424:RDM1	pGBT9:BPM1
MATH-BTB$_{BPM1}$ – DMS3		pGAD424:BPMΔBACK	pGBT9:DMS3
MATH-BTB$_{BPM1}$ – RDM1		pGAD424:BPM1ΔBACK	pGBT9:RDM1
MATH-BACK$_{BPM1}$ – DMS3		pGAD424:BPM1ΔBTB	pGBT9:DMS3
MATH-BACK$_{BPM1}$ – RDM1		pGAD424:BPM1ΔBTB	pGBT9:RDM1
BTB-BACK$_{BPM1}$ – DMS3		pGAD424:BPM1ΔMATH	pGBT9:DMS3
BTB-BACK$_{BPM1}$ – RDM1		pGAD424:BPM1ΔMATH	pGBT9:RDM1
MATH$_{BPM1}$ – DMS3		pGAD424:BPM1ΔBTBΔBACK	pGBT9:DMS3
MATH$_{BPM1}$– RDM1		pGAD424:BPM1ΔBTBΔBACK	pGBT9:RDM1
BTB$_{BPM1}$– DMS3		pGAD424:BPM1ΔMATHΔBACK	pGBT9:DMS3
BTB$_{BPM1}$– RDM1		pGAD424:BPM1ΔMATHΔBACK	pGBT9:RDM1
BACK$_{BPM1}$– DMS3		pGAD424:BPM1ΔMATHΔBTB	pGBT9:DMS3
BACK$_{BPM1}$– RDM1		pGAD424:BPM1ΔMATHΔBTB	pGBT9:RDM1
Positive control		pGAD424:RDM1	pGBT9:DMS3
DMS3 – RDM1		pGAD424:DMS3	pGBT9:RDM1
Negative controls	BPM1	pGAD424:BPM1	pGBT9
	MATH-BTB$_{BPM1}$	pGAD424:BPM1ΔBACK	pGBT9
	MATH-BACK$_{BPM1}$	pGAD424:BPM1ΔBTB	pGBT9
	BTB-BACK$_{BPM1}$	pGAD424:BPM1ΔMATH	pGBT9
	MATH$_{BPM1}$	pGAD424:BPM1ΔBTBΔBACK	pGBT9
	BTB$_{BPM1}$	pGAD424:BPM1ΔMATHΔBACK	pGBT9
	BACK$_{BPM1}$	pGAD424:BPM1ΔMATHΔBTB	pGBT9
	DMS3	pGAD424:DMS3	pGBT9
	RDM1	pGAD424:RDM1	pGBT9

3.2.6.4. Biolistic transformation of tobacco BY-2 cells

For transient transformation of BY-2 cells, DNA cassettes amplified by CloneAmp™ DNA polymerase (Takara Bio, Inc) and primer set BiFC_BY2fw and BiFC_BY2rev (**Appendix C Table C5-1**) were used. As DNA templates, plasmids containing CDS of fluorescently tagged protein of interest (BPM1 or its domain-omitted variants, DMS3, RDM1, for details on the constructs see sections 3.1.4.2 and 3.2.5.1) were utilized. PCR was performed according to manufacturer's instructions and amplified DNA cassettes were purified as described in section 3.2.3.9. Each DNA cassette consisted of prementioned CDS under the cauliflower mosaic virus (CaMV) 35S promoter and CaMV 35S terminator. Additionally, in the cassette, glufosinate (pB7WGF2 and pB7WGR2) or hygromycin (pH7WGR2) resistance gene under the nopaline synthase (NOS) promoter and NOS terminator was present.

A fresh tobacco BY-2 culture was initiated and grown for 3 to 4 days. One to two hours before transformation, cells were collected by filtering through a 50 μm nylon mesh, and spread as a thin layer onto 35 mm petri dishes with solid MS-BY2 medium (**Appendix A Table A1-2**). For preparation of DNA-coated gold particles, 2-3 μg of purified DNA cassette was added to 50 μL aliquots of a 60 mg/mL gold suspension (0.6 μm Gold Microcarriers, Bio-Rad Laboratories, Inc.) together with 0.1 M spermidine and 2.5 M $CaCl_2$. It is important that all the components are mixed together simultaneously, thus maximum of 10 μL of DNA was added to the wall of the 1.5 mL Eppendorf tube containing gold suspension while spermidine and $CaCl_2$ were pipetted each to the one side of Eppendorf tubes cap. In order to mix all the ingredients at the same time, the tube was tapped on the bench with the cap facing down and vigorously vortexed for 1 min. The DNA-coated gold suspension was further precipitated by centrifugation, washed in 250 μL of 96% ethanol and finally resuspended in 150 μL of 96% ethanol. Cells were bombarded with 7.5 μL aliquots of DNA-coated gold particles spread on macrocarrier disks, using the particle delivery system PDS1000/He (Bio-Rad Laboratories, Inc.), 1 100-psi rupture disks, a partial vacuum of 27 inch Hg and a 6 cm target distance according to manufacturer's instructions. The same cells were bombarded twice with the petri dish reposition. After transformation, plates were incubated 1 h in the dark at 26 °C and then the cells were rinsed from the plates into 35 mm petri dishes using liquid BY2-MS medium (**Appendix A Table A1-2**) and placed in the dark with shaking (110 rpm, 24 °C). Cells (100 μL) were observed under the inverted fluorescence microscope in the period of 8-42 h after the transformation.

To stabilize proteins and prevent their degradation on the proteasome 26S, the proteasome inhibitor MG132 was used. MG132 (Sigma-Aldrich, Merck KGaA) stock solution (10 mM) was dissolved in DMSO and BY-2 cells were treated with 50 μM MG132 12 h after bombardment. Cells were further incubated at 24 °C with shaking at 110 rpm in the dark until microscopy. Control cells were treated with 0.05% of pure DMSO. The percentage of fluorescent cells observed at certain time point (14-16 h or 18-20 h after transformation) and treatment (MG132 or control) was expressed in relation to the total number of observed fluorescent cells per construct (with and without MG132 treatment, 14-16 and 18-20 h after transformation).

3.2.6.5. Agroinfiltration of *Nicotiana benthamiana* epidermal cells

Binary plasmid constructs carrying *EGFP-BPM1* or its deletion variants, *BPM1-EGFP*, *mRFP1-BPM1*, *EGFP-DMS3* or *EGFP-RDM1*, were electroporated into *A. tumefaciens* for colocalization and FRET-FLIM analysis. For BiFC analysis of BPM1 homodimer formation, vectors pSPYCE or pSPYNE encoding for BPM1 or its deletion variants fusion proteins were electroporated into *A. tumefaciens.* Additionally, to improve transgene expression in plants, *A. tumefaciens* carrying pCB301-p19 plasmid (Win & Kamoun, 2004) was used. Agrobacteria were infiltrated into the *N. benthamiana* leaves according to a modified protocol by Schütze et al. (2009). Briefly, individual *A. tumefaciens* colony cultures were grown overnight in 5 mL of liquid LB medium supplemented with 50 ng/mL rifampicin, 50 ng/mL gentamicin and 100 ng/mL spectinomycin. After the presence of the transgene was verified by colony PCR (section 3.2.3.3), cells were pelleted by centrifugation at 5 000 × g for 20 min, washed in agroinfiltration buffer (10 mM MES, pH 5.7, 10 mM $MgCl_2$), resuspended in agroinfiltration solution (10 mM MES, pH 5.7, 10 mM $MgCl_2$, 150 μM acetosyringone) and incubated for 4-5 h at room temperature. Optical density of each suspension was measured using 1:10 dilutions and agroinfiltration mixtures with desired combinations of clones were prepared by calculating required volumes of agrobacterial suspensions so that each desired *A. tumefaciens* clone in the mixture had an optical density of 0.5. To each agroinfiltration mixture, a 0.5 optical density of agrobacteria carrying pCB301-p19 was added. The total volume of each agroinfiltration mixture was 3 mL. Agrobacteria were delivered into the underside of leaves of 6-8 weeks old plants using a blunt tipped plastic syringe and applying gentle pressure. Two to three leaves per plant were infiltrated with the same mixture. After agroinfiltration, plants were watered and incubated at long-day conditions (16 h light/8 h dark, 120

to 130 μmol/m^2·s, 22 °C) with 50% relative humidity and inspected by fluorescence or confocal microscopy after 2-4 days.

3.2.6.6. Floral dip transformation of *Arabidopsis thaliana*

For promoter activity analysis, *Agrobacterium tumefaciens* cells GV3101 were electroporated with vector pCambia1301 containing expression cassette *pFWA*::*GUS* (for generation of the construct see section 3.2.5.2). For positive control, original pCambia1301 vector with *GUS* under CaMV 35S promoter control was used, while for negative control vector pCambia1301 without 35S promoter region (pCambia1301Δ35S) was used. Agrobacteria carrying pCambia1301 with *pFWA*::*GUS* expression cassette or pCambia1301 original vector or pCambia1301Δ35S were introduced to flowering *A. thaliana* WT plants with majority of immature floral buds and only few siliques present via floral dip method described by Clough & Bent (1998). Overnight cultures (5 mL) for individual agrobacteria transformants were verified by colony PCR (section 3.2.3.3). One milliliter of each verified overnight culture was transferred to 200 mL of fresh LB medium supplemented with appropriate antibiotics and agrobacteria were grown overnight at 28 °C. Large (200 mL) overnight cultures were again verified by colony PCR and agrobacteria were pelleted by centrifugation at 5 000 rpm for 15 min in centrifuge DuPont Sorvall RC-5B (Sorvall Instruments, Thermo Fisher Scientific). Agrobacteria pellet was resuspended in 200 mL of 5% sucrose and 0.03% Silwet L-77 (OSi Specialties, Inc., Danbury, CT, USA) solution. Silwet L-77 is surfactant that significantly increases transformation rates of floral dip (Clough & Bent, 1998). Plants were inverted in the suspension so that whole inflorescences were submerged in it and were left like that for 2-3 min. Afterwards, plants were removed from the solution, placed in freezer bags to maintain humidity and left in dark conditions overnight. The next day, plants were returned to growth chamber under standard light conditions. Plants were floral dipped twice with one week apart and were further grown till siliques turned brown and dry so seeds could be collected.

3.2.7. Tandem affinity purification combined with mass spectrometry

3.2.7.1. Purification of BPM1 and interacting proteins from *Arabidopsis thaliana*

One gram of 12-day old seedlings overexpressing BPM1-TAP or BPM1-EGFP was used for protein extraction and further purification of BPM1 recombinant protein and its interaction partners. A triple volume (w/v) of protein extraction buffer PEB50 (**Appendix D Table D1-1**)

additionally supplemented with 0.5 mM PMSF was added to the tissue powder (section 3.2.2) and mixture was incubated for 1 h at 4 °C with occasional vortexing. The soluble protein fraction was obtained by centrifugation at 20 000 × g for 15 min at 4 °C. The extract was passed through a 0.45 μm filter. Protein extract obtained from BPM1-TAP overexpressing plants was incubated for 2 h at 4 °C under gentle rotation on Tube Roller RS-TR10 (Phoenix Instrument) with 50 μL of IgG-Sepharose 6 Fast Flow beads (GE Healthcare) pre-equilibrated with 3 mL of extraction buffer. The IgG-Sepharose beads were transferred to a 1 mL Mobicol column (MoBiTec, Göttingen, Germany) and washed three times with 15 mL of IgG wash buffer (50 mM HEPES pH 7.9, 50 mM KCl, 2.5 mM $MgCl_2$, 1 mM EDTA, 0.1% (v/v) TritonX-100, 1 mM DTT).

Protein extracts obtained from BPM1-EGFP overexpressing plants were incubated for 3 h at 4 °C under gentle rotation on Tube Roller RS-TR10 (Phoenix Instrument) with 40 μL of GFP-Trap Agarose beads (Chromotec) pre-equilibrated with 3 mL of extraction buffer. GFP-Trap Agarose beads were washed three times with 15 mL of Wash buffer (50 mM HEPES, pH 7.9, 50 mM KCl, 2.5 mM $MgCl_2$, 1 mM EDTA).

Purified protein complexes bind to either IgG-Sepharose beads or GFP-Trap Agarose beads were denatured for 10 min at 80 °C in SLB.

3.2.7.2. In-gel trypsin digestion and peptide purification

Bound complexes purified from both oeBPM1-TAP and oeBPM1-EGFP transgenic lines were separated on 12% polyacrylamide gel by SDS-PAGE and proteins were visualized with CBB staining (section 3.2.4.3). Parts of gel with proteins were cut into small (1 mm^2) slices and further processed for liquid chromatography and tandem mass spectrometry. Gel particles were washed three times with 5 mM ammonium bicarbonate (ABC) and 50% acetonitrile (ACN), dehydrated with 100% ACN, reduced with 10 mM DTT in 20 mM ABC at 56 °C and alkylated with 55 mM iodoacetamide and 20 mM ABC in the dark. After two rinses with 5 mM ABC and 50% ACN, gel slices were dehydrated in 100% ACN and rehydrated in 50 μL of digest buffer containing 625 ng of trypsin (MS Gold; Promega, Madison, WI). After 10 min, 150 μL of 20 mM ABC was added and proteins were digested at 37 °C overnight. The overnight solution was collected in a separate tube and the resulting peptides were extracted from gel slices with 3 step serial washes: the first in 30% ACN and 3% trifluoroacetic acid (TFA), the second in 80% ACN and 0.5% TFA, and finally in 100% ACN. ACN was evaporated with vacuum centrifuge (SpeedVac). Peptides were

concentrated and purified with the StageTips (P200 pipette tip with Empore^{TM} Octadecyl C18 disk cores), as described by Rappsilber et al. (2007). Briefly, StageTips were wetted by methanol and equilibrated in sample buffer (2% ACN, 0.1% TFA). Peptides were loaded onto equilibrated tips and acidified by 0.5% TFA. Peptides were then eluted from tips with 2 × 50 µL 80% ACN and 0.1% TFA, dried in SpeedVac at 37 °C for 1 h and reconstituted in 30 µL of ultrapure water. For liquid chromatography and tandem mass spectrometry analysis, 5 µL of each sample was used for further analysis as described in Jagić et al. (2022) and in **Appendix E**.

3.2.8. *In vivo* protein colocalization evaluation

To analyze whether two fluorescently labeled proteins colocalize in *N. benthamiana* epidermal cells infiltrated with agrobacteria carrying plasmids with GFP-tagged BPM1 variants and RFP-tagged DMS3 or RDM1 (section 3.2.6.5), confocal images obtained by Leica Microsystems TCS SP8 X FLIM scanning module (section 3.2.11) were processed in open-source software Fiji v1.53q (Fiji Is Just ImageJ, https://imagej.net/software/fiji/) using implemented plugin Coloc2 (https://imagej.net/plugins/coloc-2). It is treated as a colocalization between two fluorescent signals if a significant, non-random spatial correlation exists. There are two components of colocalization: spatial overlap between two signals and co-distribution of signals in proportion to one another (Di Tomaso et al., 2022). Both aspects are considered in the Coloc2 analysis. First, the region of interest (ROI) was selected with one of the ImageJ selection tools (oval for nucleus and freehand for whole cell), in one of the images. Next, Coloc2 plugin was lunched and images to analyze were selected with an indication of in which the ROI is selected. Standardized algorithms were selected, Costes treshold regression was used and the number of iterations to run the Costes statistical significance test was set to 100. Costes randomization test evaluates the probability that the value of a coefficient measured between two color channels is significantly greater than random values (Costes et al., 2004). Only coefficients with Costes *P*-values greater than 95% were taken into account. Results were expressed as Pearson's correlation coefficient (r) where r = 1 means perfect colocalization, and r = 0 means no localization. For each pair of co-expressed fluorescently tagged proteins, measurements were performed on at least 12 cells that proved to meet the Costes significance criteria.

3.2.9. Direct protein interaction analysis

3.2.9.1. Yeast two-hybrid assays

For histidine prototrophy assay, seven individual colonies of each co-transformant, obtained as described in section 3.2.6.3, were separately diluted in 250 µL of autoclaved distilled water, and ten microliters of each diluted yeast co-transformant was spotted on SD/-His/-Leu/-Trp + 3-AT to inhibit low levels of leaky *HIS3* expression (**Appendix A Table A2-2**) and incubated for two days at 30 °C. The two used vectors encode two subunits of a GAL4 transcription factor, bait pGBT9 encoding DNA binding domain and prey pGAD424 encoding activation domain, that were fused to proteins of interest. In case of protein-protein interaction, the subunits are brought in close proximity and can perform their role of an active transcription factor promoting transcription of a reporter gene essential for histidine synthesis (*HIS3*), thus rendering the co-transformants prototrophic for growth on medium lacking histidine.

To confirm interactions indicated by histidine prototrophy assay, a β-galactosidase activity assays were conducted. For those assays, another 10 µL of diluted transformants were spotted on two "master" plates and incubated for two days at 30 °C. Similar as in case of histidine prototrophy, if two fusion proteins interact and subunits of GAL4 are brought together to perform the role of an active transcription factor, the integrated *E. coli lacZ* gene leads to β-galactosidase synthesis whose activity can be visualized with the addition of specific β-galactosidase substrates.

For qualitative β-galactosidase filter assay, X-gal was used as a substrate for β-galactosidase resulting in yeast colonies turning blue when there is an interaction present. X-gal stock solution was prepared in DMF at a concentration of 20 mg/mL. A strong interaction yielded detectable blue color in less than 30 min while longer incubations of up to 5 h were required for weaker interactions. Quantitative liquid culture assay was performed using 4 mg/mL stock solution of ONPG as substrate for β-galactosidase. This assay allowed enzyme activity quantification in two-hybrid interactions depending on the intensity of yellow color developed. One unit of β-galactosidase is defined as the amount which hydrolyzes 1 µmol of substrate ONPG to o-nitrophenol and D-galactose per min per cell (Miller, 1972, 1992). Obtained interaction intensities were normalized for negative control values of corresponding BPM1 version, and interaction intensities of truncated versions were further represented as percentage of the full length BPM1 interaction intensity with either DMS3 or RDM1. Both β-galactosidase assays were performed according to Yeast Protocols Handbook (Clontech Laboratories, Inc. Takara Bio).

Strong interaction between DMS3 and RDM1 (Sasaki et al., 2014) served as positive control in all performed Y2H assays. Empty bait vector in co-transformation with fusion proteins on prey vector served as negative controls.

3.2.9.2. Pull-down

To further investigate whether BPM1 and its deletion variants interact with DMS3 and RDM1 the pull-down assay was performed. In a pull-down, the protein of interest (bait) is tagged and bound to the immobilized affinity ligand specific for the tag. Immobilized bait protein is further mixed with another tested protein (prey) to examine whether there is interaction between bait and prey. If prey protein interacts with the bait, it will stay bound to the complex during repeated ligand washing, while unbound protein will be washed away. GST-tagged BPM1 variants (60 µL of GST-BPM1, 30 µL of GST-BTB-BACK$_{BPM1}$ or 70 µL of GST-MATH-BACK$_{BPM1}$) bound to glutathione Sepharose beads were here used as bait, and His-tagged DMS3 (25 µL) or RDM1 (2 µL) as prey (purification of GST and His-tagged proteins is described in section 3.2.4.2). GST alone (20 µL) bound to glutathione Sepharose beads was used as bait in a negative control to check the specificity of the prey constructs. Pull-down reactions were carried out in total volume of 200 µL in PBS, incubated for 6 h with constant rotation on Dynal sample mixer at 4 °C. After incubation, beads with bound proteins were precipitated by centrifugation (500 × g, 4 °C, 2 min) and the unbound fraction designated as flowthrough (FT) was collected. Beads were further washed five times with 0.5-1 mL PBS while under the same centrifuge conditions. After the last wash, remaining buffer was removed with an insulin syringe (30 G). SLB buffer was added to the beads (30 µL) and to 20 µL of FT (5 µL), and samples were denatured for 5 min at 95 °C. Proteins were resolved by SDS-PAGE (section 3.2.4.3) and detected by Western blot analysis (section 3.2.4.4).

3.2.9.3. Microscale thermophoresis

For microscale thermophoresis (MST) experiments, purified His-tagged DMS3 and RDM1 (section 3.2.4.2) were used as target. GST-tagged BPM1, BTB-BACK$_{BPM1}$ and MATH-BACK$_{BPM1}$ (section 3.2.4.2) were eluted from Sepharose beads using 10 mM reduced glutathione (Sigma-Aldrich, Merck KGaA) in 50 mM Tris-HCl pH 8.0. Buffer-exchange to PBS was performed with Amicon® Ultra-4 Centrifugal Filter Units (MilliporeSigma, Merck KGaA) according to manufacturer instructions. Protein aliquots with 5% glycerol were frozen in liquid

nitrogen and stored at -80 °C until use. Protein concentrations were spectrophotometrically measured on ND-1000 Spectrophotometer immediately prior to MST experiments. Extinction coefficient and molar mass parameters were set to 22.39 and 49.08 kDa for DMS3-His, 29.45 and 22.38 kDa for RDM1-His, 84.08 and 71.02 kDa for BPM1, 58.05 and 55.9 kDa for BTB-BACK$_{BPM1}$, and 76.96 and 61.56 kDa for MATH-BACK$_{BPM1}$.

DMS3-His and RDM1-His were diluted to 200 nM in PBS-T (PBS with 0.05% Tween) and mixed with RED-NHS 2nd Generation dye (NanoTemper Technologies) in a 1:1 ratio to obtain 100 nM fluorescently labelled target protein, respectively. To confirm interaction of DMS3 or RDM1 (target) and BPM1 (ligand), a Binding Check was performed according to User Manual Monolith® NT.115 (NanoTemper Technologies). The working concentration of BPM1 was 1.13 μM. Measured fluorescence values were displayed as normalized fluorescence (F_{norm}), calculated as F1/F0 where F0 corresponds to the normalized fluorescence prior to MST activation and F1 corresponds to the normalized fluorescence after MST activation. Changes in the MST signal occur upon binding of a ligand to the target molecule and are quantified based on the altered MST signal of the target-ligand complex. To asses binding affinity between DMS3 or RDM1 (target) and BTB-BACK$_{BPM1}$ or MATH-BACK$_{BPM1}$ (ligand), a Binding Affinity assay was performed. For the DMS3-based assay, a fixed concentration of fluorescently labelled DMS3 (50 nM) was mixed with serial dilutions of ligand protein, with highest concentration set to 805 nM for BTB-BACK$_{BPM1}$ and 1.63 μM for MATH-BACK$_{BPM1}$. For the RDM1-based assay, a fixed concentration of fluorescently labelled RDM1 (50 nM) was mixed with serial dilutions of ligand protein, with highest concentration set to 2.95 μM for BTB-BACK$_{BPM1}$ and 1.14 μM for MATH-BACK$_{BPM1}$. Protein mixtures were loaded into Monolith™ NT.115 Standard Treated Capillaries and MST measurements were performed with 40% excitation power and 60% MST power on a Monolith NT.115 Instrument (NanoTemper Technologies). The change in MST signal through serial increase of ligand concentration, expressed as ΔF_{norm} was used to calculate changes in the fraction of bound target molecule to derive binding affinities. Three independent MST experiments were performed for each Binding Affinity assay. Raw MST data was fitted using PALMIST (Scheuermann et al., 2016) software version 1.5.8 following instructions by Tso & Brautigam (2016). Fast increase in temperature right after the IR laser was turned on, the T-Jump (temperature jump) was analyzed to obtain the dissociation constant, K_d values. To detect changes in T-Jump,

ligand molecule must bind fluorescently labeled target in a way that affects the physical properties of fluorophore attached to the target, and this analytical mode has shown the best matching of derived K_d values to K_d values obtained from other biophysical techniques (Scheuermann et al., 2016). K_d values are expressed as mean K_d of three experiments with 68.3% confidence intervals obtained by "error-surface projection" (ESP) implemented in the PALMIST software, that proved to be more accurate than the results of other fitting programs (Scheuermann et al., 2016; Tso & Brautigam, 2016).

3.2.9.4. Förster's resonance energy transfer - fluorescence lifetime imaging microscopy

To study *in vivo* bi-molecular protein interactions in plant cells a FRET-FLIM technique was implemented and for this purpose confocal laser scanning module TCS SP8 X FLIM (section 3.2.11) was used. Fluorescence light was detected using spectral FLIM photomultipliers. Exposure time of the individual FLIM measurement was set to approximately 1 min and the laser intensity was adjusted to attain peak photon count rate between 200 and 500 kilocounts per s. The donor fluorophore EGFP was excited at 488 nm using a pulsed white light laser with the pulse frequency set to 40 MHz. Analysis of the recorded fluorescence lifetime traces was performed using SymPhoTime64 software (PicoQuant).

To obtain the fluorescence lifetime of the donor-only sample, *N. benthamiana* epidermal cells were infiltrated with agrobacteria carrying the plasmid with donor FRET molecule (EGFP protein fused with BPM1 or RDM1 protein). Donor fluorescence lifetime, τ_0, was then estimated by fitting a mono-exponential model of fluorescence decay, $N(t) = Ae^{-t/\tau_0}$ to experimental TCSPC curves. This value of τ_0 was used as a fixed parameter in the following analysis of FRET samples. FRET is described as energy transfer through nonradiative dipole-dipole coupling between a donor and an acceptor molecule in close proximity (<10 nm) (Förster, 1948). To obtain FRET data, *N. benthamiana* epidermal cells were infiltrated with agrobacteria carrying plasmid encoding donor EGFP fused to the protein of interest and agrobacteria carrying plasmid encoding acceptor mRFP1 fused to the potential interaction partner. Donor EGFP or acceptor mRFP1 were fused to the N-terminus of the three inspected proteins (BPM1, DMS3 and RDM1). EGFP was also fused to the C-terminus of the BPM1. Therefore, three different combinations of fusion proteins for BPM1 interaction with DMS3 (EGFP-BPM1/mRFP1-DMS3, EGFP-DMS3/mRFP1-BPM1 and BPM1-EGFP/mRFP1-DMS3) and three different combinations of fusion proteins for BPM1 interaction

with RDM1 (EGFP-BPM1/mRFP1-RDM1, EGFP-RDM1/mRFP1-BPM1 and BPM1-EGFP/mRFP1-RDM1) were used for estimating *F*. Different relative position of fluorophores with respect to the labeled proteins (N or C-terminally fused) were used to test which orientation results in a maximal overall FRET effect (Radić et al., 2020). Agrobacteria carrying plasmid encoding EGFP or mRFP1 alone or in pairs were infiltrated to *N. benthamiana* epidermal cells to obtain negative controls.

For analyzing the donor fluorescence lifetime in the presence of acceptor, a double-exponential model of fluorescence decay was used, $N(t) = A_1 e^{-t/\tau_0} + A_2 e^{-t/\tau_q}$, where amplitudes A_1 and A_2 and quenched lifetime τ_q were free parameters of the fit. From the obtained amplitudes, the fraction of donor molecules that undergo FRET was calculated as $F = A_2/(A_1 + A_2)$. For each pair of fusion proteins, measurements were performed on at least 10 cells (cell nuclei to be more precise) in two independent experiments. *F* was determined for each cell and then averaged (median $[Q_1, Q_3]$).

Furthermore, EGFP fused to the N-termini of BPM1 deletion variants was tested for interaction with acceptor mRFP1 fused to the N-terminus of DMS3 or RDM1, thus adding six more different combinations (EGFP-BTB-BACK$_{BPM1}$/mRFP1-DMS3, EGFP-MATH-BACK$_{BPM1}$/mRFP1-DMS3, EGFP-MATH-BTB$_{BPM1}$/mRFP1-DMS3, EGFP-BTB-BACK$_{BPM1}$/mRFP1-RDM1, EGFP-MATH-BACK$_{BPM1}$/mRFP1-RDM1 and EGFP-MATH-BTB$_{BPM1}$/mRFP1-RDM1) for estimating *F*. Donor fluorescence lifetime in the presence of acceptor was analyzed as described above. Only one experiment using BPM1 deletion variants was performed.

3.2.10. Promoter activity analysis

3.2.10.1. *Arabidopsis thaliana* single-copy insertion screening and crossing

The number of T-DNA insertions in pFWA::GUS lines (section 3.2.6.6) was determined indirectly by monitoring the ratio of hygromycin-resistant and hygromycin-sensitive plants obtained by self-fertilization of T1 generation. For further analysis, two T1 lines that showed a monohybrid inheritance ratio (3: 1) of the selective marker were selected.

To determine the effect of BPM1 and DMS3 on RdDM-controlled *FWA* gene promoter activity, oeBPM1-EGFP, amiR-bpm, oeEGFP-DMS3 and *dms3-1* lines were crossed with both selected T1 pFWA::GUS lines. As a control of promoter activity pFWA::GUS lines were crossed with WT

plants. Considering that the transgenic traits of oeBPM1-EGFP, oeEGFP-DMS3 and amiR-bpm lines are dominant, as well as are pFWA::GUS reporter lines, it was possible to compare GUS expression already in F1 generation (reporter genes were hemizygous, containing only one transgene allele) so the corresponding control lines (pFWA::GUS × WT) were also hemizygous for *pFWA::GUS* reporter. Contrary, *dms3-1* is a recessive line, so homozygous plants (for both, *dms3-1* mutant locus and *pFWA::GUS* locus) were generated and compared to the pFWA::GUS homozygous control lines.

3.2.10.2. GUS assay and relative quantification of promoter activity

Promoter activity, or in other words the GUS expression, in pFWA::GUS crossed lines was analyzed by histochemical staining using X-Gluc as a substrate for β-glucuronidase in different tissues, and the tissues with the best expression were selected to compare the expression pattern between different lines. GUS assay was performed in 24-well cell culture plates (one well per each plant sample). X-Gluc was prepared at a final concentration of 0.5 mM in GUS reaction buffer (50 nM Potassium ferricyanide, 50 nM Potassium ferrocyanide, 100 mM Sodium Phosphate Buffer pH 7, 10 mM Sodium EDTA and 0.1% Triton X) and the solution was vacuum infiltrated into the tissue for 5 min at 27 inch Hg to facilitate entrance of the staining solution. Plates were sealed with parafilm and samples were incubated overnight at 37 ° C. The stained tissues were immersed and incubated through serial dilutions of alcohol solutions (starting with 15 min in 20% methanol, 0.25 M HCl, followed by 15 min in 60% ethanol, 7% NaOH and 5 min intervals in 40% ethanol, 20% ethanol and 10% ethanol) to remove chlorophyll which could hinder visualization of blue color. Tissues were finally fixed in a solution of 5% ethanol and 25% glycerol overnight and the promoter activity was analyzed under a binocular and a light microscope.

GUS activity in obtained images was further quantified in ImageJ v1.51. following ImageJ-Based Quantification of Histochemical GUS Staining (Béziat et al., 2017). First, images were converted to HSB (hue, saturation, and brightness) stack and the ‘saturation’ channel was used for quantifying changes in GUS activity between different reporter lines (pFWA::GUS × WT, pFWA::GUS × oeBPM1-EGFP, pFWA::GUS × amiR-bpm, pFWA::GUS × oeEGFP-DMS3, pFWA::GUS homozygotes, pFWA::GUS × *dms3-1*). ‘Saturation’ reflects the intensity of GUS staining in the image, and the signal intensity was expressed as the mean gray value measured in leaves. Five plants per line, represented by 15-20 images taken in different leaf parts (tip of the

leaf, main leaf vein, leaf serrations) were analyzed, and the mean gray values of crossed lines were calibrated to their control lines which were taken as 1. Hemizygous lines pFWA::GUS × oeBPM1-EGFP, pFWA::GUS × amiR-bpm and pFWA::GUS × oeEGFP-DMS3 were calibrated to hemizygous control pFWA::GUS × WT, while homozygous pFWA::GUS × *dms3-1* was calibrated to the mean value of pFWA::GUS homozygous line.

3.2.11. Microscopy

Bright field and fluorescent specimens were observed under Zeiss Axiovert 200M coupled with Zeiss AxioCam MRc digital camera. Filter set 13 (470/20 nm excitation, LP 505-530 nm emission) was used for EGFP fluorescence. Filter set 14 (510-560 nm excitation, 590 nm emission) was used for detection of mRFP1 fluorescence. Filter set 13 was also used for detection of YFP fluorescence in BiFC assay. Images were processed in a public domain Java image processing software ImageJ v1.51.

Confocal laser scanning microscopy (CLSM) and fluorescence lifetime imaging microscopy (FLIM) was performed using the confocal laser scanning module TCS SP8 X FLIM (Leica Microsystems, Wetzlar, Germany), equipped with the time-correlated single photon counting (TCSPC) unit (PicoQuant). For detection of EGFP, specimens were excited using an Argon 488 nm laser, and the wavelength of 500-550 nm was used for detection. For mRFP1 a White Light Laser (555 nm) was used for excitation in combination with wavelength of 580-620 nm for detection. To capture and process confocal images the Leica Application Suite X (LAS X) was used.

Results of histochemical staining for GUS enzyme activity assay (analysis of promoter activity) were analyzed with light microscopy under microscope Olympus BX51 coupled with Olympus DP70 camera and under Zeiss Stemi 2000-C Stereo Microscope coupled with Zeiss AxioCam ERc 5s.

3.2.12. Statistical analysis

Experiments were repeated at least twice on independent samples unless stated otherwise. Variance between control (24 °C without CHX) and treated (37 °C, CHX) samples in expression levels of *BPM1-EGFP* gene and in protein levels of BPM1-EGFP protein in CHX assay combined with elevated temperature treatment were analyzed by one-way ANOVA and post-hoc Duncan multiple range test was performed using Statistica™ software (TIBCO software Inc.). The effects

of elevated temperature treatment on *BPM1* gene expression in WT, oeBPM1-EGFP and oeBPM1-TAP lines were analyzed by two-tailed Student's t-test between control (24 °C) and treated (37 °C) samples after the variance between samples were determined as equal with F-test. The same was done for DMS3 protein levels between WT and oeBPM1-EGFP line, between BPM1/DMS3 and BPM1/RDM1 interaction intensities in Y2H experiment and between GUS activity of pFWA::GUS homozygotes and pFWA::GUS × *dms3-1*. Y2H interaction intensities between BPM1 deletion mutants and DMS3 or RDM1, and GUS activity between hemizygous pFWA::GUS crossed lines were first tested for normal distribution by Shapiro–Wilk test and equality of variances by Levene's test. Data were further analyzed by one-way ANOVA and post-hoc Duncan's new multiple range test where distribution was normal and variances were equal, and Kruskal-Wallis test and post-hoc Dunn's test where data significantly deviated from normal distribution and/or variances were unequal. For colocalization analysis, Costes statistical significance test and Pearson's correlation were performed as described in section 3.2.8. Comparison between Pearson's correlation coefficients (r) at the level of whole cell and specifically at the level of nucleus was done by two-tailed Student's t-test after variances were tested with F-test. Pearson's correlation coefficients between BPM1 deletion mutants and DMS3 or RDM1 were analyzed by one-way ANOVA followed by Tukey's HSD (honestly significant difference)/Kramer test if distribution was normal and variances were equal, and Kruskal-Wallis test after it was determined that the distribution is normal and variances are equal (by Shapiro-Wilk test and Levene's test). All mentioned tests were performed in Microsoft Excel 2019 using Real Statistics Resource Pack (https://www.real-statistics.com/free-download/real-statistics-resource-pack/). Statistical analysis of FRET-FLIM results was performed using the Kruskal–Wallis test implemented in MATLAB software (MathWorks), with the post-hoc Tukey–Kramer test applied for pairwise comparisons. In all analyzes, differences with a p value less than 0.05 or 0.01 were regarded as significant.

4. RESULTS

4.1. Subcellular localization and stability of BPM1

To investigate the subcellular localization and stability of BPM1 and to determine whether it is affected by a specific protein domain (MATH, BTB, or BACK), plasmids carrying CDS for green fluorescent protein (EGFP) were fused to the N-terminus of different BPM1 variants: complete BPM1 and BPM1 lacking MATH (BTB-BACK$_{BPM1}$), BTB (MATH-BACK$_{BPM1}$), or BACK (MATH -BTB$_{BPM1}$) domain were generated and transiently transformed into tobacco BY-2 cells. Expression of all fusion proteins was under the control of a strong constitutive CaMV 35S promoter. Subcellular localization of BPM1 protein variants was observed as early as 8 h after biolistic transformation. A small number of cells expressing recombinant EGFP-BPM1 protein was found 12 h after transformation (5-10 fluorescent cells per 100 μL of cell suspension) in contrast to more than 70 cells per 100 μL of cell suspension of cells expressing EGFP protein alone (data not shown). Addition of the proteasome inhibitor MG132 increased the proportion of fluorescent cells (**Table 7**), indicating susceptibility of the protein to proteasomal degradation. As shown in **Table 7**, at 14-16 hours after transformation, a higher proportion of cells with visible EGFP-BPM1 fluorescence was observed in the MG132-treated cell suspension (38%) compared with the untreated control (30%). The differences between MG132 treatment and control were even greater 18-20 h after transformation, with only 11% fluorescent cells in control and 21% in MG132 treatment, although fewer cells were generally observed at this time point. The fraction of EGFP-MATH-BTB$_{BPM1}$ fluorescent cells was doubled in the MG132-treated suspension 14-16 h after transformation (46% versus 23% in control) and remained so 18-20 h after transformation (20% versus 11%), but as with the intact EGFP-BPM1 protein, fewer cells were observed at this time point than 14-16 h after transformation. The fraction of EGFP-BTB-BACK$_{BPM1}$ fluorescent cells increased from 23% fluorescent cells in control to 34% in MG132 treatment 14-16 h after transformation, but was slightly lower in MG132 treatment 18-20 h after transformation (20% vs. 23% in control). Interestingly, the percentage of EGFP-MATH-BACK$_{BPM1}$ fluorescent cells 14-16 h after transformation was slightly lower in MG132 treatment (21%) than in control (24%) and maintained a similar pattern 18-20 h after transformation (26% treated versus 29% control), but in a few more cells. Overall, most fluorescent cells of intact BPM1 and variants containing the BTB

domain (BTB-BACK$_{BPM1}$ and MATH-BTB$_{BPM1}$) were found 14-16 h after transformation in cells treated with MG132, suggesting that this time point is the best for further studies. Interestingly, no effect of MG132 was observed in the variant lacking the BTB domain (MATH-BACK$_{BPM1}$), indicating that the BTB domain of BPM1 likely mediates its proteasomal degradation. The BTB domain of BPM1 was also shown to be responsible for homodimerization of the protein (**Appendix F Chapter F2**) and associated functions.

Table 7 Percentage of fluorescent cells with EGFP fusion proteins 14-16 and 18-20 h after biolistic transformation of tobacco BY-2 cells treated with MG132 and untreated control cells. Cells were treated 12 h after transformation with 50 μM MG132. For details see **Appendix F Chapter F1 Table F1-1**.

EGFP fusion protein	**Time points of microscopy observations and type of treatment**			
	14-16 h		18-20 h	
	control	MG132	control	MG132
EGFP-BPM1	30%	38%	11%	21%
EGFP-MATH-BTB$_{BPM1}$	23%	46%	11%	20%
EGFP-BTB-BACK$_{BPM1}$	23%	34%	23%	20%
EGFP-MATH-BACK$_{BPM1}$	24%	21%	29%	26%

Intact BPM1 was localized in the nucleus and cytoplasm in 94% of the observed cells, while only 6% of cells had strictly nuclear localization (**Figure 7 A-C, M**). In 38% of cells, EGFP-BPM1 protein was also found in the nucleolus, and in 34% of these, it was found in combination with the nucleus and cytoplasm. Deletion of any of the BPM1's domains, MATH, BTB, or BACK resulted in decreased accumulation of truncated BPM1 protein in the cytoplasm and an increase in nuclear-only localization, resulting in as much as 79% of exclusively nuclear localization in EGFP-BTB-BACK$_{BPM1}$ (with only 7% nucleolar localization; **Figure 7 D-F, N**), 45% in EGFP-MATH-BACK$_{BPM1}$, of which 16% was nucleolar (**Figure 7 G-I, O**), and 48% in EGFP-MATH-BTB$_{BPM1}$, of which 46% was nucleolar (**Figure 7 J-L, P**). The overall nucleolar fraction was significantly increased to 71% in EGFP-MATH-BTB$_{BPM1}$ (**Figure 7 P**, light green), whereas it decreased to 7% and 18% in EGFP-BTB-BACK$_{BPM1}$ (**Figure 7 N**, light green) and EGFP-MATH-BACK$_{BPM1}$ (**Figure 7 O**, light green), respectively, implying that both MATH and the BTB domain are relevant for nucleolar localization. Interestingly, the MATH-containing variants (MATH-BTB$_{BPM1}$ and MATH-BACK$_{BPM1}$) more frequently exhibited nuclear/cytoplasmic localization (**Figure 7 O-P**),

indicating a preference of the MATH domain for cytoplasmic localization or towards cytoplasmic targets.

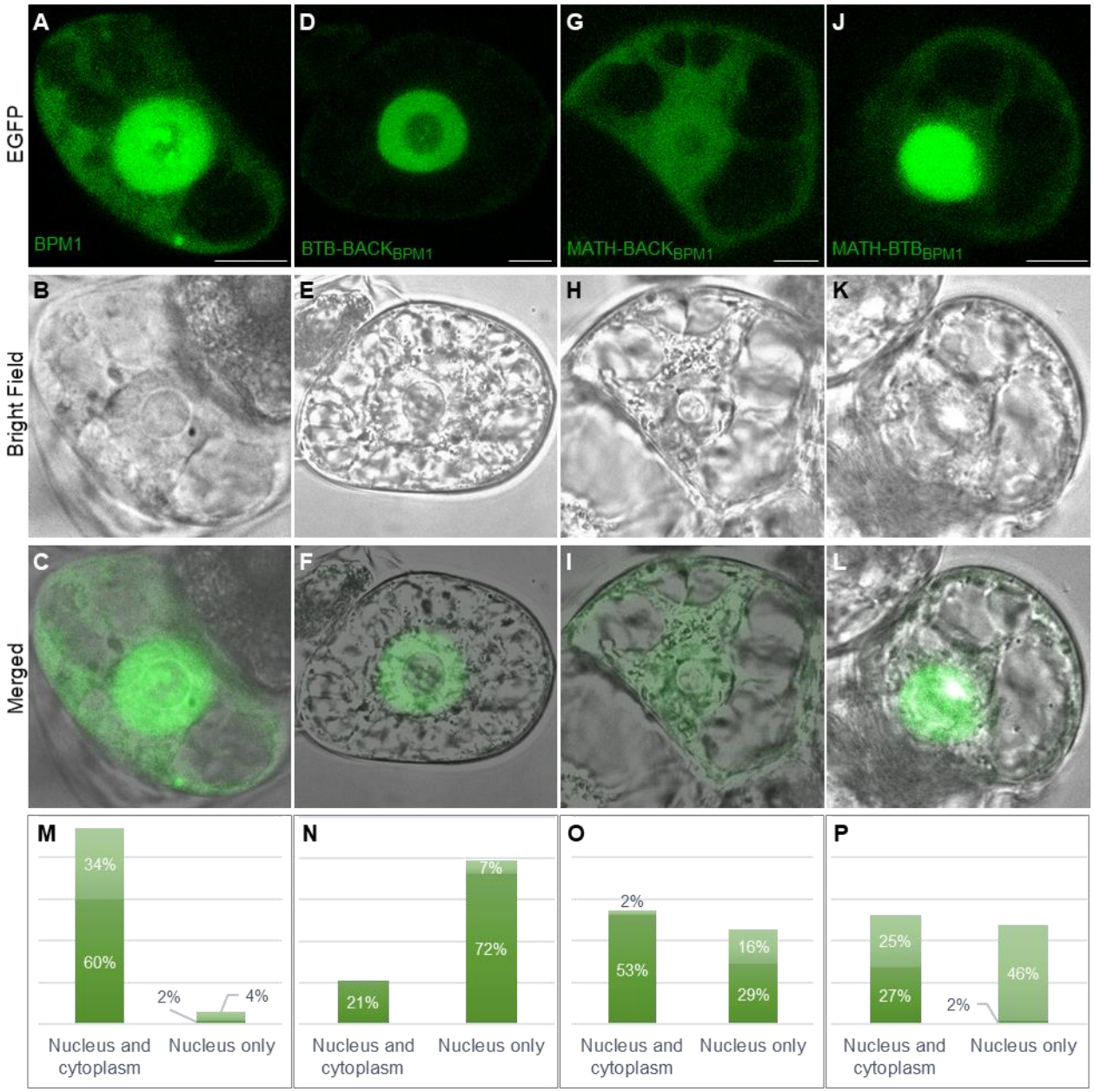

Figure 7 Protein domains alter subcellular localization of BPM1 in tobacco BY-2 cells. Intact BPM1 protein is dispersed in the cytoplasm, nucleus and nucleolus (**A-C**). BPM1 with MATH deletion delimitates localization to nucleus (**D-F**), while deletion of BTB favors cytoplasmic and nuclear localization (**G-I**). Deletion of BACK domain promotes nuclear and nucleolar localization (**J-L**). Percentage of localization of BPM1 (**M**) or MATH (**N**), BTB (**O**) or BACK (**P**) domain omitted variants in cytoplasm and nucleus or only in nucleus is shown on green bars, with indicated percentage of additional nucleolar localization (light green). For details see **Appendix F Chapter F1 Table F1-2**. Scale bar = 10 μm.

4.2. Stability of BPM1 in *Arabidopsis thaliana*

Because BPM1 protein is unstable and its stability is affected by environmental conditions (day/night and temperature, Škiljaica et al., 2020), it was necessary to determine the optimal conditions to obtain enough BPM1 protein for tandem affinity purification and mass spectrometry analysis. Immunoblotting with anti-GFP of whole protein extracts obtained from seedlings of the oeBPM1-EGFP transgenic line incubated at 37 °C for 1, 3, and 6 h under standard light conditions showed an increase in protein levels compared with control seedlings sampled at 24 °C (**Figure 8 A-B**). Significant increase was observed after a 3 h exposure at 37 °C, and there was no further increase in protein levels after a 6 h exposure (**Appendix F Chapter F3 Figure 3-1**).

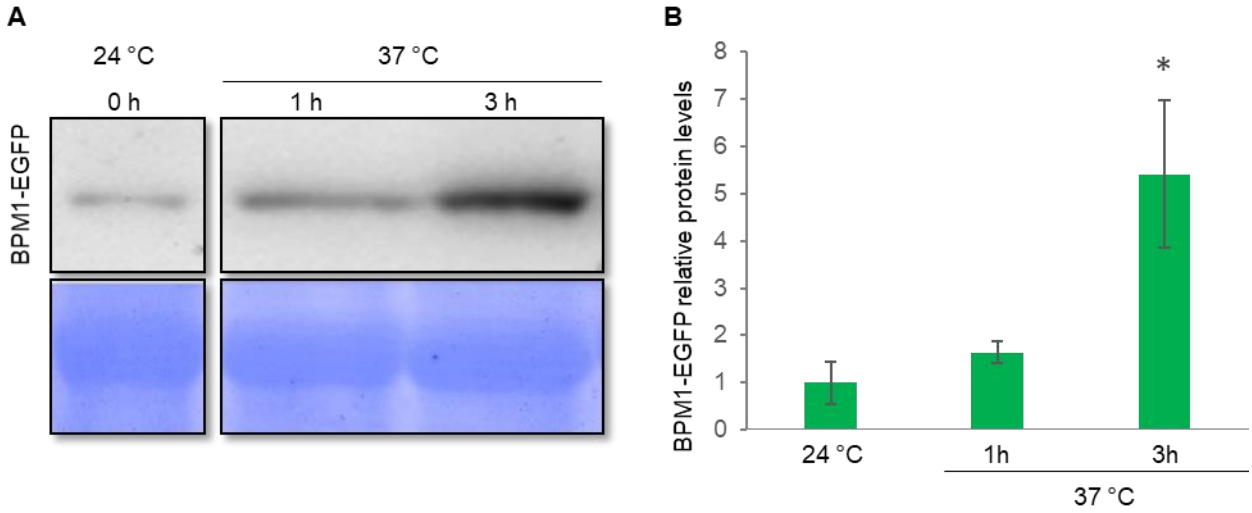

Figure 8 BPM1-EGFP accumulates after exposure to 37 °C. Seven-day-old seedlings of oeBPM1-EGFP line were sampled before treatment (0 h) and after 1 and 3 h incubation at 37 °C. **A)** Whole protein extracts were immunoblotted with anti-GFP monoclonal antibody (upper panel). For loading control, proteins were stained with CBB on PVDF membranes (lower panel). **B)** Relative BPM1-EGFP protein levels were quantified in ImageJ, normalized to CBB bands and calibrated to control conditions (24 °C, 0 h), which was taken as 1. Data is presented as means of three individual protein bands per treatment ± SD. Asterisk indicates statistically significant difference (Duncan's new multiple range test, $p < 0.05$) between three sampling conditions.

To clarify the background of heat-induced BPM1 accumulation, the effects of elevated temperature on transcription and translation and protein degradation were analyzed. Gene expression levels were analyzed by RT-qPCR and protein levels were determined by immunoblotting under different temperature conditions (24 °C and 37 °C) with or without protein synthesis inhibitor CHX. Temperature treatment (37 °C) slightly decreased *BPM1-EGFP* expression under conditions of normal translation (without CHX, **Figure 9 A**), although BPM1-EGFP protein levels were obviously higher at 37 °C compared with 24 °C (**Figure 9 B, D, E**).

When protein synthesis was inhibited with CHX, a significant increase in relative gene expression was observed at the control temperature (24 °C). As expected, no protein was detected under these conditions (**Figure 9 C**). In contrast, the relative gene expression of *BPM1-EGFP* remained unchanged after 3 h of exposure to 37 °C in CHX-treated seedlings, but BPM1-EGFP signal was detected (**Figure 9 C, F**). A similar expression pattern was observed in WT seedlings after 3 h treatment: *BPM1* gene expression was significantly increased after treatment with CHX at 24 °C, whereas there was no change in gene expression after CHX treatment at 37 °C (**Appendix F Chapter F3 Figure F3-2**). Since protein synthesis was inhibited, the accumulation of BPM1 must be due to its stabilization.

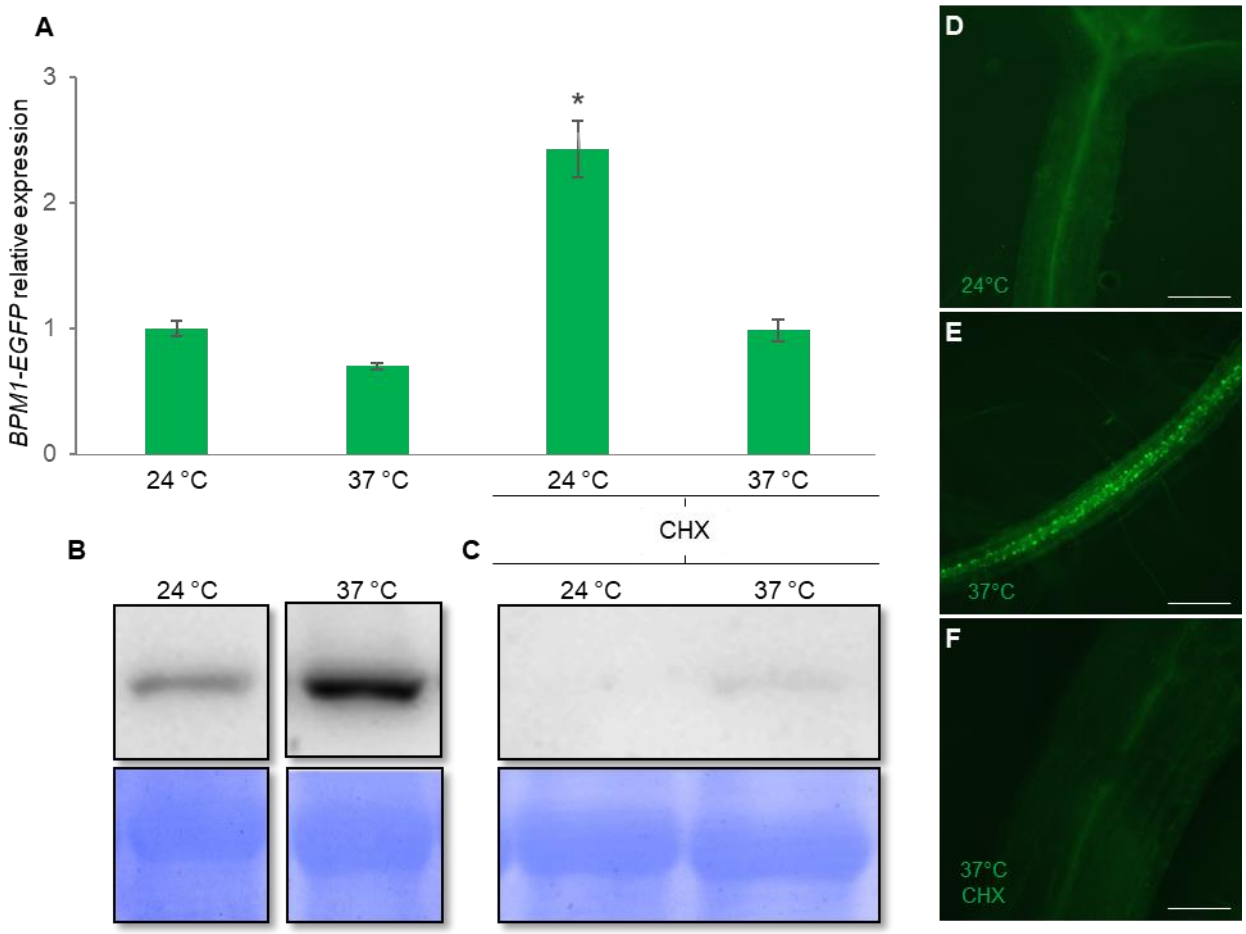

Figure 9 BPM1 protein is stabilized at 37 °C in conditions of inhibited protein synthesis. Seven-day-old seedlings of oeBPM1-EGFP line were sampled **A**) before any treatment at 24 °C, **B**) after 3 h incubation at 37°C, **C**) 3 h after treatment with protein synthesis inhibitor cycloheximide (CHX, 0.2 mg/mL) at 24 °C and 37 °C. Whole protein extracts were immunoblotted with anti-GFP monoclonal antibody (upper panel). For loading control, proteins were stained with CBB on PVDF membranes (lower panel).

Figure 9 – continued

D) *BPM1-EGFP* gene expression was analyzed at the same sampling conditions as **A**), **B**) and **C**) by quantitative RT-qPCR, normalized to *RHIP1* and calibrated to control conditions (24 °C before treatment) which was taken as 1. Expression values are shown as mean fold change of two biological replicates ± SD. Asterisk indicates statistically significant difference (Duncan's new multiple range test, $p < 0.05$) between means of different sampling conditions. Seven-day-old seedlings of oeBPM1-EGFP line were analyzed by fluorescent microscopy before (24 °C, **E**) and after 3 h incubation at 37 °C without (**F**) and with CHX (**G**) treatment. Scale bar = 100 μm.

Additionally, the stability of BPM1 protein was tested in the oeBPM1-TAP line at 37 °C. Similar to BPM1-EGFP, the accumulation of BPM1-TAP protein was pronounced in seedlings treated at 37 °C for 3 h, whereas in control samples continuously cultivated at 24 °C, the protein band was barely visible (**Figure 10**).

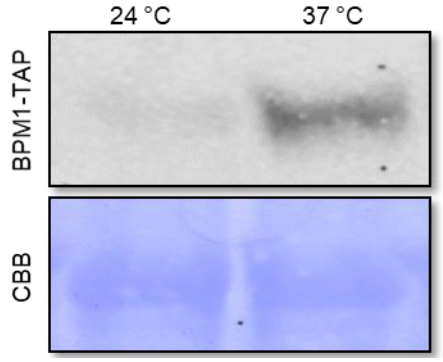

Figure 10 BPM1-TAP accumulates after exposure to 37 °C. Seven-day-old seedlings of oeBPM1-TAP line were sampled before treatment at 24 °C and after 3 h incubation at 37 °C. Whole protein extracts were immunoblotted with PAP Soluble Complex antibody (upper panel). For loading control, proteins were stained with CBB on PVDF membranes (lower panel).

Finally, the expression of the *BPM1* gene was analyzed and compared in WT and the two transgenic lines oeBPM1-EGFP and oeBPM1-TAP. After exposure to 37 °C, endogenous *BPM1* gene expression in WT was doubled (**Figure 11** blue bars) and gene expression of endogenous *BPM1* and transgenic *BPM1-TAP* together was 3.5 times higher than in untreated samples of oeBPM1-TAP plants (**Figure 11** gray bars). In the oeBPM1-EGFP line, a 30% decrease in *BPM1* gene expression (endogenous and transgenic *BPM1-EGFP* combined) was recorded after exposure to elevated temperature (**Figure 11** green bars). When comparing gene expression levels between the tested lines, *BPM1* gene expression was twice as high in the oeBPM1-TAP line compared with WT, and the differences increased slightly after exposure to elevated temperature (**Appendix F Chapter F3 Figure F3-3 A**), whilst oeBPM1-EGFP had 145-fold higher *BPM1* gene expression than WT (**Appendix F Chapter F3 Figure F3-3 B**). The difference between the promoters of the

two BPM1 overexpression lines is due to the different vectors used for plant transformation (**Appendix F Chapter F3 Figure F3-4**). Overexpression of *BPM1-TAP* is under the simple 35S promoter from pGWB529 plasmid (Nakagawa et al., 2007), thus phenotype of these plants resembles that of the WT. The overexpression of *BPM1-EGFP* is from pB7FWG2 plasmid in which translation is enhanced by the omega (Ω) sequence in the 5′ UTR (Fan et al., 2012). Overall, exposure to elevated temperature (3 h at 37 ° C) proved worthwhile to ensure stable levels of BPM1 protein in plants and was applied in further experiments. Because BPM1 gene expression and protein abundance levels differed significantly in the oeBPM1-EGFP and oeBPM1-TAP lines, both lines were selected for tandem affinity purification and mass spectrometry analysis. The first (oeBPM1-EGFP) to ensure sufficient levels of BPM1 protein for the experiment, as BPM1 has a rapid turnover and is very unstable protein (Škiljaica et al., 2020), and the second (oeBPM1-TAP) to exclude the possibility that identified potential interaction partners of BPM1 were found due to extreme overexpression by the transgenic promoter.

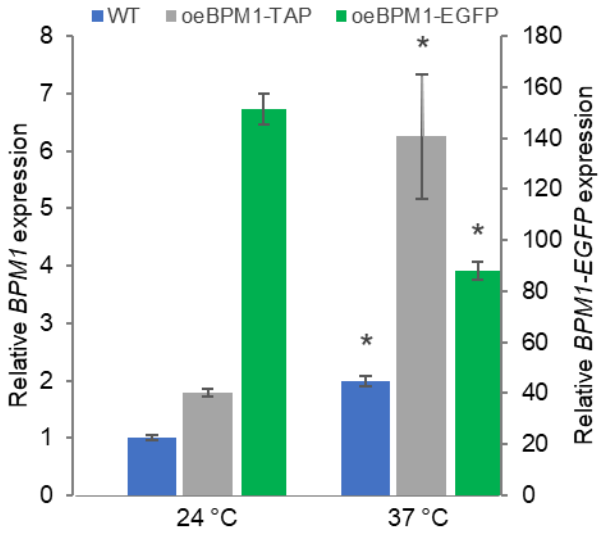

Figure 11 Expression of BPM1 is influenced by exposure to 37 °C. Seven-day-old seedlings of WT (blue), oeBPM1-TAP (gray) and oeBPM1-EGFP (green) were sampled before treatment (24 °C) and after incubation at 37 °C for 3 h. Endogenous and transgene BPM1 expression was analyzed by quantitative RT-qPCR, normalized to *RHIP1* and calibrated to WT at control conditions (24 °C), which was taken as 1. Expression values are shown as mean fold change of two biological replicates ± SD. Asterisks indicate statistically significant differences (Student's t test, $p < 0.05$) between means of control and treatment for each used plant line. Combined results of two independent experiments are presented in the chart, for separate results see **Appendix F Chapter F3 Figure F3-3**.

4.3. Identification of DMS3 and RDM1 as BPM1 interaction partners

Preliminary results on possible interaction partners of BPM1 were published in Bauer et al. (2019). In that work, mass spectrometry proteomic analysis focused on the wheat MATH-BTB protein TaMAB2 was performed. The line overexpressing a seryl-tRNA synthetase (SerRS; Kekez et al., 2016) and a line overexpressing BPM1 (oeBPM1-TAP), annotated there as protein X, were used as control lines to eliminate false-positive and nonspecific interactions of TaMAB2. The results of the analysis have been deposited to the ProteomeXchange Consortium (http://proteomecentral.proteomexchange.org) under the dataset identifier PXD014358. Intriguing discovery of the DMS3 protein as a potential BPM1-specific partner in the aforementioned work prompted further investigation into the BPM1 protein interactions and their possible role in other, thus far unrecognized cellular pathways of BPM proteins. Here, I established a protocol for tandem affinity purification of BPM1 from *Arabidopsis* seedlings that was followed by mass spectrometry in order to examine and identify BPM1 association with larger subcellular complexes. Two independent experiments were performed and obtained data sets were compared to the preliminary results on BPM1, and SerRS and TaMAB2 (Bauer et al., 2019). To stabilize BPM1, twelve-days old *Arabidopsis* seedlings overexpressing *BPM1-TAP* (line oeBPM1-TAP) or *BPM1-EGFP* (line oeBPM1-EGFP) were exposed to 37 °C. Proteins that were identified by at least two unique peptides in at least two independent experiments, and were not identified as SerRS or TaMAB2 partners (under the same criteria), were considered potential BPM1-specific partners. Only two proteins met all the criteria, with the highest score obtained for DMS3 (234.23), followed by another component of DDR complex – protein RDM1 (182.23, **Table 8**). Complete results of mass spectrometry proteomics and MaxQuant search results are deposited to the Mendeley Data cloud repository (https://data.mendeley.com/datasets/66ynzwm63d/draft?a=e0420775-072a-4cad-9890-d26d9e124105).

Table 8 List of unique BPM1 interactors identified after tandem affinity purification.

UniProt ID	Protein descriptions and functional categorization	No. of unique peptides	Score
Q8L765	BPM1	4	323.31
	DNA/chromatin modification		
Q94A79	DMS3	12	234.23
Q9LUJ3	RDM1	11	182.23

Protein extracts were generated from BPM1-overexpressing seedlings (two independent experiments). Proteins were considered as potential interaction partners of BPM1 if they were presented by at least two unique peptides in at least two independent experiments. Moreover, proteins were excluded if they were present in control experiment in which seryl-tRNA synthetase or TaMAB2 was used as a bait (proteins were considered as seryl-tRNA synthetase or TaMAB2 partners if they were presented by at least two peptides of which at least one was unique in any of the control experiments). UniProt protein identifiers are shown and total number of unique peptides and scores are represented with the best obtained values. See **Appendix F Chapter F4 Table F4-1** for details.

4.4. BPM1 colocalizes with DMS3 and RDM1

To gain insight into in the subcellular colocalization of BPM1 and its identified potential interaction partners DMS3 and RDM1, tobacco BY-2 cells were transiently co-transformed with *35S*::*EGFP-BPM1* and *35S::mRFP1-DMS3* or *35S::mRFP1-RDM1*. When expressed alone, EGFP-BPM1 accumulated predominantly in the nucleus in 94% of cells, whereas a weaker signal was detected in the cytoplasm (**Figure 7 A-C**, **M**). When co-expressed with DMS3 or RDM1, localization remained mainly unchanged (**Figure 12 A**, **E**). When co-expressed with DMS3, 92% of the signal was detected in the nucleus and cytoplasm, and when co-expressed with RDM1, 90% of the signal was detected in the nucleus and cytoplasm (**Appendix F Chapter F5 Table F5-1**). DMS3 and RDM1 were consistently localized in the nucleus and cytoplasm but not in the nucleolus (**Figure 12 B**, **F**). The strongest overlap of fluorescent signals from BPM1 with both DMS3 and RDM1 was in the nucleus, making it the most likely functional region of the three proteins (**Figure 12 C**, **G**). All mentioned cell compartments (nucleus, nucleolus and cytoplasm) are visible in the bright field images (**Figure 12 D, H**). The same localization pattern was observed for DMS3 and RDM1 when expressed alone in BY-2 cells (**Appendix F Chapter F5 Figure F5-1**).

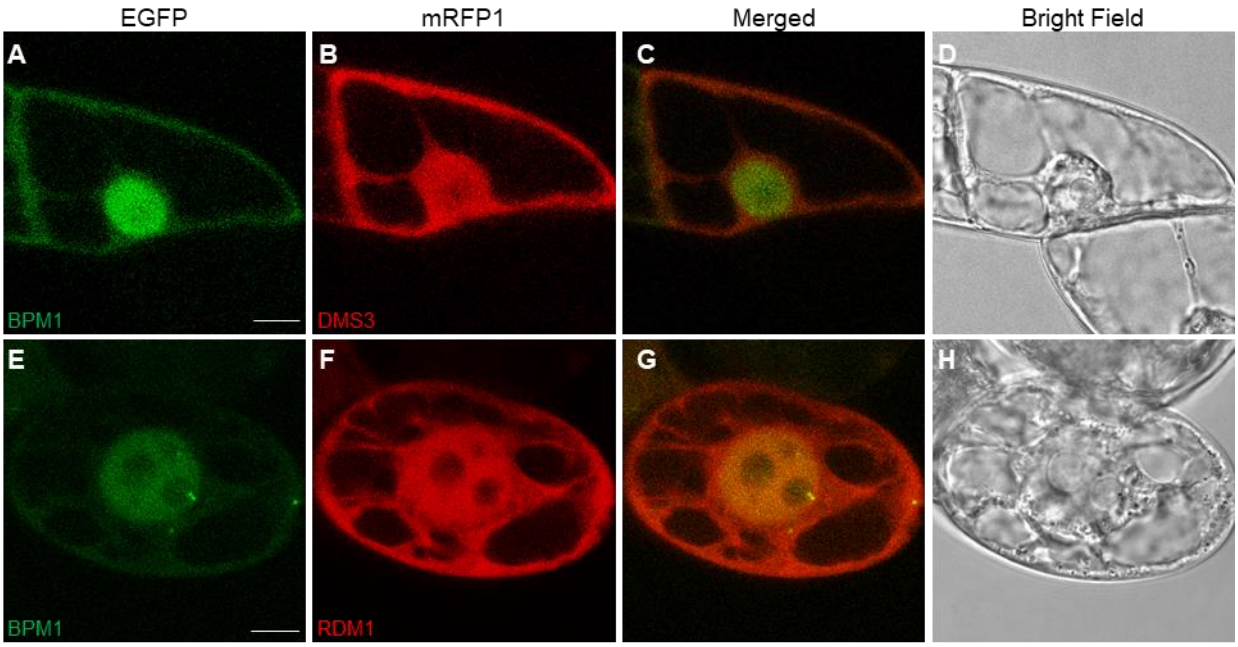

Figure 12 Subcellular colocalization of BPM1 and DMS3 or RDM1 in tobacco BY-2 cells co-expressing EGFP-BPM1 (green) and mRFP1-DMS3 (red) or mRFP1-RDM1 (red) protein. Overlap (yellow) in cytoplasm and nucleus is visible between BPM1 and DMS3 (**A-D**) and BPM1 and RDM1 (**E-H**) proteins. Scale bar = 10 μm.

Since a low percent of BY-2 cells were successfully co-transformed by Biolistic transformation, localization was also assessed in transiently transformed leaf epidermal cells of *Nicotiana benthamiana*. In cotransformation of EGFP-BPM1 with mRFP1-DMS3 or mRFP1-RDM1, fluorescent signal of BPM1 protein was detected almost exclusively in nucleus and often in agglomerates around nucleolus (**Figure 13 A**, **E**). Fluorescent signal of DMS3 (**Figure 13 B**) and RDM1 (**Figure 13 F**) was detected in the cytoplasm and nucleus as in BY-2 cells. Here, colocalization of the fluorescent signals from BPM1 and both, DMS3 or RDM1, was exclusively in the nucleus (**Figure 13 C**, **G**). The observed cells and the position of the nuclei are visible in the bright field images (**Figure 13 D, H**). The colocalization of BPM1 with DMS3 and RDM1 in the nuclei of *N. benthamiana* cells was additionally quantified and the FRET-FLIM analysis was performed.

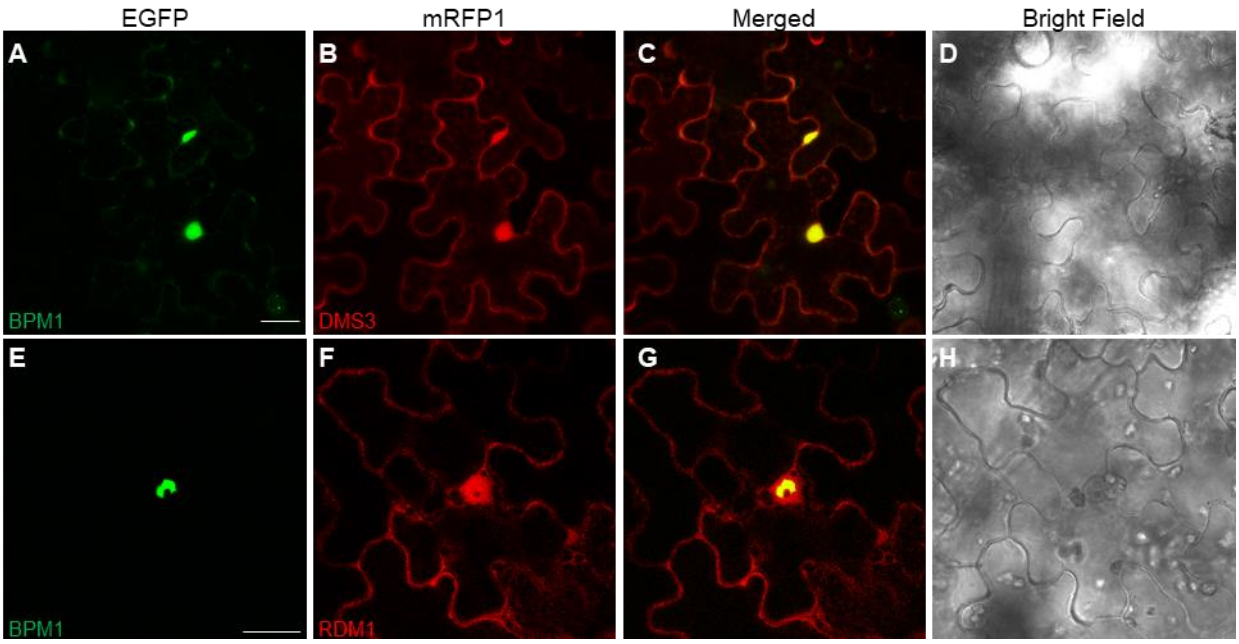

Figure 13 Subcellular colocalization of BPM1 and DMS3 or RDM1 in leaf epidermal cells of *Nicotiana benthamiana* co-expressing EGFP-BPM1 (green) and mRFP1-DMS3 (red) or mRFP1-RDM1 (red) protein. Overlap (yellow) in nucleus is visible between BPM1 and DMS3 (**A-D**) and BPM1 and RDM1 (**E-H**) proteins. Scale bar = 25 μm.

Colocalization analysis was performed using Coloc2 plugin in Fiji ImageJ. EGFP-BPM1 and mRFP1-DMS3 colocalized in *N. benthamiana* epidermal cells with Pearson's correlation coefficient median of r = 0.38 [0.23,0.51] (median $[Q_1, Q_3]$). and the majority of colocalization occurred in nucleus with r = 0.56 [0.38,0.70] (**Figure 14**, light grey). Similar colocalization was measured for EGFP-BPM1 and mRFP1-RDM1 co-expression, where in cells Pearson's correlation coefficient was r = 0.34 [0.26,0.38] and again the majority of colocalization occurred in nucleus with r = 0.44 [0.38,0.59] (**Figure 14**, dark grey).

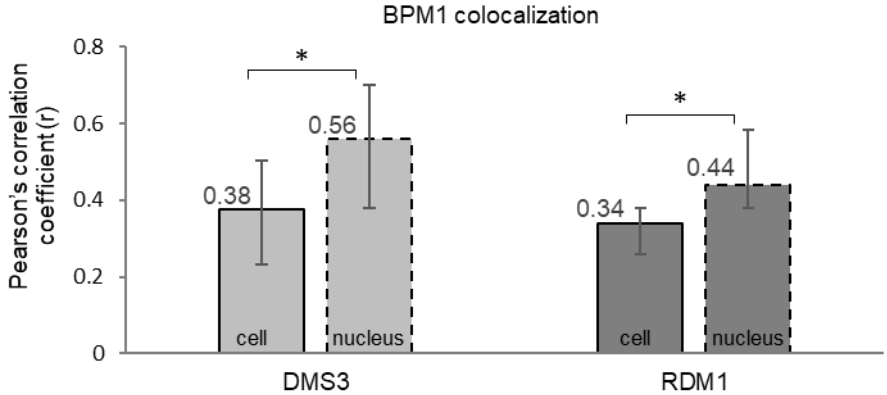

Figure 14 Colocalization analysis of BPM1 with DMS3 and RDM1, respectively, in the *N. benthamiana* epidermal cells shown in **Figure 13**.

Figure 14 - continued

Images were processed with Fiji ImageJ and colocalization was quantified using Pearson's correlation coefficient (r). Colocalization was evident in cells co-expressing EGFP-BPM1 and mRFP1-DMS3, as well as in cells co-expressing EGFP-BPM1 and mRFP1-RDM1 with fluorescent signals predominantly colocalizing in nucleus in both cases. Pearson's correlation coefficients (r) are shown as median values of N=13 for BPM1 colocalization with DMS3 and N=20 for BPM1 colocalization with RDM1, error bars correspond to r interquartile ranges. Asterisks indicate statistically significant differences (Student's t test, $p < 0.05$) between colocalization tested at the level of whole cell and specifically at the level of nucleus.

4.5. BPM1 interacts with DMS3 and RDM1 *in planta*

Following colocalization analysis, the FRET-FLIM assay was performed to identify protein interactions *in planta*. In the analysis, as a measure of the FRET effect, the fraction of fluorescent donor molecules (*F*) that transferred the energy non-radiatively to a closely apposed fluorescent acceptor molecule, was estimated. Since the position of fluorophores with the respect to the labeled proteins, whether it is fused to the N-terminus or C-terminus, can differently contribute to the overall FRET effect (Radić et al., 2020), different FRET reporter orientations were tested. EGFP and mRFP1 were fused N-terminally to all tested proteins (BPM1, DMS3 and RDM1). Additionally, EGFP was fused C-terminally to the BPM1. Therefore, three combinations were tested for interaction of BPM1 with DMS3 (EGFP-BPM1/mRFP1-DMS3, BPM1-EGFP/mRFP1-DMS3 and mRFP1-BPM1/EGFP-DMS3) and three combinations for interaction of BPM1 with RDM1 (EGFP-BPM1/mRFP1-RDM1, BPM1-EGFP/mRFP1-RDM1 and mRFP1-BPM1/EGFP-RDM1). The best orientation resulting in the highest fractional FRET population *F* proved to be the N-terminal EGFP fusion to BPM1, and N-terminal mRFP1 fusion to either DMS3 or RDM1. Measurement results of all tested orientations are given in the **Table 9**. The co-expression of EGFP-BPM1 with mRFP1-DMS3 resulted in $F = 0.1$ [0.07,0.15] and the co-expression of EGFP-BPM1 with mRFP1-RDM1 resulted in $F = 0.13$ [0.10,0.16]. As a negative control, the background FRET signal measured in *N. benthamiana* leaf epidermal cells co-expressing EGFP alone as a donor and mRFP1 alone as an acceptor was used and measured fraction of FRET in negative control was $F = 0.04$ [0.03,0.05]. Measured *F* values for BPM1 interactions with DMS3 and RDM1 were significantly larger than the negative control value, thus strongly indicating an *in vivo* interaction of BPM1 with DMS3 and RDM1 in nucleus of the *N. benthamiana* cells. The FRET between the co-expressed EGFP-DMS3 and mRFP1-RDM1 served as a positive control and was measured as $F = 0.17$ [0.15,0.18] (**Table 9**, two last rows).

Table 9 Fraction of fluorescent donor molecules (F) measured in nuclei of *Nicotiana benthamiana* epidermal cells. From left to right: the measured donor/acceptor pair, median fraction of donor molecules that undergo FRET (*F*), interquartile range of the measured F and the significance (p-value) of the measured F compared to the EGFP/mRFP1 control combination (Tukey–Kramer test).

FRET pair	Median	Interquartile range	p-value when compared to EGFP/mRFP1
EGFP-BPM1/mRFP1-DMS3	0.10	0.07 - 0.15	0.01
EGFP-BPM1/mRFP1-RDM1	0.13	0.10 - 0.16	0.0006
BPM1-EGFP /mRFP1-DMS3	0.11	0.03 - 0.23	0.04
BPM1-EGFP/mRFP1-RDM1	0.05	0.03 - 0.05	1
mRFP1-BPM1/ EGFP -DMS3	0.04	0.02 - 0.07	1
mRFP1-BPM1/ EGFP -RDM1	0.07	0.02 - 0.15	0.06
EGFP-DMS3/mRFP1-RDM1	0.17	0.15 - 0.18	$< 10^{-7}$
EGFP/mRFP1	0.04	0.03 - 0.05	

4.6. BPM1 directly interacts with DMS3 and RDM1

Mass spectrometry, FRET-FLIM and colocalization data (**Tables 8** and **9,** and **Figure 14**) suggested that BPM1 interacts with DMS3 and RDM1. Nevertheless, I performed several protein-protein interaction assays to unambiguously determine whether those interactions are direct or indirect.

Yeast two-hybrid assay, where DMS3 or RDM1 were used as bait, and BPM1 as prey, indicated direct interaction of BPM1 with both proteins. Both combinations, BPM1/DMS3 and BPM1/RDM1 proved to be prototrophic for histidine since uniform growth of yeasts was noticed on histidine lacking medium (**Figure 15 A**). When empty pGBT9 plasmid expressing only DNA binding domain of GAL4 transcription factor was used as bait and BPM1 fused to activation domain was used as prey (negative control), no yeast growth was observed on histidine lacking medium, while positive control (interaction of DMS3 and RDM1) exhibited strong growth on the same medium. Interactions were additionally validated and quantified by β-galactosidase assays. Weak blue coloring was observed for both inspected interactions (BPM1/DMS3 and BPM1/RDM1) after incubation with β-galactosidase substrate X-gal. Blue color was first detected after 2 h incubation (**Figure 15 B**). Unlike those interactions, positive control (DMS3/RDM1) was clearly blue after only 15 min incubation. No coloring was observed in negative control even after 5 h (a method limitation). When quantified using ONPG as β-galactosidase substrate, BPM1

showed slightly higher affinity for DMS3 (1.01 Miller units) than for RDM1 (0.72 Miller units, **Figure 15 C**). Displayed values of interaction intensities were obtained by normalizing the experimentally obtained values for negative control (DNA binding domain alone in co-transformation with AD-BPM1). As a positive control, a known interaction between DMS3 and RDM1 was used (Sasaki et al., 2014) and affinity of RDM1 for DMS3 was 17.49 Miller units, confirming a very strong interaction.

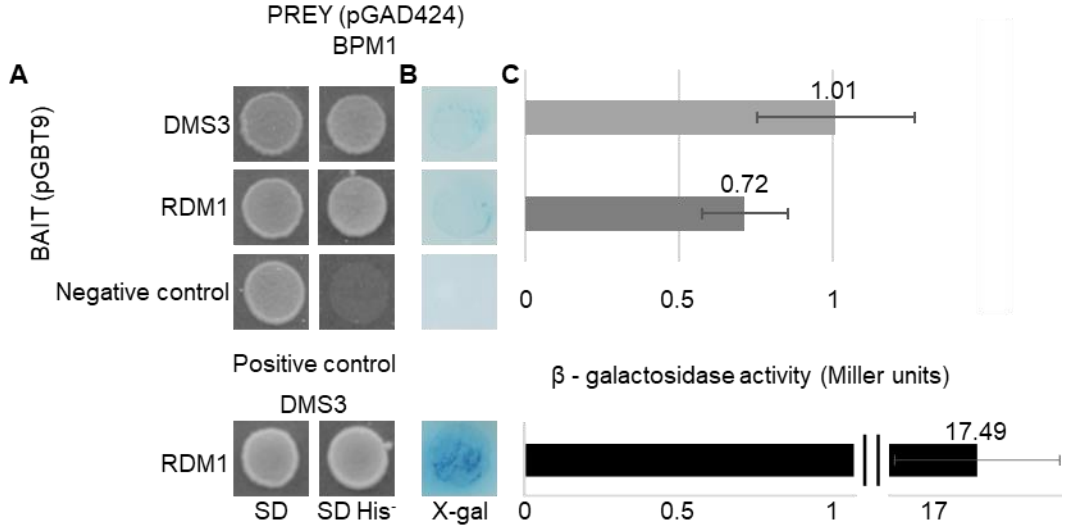

Figure 15 Y2H protein interaction assays indicated direct interaction of BPM1 with DMS3 and RDM1, respectively. **A)** In histidine prototrophy assay, growth of prototrophic yeasts was detected for both, BPM1/DMS3 and BPM1/RDM1 co-transformants. For each co-transformation ten individual colonies were analyzed. Specificity of the prey construct was confirmed by co-transformation with empty bait vectors (negative control). DMS3/RDM1 interaction served as a positive control. **B)** In the qualitative β-galactosidase assay weak blue coloring for BPM1/DMS3 and BPM1/RDM1 was observed after 2 h incubation with X-gal substrate. Positive control was blue after 15 min incubation. Negative control remained colorless. **C)** In the quantitative β-galactosidase assay, interaction intensities for BPM1 and DMS3 or RDM1 were normalized for negative control values and are indicated as units of β-galactosidase activity (Miller units). Data are presented as means of three independent experiments ± SD. DMS3-RDM1 interaction served as a positive control. No significant difference was observed (Student's t test, $p < 0.05$) between interaction intensities of BPM1 and DMS3 or RDM1.

In a pull-down assay, purified prey proteins, His-DMS3 and His-RDM1 were coprecipitated with glutathione Sepharose bound GST-tagged BPM1 (**Figure 16 A**). GST protein alone did not bind either His-DMS3 or His-RDM1 thus the specificity of DMS3-BPM1 and RDM1-BPM1 interactions was validated. The same proteins were additionally used for microscale thermophoresis, where eluted GST-BPM1 protein was used as a ligand, and His-tagged DMS3 or RDM1 were used as targets. MST measures the movement of molecules in a microscopic temperature gradient under constant buffer conditions, and this motion depends on the size, charge

and solvation entropy of the molecules (Jerabek-Willemsen et al., 2014). If there is an interaction between target molecule and a ligand molecule, a shift in fluorescent signal will be observed in comparison to the signal of target molecule alone. Change in fluorescence amplitude of 18.5 was detected for RDM1-BPM1 and 22.8 for DMS3-BPM1, thus confirming BPM1 interaction with both proteins, RDM1 and DMS3 (**Figure 16 B**).

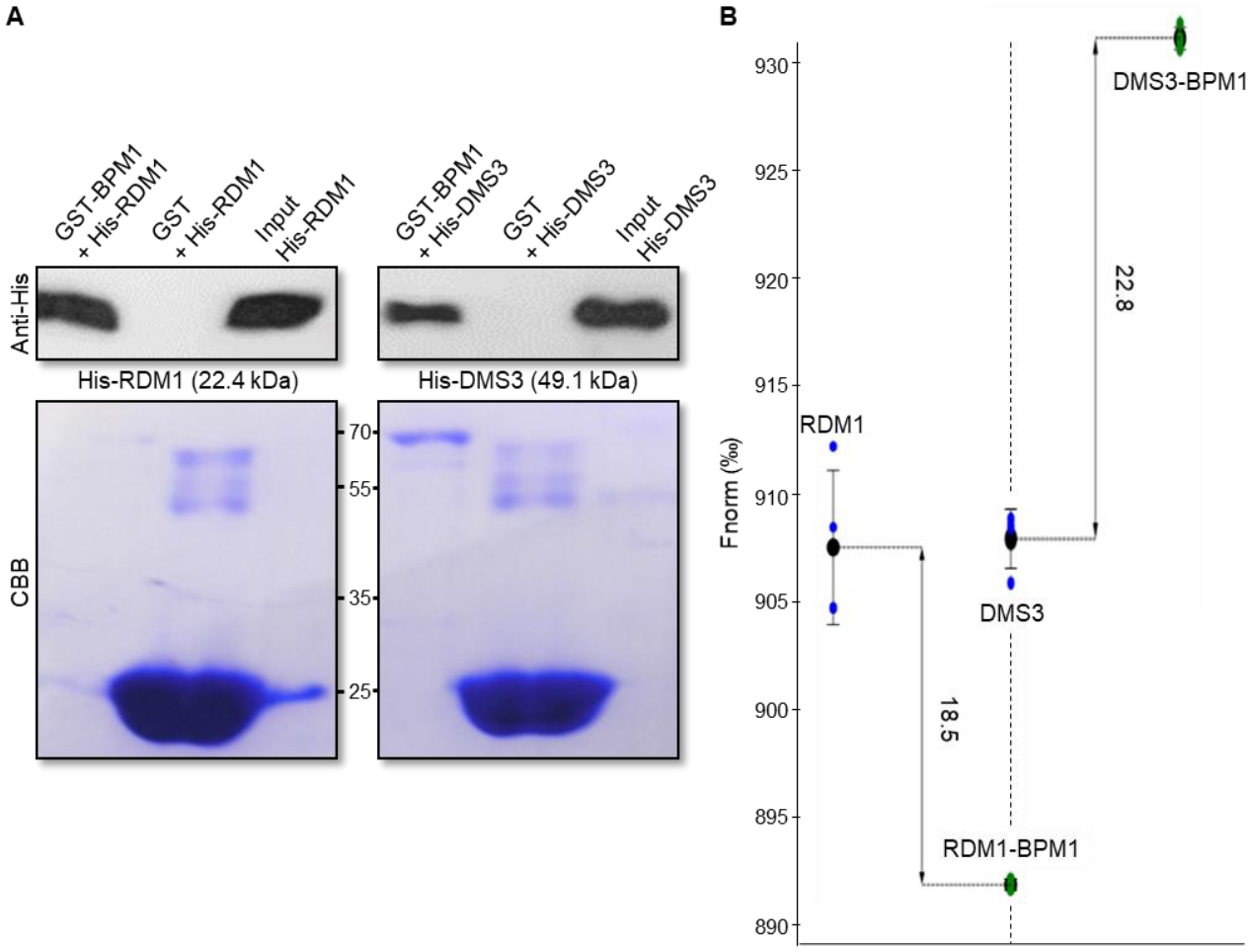

Figure 16 Interaction of BPM1 with RDM1 and DMS3 analyzed by *in vitro* pull-down assays. **A**) His-tagged prey proteins DMS3 and RDM1 were detected with anti-His monoclonal antibody in pull-down assay where GST-tagged BPM1 bound to the glutathione Sepharose beads served as bait. GST-BPM1 (70.3 kDa) is visible on Coomassie Brilliant Blue (CBB) stained PVDF membrane below. Specificity of prey constructs was confirmed by incubation with GST alone (negative control). "Input" represents purified prey proteins taken before pull-down assay was carried on. **B**) MST analysis of BPM1 interaction with RDM1 and DMS3, respectively. Interaction between His-labeled RDM1 or His-labeled DMS3 with BPM1 was confirmed by change in fluorescence amplitude between RDM1-only (blue) and RDM1-BPM1 complex (green), and DMS3-only (blue) and DMS3-BPM1 complex (green). Data are presented as means of four technical replicates ± SD. Similar results were obtained in two independent experiments.

4.7. Interaction between BPM1 and DMS3 is dominantly mediated by MATH domain

To determine which domain(s) of BPM1 interact with DMS3, BPM1 variants missing one of the three domains (MATH, BTB or BACK) were generated for use in Y2H, pull-down and MST, and for colocalization and FRET-FLIM analysis *in planta* (for schematic representation see **Figure 17**, double-domain variants of BPM1). In Y2H, DMS3 was used as bait, while truncated versions of BPM1 were used as prey. In histidine prototrophy assay, for all three BPM1 deletion mutants (BTB-BACK$_{BPM1}$/DMS3, MATH-BACK$_{BPM1}$/DMS3 and MATH-BTB$_{BPM1}$/DMS3) growth of prototrophic yeasts was observed (**Figure 18 A**) indicating interaction with DMS3 in all tested combinations. Although there was no statistically significant difference between inspected combinations in quantitative β-galactosidase assay (**Figure 18 B**), deletion of BACK domain (MATH-BTB$_{BPM1}$) had the weakest effect on the interaction leading to 84% of the full-length BPM1/DMS3 interaction intensity. Deletion of BTB domain (MATH-BACK$_{BPM1}$) led to 66% of the full-length BPM1/DMS3 interaction intensity, and deletion of MATH domain appeared to have the greatest effect on the interaction with DMS3 since the interaction intensity of this protein variant (BTB-BACK$_{BPM1}$) was reduced to only 51% of the interaction intensity of the full-length BPM1 protein.

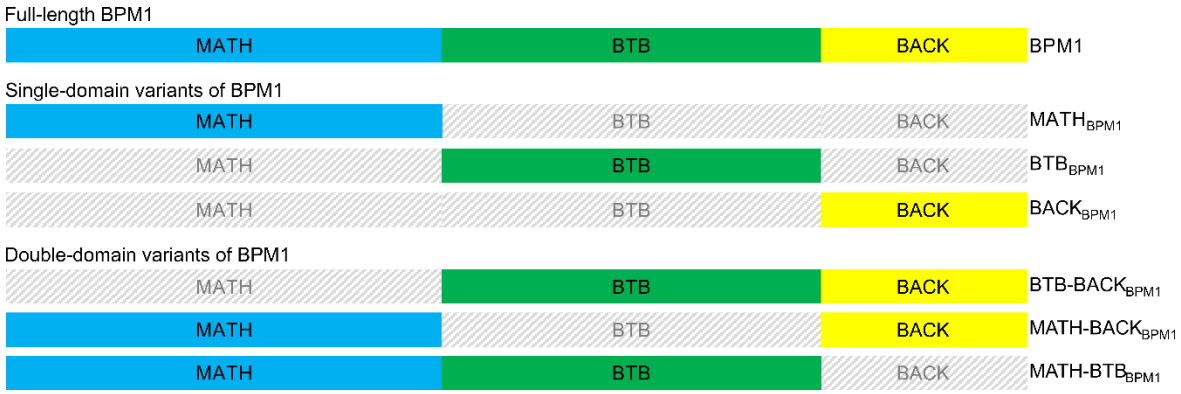

Figure 17 Schematic representation of the full-length BPM1 protein, and single-domain and double-domain BPM1 mutant variants. For details see **Figure 6**.

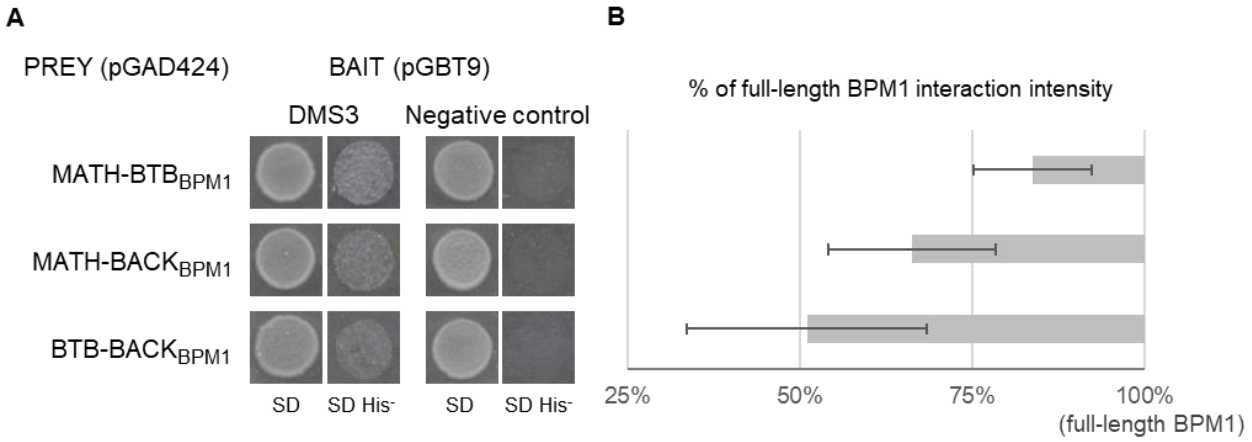

Figure 18 Double-domain variants (MATH-BTB, MATH-BACK and BTB-BACK) of BPM1 interact with DMS3 in Y2H protein interaction assays. **A**) Histidine prototrophy assay showing interaction between BPM1 and DMS3. Similar results were obtained in three individual experiments, for each experiment seven individual colonies were analyzed. Specificity of the pray construct was confirmed by co-transformation with empty bait vectors (negative control). **B**) In the β-galactosidase assay, interaction intensities of truncated BPM1 proteins with DMS3 are represented as percentage of full-length BPM1 interaction values. Data is presented as means of three individual experiments ± SEM. No significant difference was observed (Duncan's new multiple range test, $p < 0.05$) between interaction intensities of BPM1 double-domain variants and DMS3.

To further elucidate the role of the individual domains, single-domain protein variants were generated leaving only one domain of the BPM1 protein present in the Y2H prey construct as depicted in the **Figure 17** (single-domain variants of BPM1). Surprisingly, all single-domain variants of BPM1 interacted with DMS3 in histidine prototrophy assay (**Figure 19 A**), but individual colonies indicated varying interaction intensities (Jagić et al., 2022). In quantitative β-galactosidase assay individual domains showed less affinity for binding DMS3 than full-length BPM1 (**Figure 19 B**). Here, the $MATH_{BPM1}$ had the highest interaction intensity with DMS3 which was 75% of the interaction intensity of the full-length BPM1 protein. Interaction intensity of BTB domain (BTB_{BPM1}) was reduced to 58% of the full-length BPM1 interaction. The lowest interaction intensity was recorded for $BACK_{BPM1}$ protein variant showing only 40% of the full-length BPM1/DMS3 interaction suggesting that this domain is the least important for interaction with DMS3. Altogether, Y2H results point out the importance of the MATH domain for interaction with DMS3.

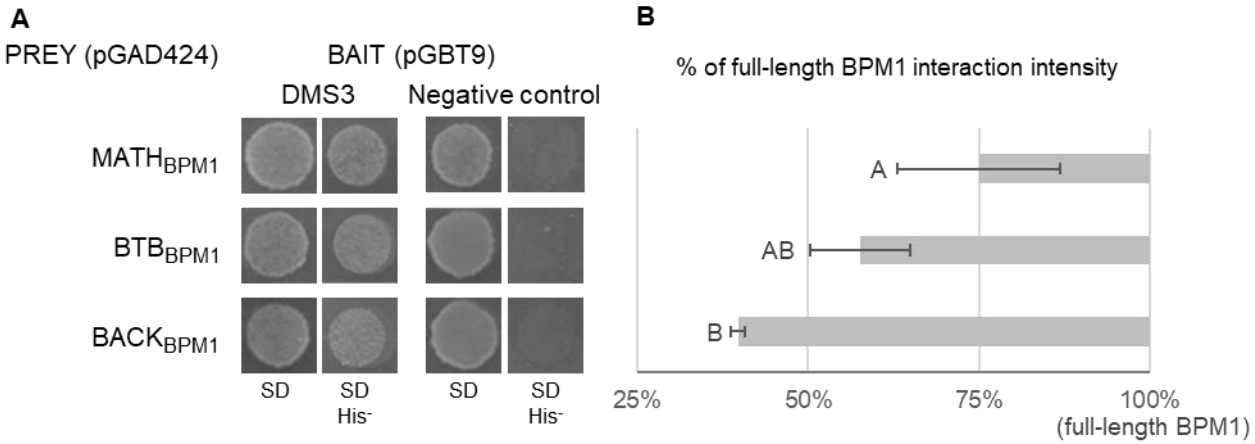

Figure 19 Single-domain variants (MATH, BTB or BACK) of BPM1 interact with DMS3 in Y2H protein interaction assays. **A)** Histidine prototrophy assay showing interaction between BPM1 and DMS3. Similar results were obtained in three individual experiments, for each experiment seven individual colonies were analyzed. Specificity of the pray construct was confirmed by co-transformation with empty bait vectors (negative control). **B**) In the β-galactosidase assay, interaction intensities of truncated BPM1 proteins with DMS3 are represented as percentage of full-length BPM1 interaction values. Data is presented as means of three individual experiments ± SEM. Columns marked with different letters indicate a significant difference (Dunn's test, $p < 0.05$) between interaction intensities of BPM1 single-domain variants and DMS3.

Moreover, two combinations were analyzed in the pull-down assay: GST-tagged BTB-BACK$_{BPM1}$ and MATH-BACK$_{BPM1}$ with the aim of comparing the importance of the BTB and MATH domains for interaction with DMS3. The two constructs served as bait proteins and the interaction of both with His-tagged DMS3 prey was confirmed by immunodetection with anti-His monoclonal antibody (**Figure 20 A** and **B**). To quantify these interactions, MST was performed. A fixed concentration of His-tagged DMS3 target protein was combined with serial dilutions of BTB-BACK$_{BPM1}$ or MATH-BACK$_{BPM1}$, and the changes in MST signal (normalized fluorescence changes, ΔF_{norm}) throughout temperature gradient were measured. The changes detected were expressed as interaction affinities of the BPM1 variants to the DMS3 protein. The measured Kd values were as follows: 900 [600,1600] nM for BTB-BACK$_{BPM1}$ (**Figure 20 C**) and 480 [440,530] nM for MATH-BACK$_{BPM1}$ (**Figure 20 D**) both suggesting interaction. The confidentially lower Kd value for MATH-BACK$_{BPM1}$ confirmed the Y2H assumption that the MATH domain is more important for interaction with DMS3.

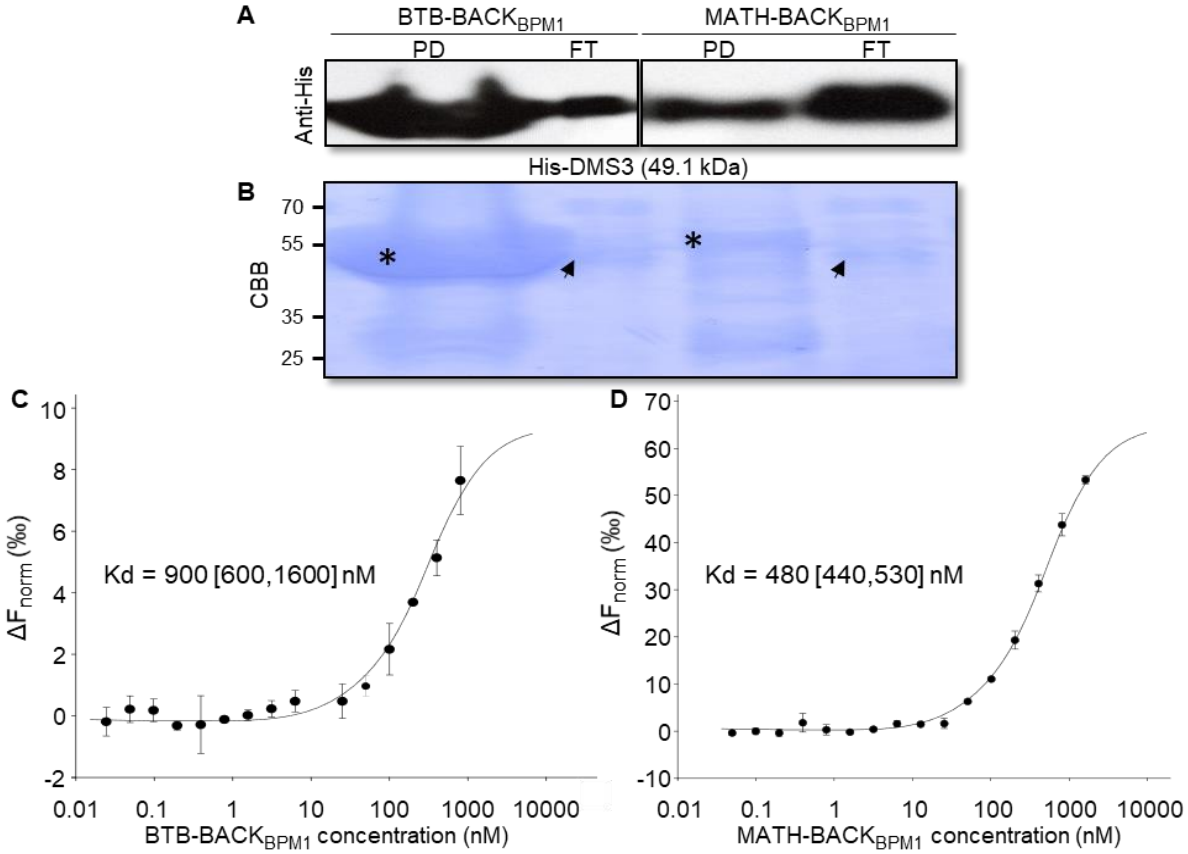

Figure 20 Double-domain variants (BTB-BACK and MATH-BACK) of BPM1 interact with DMS3 in pull-down assay and MST. GST-tagged constructs of BTB-BACK$_{BPM1}$ and MATH-BACK$_{BPM1}$ were used as baits/ligands, whilst His-tagged DMS3 was used as prey/target. His-DMS3 in pull-down (PD) and flow through (FT) was detected with anti-His monoclonal antibody (**A**). Bait proteins are indicated on CBB stained PVDF membrane with asterisks in PD (GST-BTB-BACK$_{BPM1}$ = 55.4 kDa, GST-MATH-BACK$_{BPM1}$ = 57.3 kDa), arrows indicate prey protein in FT (His-DMS3 = 49.1 kDa) (**B**). DMS3 affinity between BTB-BACK$_{BPM1}$ and MATH-BACK$_{BPM1}$ was quantified by titrating the ligand against a fixed concentration of His-labelled DMS3 target. The resulting Kd values were 900 [600,1600] nM for BTB-BACK$_{BPM1}$ (**C**) and 480 [440,530] nM for MATH-BACK$_{BPM1}$ (**D**). Fitted MST data is displayed as F$_{norm}$ values relative to ligand concentration as means of three biological replicates ± SD. Kd values are expressed as Kd mean [Kd confidence interval].

4.8. Subcellular colocalization of BPM1 and DMS3 is influenced by BACK domain, while MATH domain contributes to their interaction *in planta*

Considering the previously described better characteristics of the epidermal cells of *N. benthamiana* compared with the BY-2 cells (section 4.4), colocalization analyzes and FRET-FLIM were performed in the *N. benthamiana* epidermal cells. The fluorescence signals of BPM1 deletion mutants and DMS3 were almost exclusively detected in the nucleus, so quantitative colocalization analysis was performed in this compartment (**Figure 21 A-L**). The best colocalization with DMS3 was calculated for MATH-$BACK_{BPM1}$, r = 0.42 [0.26,0.52] (**Figure 21 M**). The presence of the BTB and BACK domains (BTB-$BACK_{BPM1}$) resulted in an intermediate colocalization coefficient, r = 0.38 [0.23,0.45], whereas the weakest colocalization was observed when the BACK domain (MATH-BTB_{BPM1}) was absent, r = 0.29 [0.22,0.30]. The BACK domain thus might have some role in mediating the DMS3 interaction by affecting protein colocalization. Moreover, the MATH domain, in cooperation with the BACK domain, showed affinity for both nuclear and cytoplasmic located targets in BY-2 cells, whereas the BTB domain showed a preference for exclusively nuclear localization of the BPM1 protein when DMS3 is present in the cell (**Appendix F Chapter F5 Figure F5-2**).

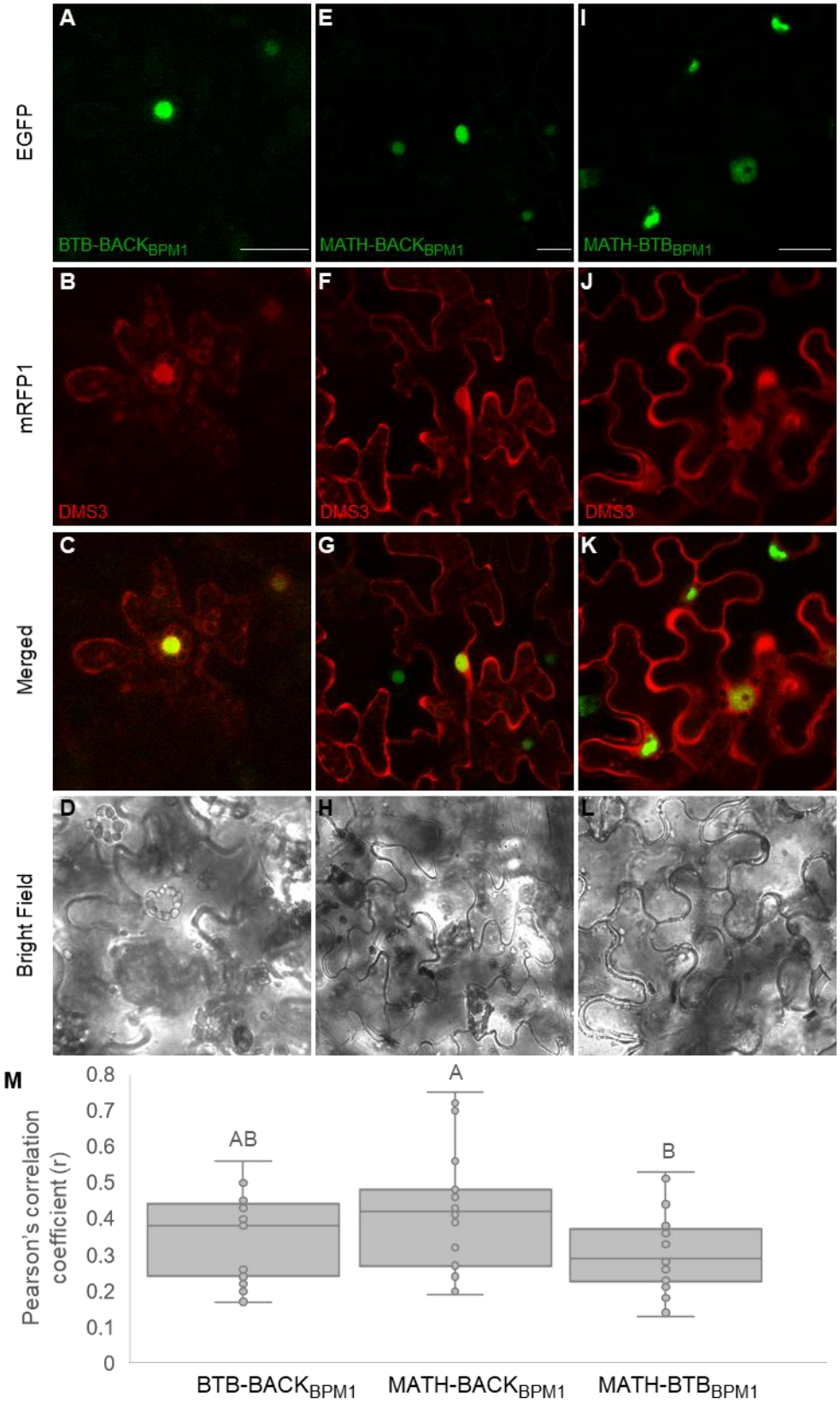

Figure 21 Subcellular colocalization of BPM1 deletion mutants and DMS3 in *N. benthamiana*.

Figure 21 – continued

Overlap in leaf epidermal cells co-expressing EGFP-tagged BPM1 variants missing MATH, BTB or BACK domain and mRFP1-DMS3 protein is visible in nucleus between all three variants of BPM1 protein (green) and DMS3 protein (red): BTB-BACK$_{BPM1}$ and DMS3 (**A-D**), MATH-BACK$_{BPM1}$ and DMS3 (**E-H**), and MATH-BTB$_{BPM1}$ and DMS3 (**I-L**). Scale bar = 25 μm. Colocalization analysis of BPM1 deletion mutants with DMS3 (**M**). Images were processed with Fiji ImageJ and colocalization was quantified using Pearson's correlation coefficient (r). Results are shown as median r values (N = 17 for BTB-BACK$_{BPM1}$ and MATH-BACK$_{BPM1}$ and N = 24 for MATH-BTB$_{BPM1}$) with indicated r interquartile ranges. whiskers indicating minimum and maximum measured values. Boxes marked with different letters indicate a significant difference (Tukey's HSD/Kramer test, $p < 0.05$) between the tested colocalizations.

Following colocalization analysis in *N. benthamiana*, interaction of BPM1 deletion mutants with DMS3 was examined *in planta* by FRET-FLIM. Fractional FRET population was measured only in the orientation that exhibited the best results with full-length BPM1: N-terminal EGFP fusion to BPM1 and N-terminal mRFP1 fusion to DMS3 (**Table 9**). Measured *F* values were as follows: $F = 0.11$ [0.05,0.13] for BTB-BACK$_{BPM1}$, $F = 0.11$ [0.09,0.18] for MATH-BACK$_{BPM1}$ and $F = 0.12$ [0.05,0.15] for MATH-BTB$_{BPM1}$ (**Figure 22**). No significant preference for DMS3 was recorded between three domain-deletion variants of BPM1, although MATH-BACK$_{BPM1}$ showed increased tendency for the interaction. All variants significantly differed from the negative control hence indicating their interaction with DMS3.

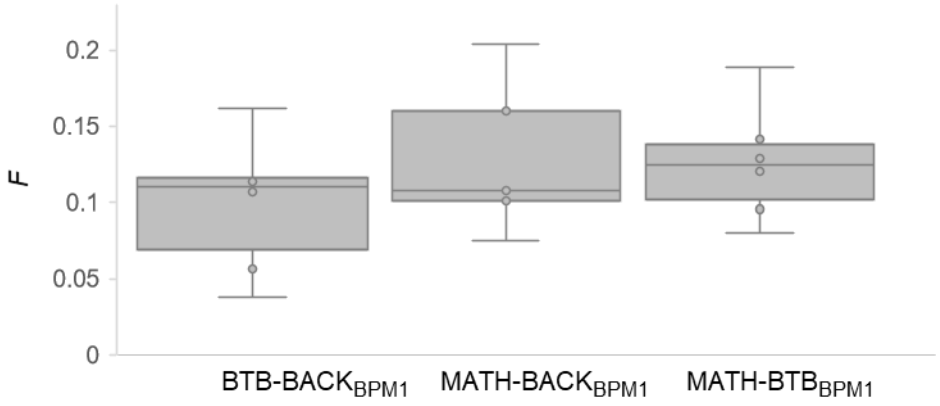

Figure 22 Fraction of fluorescent donor molecules that undergo FRET (F) for EGFP-BPM1 deletion variants (BTB-BACK$_{BPM1}$, MATH-BACK$_{BPM1}$ and MATH-BTB$_{BPM1}$) in combination with mRFP1-DMS3. All BPM1 deletion variants can interact in vivo with DMS3. Box-plot shows median F values with indicated interquartile interval, whiskers indicating minimum and maximum measured values. There was no significant difference (Tukey's HSD/Kramer test, $p < 0.05$) between the tested groups. For details see **Appendix F Chapter F6 Table F6-1**.

4.9. DMS3 is not targeted for degradation by BPM1

Taken all together, MATH domain showed the highest affinity for DMS3. Since MATH domain is known to bind and target proteins for ubiquitination and subsequent protein degradation, influence of BPM1 overexpression on endogenous protein levels of DMS3 in *A. thaliana* seedlings was tested. No difference was observed between endogenous DMS3 protein levels in WT and in BPM1-overexpressing (oeBPM1-EGFP) plants after Western blotting with native anti-DMS3 antibody (**Figure 23 A** and **B**), suggesting that DMS3 is not a target for BPM1-mediated ubiquitination and degradation by $CUL3^{BPM}$ E3 ubiquitin ligases pathway.

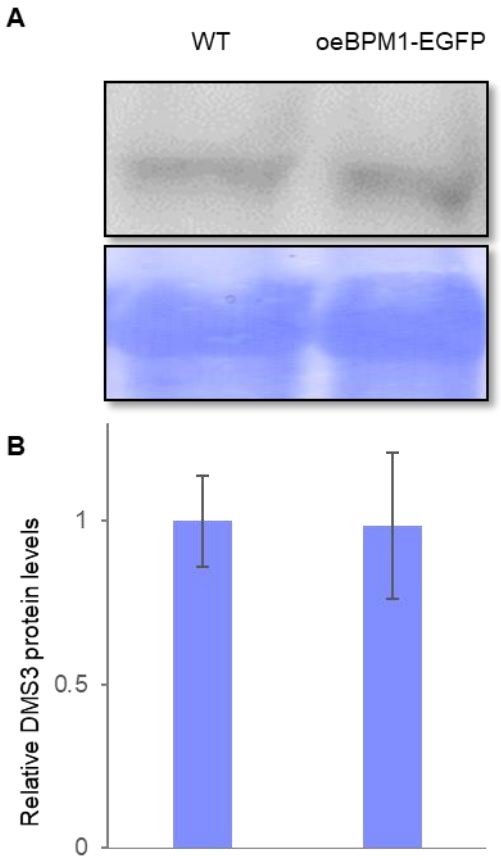

Figure 23 DMS3 protein levels in WT and oeBPM1-EGFP line were invariable. **A**) Total proteins were extracted from eleven-day-old seedlings and DMS3 levels were detected by Western blotting using an anti-DMS3 antibody (upper panel). For loading control, proteins were stained with CBB on PVDF membranes (lower panel). Two independent experiments were performed. **B**) Relative DMS3 protein levels were quantified in ImageJ and normalized to CBB bands. Data is presented as means of two independent experiments comprising of two individual protein bands per line ± SD. No significant difference was observed (Student's t test, $p < 0.05$) between DMS3 protein levels in WT and oeBPM1-EGFP.

4.10. BTB domain in combination with MATH dominantly mediated interaction with RDM1

To examine domain-specific roles of BPM1 in interaction with RDM1, the same BPM1 deletion mutants that were used to determine interaction with DMS3 (BTB-BACK$_{BPM1,}$ MATH-BACK$_{BPM1}$, MATH-BTB$_{BPM1}$) were used (**Figure 17**, double-domain variants of BPM1). In Y2H, RDM1 was used as bait, while BPM1 deletion mutants were used as prey. All variants interacted with RDM1 as shown by growth of prototrophic yeasts in all three combinations (MATH-BTB$_{BPM1}$/RDM1, MATH-BACK$_{BPM1}$/RDM1 and BTB-BACK$_{BPM1}$/RDM1) in histidine prototrophy assay (**Figure 24 A**). In quantitative β-galactosidase assay with ONPG used as a β-galactosidase substrate, only MATH-BTB$_{BPM1}$/RDM1 showed an increase in averaged interaction intensity (117%) in comparison to the intact BPM1/RDM1. The lack of BTB domain (MATH-BACK$_{BPM1}$) led to the 69% of the interaction intensity of intact BPM1 with RDM1, whereas lack of MATH domain (BTB-BACK$_{BPM1}$) resulted in 54% of the full-length BPM1/RDM1 interaction intensity (**Figure 24 B**). However, considering there was a lot of variances between inspected combinations (large standard deviations), no statistically significant difference was observed.

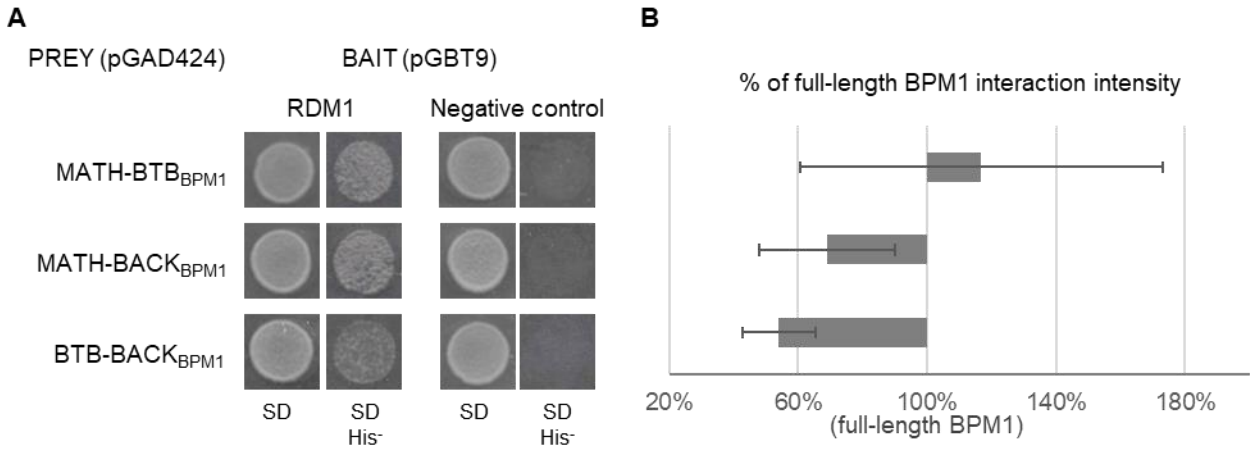

Figure 24 Double-domain variants (MATH-BTB, MATH-BACK and BTB-BACK) of BPM1 interact with RDM1 in Y2H protein interaction assays. **A**) Histidine prototrophy assay showing interaction between BPM1 and RDM1. Similar results were obtained in three individual experiments, for each experiment seven individual colonies were analyzed. Specificity of the pray construct was confirmed by co-transformation with empty bait vectors (negative control). **B**) In the β-galactosidase assay, interaction intensities of truncated BPM1 proteins with RDM1 are represented as percentage of full-length BPM1 interaction values. Data is presented as means of three individual experiments ± SEM. No significant difference was observed (Duncan's new multiple range test, $p < 0.05$) between tested interaction intensities.

The role of the individual domains of BPM1 in interaction with RDM1 was also tested. Single-domain protein variants of BPM1 ($MATH_{BPM1}$, BTB_{BPM1}, $BACK_{BPM1}$, **Figure 17**, single-domain variants of BPM1) were used as prey in Y2H experiment with RDM1 used as bait. Yeasts co-transformed with all three combinations ($MATH_{BPM1}$/RDM1, BTB_{BPM1}/RDM1, $BACK_{BPM1}$/RDM1) have grown on media lacking histidine, all suggesting a direct interaction (**Figure 25 A**). In quantitative β-galactosidase assay, MATH only variant ($MATH_{BPM1}$) experienced 82% of full-length BPM1 interaction intensity, while BTB_{BPM1} had the highest interaction intensity with RDM1 exceeding the interaction intensity of the full-length BPM1 protein and resulted in 118% of the full length BPM1/RDM1 interaction intensity (**Figure 25 B**). On the other side, $BACK_{BPM1}$/RDM1 showed only 53% of interaction intensity of full-length BPM1 for binding RDM1. Although, $MATH_{BPM1}$ was not significantly different from either of the variants, BTB_{BPM1} had statistically greater interaction intensity with RDM1 than $BACK_{BPM1}$. Thus, BTB might be the most relevant domain for interaction with RDM1, while BACK domain is again the least important for the interaction.

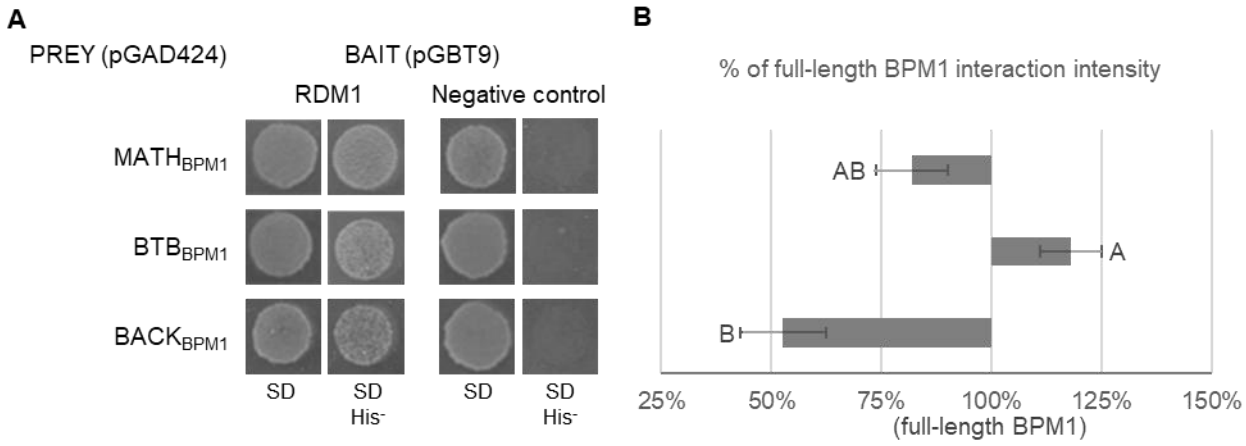

Figure 25 Single-domain variants (MATH, BTB or BACK) of BPM1 interact with RDM1 in Y2H protein interaction assays. **A**) Histidine prototrophy assay showing interaction between BPM1 and RDM1. Similar results were obtained in three individual experiments, for each experiment seven individual colonies were analyzed. Specificity of the pray construct was confirmed by co-transformation with empty bait vectors (negative control). **B**) In the β-galactosidase assay, interaction intensities of truncated BPM1 proteins with RDM1 are represented as percentage of full-length BPM1 interaction values. Data is presented as means of three individual experiments ± SEM. Columns marked with different letters indicate a significant difference (Duncan's new multiple range test, $p < 0.05$) between interaction activities of BPM1 single-domain variants and RDM1.

In pull-down assay where GST-BTB-BACK$_{BPM1}$ and GST-MATH-BACK$_{BPM1}$ protein served as bait and His-tagged RDM1 was used as prey, in both cases coprecipitation of prey protein was detected using anti-His monoclonal antibody, further confirming there is a direct interaction between BTB-BACK$_{BPM1}$ and MATH-BACK$_{BPM1}$ with RDM1 (**Figure 26 A** and **B**). To attempt to quantify the interactions, MST was performed. Fixed concentrations of His-tagged RDM1 protein were combined with serial dilutions of BTB-BACK$_{BPM1}$ or MATH-BACK$_{BPM1}$ and changes in MST signal (ΔF_{norm}) throughout temperature gradient were measured. The measured Kd values were highly similar: 700 [500,1300] nM for BTB-BACK$_{BPM1}$ (**Figure 26 C**) and 600 [300,1400] nM for MATH-BACK$_{BPM1}$ (**Figure 26 D**) thus confirming interaction but making it impossible to differentiate the importance of BTB or MATH domain in combination with BACK for interaction with RDM1.

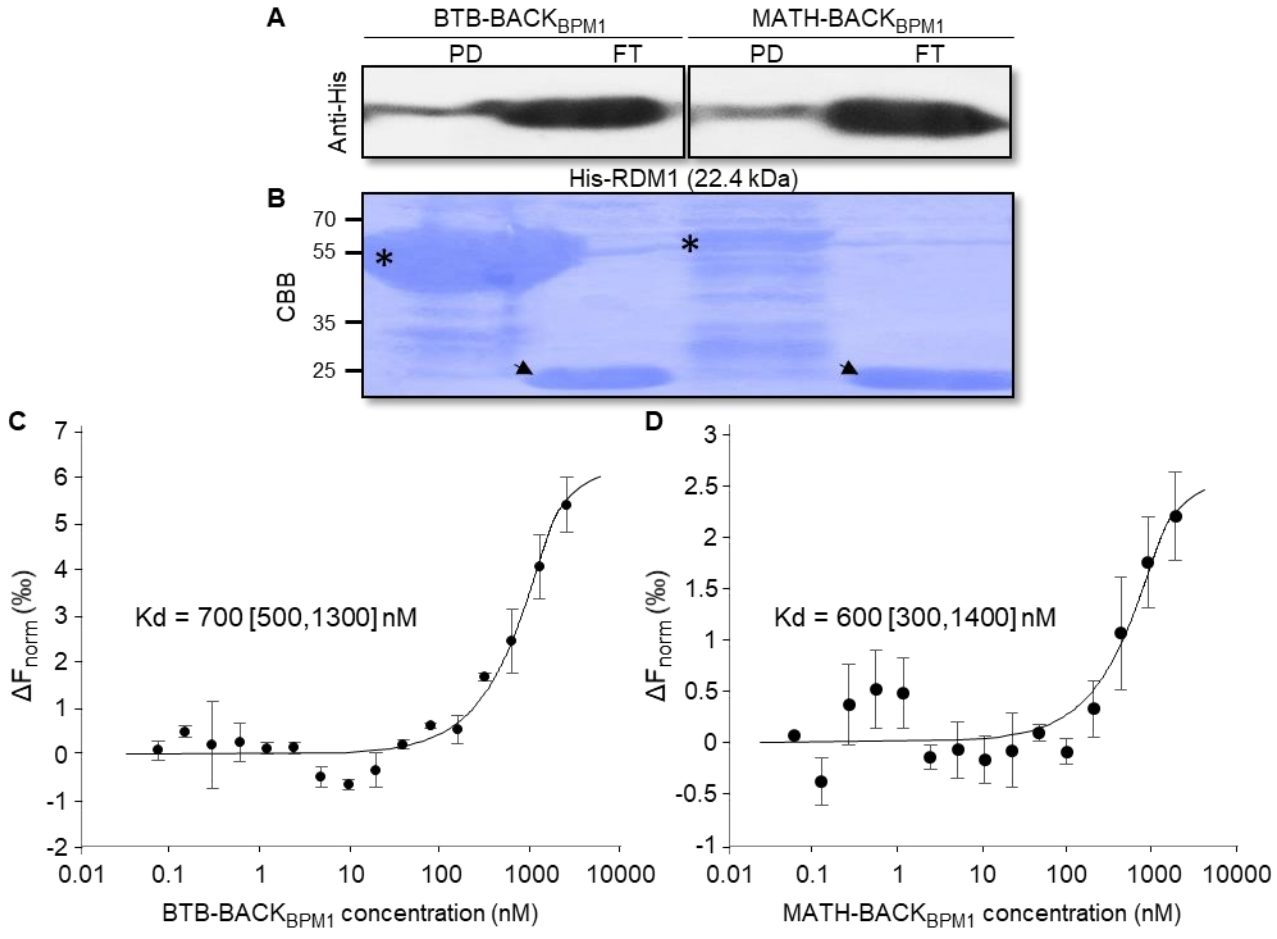

Figure 26 Double-domain variants (BTB-BACK and MATH-BACK) of BPM1 interact with RDM1 in pull-down assay and MST.

Figure 26 - continued

GST-tagged constructs of BTB-BACK$_{BPM1}$ and MATH-BACK$_{BPM1}$ were used as baits/ligands, whilst His-tagged RDM1 was used as prey/target. His-RDM1 in pull-down (PD) and flow through (FT)* was detected with anti-His monoclonal antibody (**A**). Bait proteins are indicated on CBB stained PVDF membrane with asterisks in PD (GST-BTB-BACK$_{BPM1}$ = 55.4 kDa, GST-MATH-BACK$_{BPM1}$ = 57.3 kDa), arrows indicate prey protein in FT (His-RDM1 = 22.4 kDa) (**B**). RDM1 affinity between BTB-BACK$_{BPM1}$ and MATH-BACK$_{BPM1}$ was quantified by titrating the ligand against a fixed concentration of His-labelled RDM1 target. The resulting Kd values were 700 [500,1300] nM for BTB-BACK$_{BPM1}$ (**C**) and 600 [300,1400] nM for MATH-BACK$_{BPM1}$ (**D**). Fitted MST data is displayed as F_{norm} values relative to ligand concentration as means of three biological replicates ± SD. Kd values are expressed as Kd mean [Kd confidence interval].
* Enormous quantities of His-labelled RDM1 protein were purified largely exceeding amounts of GST-tagged BTB-BACK$_{BPM1}$ and MATH-BACK$_{BPM1}$ as obvious from **B**) therefore the bands in FT are much stronger than the ones in PD (**A**).

4.11. BTB-BACK domain combination increases nuclear colocalization and interaction of BPM1 with RDM1 *in planta*

Colocalization analysis and FRET-FLIM were performed in *N. benthamiana* epidermal cells co-transformed with EGFP-BPM1 deletion mutants and mRFP1-RDM1. Overlap of the EGFP and mRFP1 fluorescent signal was again in the nucleus and colocalization analysis was done in this compartment (**Figure 27 A-L**). Colocalization between BTB-BACK$_{BPM1}$ and RDM1 was calculated to r = 0.59 [0.48,0.67], colocalization between MATH-BACK$_{BPM1}$ and RDM1 to r = 0.49 [0.40,0.61] and between MATH-BTB$_{BPM1}$ and RDM1 to r = 0.54 [0.48,0.67] (**Figure 27 M**). There was no statistically significant difference observed, but the presence of BTB domain, especially when combined with BACK showed an increased trend for colocalization with RDM1. Furthermore, subcellular localization of BPM1 deletion mutants when co-expressed with RDM1 was examined in BY-2 cells (**Appendix F Chapter F5**). All BPM1 deletion mutants localized exclusively in nucleus indicating that the presence of RDM1 in cells seems to elicit BPM1 to nucleus regardless of the domains omitted (**Appendix F Chapter F5 Figure F5-3**).

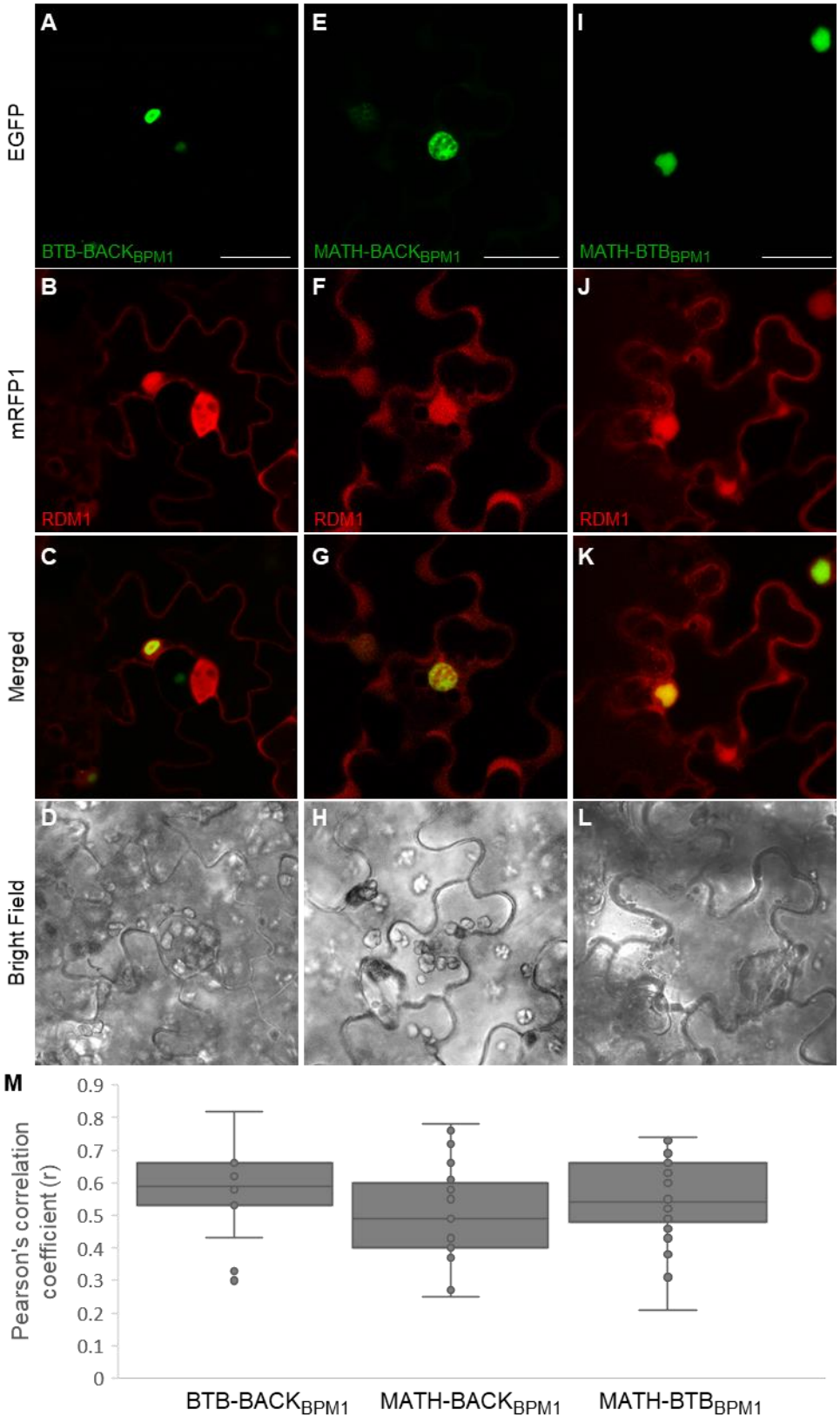

Figure 27 Subcellular colocalization of BPM1 deletion mutants and RDM1 in *N. benthamiana*. Overlap in leaf epidermal cells co-expressing EGFP-tagged BPM1 variants missing MATH, BTB or BACK domain and mRFP1-RDM1 protein is visible in nucleus between all three variants of BPM1 protein (green) and RDM1 protein (red): BTB-BACK$_{BPM1}$ and RDM1 (**A-D**), MATH-BACK$_{BPM1}$ and RDM1 (**E-H**), and MATH-BTB$_{BPM1}$ and RDM1 (**I-L**).

Figure 27 – continued

Scale bar = 25 μm. Colocalization analysis of BPM1 deletion mutants with RDM1 in the cell nuclei (**M**). Images were processed with Fiji ImageJ and colocalization was quantified using Pearson's correlation coefficient (r). Results are shown as median r values (N =17 for BTB-BACK$_{BPM1}$, N=25 for MATH-BTB$_{BPM1}$ and N = 33 for MATH-BACK$_{BPM1}$ with indicated r interquartile ranges. whiskers indicating minimum and maximum measured values. There was no significant difference (Tukey's HSD/Kramer test, $p < 0.05$) between the tested colocalizations.

After colocalization analysis, interaction of EGFP-BPM1 deletion mutants with mRFP1-RDM1 was inspected by FRET-FLIM. Even though, BTB-BACK$_{BPM1}$ showed upward trend for interaction with RDM1 in FRET-FLIM, all measured *F* values were around the same median as follows: *F* = 0.15 [0.12,0.23] for BTB-BACK$_{BPM1}$, *F* = 0.14 [0.06,0.16] for MATH-BACK$_{BPM1}$ and *F* = 0.13 [0.11,0.15] for MATH-BTB$_{BPM1}$ (**Figure 28**). All combinations indicated interaction with RDM1 (they were significantly larger than EGFP/mRFP1 negative control values) and the BTB-BACK domain combination again slightly increased the *F* value for the interaction, although no statistical significance was observed.

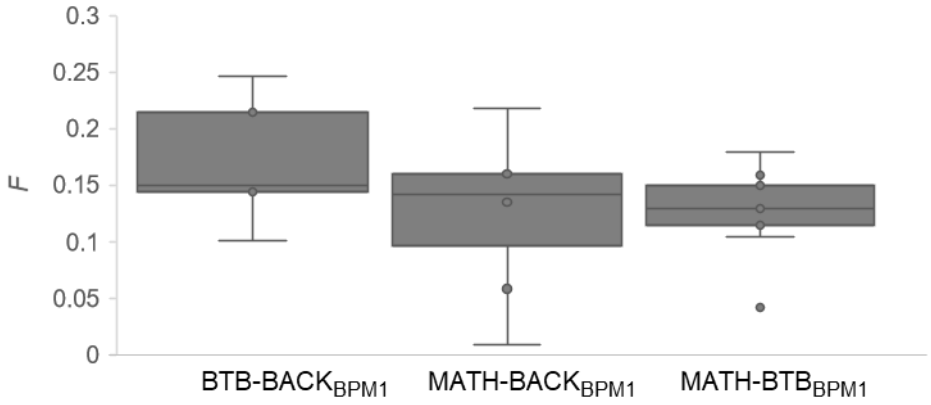

Figure 28 Fraction of fluorescent donor molecules that undergo FRET (F) for EGFP-BPM1 deletion variants in combination with mRFP1-RDM1. All BPM1 deletion variants can interact in vivo with RDM1. Box-plot shows median F values with indicated interquartile interval, whiskers indicating minimum and maximum measured values. There was no significant difference (Tukey's HSD/Kramer test, $p < 0.05$) between the tested groups. For details see **Appendix F Chapter F6 Table F6-1**.

4.12. BPM1 reduces promoter activity of RdDM regulated gene *FWA*

In this work, it was shown that BPM1 protein is involved in the BPM1 interaction with DMS3 and RDM1, important components of RdDM, rising a question about the physiological role of these interactions. For this purpose, promoter activity of *FWA*, a gene whose expression is regulated by RdDM in promoter region (Chan et al., 2004; Soppe et al., 2000), was analyzed. To examine the influence of BPM1 on promoter activity of *FWA*, GUS assay was conducted in BPM1 overexpressing plants (oeBPM1-EGFP) and plants with downregulation of *BPM 1*, *4*, *5* and *6* (amiR-bpm). First, *A. thaliana* WT plants transformed with *pFWA::GUS* expression cassette were analyzed to select the best lines and determine the most suitable tissues for analysis. Two lines, pFWA::GUS 1-4 and pFWA::GUS 1-12 were selected and rosette leaves proved to be the best for histochemical X-Gluc staining. Blue coloring was observed through vascular tissue: in hydathodes of leaf tips and leaf serrations, in primary leaf vein and scarcely in lateral veins (**Figure 29**).

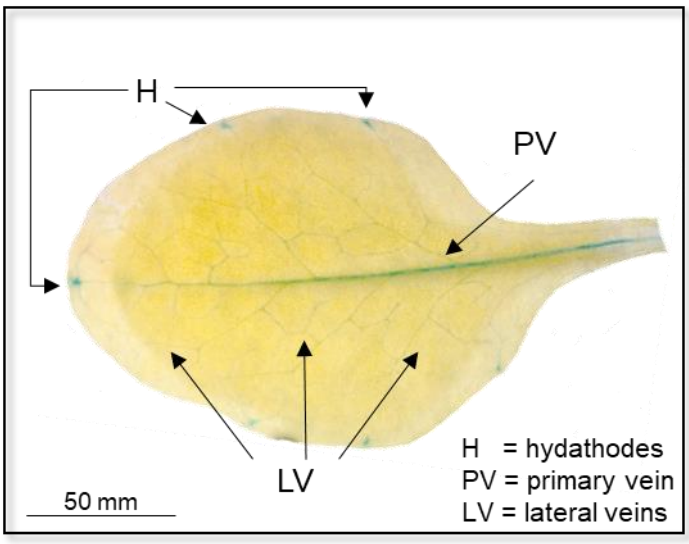

Figure 29 *pFWA* promoter activity in one of the selected lines, pFWA::GUS 1-4. Blue staining is visible in vascular tissue of *A. thaliana* rosette leaf, precisely in hydathodes (H), primary leaf vein (PV) and in lateral veins (LV). Scale bar = 50 mm.

To analyze influence of BPM1 on *pFWA* activity, selected lines were crossed with oeBPM1-EGFP and amiR-bpm lines thus generating BPM-reporter lines. Furthermore, selected lines were also crossed with oeEGFP-DMS3 line and *dms3-1* mutant line thus generating DMS3-reporting lines to visualize RdDM-influenced pattern of GUS staining. Stronger coloring observed in GUS assay reflects higher promoter activity. Images and normalized results of promoter activity represented as heatmaps are presented in **Figure 30** (for heatmap legend see **Figure 30 A**). As a control and for normalization of obtained GUS activity results, pFWA::GUS

lines were crossed with WT (for normalization of pFWA::GUS × oeBPM1-EGFP, pFWA::GUS × amiR-bpm and pFWA::GUS × oeEGFP-DMS3) or self-pollinated to obtain plants homozygous for *pFWA::GUS* T-DNA insertions (T3 generation). Control lines (crossings: pFWA::GUS 1-4 × WT and pFWA::GUS 1-12 × WT, and pFWA::GUS 1-4 homozygous plants) were displayed as 1 (**Figure 30 B** and **E**). The highest *pFWA* promoter activity was measured in pFWA::GUS × amiR-bpm plants with intense blue coloring observed inside entire leaf vasculature, in leaf hydathodes and through leaf mesophyll (**Figure 30 C**). When normalized, promoter activity of pFWA::GUS × amiR-bpm appears to be 1.45 times higher than that obtained for the pFWA::GUS 1-4 × WT, and 1.34 times higher than that of the pFWA::GUS 1-12 × WT. Significantly lower promoter activity was observed for pFWA::GUS × oeBPM1-EGFP plants and it was estimated to 0.84 of the control value for crossing with pFWA::GUS 1-4 and 0.98 of the control value for pFWA::GUS 1-12 crossing (**Figure 30 D**). Similar values were obtained for pFWA::GUS × oeEGFP-DMS3 where crossing with pFWA::GUS 1-4 resulted in 0.75 of the control value, and crossing with pFWA::GUS 1-12 resulted in 1.01 of the control value (**Figure 30 G)**. pFWA::GUS × *dms3-1* had slightly higher promoter activity (1.11, **Figure 30 F**) than pFWA::GUS 1-4 homozygous plants (**Figure 30 E**) but without statistical significance (**Appendix F Chapter F7 Figure F7-1 B**).

Overall, results of the promoter analysis indicated involvement of BPM1 in regulation of *FWA* gene expression, where *BPM1* overexpression led to reduction in promoter activity of *FWA*, similar as does overexpression of *DMS3*, while downregulation of *BPM* genes led to the enhanced promoter activity that resulted in even greater activity than inactive DMS3 protein. The overlapping trend of BPM1 and DMS3 effect on *FWA* promoter activity, together with the known role of DMS3 in RdDM (Law et al., 2010) and the known effect of RdDM on *pFWA* activity (Chan et al., 2004; Soppe et al., 2000), supports the assumption that DMS3 is not degraded by BPM1-mediated CUL3-dependent protein degradation.

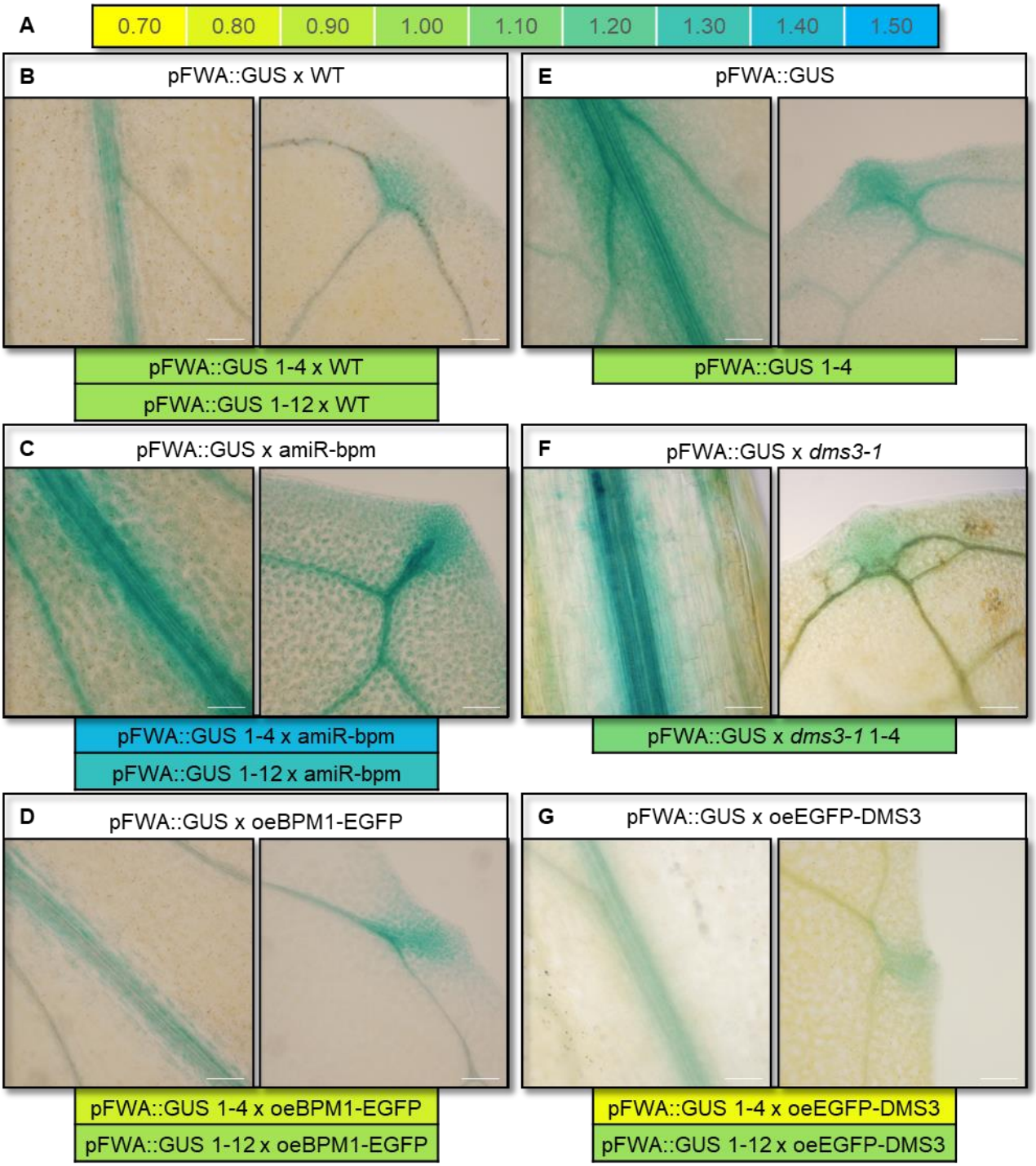

Figure 30 *FWA* gene promoter activity visualized by histochemical GUS staining in *Arabidopsis thaliana* leaves. **A**) Heatmap legend showing spectrum of normalized values and their relation to colors. Shown are images (primary vein and hydathode) of crossed lines: pFWA::GUS × WT (**B**), pFWA::GUS × amiR-bpm (**C**), pFWA::GUS × oeBPM1-EGFP (**D**), pFWA::GUS T3 homozygotes (**E**), pFWA::GUS × *dms3-1* (**F**) and pFWA::GUS × oeEGFP-DMS3 (**G**). Scale bar = 100 µm. Beneath every pair of images is a heatmap reflecting level of promoter activity in designated reporter lines (pFWA::GUS 1-4 and pFWA::GUS 1-12 crossed with WT, amiR-bpm, oeBPM1-EGFP or oeEGFP-DMS3, and pFWA::GUS 1-4 T3 generation or crossed with *dms3-1*). Bar plots with indicated measured mean values, standard deviation and statistical analysis are shown in **Appendix F Chapter F7 Figure F7-1**.

5. DISCUSSION

It is known that the MATH-BTB proteins are mainly responsible for CUL3-mediated proteasomal degradation (Gingerich et al., 2007; Pintard et al., 2003). In addition, the *Arabidopsis* MATH-BTB protein family (the BPM protein family) is involved in the regulation of transcription mediated by proteasomal degradation of various TFs, and is thus responsible for accurate plant development and stress response (Al-Saharin et al., 2022). This work reports a novel CUL3-independent role of *Arabidopsis* MATH-BTB protein BPM1 and possibly other MATH-BTB proteins in RNA-directed DNA methylation (RdDM). The RdDM is an important epigenetic mechanism of *de novo* DNA methylation that plays an important role in transposon control, stress response, reproduction, and genomic imprinting during embryogenesis (Matzke & Mosher, 2014). BPM1 was involved in RdDM via interaction with DMS3 and RDM1, two crucial components of the DDR complex responsible for the correct positioning of RdDM machinery at targeted genomic loci (Zhong et al., 2012). Subcellular colocalization and direct protein-protein interactions between BPM1 and both DMS3 and RDM1 were demonstrated by several different approaches. Given the known role of BPM1 in protein degradation, it was expected that BPM1 would also play a role here in the degradation of DMS3 and RDM1. Since stoichiometric balance between the components of the DDR complex is essential for its proper function, this interaction would directly link BPM1 to RdDM regulation. As a first step to clarify the role of BPM1 in RdDM regulation, domain-specific interactions with DMS3 and RDM1 were tested. The interactions were mediated not exclusively by the substrate-targeting MATH domain but also by the CUL3-binding BTB domain, indicating a cullin-independent function of BPM1 in the regulation of proteins involved in RdDM.

The newly discovered role of BPM1 protein in RdDM, as well as its known functions in CUL3-mediated protein degradation, raised the question of the regulation of BPM1 functionality. BPM1 was found to be regulated at multiple levels, from pre-translational RNA silencing and post-translational self-regulation to homo- and heterodimerization, providing the basis for its physiological function either in the CRL3 complex or in the integrative regulation of transcription and methylation suggested by the results of this research.

5.1. Pre-translational and post-translational self-regulation of BPM1

The *Arabidopsis* MATH-BTB proteins BPM1 and BPM3 have been previously characterized as unstable due to their rapid turnover via the proteasome degradation pathways (Chico et al., 2020; Škiljaica et al., 2020). For both proteins, it was shown that despite their overexpression by the strong 35S promoter, only very low protein levels can be detected in cells. Moreover, their stability is shown to be strongly influenced by environmental conditions. Detailed analysis of BPM1 stability shows that darkness and salt stress promote BPM1 degradation, whereas elevated temperature promotes BPM1 stabilization and accumulation (Škiljaica et al., 2020). Moreover, the addition of jasmonates strongly stabilizes the otherwise unstable BPM3, while the same treatment has no effect on BPM6, which is generally found to be more stable (Chico et al., 2020). In this work, the BPM1 transgene was shown to be unstable *in planta* in BPM1-overexpressing transgenic lines (oeBPM1-EGFP and oeBPM1-TAP), but also in BY-2 cells, in which the *EGFP-BPM1* transgene was transiently expressed. To elucidate the background of this instability, the protein synthesis inhibitor CHX and the proteasome inhibitor MG132 were used. CHX interferes with the translocation step, leading to an obstruction of transcriptional elongation (Lawana et al., 2014). When the tissue is treated with CHX, no new protein synthesis occurs, so protein levels reflect the translational state of the cells at the time of sampling. After *Arabidopsis* seedlings were treated with CHX for only 1 h at 24 °C, no BPM1 protein was detected, confirming the rapid turnover of BPM1. However, increasing the temperature to 37 °C stabilized the protein, and some BPM1 was detected even after 3 h of CHX treatment. When protein synthesis was inhibited at 24 °C, *BPM1* transcript levels were significantly increased in both WT and oeBPM1-EGFP, but there was no change in expression when seedlings were exposed to 37 °C. This finding could be explained by a kind of protein self-regulation at the level of transcription. When a protein, in this case BPM1, is not present in the cell due to inhibition of its synthesis and rapid turnover, expression is increased to compensate for the missing protein. The mechanism of BPM1 self-regulation could be a feedback regulation (Roy et al., 2020) in which BPM1 targets its own TF for proteasomal degradation to ensure its appropriate level and function. However, this assumption only applies to transcription from the native BPM1 promoter. However, in this work, the same trend was observed for the constitutive CaMV 35S promoter-controlled *BPM1-EGFP* transgene. This suggests additional post-transcriptional control of *BPM1* expression, potentially mediated by RNA silencing. RNA silencing plays an important role in plant development and in response to viral infection, transgene overexpression, and abiotic stress (Brodersen & Voinnet, 2006). In

the case of post-transcriptional regulation, translation inhibited by CHX would firstly lead to increased expression of a number of genes, including BPM1, and secondly, elevated temperature as an abiotic stressor would trigger specific RNA silencing and cleavage of the *BPM1* mRNA transcript, thereby normalizing its expression levels. Post-transcriptional regulation could also be the cause of the reduced *BPM1-EGFP* transgene expression at 37 °C in the conditions of normal protein translation.

Consistent with the idea of post-transcriptional RNA silencing, Huang et al. (2021) showed that *Arabidopsis* PUMILIO PROTEIN24 (APUM24), an atypical Pum and FBF (PUF) protein, reduces the mRNA stability of all *BPM* transcripts. PUF proteins are known to play a role in ribosomal RNA processing, mRNA stability and translation (Abbasi et al., 2010; Wickens et al., 2002). Because APUM24 localizes to the nucleolus and negatively affects *BPM* transcription levels, but has no direct effect on protein levels, it most likely plays a role in RNA processing rather than translation (Huang et al., 2021; Shanmugam et al., 2017). The exact mechanism of APUM24-mediated regulation of *BPM* transcripts and whether it is influenced by elevated temperature or the *BPM1* transgene remain to be elucidated. On the other hand, Santos et al. (2019) reported rapid CHX-induced transcription of genes involved in ribosome biogenesis in budding yeast, while Bauer et al. (2019) reported a possible interaction of the wheat MATH-BTB protein TaMAB2 with proteins involved in translation, mainly the eukaryotic translation factors eIF3A, eIF3C, IF-2, and the 30S ribosomal protein S9. In this experiment, the oeBPM1-TAP line is used as a control, and the same putative interactors are identified. As mentioned by Santos et al. (2019), CHX treatment is expected to lead to increased transcription of the detected translation initiation factors. If BPM1 is involved in the regulation of the above translation initiation factors, the upregulation of *BPM1* could occur in the same package.

Persistent BPM1 protein levels after CHX treatment at 37 °C together with the absence of BPM1 after CHX treatment at 24 °C indicated important regulation of BPM1 either at the level of protein synthesis or protein degradation. The induced accumulation of BPM1-EGFP in the root tips of oeBPM1-EGFP seedlings treated with the proteasome inhibitor MG132 or the CUL neddylation inhibitor MLN4924 suggests that the degradation of BPM1 is mediated through the ubiquitin-proteasome pathway (Škiljaica et al., 2020). It remains unclear whether this degradation occurs via CUL3 or another E3 ligase pathway. The MATH-recognizing SBC-like motif (Morimoto et al., 2017) was found upstream of the MATH domain of BPM1, suggesting that BPM1 might be degraded via the CRL3 pathway with BPM protein as a substrate specificity module ($CRL3^{BPM}$). On the other hand, an N-terminal DSGxxT phosphodegron

(resembling the canonical DSGxxS) located within the MATH domain of BPM1 might be sufficient to recruit CRL1 and initiate CUL1-mediated ubiquitination and subsequent degradation (Leljak Levanić et al., 2012). There are few recent studies on dimerization quality control that monitors and prevents aberrant dimerization of BTB proteins undergoing CRL1 mediated degradation (Mena et al., 2018, 2020; Padovani et al., 2022). It seems that mainly BTB homodimers act as functional adaptors of CUL3 ligases, whereas extensive BTB domain conservation leads to the frequent formation of inactive heterodimers that fail to stabilize an intermolecular β-sheet around a highly divergent sequence in the BTB domain (Mena et al., 2020), and proper stoichiometry of the CRL3 complex is crucial for its stability and functionality (Padovani et al., 2022). *Arabidopsis* BPM proteins are capable of forming heterodimers with each other (Weber et al., 2005), but their functionality and stability have not yet been tested.

In this work, the effect of MG132, a potent but reversible 26S proteasome degradation inhibitor (Lee & Goldberg, 1996), on the stability of BPM1 and its domain-omitted variants was analyzed in BY-2 cells. Compared with the untreated control, inhibition of 26S proteasome degradation resulted in more BY-2 cells expressing fluorescently labeled full-length BPM1 or BTB domain-containing variants (BTB-BACK$_{BPM1}$ and MATH-BTB$_{BPM1}$). No effect of MG132 on protein stability of the BTB-domain omitted variant (MATH-BACK$_{BPM1}$) was observed. The BTB domain is a CUL3-binding domain (Weber et al., 2005), so, as expected, BPM1 lacking the BTB domain was unable to assemble the CUL3 E3 ligase complex (nor the BPM1 homodimer, as will be discussed later), thereby losing its ubiquitination and self-ubiquitination activity. On the other hand, the BTB-omitted protein variant with the phosphodegron-containing MATH domain (MATH-BACK$_{BPM1}$) was probably unable to recruit the CUL1-mediated E3 ligase, as this would lead to an increased number of fluorescent cells after MG132 treatment. In contrast, no degradation of MATH-BACK$_{BPM1}$ was observed, suggesting overall self-regulated auto-ubiquitination and degradation of BPM1 via the CUL3-mediated degradation pathway. The increase in the number of cells expressing fluorescently labeled BTB-BACK$_{BPM1}$, a variant lacking the phosphodegron-containing MATH domain, after treatment with MG132 also confirmed that degradation does not occur via the phosphodegron-dependent CUL1 E3 ligase.

In cells expressing full-length BPM1 and the MATH-BTB$_{BPM1}$ variant, MG132 had the greatest effect on stabilizing the protein, suggesting that both the MATH and BTB domains are essential for efficient self-regulation. In addition, Lee and Goldberg (1996) report loss of the

inhibitory effect of MG132 after 4-5 h of incubation and subsequent recovery of proteasomal degradation activity. This was also the case in this work, as six hours after addition of MG132, the effect of the proteasome inhibitor wore off, and the number of fluorescent cells decreased in both cases (MG132 treatment and control). Protein variants lacking either the BTB or MATH domain but containing the BACK domain (BTB-BACK$_{BPM1}$ and MATH-BACK$_{BPM1}$) were found to be more stable over time and more resistant to proteasomal degradation. Although there are limited data on the role of the BACK domain in plants, it is proposed that the BACK domain in human SPOP ensures the proper orientation of substrate proteins within the CUL3-based E3 ligase complex and fine-tunes E3 ligase activity (Errington et al., 2012; Stogios & Privé, 2004).

5.2. BPM1 functions are facilitated by its subcellular localization

The subcellular localization of all six *Arabidopsis* BPM proteins in tobacco epidermal cells was previously described in Weber & Hellmann (2009). According to these data, BPM1 and BPM2 localize mainly in the nucleus, BPM3-5 in the cytosol and nucleus, and BPM4 exclusively in the cytosol. The different subcellular localization is likely related to the different localization of BPM substrates. Transcription factors RAP2.4, WRI1, DREB2a belonging to the AP2/ERF family, the Hd-Zip/HB TF family member HB6, and the bHLH TFs MYC2-4 are mainly localized in the nucleus (Chen et al., 2013; Fernández-Calvo et al., 2011; Himmelbach et al., 2002; Lorenzo et al., 2004; Morimoto et al., 2013; Weber & Hellmann, 2009; Withers et al., 2012). The R2R3 MYB members MYB25 and MYB109 and PP2CA are localized in nuclear speckles, which are assumed to be the sites of active transcription (Beathard et al., 2021; Julian et al., 2019), whereas the R2R3 MYB members, MYB56 and MYB1, are localized in the nucleus and cytosol (Beathard et al., 2021; Chen et al., 2015). The common interactor of almost all functionally characterized BPM proteins, CUL3, is localized in the cytoplasm and nucleus but not in the nucleolus, suggesting that substrate proteins may be ubiquitinated in the cytoplasm and nucleus and possibly marked for degradation by the 26S proteasome (Leljak Levanić et al., 2012; Weber & Hellmann, 2009). To investigate how specific BPM1 domains affect the subcellular localization of the protein, full-length BPM1 and its domain-omitted variants were fluorescently labeled. In addition, bimolecular fluorescence complementation (BiFC) was used to assess the ability of all the above BPM1 variants to form homodimers and to determine the subcellular localization of these interactions. BiFC is a method based on complementation between two non-fluorescent YFP fragments brought together by interactions

between the tested proteins fused to each fragment (Hu et al., 2002). When and where the BPM1 homodimer is formed, the YFP signal is observed. Both the full-length BPM1 protein and the full-length BPM1 homodimers were mainly localized in the nucleus and cytoplasm of BY-2 cells, with a stronger signal in the nucleus including the nucleolus and a weaker signal in the cytoplasm, suggesting that homodimerization is an important step in the nucleus-related downstream functions of BPM1. Additionally, a considerable number of agglomerates were observed around and within the nucleolus. The same pattern of subcellular localization was observed by Leljak Levanić et al. (2012), and a bipartite nuclear localization signal at the C-terminal end of BPM1 was sufficient to bring the protein into the nucleus and nucleolus. In addition, two nuclear export signals were found, one within the BTB domain and another within the BACK domain, but their significance for subcellular localization remains to be determined. The presence or absence of a specific BPM1 domain also affected subcellular localization. The BTB-BACK$_{BPM1}$ variant containing both domains involved in CUL3 binding was predominantly localized only in the nucleus, whereas variants containing the substrate-binding MATH domain (MATH-BTB$_{BPM1}$ and MATH-BACK$_{BPM1}$) were dispersed through the cytoplasm and nucleus. Moreover, the absence of the MATH domain resulted in nuclear-only localization of a homodimer. This result suggests a preferential nuclear localization of the CUL3-BPM1 assembly, whereas various BPM1 substrates alter the localization of the CRL3^{BPM1} complex with the respect to their subcellular localization. Moreover, no homodimers were observed between the BTB-less MATH-BACK$_{BPM1}$ variant. This was expected since BPM1 homodimer formation is mediated by the BTB domain (Weber et al., 2005). As mentioned earlier, the BTB domain was also shown to be essential for self-regulation of BPM1 turnover and thus functional availability. Interestingly, the absence of the BACK domain in the MATH-BTB$_{BPM1}$ protein variant resulted in more protein in or around the nucleolus where CUL3 is not present (Leljak Levanić et al., 2012). Accordingly, MATH-BTB$_{BPM1}$ homodimers localized exclusively to the nucleus, with the predominant signal found in the nucleolus. This suggested that MATH and BTB might have other interactors besides CUL3 and potentially CUL3-independent functions. The best studied process occurring in the nucleolus is ribosome biogenesis (Muñoz-Díaz & Sáez-Vásquez, 2022), again suggesting possible involvement of MATH-BTB proteins in regulating the protein translation machinery (Bauer et al., 2019), but this connection remains to be explored. Besides nucleolus, nuclear speckles are another type of nuclear body in which the observed BPM1 accumulation has been localized. Various splicing factors, transcription factors, and 3’ processing factors are stored in

the nuclear speckles (Lorković et al., 2008; Muñoz-Díaz & Sáez-Vásquez, 2022), and among others, the known BPM targets MYB25, MYB109 and PP2CA are localized there (Beathard et al., 2021; Julian et al., 2019). Another interesting sub-compartment of the nucleus are Cajal bodies, considering the BPM1 agglomerates found within and around the nucleolus. Cajal bodies are dynamic membraneless organelles that are associated with the nucleolus and can move into or out of it (Muñoz-Díaz & Sáez-Vásquez, 2022). Some known functions that occur in these compartments are biogenesis of small RNAs (small nuclear RNAs, micro RNAs and siRNAs), formation of spliceosomal particles, and gene silencing (Muñoz-Díaz & Sáez-Vásquez, 2022; Pontes & Pikaard, 2008). Membraneless organelles, such as nucleoli, Cajal bodies, and nuclear speckles, potentially control and accelerate biochemical reactions through their spatiotemporal compartmentalization (Gomes & Shorter, 2019). They are formed by a liquid-liquid phase separation process that leads to a substantial increase in the concentration of certain molecules within the organelle (Li et al., 2012). A common feature of proteins that undergo phase separation in a biologically meaningful manner is the presence of multivalent binding domains, and MATH-BTB proteins fit this description (Gomes & Shorter, 2019; Pierce et al., 2016). Multivalency increases with the protein's ability to oligomerize and can result from protein-protein interactions between ordered domains, but also from intrinsically disordered domains that often contain multiple short-linear motifs (Li et al., 2012; Pierce et al., 2016).

With the aim of elucidating the diverse localization patterns of the BPM1 protein, new BPM1 functions, and the potential influence of yet unknown BPM1 partners on its subcellular localization, mass spectrometry analysis was performed after tandem affinity purification of BPM1 interaction complexes. Lines overexpressing BPM1 (oeBPM1-TAP and oeBPM1-EGFP) were used. Expression of *BPM1* occurred under the constitutive CaMV 35S promoter, but the promoter in the oeBPM1-TAP line was simple, so the level of BPM1 overexpression was low and the plants resembled the WT phenotype. In contrast, *BPM1* in the oeBPM1-EGFP line was expressed by an enhanced promoter, so the increase in mRNA transcription was significant and the plant phenotype is considerably pronounced (disordered rosette and flower development, Škiljaica et al., 2020). The two lines were used to overcome a potential influence of the overexpressed transgenic protein on protein interactions with potential endogenous partners as pointed by Amack & Antunes (2020). In view of the above, fewer potential partners were identified for BPM1-EGFP than for BPM1-TAP, but none of the identified proteins belonged to the CRL3 complex. In addition, a strict selection was made and all interactors in common with the control MATH-BTB protein TaMAB2 were excluded. In both analyzes,

DMS3 and RDM1, essential parts of the DDR complex involved in the correct positioning of the RdDM machinery at the target loci (Matzke & Mosher, 2014; Wongpalee et al., 2019), were found to be the BPM1-specific interactors. DMS3 and RDM1 are both predicted to be localized in the nucleus, but their subcellular localization is poorly understood. RDM1 has been shown to interact and colocalize with POL II, AGO4, and DRM2 in the nucleoplasm and with POL V in the perinucleolar processing center (Gao et al., 2010), whereas no data are available on the localization of DMS3. In this work, DMS3 and RDM1 were localized in both the cytoplasm and nucleus of BY-2 cells, but no nucleolar localization was observed. The presence of DMS3 or RDM1 did not affect the subcellular localization of full-length BPM1 protein or the BTB-BACK$_{BPM1}$ variant, and *vice versa*. The presence of RDM1 in cells affected the localization of MATH-containing BPM1 variants and caused them to localize predominantly in the nucleus, suggesting possible shared functions of nuclear fraction of BPM1 and RDM1. The presence of DMS3 increased the proportion of nuclear-only localization of MATH-BTB$_{BPM1}$, whereas it attracted MATH-BACK$_{BPM1}$ more to the cytoplasm, suggesting that DMS3 and BPM1 share some functions within both cellular compartments, nucleus and cytoplasm. The result was more obvious in the epidermal leaf cells of *N. benthamiana*. When expressed in *N. benthamiana* cells, DMS3 and RDM1 shared exclusive nuclear localization with all BPM1 variants, with DMS3 and RDM1 signal dispersed throughout the nucleoplasm, whereas BPM1 signal was more compact in the nucleus, with a frequent tendency to cluster around the nucleolus and possibly concentrate in some of the membraneless nuclear bodies.

5.3. BPM1 positively affects DNA methylation through the interactions with DMS3 and RDM1

As stated before, *Arabidopsis* BPM1-6 proteins are known to bind transcription factors from the AP2/ERF family (Chen et al., 2013; Ma et al., 2015; Morimoto et al., 2017; Phukan et al., 2017; Weber & Hellmann, 2009), Hd-Zip/HB family (Lechner et al., 2011), R2R3 MYB family (Beathard et al., 2021; Chen et al., 2015) and bHLH TF family (Chico et al., 2020). In addition, type 2C protein phosphatases are recognized as substrates for protein degradation mediated by the CUL3^{BPM} E3 ligase (Julian et al., 2019). Until this study, all the aforementioned BPM interactors were shown to be degraded by CUL3-mediated proteasomal degradation pathway (Al-Saharin et al., 2022). In this process, the MATH domain binds specific substrates by recognizing the SBC or SBC-like motif (Morimoto et al., 2017; Zhuang et al., 2009) or PEST motif (Belizario et al., 2008; Mooney et al., 2019), while the BTB domain is required for CUL3 binding and subsequent formation of the CRL3 complex, and for BPM homodimer formation

(Figueroa et al., 2005; Gingerich et al., 2005; Weber et al., 2005). Conserved NH_2-terminal region of CUL3 and eight specific residues (Asp-12, His-25, Ile-52, Ile-54, Asp-56, Asp-101, Tyr-103 and Leu-105) of BPM1's BTB domain are essential for CUL3-BPM1 interaction (Škiljaica, 2022; Weber et al., 2005).

In this work, the direct interaction of BPM1 with DMS3 and RDM1 was demonstrated using four different approaches (qualitative and quantitative Y2H experiments, pull-down and MST). In Y2H, reverse protein-tag orientations were tried, but the interaction occurred only when BPM1 was fused to the GAL4 activating domain, whereas no interaction occurred when BPM1 was fused to the DNA binding domain (data not shown). The positive control, DMS3 and RDM1, confirmed a strong interaction independent of tag orientations, as shown in Sasaki et al. (2014). The lack of interaction could be due to possible misfolding of BPM1 with a particular tag or due to steric constraints of the particular protein tag that may impose on the GAL4 reporter system (Striebinger et al., 2013). In addition, several attempts to purify His-tagged BPM1 and its deletion variants for pull-down assay with GST-tagged DMS3 or RDM1 are made, but nothing resulted in successful purification. Induction of expression of full-length BPM1 and MATH-$BACK_{BPM1}$ variant was unsuccessful, whereas BTB-$BACK_{BPM1}$ was insoluble and detected only in the inclusion bodies in the pellet (Miškec, 2019). Although induction was successful for the GST-tagged BPM1 variants, large differences in the amount of purified protein were observed in this work. GST-BTB-$BACK_{BPM1}$ was stable, excessively expressed, and soluble, so it was easily purified in large amounts. On the other hand, GST-MATH-$BACK_{BPM1}$ appeared to be destabilized, poorly expressed, and still very insoluble, so it was obtained in much smaller amounts. The difficulties encountered in this work led to the assumption that the correct folding of BPM1 was influenced by the fused tag and that it contributed greatly to the stability of the protein and its ability to participate in various interactions. In addition, colocalization of BPM1 with DMS3 or RDM1 was detected in the nucleus. Because colocalization itself cannot indicate whether two proteins are interacting but only that they are both tightly localized in a particular region (Dunn et al., 2011), the fifth interaction analysis was performed using FRET-FLIM *in planta*. The advantages of FRET-FLIM compared with used biochemical methods are that it is performed *in vivo* in plant cells, is highly sensitive and specific, and provides information about the location of interaction (Cui et al., 2019). Thus, interactions between BPM1 and DMS3 and BPM1 and RDM1 were confirmed within the nucleus. Again, the proper folding of BPM1 and the influence of the tag on the ability to interact came to the fore. Different tags (EGFP or mRFP1) and their orientations

showed different results, and only when EGFP was N-terminally fused to BPM1 (EGFP-BPM1) did the protein show interaction with DMS3 or RDM1. Other orientations were ambiguous, which is not unusual because the relative position of the fluorophores with respect to the labeled proteins (N- or C-terminal fusion) contributes differently to the overall FRET effect (Radić et al., 2020) and BPM1 has already been shown to be sensitive to improper folding and the presence of different tags.

The interaction with RDM1 was mediated by the BTB domain of BPM1, with a significant contribution from the MATH domain. There is a potential 24 amino acid long PEST motif in the RDM1 protein sequence (between positions 10 and 35, predicted by https://emboss.bioinformatics.nl/cgi-bin/emboss/epestfind) that could explain the interaction with the MATH domain. Since the MATH domain targets substrates for ubiquitination and subsequent proteasomal degradation (Chen et al., 2013; Lechner et al., 2011; Weber & Hellmann, 2009; Zhuang et al., 2009), one would expect the same fate for RDM1. However, in Jagić et al. (2022), the indirect effect of BPM1 on EGFP-RDM1 levels is analyzed under BPM1-stabilizing conditions (37 °C) and no changes are observed compared with the control conditions, suggesting that RDM1 is not degraded under these conditions. Moreover, in the same work, EGFP-RDM1 ubiquitination is tested with the anti-Ubiquitin antibody, indicating that EGFP-RDM1 is not ubiquitinated in the RDM1 overexpressing line. In addition, the higher affinity of the BTB domain for interaction with RDM1 in Y2H quantitative assay, compared with the full-length BPM1 (or any other deletion variant), pointed to the potential competition between CUL3 and RDM1 for interaction with BPM1, giving BPM1 a potentially important role in balancing protein degradation and DNA methylation.

Furthermore, it was found that interaction with DMS3 is preferentially mediated by the MATH domain, although neither the SBC nor the PEST motif is present in the DMS3 protein sequence. Considering that the MATH domain is responsible for substrate targeting in the CRL3 ubiquitination pathway, the simplest explanation would be that DMS3 is ubiquitinated and degraded via this pathway. In contrast, the protein levels of endogenous DMS3 protein were not affected by BPM1 overexpression in the *Arabidopsis thaliana* seedlings, whereas the effect of DMS3 and BPM1 overexpression on the RdDM-regulated promoter of the *FWA* gene was similar. Methylation in the promoter region of *FWA* leads to transcriptional silencing, whereas hypomethylation in the same region leads to upregulation of *FWA* expression (Dai et al., 2021; Greenberg et al., 2011; Soppe et al., 2000). If DMS3 was degraded by the $CRL3^{BPM1}$ pathway, a decrease in endogenous DMS3 protein levels in the BPM1-overexpressing line (compared to WT) would be expected, and the effect of DMS3 overexpression on *pFWA* would

be in contrast to the effect of BPM1 overexpression. The expected increased degradation of DMS3 in the oeBPM1-EGFP line would lead to disturbed stoichiometric balance of the DDR complex, because proper formation of DMS3-RDM1 is essential for the complex assembly (Wongpalee et al., 2019), so RdDM levels would decrease and the *pFWA* promoter would be more active. In contrast, the results of this study showed a decrease in *FWA* promoter activity in the BPM1 and DMS3 overexpressing lines, whereas it was slightly increased in the *dms3-1* mutant line. On the other hand, promoter activity was significantly increased in the line with downregulation of four of the six BPM proteins (amiR-bpm). Moreover, in Jagić et al. (2022), DNA methylation in the proximal promoter region of *FWA* is analyzed and the increase in the total number of methylated cytosines was found in the oeBPM1-EGFP line compared with WT, along with an increase in CHH methylation, which is an indicator of the RdDM pathway. In contrast, methylation is significantly reduced in the *dms3-1* mutant line in all methylation contexts. In addition, an increase in EGFP-DMS3 signal is detected in the roots of the DMS3 overexpressing line when seedlings were treated at a BPM1-stabilizing temperature (37 °C). moreover, the EGFP-DMS3 protein is found to be ubiquitinated in the *cul3hyp* genetic background (Jagić et al., 2022), which has reduced function of the CUL3-based E3 ligase (Thomann et al., 2009). Furthermore, Zhong et al. (2019) showed that DMS3 is ubiquitinated and degraded via the APC/C pathway. All in all, interaction of BPM1 with DMS3 did not lead to the degradation of DMS3 despite its preferential binding to the MATH domain, again putting the BPM1 somewhere in between proteasomal degradation and *de novo* DNA methylation.

Although the BACK domain showed the least importance in mediating BPM1 interactions with DMS3 or RDM1 in Y2H, it proved to be important for colocalization of BPM1 with both proteins tested. In combination with the main domain responsible for the interaction (MATH-BACK for DMS3 and BTB-BACK for RDM1), the BACK domain led to a higher colocalization coefficient and higher FRET values in the nucleus. *Arabidopsis* BACK domain has not yet been characterized, but when compared with the role of the BACK domain in the human SPOP protein, it is thought to be involved in oligomerization of the protein, interaction with CUL3 and correct orientation of targeted substrates (Errington et al., 2012; Stogios & Privé, 2004).

Finally, it is important to point out that BPM1 was involved in interactions with DMS3 and RDM1 through the BTB domain and even more through the MATH domain, but does not direct these two proteins to proteasomal degradation. Considering that the MATH domain is known to specifically target numerous transcription factors for degradation, whereas the BTB domain binds CUL3 to form an active E3 ligase complex, a certain competition between the two distinct

functions of the BPM1 protein exists. On the one hand, BPM1 recognizes specific TFs and interacts with them, leading to their proteasomal degradation and deactivating their transcriptional activity. On the other hand, BPM1 is involved in the recruitment of the DNA methylation machinery to specific loci. Whether and in what way BPM1 mediates between these two mechanisms and whether TFs and POL II generated transcripts are involved in localization of the POL V methylation machinery through BPM1, as suggested in **Figure 31**, remains to be elucidated.

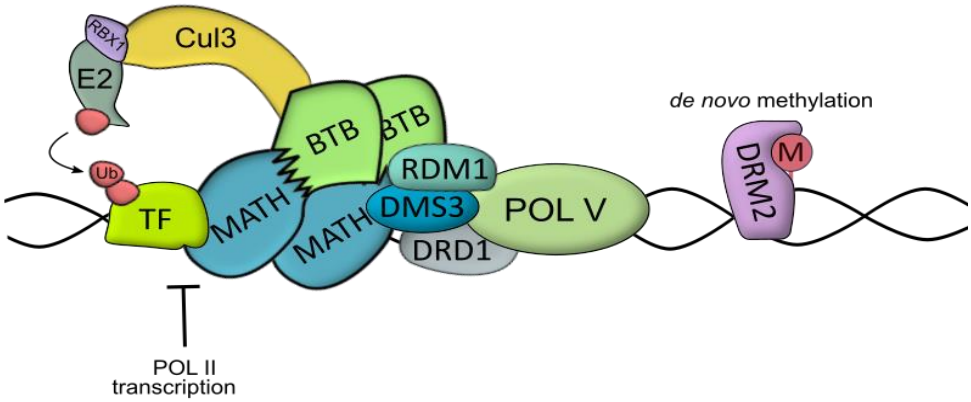

Figure 31. Proposed mechanism of MATH-BTB protein balancing between transcription and DNA methylation. POL II transcription is deactivated by MATH-BTB-mediated TF ubiquitination and subsequent degradation, whereas on the other hand DNA methylation at specific genomic loci is stimulated by MATH-BTB-mediated DDR recruitment of POL V. The MATH-BTB protein is involved in these processes as a homodimer in which the MATH domain serves as a binding module for TF on one side and DMS3 on the other, while the BTB domain binds CUL3 on one side and RDM1 on the other facilitated by the MATH domain. Generated in Inkscape vector graphics editor.

Whether BPM1 participates in the interactions with DMS3 and RDM1 as an oligomer, whether DMS3 and RDM1 are involved in the interaction as homodimers, and whether the established DMS3-RDM1 complex, which is a prerequisite for the full DDR complex assembly (Wongpalee et al., 2019), interacts with BPM1 remains to be determined. The BACK domain may be involved here in appropriate orientation of the proteins in the BPM1-DMS3-RDM1 assembly, as BPM1 has been shown to be sensitive to misguided orientation and protein misfolding.

Increase in global DNA methylation in BPM1-overexpressing plants, increase in DNA methylation of RdDM-targeted promoter regions of *FWA* and *CML41* genes (Baev et al., 2010; Soppe et al., 2000) in the same plants, as well as an increase in DNA methylation of *FBW2*, *RKP*, and *AGL14* regions that overlapped between BPM1 and DMS3 in chromatin immunoprecipitation analysis (Vuk, 2022), all point to the stimulatory role of BPM1 on RdDM activity, whereas the exact mechanism of BPM1 involvement in RdDM remains to be further elucidated.

6. CONCLUSIONS

Based on the presented data, the following conclusions can be drawn:

- The BPM1 protein, and probably other BPMs, have different protein interaction partners and are involved in various fundamental roles in the cell. In addition to its known role in the regulation of transcription by interacting with CUL3 and various TFs, which are then degraded by $CRL3^{BPM}$-mediated proteasomal degradation, BPM1 interacts with DMS3 and RDM1, crucial components of the DDR complex responsible for the precise positioning of RdDM machinery at target loci, thus having a novel role in an RdDM pathway.
- DMS3 and RDM1 are not degraded via the $CRL3^{BPM1}$-26S proteasome pathway and their interactions with BPM1 are independent of BPM1's role in CRL3.
- Differential subcellular localization of BPM1 is mediated by the presence of its domains: the CUL3-binding BTB-BACK domain combination leads to preferential nuclear localization, whereas the substrate-binding MATH domain contributes to a more uniform localization between the nucleus and cytoplasm. The MATH-BTB combination lacking the BACK domain is related to the nucleolar localization of the protein.
- BPM1 is regulated at two levels: probably by RNA silencing and post-translationally by autoubiquitination and subsequent proteasomal degradation. The BTB domain is essential for post-translational self-regulation of BPM1, whereas the BACK domain contributes to the stability of the protein.
- The interaction of BPM1 with DMS3 is predominantly mediated by the substrate-binding MATH domain, but the interaction does not affect endogenous DMS3 protein levels.
- The interaction of BPM1 with RDM1 is predominantly mediated by the BTB domain, with a significant contribution from the MATH domain.
- Interaction of BPM1 with DMS3 and RDM1 *in planta* occurs in the cell nuclei. Subcellular colocalization and interaction with DMS3 is facilitated by MATH-BACK domain combination, whereas colocalization and interaction with RDM1 is facilitated by BTB-BACK domain combination.
- BPM1 reduces the promoter activity of the RdDM-silenced *FWA* gene, indicating a stimulatory role in *de novo* DNA methylation.

7. REFERENCES

Abbasi, N, Kim, HB, Park, N Il, Kim, HS, Kim, YK, Park, Y Il, & Choi, SB. (2010). APUM23, a nucleolar Puf domain protein, is involved in pre-ribosomal RNA processing and normal growth patterning in Arabidopsis. *Plant Journal*, **64** (6), 960-976. https://doi.org/10.1111/j.1365-313X.2010.04393.x

Agatep, R, Kirkpatrick, RD, Parchaliuk, DL, Woods, RA, & Gietz, RD. (1998). Transformation of *Saccharomyces cerevisiae* by the lithium acetate/single-stranded carrier DNA/polyethylene glycol protocol. *Technical Tips Online*, **3** (1), 133-137. https://doi.org/10.1016/s1366-2120(08)70121-1

Al-Saharin, R, Mooney, S, Dissmeyer, N, & Hellmann, H. (2022). Using CRL3^{BPM} E3 ligase substrate recognition sites as tools to impact plant development and stress tolerance in *Arabidopsis thaliana*. *Plant Direct*, **6** (12), 1-14. https://doi.org/10.1002/pld3.474

Amack, SC, & Antunes, MS. (2020). CaMV35S promoter – A plant biology and biotechnology workhorse in the era of synthetic biology. *Current Plant Biology*, **24**, 100179. https://doi.org/10.1016/J.CPB.2020.100179

Aufsatz, W, Mette, MF, Van Der Winden, J, Matzke, AJM, & Matzke, M. (2002). RNA-directed DNA methylation in Arabidopsis. *Proceedings of the National Academy of Sciences of the United States of America*, **99**, 16499-16506. https://doi.org/10.1073/pnas.162371499

Baev, V, Naydenov, M, Apostolova, E, Ivanova, D, Doncheva, S, Minkov, I, & Yahubyan, G. (2010). Identification of RNA-dependent DNA-methylation regulated promoters in Arabidopsis. *Plant Physiology and Biochemistry*, **48** (6), 393-400. https://doi.org/10.1016/J.PLAPHY.2010.03.013

Bartels, A, Han, Q, Nair, P, Stacey, L, Gaynier, H, Mosley, M, Huang, QQ, Pearson, JK, Hsieh, TF, An, YQC, & Xiao, W. (2018). Dynamic DNA methylation in plant growth and development. *International Journal of Molecular Sciences*, **19** (7). https://doi.org/10.3390/ijms19072144

Bauer, N, Škiljaica, A, Malenica, N, Razdorov, G, Klasić, M, Juranić, M, Močibob, M, Sprunck, S, Dresselhaus, T, & Leljak Levanić, D. (2019). The MATH-BTB protein TaMAB2 accumulates in ubiquitin-containing foci and interacts with the translation initiation machinery in Arabidopsis. *Frontiers in Plant Science*, **10**, 1-16. https://doi.org/10.3389/fpls.2019.01469

Beathard, C, Mooney, S, Al-Saharin, R, Goyer, A, & Hellmann, H. (2021). Characterization of *Arabidopsis thaliana* R2R3 S23 MYB transcription factors as novel targets of the ubiquitin proteasome-pathway and regulators of salt stress and abscisic acid response. *Frontiers in Plant Science*, **12**, 1-15. https://doi.org/10.3389/fpls.2021.629208

Belizario, J, Alves, J, Garay-Malpartida, M, & Occhiucci, J. (2008). Coupling caspase cleavage and proteasomal degradation of proteins carrying PEST motif. *Current Protein & Peptide Science*, **9** (3), 210-220. https://doi.org/10.2174/138920308784534023

Béziat, C, Kleine-Vehn, J, & Feraru, E. (2017). Histochemical staining of β-glucuronidase

and its spatial quantification. *Methods in Molecular Biology*, **1497**, 73-80. https://doi.org/10.1007/978-1-4939-6469-7_8

Böhmdorfer, G, Sethuraman, S, Jordan Rowley, M, Krzyszton, M, Hafiz Rothi, M, Bouzit, L, & Wierzbicki, AT. (2016). Long non-coding RNA produced by RNA polymerase V determines boundaries of heterochromatin. *eLife*, **5**, 1-24. https://doi.org/10.7554/eLife.19092

Brodersen, P, & Voinnet, O. (2006). The diversity of RNA silencing pathways in plants. *Trends in Genetics*, **22** (5), 268-280. https://doi.org/10.1016/j.tig.2006.03.003

Bulatov, E, & Ciulli, A. (2015). Targeting Cullin-RING E3 ubiquitin ligases for drug discovery: structure, assembly and small-molecule modulation. *Biochemical Journal*, **467** (3), 365-386. https://doi.org/10.1042/BJ20141450

Canning, P, Cooper, CDO, Krojer, T, Murray, JW, Pike, ACW, Chaikuad, A, Keates, T, Thangaratnarajah, C, Hojzan, V, Ayinampudi, V, Marsden, BD, Gileadi, O, Knapp, S, Von Delft, F, & Bullock, AN. (2013). Structural basis for Cul3 protein assembly with the BTB-Kelch family of E3 ubiquitin ligases. *The Journal of Biological Chemistry*, **288** (11), 7803. https://doi.org/10.1074/JBC.M112.437996

Chaharbakhshi, E, & Jemc, JC. (2016). Broad-complex, Tramtrack, and Bric-à-brac (BTB) Proteins: critical regulators of development. *Genesis*, **54** (10), 505-518. https://doi.org/10.1002/dvg.22964

Chan, SWL, Zilberman, D, Xie, Z, Johansen, LK, Carrington, JC, & Jacobsen, SE. (2004). RNA silencing genes control *de novo* DNA methylation. *Science*, **303** (5662), 1336. https://doi.org/10.1126/science.1095989

Chen, L, Bernhardt, A, Lee, J, & Hellmann, H. (2015). Identification of Arabidopsis MYB56 as a novel substrate for $CRL3^{BPM}$ E3 ligases. *Molecular Plant*, **8** (2), 242-250. https://doi.org/10.1016/j.molp.2014.10.004

Chen, L, Lee, JH, Weber, H, Tohge, T, Witt, S, Roje, S, Fernie, AR, & Hellmann, H. (2013). Arabidopsis BPM proteins function as substrate adaptors to a CULLIN3-based E3 ligase to affect fatty acid metabolism in plants. *The Plant Cell*, **25** (6), 2253-2264. https://doi.org/10.1105/tpc.112.107292

Chico, JM, Lechner, E, Fernandez-Barbero, G, Canibano, E, García-Casado, G, Franco-Zorrilla, JM, Hammann, P, Zamarreño, AM, García-Mina, JM, Rubio, V, Genschik, P, & Solano, R. (2020). $CUL3^{BPM}$ E3 ubiquitin ligases regulate MYC2, MYC3, and MYC4 stability and JA responses. *Proceedings of the National Academy of Sciences*, **117** (11), 6205-6215. https://doi.org/10.1073/pnas.1912199117

Choi, CM, Gray, WM, Mooney, S, & Hellmann, H. (2014). Composition, roles, and regulation of Cullin-based ubiquitin E3 ligases. *The Arabidopsis Book*, **12**, e0175. https://doi.org/10.1199/tab.0175

Clough, SJ, & Bent, AF. (1998). Floral dip: a simplified method for Agrobacterium-mediated transformation of *Arabidopsis thaliana*. *The Plant Journal : For Cell and Molecular Biology*, **16** (6), 735-743. https://doi.org/10.1046/j.1365-313x.1998.00343.x

Collins, GA, & Tansey, WP. (2006). The proteasome: a utility tool for transcription? *Current Opinion in Genetics & Development*, **16** (2), 197-202. https://doi.org/10.1016/J.GDE.2006.02.009

Costes, S V., Daelemans, D, Cho, EH, Dobbin, Z, Pavlakis, G, & Lockett, S. (2004). Automatic and quantitative measurement of protein-protein colocalization in live cells. *Biophysical Journal*, **86** (6), 3993-4003. https://doi.org/10.1529/biophysj.103.038422

Cui, JY, Fu, ZD, & Dempsey, J. (2018). The role of histone methylation and methyltransferases in gene regulation. In *Toxicoepigenetics: Core principles and applications*. Elsevier Inc. https://doi.org/10.1016/B978-0-12-812433-8.00002-2

Cui, Y, Zhang, X, Yu, M, Zhu, Y, Xing, J, & Lin, J. (2019). Techniques for detecting protein-protein interactions in living cells: principles, limitations, and recent progress. *Science China Life Sciences 2019 62:5*, **62** (5), 619-632. https://doi.org/10.1007/S11427-018-9500-7

Dai, X, Wang, J, Song, Y, Liu, Z, Xue, T, Qiao, M, Yu, Y, Xin, W, & Xiang, F. (2021). Cytosine methylation of the FWA promoter promotes direct in vitro shoot regeneration in *Arabidopsis thaliana*. *Journal of Integrative Plant Biology*, **63** (8), 1491-1504. https://doi.org/10.1111/JIPB.13156

Deichmann, U. (2016). Epigenetics: The origins and evolution of a fashionable topic. *Developmental Biology*, **416** (1), 249-254. https://doi.org/10.1016/J.YDBIO.2016.06.005

Di Tomaso, MV, Alberdi, LV, Olsson, D, Cancela, S, Fernández, A, Rosillo, JC, Ábalos, ALR, Zabaleta, MÁ, Calero, M, & Kun, A. (2022). Colocalization analysis of Peripheral Myelin Protein-22 and Lamin-B1 in the Schwann cell nuclei of Wt and TrJ mice. *Biomolecules*, **12** (3), 1-23. https://doi.org/10.3390/biom12030456

Domman, D, Collingro, A, Lagkouvardos, I, Gehre, L, Weinmaier, T, Rattei, T, Subtil, A, & Horn, M. (2014). Massive expansion of ubiquitination-related gene families within the Chlamydiae. *Molecular Biology and Evolution*, **31** (11), 2890-2904. https://doi.org/10.1093/molbev/msu227

Duan, C, Zhang, H, Tang, K, Zhu, X, Qian, W, Hou, Y, Wang, B, Lang, Z, Zhao, Y, Wang, X, Wang, P, Zhou, J, Liang, G, Liu, N, Wang, C, & Zhu, J. (2015). Specific but interdependent functions for Arabidopsis AGO 4 and AGO 6 in RNA-directed DNA methylation. *The EMBO Journal*, **34** (5), 581-592. https://doi.org/10.15252/EMBJ.201489453

Duda, DM, Olszewski, JL, Tron, AE, Hammel, M, Lambert, LJ, Waddell, MB, Mittag, T, DeCaprio, JA, & Schulman, BA. (2012). Structure of a Glomulin-RBX1-CUL1 complex: inhibition of a RING E3 ligase through masking of its E2-binding surface. *Molecular Cell*, **47** (3), 371. https://doi.org/10.1016/J.MOLCEL.2012.05.044

Dunn, KW, Kamocka, MM, & McDonald, JH. (2011). A practical guide to evaluating colocalization in biological microscopy. *American Journal of Physiology - Cell Physiology*, **300** (4), 723-742. https://doi.org/10.1152/ajpcell.00462.2010

Errington, WJ, Khan, MQ, Bueler, SA, Rubinstein, JL, Chakrabartty, A, & Privé, GG. (2012). Adaptor protein self-assembly drives the control of a Cullin-RING ubiquitin

ligase. *Structure*, **20** (7), 1141–1153. https://doi.org/10.1016/J.STR.2012.04.009

Fan, Q, Treder, K, & Miller, WA. (2012). Untranslated regions of diverse plant viral RNAs vary greatly in translation enhancement efficiency. *BMC Biotechnology*, **12** (22), http://www.biomedcentral.com/1472-6750/12/22

Feilotter, HE, Hannon, GJ, Ruddell, CJ, & Beach, D. (1994). Construction of an improved host strain for two hybrid screening. *Nucleic Acids Research*, **22** (8), 1502. https://doi.org/10.1093/NAR/22.8.1502

Felsenfeld, G. (2014). The evolution of epigenetics. *Perspectives in Biology and Medicine*, **57** (1), 132-148. https://doi.org/10.1353/pbm.2014.0004

Fernández-Calvo, P, Chini, A, Fernández-Barbero, G, Chico, JM, Gimenez-Ibanez, S, Geerinck, J, Eeckhout, D, Schweizer, F, Godoy, M, Franco-Zorrilla, JM, Pauwels, L, Witters, E, Puga, MI, Paz-Ares, J, Goossens, A, Reymond, P, de Jaeger, G, & Solano, R. (2011). The Arabidopsis bHLH transcription factors MYC3 and MYC4 are targets of JAZ repressors and act additively with MYC2 in the activation of jasmonate responses. *The Plant Cell*, **23** (2), 701. https://doi.org/10.1105/TPC.110.080788

Figueroa, P, Gusmaroli, G, Serino, G, Habashi, J, Ma, L, Shen, Y, Feng, S, Bostick, M, Callis, J, Hellmann, H, & Xing, WD. (2005). Arabidopsis has two redundant Cullin3 proteins that are essential for embryo development and that interact with RBX1 and BTB proteins to form multisubunit E3 ubiquitin ligase Complexes in Vivo. *The Plant Cell*, **17** (4), 1180. https://doi.org/10.1105/TPC.105.031989

Finley, D. (2009). Recognition and processing of ubiquitin-protein conjugates by the proteasome. *Annual Review of Biochemistry*, **78**, 477-513. https://doi.org/10.1146/annurev.biochem.78.081507.101607

Förster, T. (1948). Zwischenmolekulare Energiewanderung und Fluoreszenz. *Annalen Der Physik*, **437** (1-2), 55-75. https://doi.org/10.1002/ANDP.19484370105

Gao, C, Pallett, MA, Croll, TI, Smith, GL, & Graham, SC. (2019). Molecular basis of cullin-3 (Cul3) ubiquitin ligase subversion by vaccinia virus protein A55. *Journal of Biological Chemistry*, **294** (16), 6416-6429. https://doi.org/10.1074/JBC.RA118.006561

Gao, Z, Liu, HL, Daxinger, L, Pontes, O, He, X, Qian, W, Lin, H, Xie, M, Lorkovic, ZJ, Zhang, S, Miki, D, Zhan, X, Pontier, D, Lagrange, T, Jin, H, Matzke, AJM, Matzke, M, Pikaard, CS, & Zhu, JK. (2010). An RNA polymerase II- and AGO4-associated protein acts in RNA-directed DNA methylation. *Nature*, **465** (7294), 106-109. https://doi.org/10.1038/nature09025

Gatica, D, Lahiri, V, & Klionsky, DJ. (2018). Cargo recognition and degradation by selective autophagy. *Nature Cell Biology*, **20** (3), 233-242. https://doi.org/10.1038/s41556-018-0037-z

Genschik, P, Sumara, I, & Lechner, E. (2013). The emerging family of CULLIN3-RING ubiquitin ligases (CRL3s): cellular functions and disease implications. *EMBO Journal*, **32** (17), 2307-2320. https://doi.org/10.1038/emboj.2013.173

Gilkerson, J, Hu, J, Brown, J, Jones, A, Sun, TP, & Callis, J. (2009). Isolation and

characterization of cul1-7, a recessive allele of CULLIN1 that disrupts SCF function at the C terminus of CUL1 in *Arabidopsis thaliana*. *Genetics*, **181** (3), 945. https://doi.org/10.1534/GENETICS.108.097675

Gilkerson, J, Tam, R, Zhang, A, Dreher, K, & Callis, J. (2016). Cycloheximide assays to measure protein degradation *in vivo* in plants. *BIO-PROTOCOL*, **6** (17). https://doi.org/10.21769/BIOPROTOC.1919

Gingerich, DJ, Gagne, JM, Salter, DW, Hellmann, H, Estelle, M, Ma, L, & Vierstra, RD. (2005). Cullins 3a and 3b assemble with members of the broad complex/tramtrack/ bric-a-brac (BTB) protein family to form essential ubiquitin-protein ligases (E3s) in *Arabidopsis*. *Journal of Biological Chemistry*, **280** (19), 18810-18821. https://doi.org/10.1074/jbc.M413247200

Gingerich, DJ, Hanada, K, Shiu, SH, & Vierstra, RD. (2007). Large-scale, lineage-specific expansion of a bric-a-brac/tramtrack/broad complex ubiquitin-ligase gene family in rice. *Plant Cell*, **19** (8), 2329-2348. https://doi.org/10.1105/tpc.107.051300

Gomes, E, & Shorter, J. (2019). The molecular language of membraneless organelles. *The Journal of Biological Chemistry*, **294** (18), 7115. https://doi.org/10.1074/JBC.TM118.001192

Greenberg, MVC, Ausin, I, Chan, SWL, Cokus, SJ, Cuperus, JT, Feng, S, Law, JA, Chu, C, Pellegrini, M, Carrington, JC, & Jacobsen, SE. (2011). Identification of genes required for *de novo* DNA methylation in Arabidopsis. *Epigenetics*, **6** (3), 344-354. https://doi.org/10.4161/epi.6.3.14242

Haas, AL, Warms, JVB, Hershkog, A, & Rose7, IA. (1982). Ubiquitin-activating enzyme. Mechanism and role in protein-ubiquitin conjugation. *The Journal Of Biological Chemistry*, **257** (5), 2513-2548. https://doi.org/10.1016/S0021-9258(18)34958-5

Han, Q, Bartels, A, Cheng, X, Meyer, A, An, Y-QC, Hsieh, T-F, & Xiao, W. (2019). Epigenetics regulates reproductive development in plants. *Plants*, **8** (12), 564. https://doi.org/10.3390/PLANTS8120564

Harrison, SJ, Mott, EK, Parsley, K, Aspinall, S, Gray, JC, & Cottage, A. (2006). A rapid and robust method of identifying transformed *Arabidopsis thaliana* seedlings following floral dip transformation. *Plant Methods*, **2** (1), 1-7. https://doi.org/10.1186/1746-4811-2-19

Hatakeyama, S, & Nakayama, KII. (2003). U-box proteins as a new family of ubiquitin ligases. *Biochemical and Biophysical Research Communications*, **302** (4), 635-645. https://doi.org/10.1016/S0006-291X(03)00245-6

Hershko, A, & Ciechanover, A. (1998). The ubiquitin system. *Annual Review of Biochemistry*, **67**, 425-479. https://doi.org/10.1038/458421a

Himmelbach, A, Hoffmann, T, Leube, M, Höhener, B, & Grill, E. (2002). Homeodomain protein ATHB6 is a target of the protein phosphatase ABI1 and regulates hormone responses in Arabidopsis. *The EMBO Journal*, **21** (12), 3029. https://doi.org/10.1093/EMBOJ/CDF316

Hu, CD, Chinenov, Y, & Kerppola, TK. (2002). Visualization of interactions among bZIP and Rel family proteins in living cells using bimolecular fluorescence complementation. *Molecular Cell*, **9** (4), 789-798. https://doi.org/10.1016/S1097-2765(02)00496-3

Huang, R, Liu, M, Gong, G, Wu, P, Patra, B, Yuan, L, Qin, H, Wang, X, Wang, G, Liao, H, Gao, L, Yang, C, Li, H, & Zhang, S. (2021). The Pumilio RNA-binding protein APUM24 regulates seed maturation by fine-tuning the BPM-WRI1 module in Arabidopsis. *Journal of Integrative Plant Biology*, **63** (7), 1240-1259. https://doi.org/10.1111/jipb.13092

Huang, Y, Ji, L, Huang, Q, Vassylyev, DG, Chen, X, & Ma, JB. (2009). Structural insights into mechanisms of the small RNA methyltransferase HEN1. *Nature*, **461** (7265), 823. https://doi.org/10.1038/NATURE08433

Huettel, B, Kanno, T, Daxinger, L, Aufsatz, W, Matzke, AJM, & Matzke, M. (2006). Endogenous targets of RNA-directed DNA methylation and Pol IV in Arabidopsis. *EMBO Journal*, **25** (12), 2828-2836. https://doi.org/10.1038/SJ.EMBOJ.7601150

Jagić, M, Vuk, T, Škiljaica, A, Markulin, L, Vičić Bočkor, V, Tokić, M, Miškec, K, Razdorov, G, Habazin, S, Šoštar, M, Weber, I, Bauer, N, & Leljak Levanić, D. (2022). BPM1 regulates RdDM - mediated DNA methylation via a cullin 3 independent mechanism. *Plant Cell Reports*, **3**. https://link.springer.com/article/10.1007/s00299-022-02911-9

Jerabek-Willemsen, M, André, T, Wanner, R, Roth, HM, Duhr, S, Baaske, P, & Breitsprecher, D. (2014). MicroScale Thermophoresis: Interaction analysis and beyond. *Journal of Molecular Structure*, **1077**, 101-113. https://doi.org/10.1016/j.molstruc.2014.03.009

Johnson, LM, Du, J, Hale, CJ, Bischof, S, Feng, S, Chodavarapu, RK, Zhong, X, Marson, G, Pellegrini, M, Segal, DJ, Patel, DJ, & Jacobsen, SE. (2014). SRA-and SET-domain-containing proteins link RNA polymerase V occupancy to DNA methylation. *Nature*, **507** (7490), 124-128. https://doi.org/10.1038/nature12931

Julian, J, Coego, A, Lozano-Juste, J, Lechner, E, Wu, Q, Zhang, X, Merilo, E, Belda-Palazon, B, Park, SY, Cutler, SR, An, C, Genschik, P, & Rodriguez, PL. (2019). The MATH-BTB BPM3 and BPM5 subunits of Cullin3-RING E3 ubiquitin ligases target PP2CA and other clade A PP2Cs for degradation. *Proceedings of the National Academy of Sciences of the United States of America*, **116** (31), 15725-15734. https://doi.org/10.1073/pnas.1908677116

Juranić, M, & Dresselhaus, T. (2014). Phylogenetic analysis of the expansion of the MATH-BTB gene family in the grasses. *Plant Signaling & Behavior*, **9** (4), e28242. https://doi.org/10.4161/PSB.28242

Juranić, M, Srilunchang, K-o, Krohn, NG, Leljak-Levanic, D, Sprunck, S, & Dresselhaus, T. (2012). Germline-specific MATH-BTB substrate adaptor MAB1 regulates spindle length and nuclei identity in maize. *The Plant Cell*, **24** (12), 4974–4991. https://doi.org/10.1105/tpc.112.107169

Kamura, T, Maenaka, K, Kotoshiba, S, Matsumoto, M, Kohda, D, Conaway, RC, Conaway, JW, & Nakayama, KI. (2004). VHL-box and SOCS-box domains determine

binding specificity for Cul2-Rbx1 and Cul5-Rbx2 modules of ubiquitin ligases. *Genes & Development*, **18** (24), 3055. https://doi.org/10.1101/GAD.1252404

Kankel, MW, Ramsey, DE, Stokes, TL, Flowers, SK, Haag, JR, Jeddeloh, JA, Riddle, NC, Verbsky, ML, & Richards, EJ. (2003). Arabidopsis MET1 cytosine methyltransferase mutants. *Genetics*, **163** (3), 1109-1122. https://doi.org/10.1093/genetics/163.3.1109

Kanno, T, Bucher, E, Daxinger, L, Huettel, B, Böhmdorfer, G, Gregor, W, Kreil, DP, Matzke, M, & Matzke, AJM. (2008). A structural-maintenance-of-chromosomes hinge domain-containing protein is required for RNA-directed DNA methylation. *Nature Genetics*, **40** (5), 670-675. https://doi.org/10.1038/ng.119

Kanno, T, Mette, MF, Kreil, DP, Aufsatz, W, Matzke, M, & Matzke, AJM. (2004). Involvement of putative SNF2 chromatin remodeling protein DRD1 in RNA-directed DNA methylation. *Current Biology*, **14** (9), 801-805. https://doi.org/10.1016/J.CUB.2004.04.037

Kekez, M, Bauer, N, Saric, E, & Rokov-Plavec, J. (2016). Exclusive cytosolic localization and broad tRNASer specificity of *Arabidopsis thaliana* seryl-tRNA synthetase. *Journal of Plant Biology*, **59** (1), 44-54. https://doi.org/10.1007/s12374-016-0370-3

Kerscher, O, Felberbaum, R, & Hochstrasser, M. (2006). Modification of proteins by ubiquitin and ubiquitin-like proteins. *Annual Review of Cell and Developmental Biology*, **22**, 159-180. https://doi.org/10.1146/annurev.cellbio.22.010605.093503

Khaminets, A, Behl, C, & Dikic, I. (2016). Ubiquitin-dependent and independent signals in selective autophagy. *Trends in Cell Biology*, **26** (1), 6-16. https://doi.org/10.1016/j.tcb.2015.08.010

Kisselev, AF, Akopian, TN, Woo, KM, & Goldberg, AL. (1999). The sizes of peptides generated from protein by mammalian 26 and 20 S proteasomes. *Journal of Biological Chemistry*, **274** (6), 3363-3371. https://doi.org/10.1074/jbc.274.6.3363

Koncz, C, & Schell, J. (1986). The promoter of TL-DNA gene 5 controls the tissue-specific expression of chimaeric genes carried by a novel type of Agrobacterium binary vector. *Molecular & general genetics*, **204**, 383-396.

Law, JA, Ausin, I, Johnson, LM, Vashisht, AA, Zhu, JK, Wohlschlegel, JA, & Jacobsen, SE. (2010). A protein complex required for Polymerase V transcripts and RNA-directed DNA methylation in Arabidopsis. *Current Biology*, **20** (10), 951-956. https://doi.org/10.1016/j.cub.2010.03.062

Lawana, V, Korrapati, MC, & Mehendale, HM. (2014). Cycloheximide. *Encyclopedia of Toxicology: Third Edition*, 1103–1105. https://doi.org/10.1016/B978-0-12-386454-3.00298-0

Lechner, E, Leonhardt, N, Eisler, H, Parmentier, Y, Alioua, M, Jacquet, H, Leung, J, & Genschik, P. (2011). MATH/BTB CRL3 receptors target the homeodomain-leucine zipper ATHB6 to modulate abscisic acid signaling. *Developmental Cell*, **21** (6), 1116-1128. https://doi.org/10.1016/j.devcel.2011.10.018

Lee, C, Schwartz, MP, Prakash, S, Iwakura, M, & Matouschek, A. (2001). ATP-dependent

proteases degrade their substrates by processively unraveling them from the degradation signal. *Molecular Cell*, **7** (3), 627-637. https://doi.org/10.1016/S1097-2765(01)00209-X

Lee, DH, & Goldberg, AL. (1996). Selective inhibitors of the proteasome-dependent and vacuolar pathways of protein degradation in *Saccharomyces cerevisiae*. *Journal of Biological Chemistry*, **271** (44), 27280-27284. https://doi.org/10.1074/JBC.271.44.27280

Leljak-Levanić, D, Juranić, M, & Sprunck, S. (2013). De novo zygotic transcription in wheat (*Triticum aestivum* L.) includes genes encoding small putative secreted peptides and a protein involved in proteasomal degradation. *Plant Reproduction*, **26** (3), 267-285. https://doi.org/10.1007/s00497-013-0229-4

Leljak Levanić, D, Horvat, T, Martinčić, J, & Bauer, N. (2012). A novel bipartite nuclear localization signal guides BPM1 protein to nucleolus suggesting its Cullin3 independent function. *PLoS ONE*, **7** (12), 1-10. https://doi.org/10.1371/journal.pone.0051184

Lespinet, O, Wolf, YI, Koonin, E V., & Aravind, L. (2002). The role of lineage-specific gene family expansion in the evolution of eukaryotes. *Genome Research*, **12** (7), 1048. https://doi.org/10.1101/GR.174302

Li, P, Banjade, S, Cheng, HC, Kim, S, Chen, B, Guo, L, Llaguno, M, Hollingsworth, J V., King, DS, Banani, SF, Russo, PS, Jiang, QX, Nixon, BT, & Rosen, MK. (2012). Phase transitions in the assembly of multi-valent signaling proteins. *Nature*, **483** (7389), 336. https://doi.org/10.1038/NATURE10879

Lindroth, AM, Cao, X, Jackson, JP, Zilberman, D, McCallum, CM, Henikoff, S, & Jacobsen, SE. (2001). Requirement of CHROMOMETHYLASE3 for maintenance of CpXpG methylation. *Science*, **292** (5524), 2077-2080. https://doi.org/10.1126/science.1059745

Liu, ZW, Shao, CR, Zhang, CJ, Zhou, JX, Zhang, SW, Li, L, Chen, S, Huang, HW, Cai, T, & He, XJ. (2014). The SET domain proteins SUVH2 and SUVH9 are required for Pol V occupancy at RNA-directed DNA methylation loci. *PLoS Genetics*, **10** (1). https://doi.org/10.1371/JOURNAL.PGEN.1003948

Lorenzo, O, Chico, JM, Sánchez-Serrano, JJ, & Solano, R. (2004). JASMONATE-INSENSITIVE1 encodes a MYC transcription factor essential to discriminate between different jasmonate-regulated defense responses in Arabidopsis. *The Plant Cell*, **16** (7), 1938. https://doi.org/10.1105/TPC.022319

Lorković, ZJ, Hilscher, J, & Barta, A. (2008). Co-localisation studies of Arabidopsis SR splicing factors reveal different types of speckles in plant cell nuclei. *Experimental Cell Research*, **314** (17), 3175-3186. https://doi.org/10.1016/J.YEXCR.2008.06.020

Lorković, ZJ, Naumann, U, Matzke, AJM, & Matzke, M. (2012). Involvement of a GHKL ATPase in RNA-directed DNA methylation in *Arabidopsis thaliana*. *Current Biology*, **22** (10), 933-938. https://doi.org/10.1016/j.cub.2012.03.061

Luke-Glaser, S, Pintard, L, Lu, C, Mains, PE, & Peter, M. (2005). The BTB protein MEL-26 promotes cytokinesis in *C. elegans* by a CUL-3-independent mechanism. *Current Biology*, **15** (18), 1605-1615. https://doi.org/10.1016/j.cub.2005.07.068

Ma, W, Kong, Q, Grix, M, Mantyla, JJ, Yang, Y, Benning, C, & Ohlrogge, JB. (2015). Deletion of a C-terminal intrinsically disordered region of WRINKLED1 affects its stability and enhances oil accumulation in Arabidopsis. *Plant Journal*, **83** (5), 864-874. https://doi.org/10.1111/tpj.12933

Marshall, RS, & Vierstra, RD. (2019). Dynamic regulation of the 26S proteasome: From synthesis to degradation. *Frontiers in Molecular Biosciences*, **6**, 40. https://doi.org/10.3389/FMOLB.2019.00040/BIBTEX

Matzke, MA, Kanno, T, & Matzke, AJM. (2015). RNA-directed DNA methylation: The evolution of a complex epigenetic pathway in flowering plants. *Annual Review of Plant Biology*, **66**, 243-267. https://doi.org/10.1146/ANNUREV-ARPLANT-043014-114633

Matzke, MA, & Mosher, RA. (2014). RNA-directed DNA methylation: An epigenetic pathway of increasing complexity. *Nature Reviews Genetics*, **15** (6), 394-408. https://doi.org/10.1038/nrg3683

Melnick, A, Ahmad, KF, Arai, S, Polinger, A, Ball, H, Borden, KL, Carlile, GW, Prive, GG, & Licht, JD. (2000). In-depth mutational analysis of the promyelocytic leukemia zinc finger BTB/POZ domain reveals motifs and residues required for biological and transcriptional functions. *Molecular and Cellular Biology*, **20** (17), 6550-6567. https://doi.org/10.1128/mcb.20.17.6550-6567.2000

Mena, EL, Jevtić, P, Greber, BJ, Gee, CL, Lew, BG, Akopian, D, Nogales, E, Kuriyan, J, & Rape, M. (2020). Structural basis for dimerization quality control. *Nature*, **586** (7829), 452-456. https://doi.org/10.1038/s41586-020-2636-7

Mena, EL, Kjolby, RAS, Saxton, RA, Werner, A, Lew, BG, Boyle, JM, Harland, R, & Rape, M. (2018). Dimerization quality control ensures neuronal development and survival. *Science*, **362** (6411). https://doi.org/10.1126/SCIENCE.AAP8236/SUPPL_FILE/AAP8236_TABLE_S1.XLSX

Miller, JH. (1972). *Experiments in molecular genetics*. Cold Spring Harbor Laboratory, Cold Spring Harbor, NY. https://openlibrary.org/books/OL5298363M/Experiments_in_molecular_genetics

Miller, JH. (1992). *A short course in bacterial genetics*. Cold Spring Harbor Laboratory Press, Cold Spring Harbor. https://www.worldcat.org/title/short-course-in-bacterial-genetics-a-laboratory-manual-and-handbook-for-escherichia-coli-and-related-bacteria/oclc/23386589

Miškec, K. (2019). *Uloga konzerviranih domena MATH, BTB, i SPOP proteina BPM1 u interakciji s proteinima DMS3, RDM1 i HB6*. Master's thesis, University of Zagreb, Faculty of Science. https://urn.nsk.hr/urn:nbn:hr:217:307008

Mooney, S, Al-Saharin, R, Choi, CM, Tucker, K, Beathard, C, & Hellmann, HA. (2019). Characterization of *Brassica rapa* RAP2.4-related proteins in stress response and as CUL3-dependent E3 ligase substrates. *Cells*, **8** (4), 336. https://doi.org/10.3390/CELLS8040336

Moore, LD, Le, T, & Fan, G. (2013). DNA methylation and its basic function. *Neuropsychopharmacology*. https://doi.org/10.1038/npp.2012.112

Morimoto, K, Mizoi, J, Qin, F, Kim, JS, Sato, H, Osakabe, Y, Shinozaki, K, & Yamaguchi-Shinozaki, K. (2013). Stabilization of Arabidopsis DREB2A is required but not sufficient for the induction of target genes under conditions of stress. *PLoS ONE*, **8** (12), 80457. https://doi.org/10.1371/JOURNAL.PONE.0080457

Morimoto, K, Ohama, N, Kidokoro, S, Mizoi, J, Takahashi, F, Todaka, D, Mogami, J, Sato, H, Qin, F, Kim, J-S, Fukao, Y, Fujiwara, M, Shinozaki, K, & Yamaguchi-Shinozaki, K. (2017). BPM-CUL3 E3 ligase modulates thermotolerance by facilitating negative regulatory domain-mediated degradation of DREB2A in Arabidopsis. *Proceedings of the National Academy of Sciences*, 201704189. https://doi.org/10.1073/pnas.1704189114

Muñoz-Díaz, E, & Sáez-Vásquez, J. (2022). Nuclear dynamics: Formation of bodies and trafficking in plant nuclei. *Frontiers in Plant Science*, **13**, 3075. https://doi.org/10.3389/FPLS.2022.984163/BIBTEX

Murashige, T, & Skoog, F. (1962). A revised medium for rapid growth and bio assays with tobacco tissue cultures. *Physiologia Plantarum*, **15**, 473-497. https://doi.org/10.1111/j.1399-3054.1962.tb08052.x

Nakagawa, T, Suzuki, T, Murata, S, Nakamura, S, Hino, T, Maeo, K, Tabata, R, Kawai, T, Tanaka, K, Niwa, Y, Watanabe, Y, Nakamura, K, Kimura, T, & Ishiguro, S. (2007). Improved Gateway binary vectors: High-performance vectors for creation of fusion constructs in transgenic analysis of plants. *Bioscience, Biotechnology, and Biochemistry*, **71** (8), 2095-2100. https://doi.org/10.1271/BBB.70216

Nguyen, HC, Wang, W, & Xiong, Y. (2017). Cullin-RING E3 ubiquitin ligases: bridges to destruction. *Sub-Cellular Biochemistry*, **83**, 323. https://doi.org/10.1007/978-3-319-46503-6_12

Novy, R, Drott, D, Yaeger, K, & Mierendorf, R. (2001). Overcoming the codon bais of *E. coli* for enhanced protein expression. *InNovations*, **12**, 4-6.

Nuthikattu, S, Mccue, AD, Panda, K, Fultz, D, Defraia, C, Thomas, EN, & Slotkin, RK. (2013). The initiation of epigenetic silencing of active transposable elements is triggered by RDR6 and 21-22 nucleotide small interfering RNAs. *Plant Physiology*, **162**, 116-131. https://doi.org/10.1104/pp.113.216481

Padovani, C, Jevtić, P, & Rapé, M. (2022). Quality control of protein complex composition. *Molecular Cell*, **82** (8), 1439-1450. https://doi.org/10.1016/J.MOLCEL.2022.02.029

Passmore, LA, & Barford, D. (2004). Getting into position: The catalytic mechanisms of protein of protein ubiquitylation. *Biochemical Journal*, **379** (3), 513-525. https://doi.org/10.1042/BJ20040198

Perez-Torrado, R, Yamada, D, & Defossez, PA. (2006). Born to bind: The BTB protein-protein interaction domain. *BioEssays*, **28** (12), 1194-1202. https://doi.org/10.1002/bies.20500

Petroski, MD, & Deshaies, RJ. (2005). Function and regulation of cullin–RING ubiquitin ligases. *Nature Reviews Molecular Cell Biology*, **6** (1), 9-20. https://doi.org/10.1038/nrm1547

Pfaffl, MW, Tichopad, A, Prgomet, C, & Neuvians, TP. (2004). Determination of stable housekeeping genes, differentially regulated target genes and sample integrity: BestKeeper – Excel-based tool using pair-wise correlations. *Biotechnology Letters*, **26** (6), 509-515. https://doi.org/10.1023/B:BILE.0000019559.84305.47

Phukan, UJ, Jeena, GS, Tripathi, V, & Shukla, RK. (2017). Regulation of Apetala2/ethylene response factors in plants. *Frontiers in Plant Science*, **8**, 1-18. https://doi.org/10.3389/fpls.2017.00150

Pierce, WK, Grace, CR, Lee, J, Nourse, A, Marzahn, MR, Watson, ER, High, AA, Peng, J, Schulman, BA, & Mittaga, T. (2016). Multiple weak linear motifs enhance recruitment and processivity in SPOP-mediated substrate ubiquitination. *Journal of Molecular Biology*, **428** (6), 1256-1271. https://doi.org/10.1016/j.jmb.2015.10.002

Pintard, L, Willems, A, & Peter, M. (2004). Cullin-based ubiquitin ligases: Cul3-BTB complexes join the family. *EMBO Journal*, **23** (8), 1681-1687. https://doi.org/10.1038/SJ.EMBOJ.7600186

Pintard, L, Willis, JH, Willems, A, Johnson, JLF, Srayko, M, Kurz, T, Glaser, S, Mains, PE, Tyers, M, Bowerman, B, & Peter, M. (2003). The BTB protein MEL-26 is a substrate-specific adaptor of the CUL-3 ubiquitin-ligase. *Nature*, **425** (6955), 311-316. https://doi.org/10.1038/nature01959

Pontes, O, Li, CF, Nunes, PC, Haag, J, Ream, T, Vitins, A, Jacobsen, SE, & Pikaard, CS. (2006). The Arabidopsis chromatin-modifying nuclear siRNA pathway involves a nucleolar RNA processing center. *Cell*, **126** (1), 79-92. https://doi.org/10.1016/j.cell.2006.05.031

Pontes, O, & Pikaard, CS. (2008). siRNA and miRNA processing: new functions for Cajal bodies. *Current Opinion in Genetics & Development*, **18** (2), 197-203. https://doi.org/10.1016/j.gde.2008.01.008

Primorac, I, & Musacchio, A. (2013). Panta rhei: The APC/C at steady state. *Journal of Cell Biology*, **201** (2), 177-189. https://doi.org/10.1083/JCB.201301130

Radić, M, Šoštar, M, Weber, I, Ćetković, H, Slade, N, & Bosnar, MH. (2020). The subcellular localization and oligomerization preferences of NME1/NME2 upon radiation-induced dna damage. *International Journal of Molecular Sciences*, **21** (7), 1-19. https://doi.org/10.3390/ijms21072363

Ramakers, C, Ruijter, JM, Lekanne Deprez, RH, & Moorman, AFM. (2003). Assumption-free analysis of quantitative real-time polymerase chain reaction (PCR) data. *Neuroscience Letters*, **339**, 62-66. https://doi.org/10.1016/S0304-3940(02)01423-4

Rappsilber, J, Mann, M, & Ishihama, Y. (2007). Protocol for micro-purification, enrichment, pre-fractionation and storage of peptides for proteomics using StageTips. *Nature Protocols*, **2** (8), 1896-1906. https://doi.org/10.1038/nprot.2007.261

Reggiori, F, & Klionsky, DJ. (2013). Autophagic processes in yeast: mechanism, machinery and regulation. *Genetics*, **194** (2), 341. https://doi.org/10.1534/GENETICS.112.149013

Rendulić, T. (2018). *Protein interaction analysis of BPM1, DMS3 and RDM1 in tobacco cells*

using bimolecular fluorescent complementation. Master's thesis, University of Zagreb, Faculty of Science. urn:nbn:hr:217:006801

Roberts, D, Pedmale, U V., Morrow, J, Sachdev, S, Lechner, E, Tang, X, Zheng, N, Hannink, M, Genschik, P, & Liscum, E. (2011). Modulation of phototropic responsiveness in Arabidopsis through ubiquitination of Phototropin 1 by the CUL3-Ring E3 ubiquitin ligase $CRL3^{NPH3}$. *The Plant Cell*, **23** (10), 3627-3640. https://doi.org/10.1105/TPC.111.087999

Ronai, ZA. (2016). Monoubiquitination in proteasomal degradation. *Proceedings of the National Academy of Sciences of the United States of America*, **113** (32), 8894-8896. https://doi.org/10.1073/pnas.1610186113

Rotin, D, & Kumar, S. (2009). Physiological functions of the HECT family of ubiquitin ligases. *Nature Reviews Molecular Cell Biology*, **10** (6), 398-409. https://doi.org/10.1038/nrm2690

Roy, B, Granas, D, Bragg, F, Cher, JAY, White, MA, & Stormo, GD. (2020). Autoregulation of yeast ribosomal proteins discovered by efficient search for feedback regulation. *Communications Biology*, **3** (1), 1-9. https://doi.org/10.1038/s42003-020-01494-z

Russell, WM, & Klaenhammer, TR. (2001). Identification and cloning of gusA, encoding a new-glucuronidase from *Lactobacillus gasseri* ADH. *Applied and Environmental Microbiology*, **67** (3), 1253-1261. https://doi.org/10.1128/AEM.67.3.1253

Samant, RS, Livingston, CM, Sontag, EM, & Frydman, J. (2018). Distinct proteostasis circuits cooperate in nuclear and cytoplasmic protein quality control. *Nature*, **563** (7731), 407-411. https://doi.org/10.1038/s41586-018-0678-x

Santos, DA, Shi, L, Tu, BP, & Weissman, JS. (2019). Cycloheximide can distort measurements of mRNA levels and translation efficiency. *Nucleic Acids Research*, **47** (10), 4974-4985. https://doi.org/10.1093/nar/gkz205

Sarikas, A, Hartmann, T, & Pan, ZQ. (2011). The cullin protein family. *Genome Biology*, **12** (4), 1-12. https://doi.org/10.1186/GB-2011-12-4-220/FIGURES/1

Sasaki, T, Lorković, ZJ, Liang, SC, Matzke, AJM, & Matzke, M. (2014). The ability to form homodimers is essential for RDM1 to function in RNA-directed DNA methylation. *PLoS ONE*, **9** (2), 1-8. https://doi.org/10.1371/journal.pone.0088190

Scheuermann, TH, Padrick, SB, Gardner, KH, & Brautigam, CA. (2016). On the acquisition and analysis of microscale thermophoresis data. *Analytical Biochemistry*, **496**, 79-93. https://doi.org/10.1016/j.ab.2015.12.013

Schütze, K, Harter, K, & Chaban, C. (2009). Bimolecular fluorescence complementation (BiFC) to study protein-protein interactions in living plant cells. In *Plant Signal Transduction: Methods and Protocols*, 189-202. Humana Press. https://doi.org/10.1007/978-1-59745-289-2_12

Shanmugam, T, Abbasi, N, Kim, HS, Kim, HB, Park, N Il, Park, GT, Oh, SA, Park, SK, Muench, DG, Choi, Y, Park, Y Il, & Choi, SB. (2017). An Arabidopsis divergent

pumilio protein, APUM24, is essential for embryogenesis and required for faithful pre-rRNA processing. *Plant Journal*, **92** (6), 1092-1105. https://doi.org/10.1111/tpj.13745

Škiljaica, A. (2022). *The role of MATH-BTB family proteins TaMAB2 and AtBPM1 in plant development and stress response*. Doctoral thesis, University of Zagreb, Faculty of Science. urn:nbn:hr:217:744869

Škiljaica, A, Jagić, M, Vuk, T, Leljak Levanić, D, Bauer, N, & Markulin, L. (2022). Evaluation of reference genes for RT-qPCR gene expression analysis in Arabidopsis thaliana exposed to elevated temperatures. *Plant Biology*. https://doi.org/10.1111/plb.13382

Škiljaica, A, Lechner, E, Jagić, M, Majsec, K, Malenica, N, & Genschik, P. (2020). The protein turnover of Arabidopsis BPM1 is involved in regulation of flowering time and abiotic stress response. *Plant Molecular Biology*. https://doi.org/10.1007/s11103-019-00947-2

Smaldone, G, Pirone, L, Pedone, E, Marlovits, T, Vitagliano, L, & Ciccarelli, L. (2016). The BTB domains of the potassium channel tetramerization domain proteins prevalently assume pentameric states. *FEBS Letters*, **590** (11), 1663-1671. https://doi.org/10.1002/1873-3468.12203

Smit, JJ, Sixma, TK, Irp, H, & Ring, I. (2014). RBR E3-ligases at work. *EMBO Reports*, **15** (2), 142-154.

Soppe, WJJ, Jacobsen, SE, Alonso-Blanco, C, Jackson, JP, Kakutani, T, Koornneef, M, & Peeters, AJM. (2000). The late flowering phenotype of fwa mutants is caused by gain-of-function epigenetic alleles of a homeodomain gene. *Molecular Cell*, **6** (4), 791-802. https://doi.org/10.1016/S1097-2765(05)00090-0

Stewart, MD, Ritterhoff, T, Klevit, RE, & Brzovic, PS. (2016). E2 enzymes: More than just middle men. *Cell Research*, **26** (4), 423-440. https://doi.org/10.1038/cr.2016.35

Stogios, PJ, Downs, GS, Jauhal, JJS, Nandra, SK, & Privé, GG. (2005). Sequence and structural analysis of BTB domain proteins. *Genome Biology*, **6** (10), 1-18. https://doi.org/10.1186/gb-2005-6-10-r82

Stogios, PJ, & Privé, GG. (2004). The BACK domain in BTB-kelch proteins. *Trends in Biochemical Sciences*, **29** (12), 634-637. https://doi.org/10.1016/J.TIBS.2004.10.003

Striebinger, H, Koegl, M, & Bailer, SM. (2013). A high-throughput yeast two-hybrid protocol to determine virus-host protein interactions. *Methods in Molecular Biology*, **1064**, 1-15. https://doi.org/10.1007/978-1-62703-601-6_1

Sunnerhagen, M, Pursglove, S, & Fladvad, M. (2002). The new MATH: Homology suggests shared binding surfaces in meprin tetramers and TRAF trimers. *FEBS Letters*, **530**, 1-3. https://doi.org/10.1016/S0014-5793(02)03330-6

Tanaka, K. (2009). The proteasome: Overview of structure and functions. *Proceedings of the Japan Academy. Series B, Physical and Biological Sciences*, **85** (1), 12. https://doi.org/10.2183/PJAB.85.12

Thomann, A, Lechner, E, Hansen, M, Dumbliauskas, E, Parmentier, Y, Kieber, J, Scheres, B, & Genschik, P. (2009). Arabidopsis CULLIN3 genes regulate primary root growth and patterning by ethylene-dependent and -independent mechanisms. *PLOS Genetics*, **5** (1), e1000328. https://doi.org/10.1371/JOURNAL.PGEN.1000328

Tso, S-C, & Brautigam, CA. (2016). Measuring the KD of protein–ligand interactions using microscale thermophoresis. In *Protein-Ligand Interactions: Methods and Applications*, Third Edition, 161-181. Springer Nature. https://doi.org/10.1007/978-4-431-55985-6_16

Vandesompele, J, De Preter, K, Pattyn, F, Poppe, B, Van Roy, N, De Paepe, A, & Speleman, F. (2002). Accurate normalization of real-time quantitative RT-PCR data by geometric averaging of multiple internal control genes. *Genome Biology*, **3** (7), 1-12. https://doi.org/10.1186/gb-2002-3-7-research0034

Vuk, T. (2022). *Uloga proteina BPM1 u mehanizmu metilacije DNA de novo tijekom razvoja uročnjaka (Arabidopsis thaliana L.)*. Doctoral thesis, University of Zagreb, Faculty of Science. urn:nbn:hr:217:895020

Waddington, CH. (2012). The epigenotype. 1942. *International Journal of Epidemiology*, **41** (1), 10-13. https://doi.org/10.1093/ije/dyr184

Walter, M, Chaban, C, Schütze, K, Batistic, O, Weckermann, K, Näke, C, Blazevic, D, Grafen, C, Schumacher, K, Oecking, C, Harter, K, & Kudla, J. (2004). Visualization of protein interactions in living plant cells using bimolecular fluorescence complementation. *The Plant Journal*, **40** (3), 428-438. https://doi.org/10.1111/J.1365-313X.2004.02219.X

Weber, H, Bernhardt, A, Dieterle, M, Hano, P, Mutlu, A, Estelle, M, Genschik, P, & Hellmann, H. (2005). Arabidopsis AtCUL3a and AtCUL3b form complexes with members of the BTB/POZ-MATH protein family. *Plant Physiology*, **137** (1), 83-93. https://doi.org/10.1104/PP.104.052654

Weber, H, & Hellmann, H. (2009). *Arabidopsis thaliana* BTB/POZ-MATH proteins interact with members of the ERF/AP2 transcription factor family. *FEBS Journal*, **276** (22), 6624-6635. https://doi.org/10.1111/j.1742-4658.2009.07373.x

Wickens, M, Bernstein, DS, Kimble, J, & Parker, R. (2002). A PUF family portrait: 3′UTR regulation as a way of life. *Trends in Genetics*, **18** (3), 150-157. https://doi.org/10.1016/s0168-9525(01)02616-6

Wicker, T, & Keller, B. (2007). Genome-wide comparative analysis of copia retrotransposons in Triticeae, rice, and Arabidopsis reveals conserved ancient evolutionary lineages and distinct dynamics of individual copia families. *Genome Research*, **17** (7), 1072. https://doi.org/10.1101/GR.6214107

Wierzbicki, AT, Cocklin, R, Mayampurath, A, Lister, R, Jordan Rowley, M, Gregory, BD, Ecker, JR, Tang, H, & Pikaard, CS. (2012). Spatial and functional relationships among Pol V-associated loci, Pol IV-dependent siRNAs, and cytosine methylation in the Arabidopsis epigenome. *Genes and Development*, **26** (16), 1825-1836. https://doi.org/10.1101/gad.197772.112

Wierzbicki, AT, Haag, J, & Pikaard, C. (2008). Noncoding transcription by RNA polymerase

Pol IVb/Pol V mediates transcriptional silencing of overlapping and adjacent genes. *Cell*, **135** (4), 635-648. https://doi.org/10.1016/J.CELL.2008.09.035

Wilton, BA, Campbell, S, Van Buuren, N, Garneau, R, Furukawa, M, Xiong, Y, & Barry, M. (2008). Ectromelia virus BTB/kelch oroteins, EVM150 and EVM167, interact with cullin-3-based ubiquitin ligases. *Virology*, **374** (1), 82. https://doi.org/10.1016/J.VIROL.2007.11.036

Win, J, & Kamoun, S. (2004). pCB301-p19 : A binary plasmid vector to enhance transient expression of transgenes by agroinfiltration. http://www.kamounlab.net.

Withers, J, Yao, J, Mecey, C, Howe, GA, Melotto, M, & He, SY. (2012). Transcription factor-dependent nuclear localization of a transcriptional repressor in jasmonate hormone signaling. *Proceedings of the National Academy of Sciences of the United States of America*, **109** (49), 20148-20153. https://doi.org/10.1073/pnas.1210054109

Wongpalee, SP, Liu, S, Gallego-Bartolomé, J, Leitner, A, Aebersold, R, Liu, W, Yen, L, Nohales, MA, Kuo, PH, Vashisht, AA, Wohlschlegel, JA, Feng, S, Kay, SA, Zhou, ZH, & Jacobsen, SE. (2019). CryoEM structures of Arabidopsis DDR complexes involved in RNA-directed DNA methylation. *Nature Communications*, **10** (3916). https://doi.org/10.1038/s41467-019-11759-9

Xie, J, Jin, Y, & Wang, G. (2019). The role of SCF ubiquitin-ligase complex at the beginning of life. *Reproductive Biology and Endocrinology*, **17** (1), 1-9. https://doi.org/10.1186/S12958-019-0547-Y/FIGURES/2

Yang, Q, Zhao, J, Chen, D, & Wang, Y. (2021). E3 ubiquitin ligases: styles, structures and functions. *Molecular Biomedicine*, **2** (1), 1-17. https://doi.org/10.1186/S43556-021-00043-2

Zapata, JM, Pawlowski, K, Haas, E, Ware, CF, Godzik, A, & Reed, JC. (2001). A diverse family of proteins containing tumor necrosis factor receptor-associated factor domains. *Journal of Biological Chemistry*, **276** (26), 24242-24252. https://doi.org/10.1074/JBC.M100354200

Zemach, A, Kim, MY, Hsieh, P-H, Coleman-Derr, D, Eshed-Williams, L, Thao, K, Harmer, SL, & Zilberman, D. (2013). The nucleosome remodeler DDM1 allows DNA methyltransferases to access H1-containing heterochromatin. *Cell*, **153** (1), 193. https://doi.org/10.1016/J.CELL.2013.02.033

Zhang, H, Lang, Z, & Zhu, J-K. (2018). Dynamics and function of DNA methylation in plants. *Nature Reviews Molecular Cell Biology 2018 19:8*, **19** (8), 489-506. https://doi.org/10.1038/s41580-018-0016-z

Zheng, B, Wang, Z, Li, S, Yu, B, Liu, J-Y, & Chen, X. (2009). Intergenic transcription by RNA Polymerase II coordinates Pol IV and Pol V in siRNA-directed transcriptional gene silencing in Arabidopsis. *Genes & Development*, **23** (24), 2850. https://doi.org/10.1101/GAD.1868009

Zhong, S, Xu, Y, Yu, C, Zhang, X, Li, L, Ge, H, Ren, G, Wang, Y, Ma, J, Zheng, Y, & Zheng, B. (2019). Anaphase-promoting complex/cyclosome regulates RdDM activity by degrading DMS3 in Arabidopsis. *Proceedings of the National Academy of Sciences of the*

United States of America, **116** (9), 3899-3908. https://doi.org/10.1073/pnas.1816652116

Zhong, X, Hale, CJ, Law, JA, Johnson, LM, Feng, S, Tu, A, & Jacobsen, SE. (2012). DDR complex facilitates global association of RNA polymerase v to promoters and evolutionarily young transposons. *Nature Structural and Molecular Biology*, **19** (9), 870-875. https://doi.org/10.1038/nsmb.2354

Zhuang, M, Calabrese, MF, Liu, J, Waddell, MB, Nourse, A, Hammel, M, Miller, DJ, Walden, H, Duda, DM, Seyedin, SN, Hoggard, T, Harper, JW, White, KP, & Schulman, BA. (2009). Structures of SPOP-substrate complexes: insights into molecular architectures of BTB-Cul3 ubiquitin ligases. *Molecular Cell*, **36** (1), 39-50. https://doi.org/10.1016/j.molcel.2009.09.022

Zimmerman, ES, Schulman, BA, & Zheng, N. (2010). Structural assembly of cullin-RING ubiquitin ligase complexes. *Current Opinion in Structural Biology*, **20** (6), 714-721. https://doi.org/10.1016/j.sbi.2010.08.010

Online sources:

Biolisitc® PDS-1000/He Particle Delivery System Instruction Manual. Bio-Rad Laboratories, Inc. Available at: https://www.bio-rad.com/webroot/web/pdf/lsr/literature/10000070900.pdf

Densitometry using ImageJ. SYBIL. Available at: https://www.sybil-fp7.eu/node/95

In-Fusion® HD Cloning Kit User Manual. Takara Bio, Inc. Available at: https://www.takarabio.com/documents/User%20Manual/In/In-Fusion%20HD%20Cloning%20Kit%20User%20Manual_102518.pdf

PALMIST software version 1.5.8 and The PALMIST Manual. Available at: http://biophysics.swmed.edu/MBR/software.html

Q5® Site-Directed Mutagenesis Kit – Instruction Manual (2013). New England Biolabs, Inc. Available at: https://international.neb.com/protocols/2013/01/26/q5-site-directed-mutagenesis-kit-protocol-e0554

Software Manual MO.Affinity Analysis. NanoTemper Technologies. Available at: https://www2.helsinki.fi/sites/default/files/atoms/files/manual_mo.affinity_analysis.pdf

User Manual Monolith® NT.115. NanoTemper Technologies. Available at: https://www2.helsinki.fi/sites/default/files/atoms/files/manual_nt115.pdf

Yeast Protocols Handbook (2009). Clontech Laboratories, Inc. Takara Bio. Available at: https://www.takara.co.kr/file/manual/pdf/PT3024-1.pdf

8. APPENDIX

Appendix A. Media recipes and antibiotics

1. Plant growth media

Table A1-1 Composition of MS nutrient medium for the *Arabidopsis thaliana* germination

	MS nutrient medium	**mg/L**
MACROELEMENTS		
	KNO_3	1900
	NH_4NO_3	1650
	$CaCl_2$ x H_2O	755
	KH_2PO_4	170
	$MgSO_4$ x 7 H_2O	370
MICROELEMENTS	H_3BO_3	6.2
	$CoCl_2$ x 6 H_2O	0.025
	KI	0.83
	Na_2MoO_4 x 2 H_2O	0.25
	$CuSO_4$ x 5 H_2O	0.025
	$MnSO_4$ x 4 H_2O	16.9
	$ZnSO_4$ x 7 H_2O	8.6
	$FeSO_4$ x 7 H_2O	27.8
	Na_2EDTA	37.3
ORGANIC COMPOUNDS	sucrose	20000
	myo-Inositol	100
	glycine	2
	nicotinic acid	0.5
	pyridoxine-HCl	0.5
	thiamine-HCl	0.1
	agar	8000
	Adjusted pH to 5.8 and autoclaved	

Table A1-2 Composition of MS-BY2 nutrient medium for the BY-2 cells growth

	MS nutrient medium	**mg/L**
MACROELEMENTS	KNO_3	1900
	NH_4NO_3	1650
	$CaCl_2$ x H_2O	755
	KH_2PO_4	210
	$MgSO_4$ x 7 H_2O	370
MICROELEMENTS	H_3BO_3	6.2
	$CoCl_2$ x 6 H_2O	0.025
	KI	0.83
	Na_2MoO_4 x 2 H_2O	0.25
	$CuSO_4$ x 5 H_2O	0.025
	$MnSO_4$ x 4 H_2O	16.9
	$ZnSO_4$ x 7 H_2O	8.6
	$FeSO_4$ x 7 H_2O	27.8
	Na_2EDTA	37.3
ORGANIC COMPOUNDS	sucrose	30000
	myo-inositol	100
	thiamine-HCl	1
	2.4-D	1
	pyridoxine-HCl	0.5
Adjusted pH to 5.7 and autoclaved		

2. Yeast media

Table A2-1 Composition of YPD medium

YPD medium	**g/L**
Yeast extract	10
Peptone	20
Glucose	20
Agar (for plates only)	20
Adjusted pH to 6.5 and autoclaved	

Table A2-2 Composition of minimal SD medium

SD/-HIS/-LEU/-TRP medium*	**g/L**
Yeast nitrogen base without amino acids	6.7
Glucose	20
Yeast synthetic Drop-out Medium Supplements, without histidine, leucine, and tryptophan	0.62
Succinic acid	10
Agar (for plates only)	20
Adjusted pH to 7 and autoclaved	

*For selection of co-transformed yeasts, minimal SD medium was supplemented with 50 mg/L histidine (SD/-Leu/-Trp medium or "master" plates). For histidine prototrophy assay minimal SD medium was supplemented with 13 mM 3-AT (SD/-His/-Leu/-Trp + 3-AT).

3. Bacteria media

Table A3-1 Composition of LB medium

LB medium	**g/L**
Tryptone	10
Yeast extract	5
NaCl	10
Agar (for plates only)	15
Adjusted pH to 7 and autoclaved	

Table A3-2 List of antibiotics used for *E. coli* or *A. tumefaciens* selection with their working concentrations.

	E. coli	***A. tumefaciens***
Antibiotic	**ng/mL**	**ng/mL**
Ampicillin	100	/
Spectinomycin	50	100
Kanamycin	50	/
Chloramphenicol	34	/
Rifampicin	/	50
Gentamicin	/	50

Table A3-3 Composition of 4 × YT medium

4 × YT medium	**g/L**
Tryptone	32
Yeast extract	20
NaCl	5
Adjusted pH to 7 and autoclaved	

Appendix B. Cloning information

Table B1-1 Vectors used for Yeast two-hybrid assays.

Transgene	Vector name	Bacterial selection	Yeast selection
BPM1	pGAD424:BPM1	Ampicillin	-Leucine
	pGBT9:BPM1	Ampicillin	-Tryptophan
DMS3	pGAD424:DMS3	Ampicillin	-Leucine
	pGBT9:DMS3	Ampicillin	-Tryptophan
RDM1	pGAD424:RDM1	Ampicillin	-Leucine
	pGBT9:RDM1	Ampicillin	-Tryptophan

Table B1-2 Plasmids BPM1 used for localization and colocalization studies, and generation of domain-omitted BPM1 constructs with their application and bacterial selection.

Vector name	Application	Bacterial selection
pB7WGF2:BPM1	N-terminal GFP tag	Spectinomycin
pSPYNE:BPM1	split YFP N-terminal fragment	Kanamycin
pSPYCE:BPM1	split YFP C-terminal fragment	Kanamycin

Appendix C. Oligonucleotide sequences

1. Oligonucleotides for cDNA verification and gene expression

Table C1-1 Oligonucleotide sequences for cDNA verification (distinction from gDNA) and their melting temperatures (T_m).

Primer name	**Primer sequence 5' – 3'**	**T_m / °C**
ACT3_fw	CTGGCATCATACTTTCTACAATG	59
ACT3_rev	CACCACTGAGCACAATGTTAC	59

Table C1-2 Primers used for gene expression analysis in qRT-PCR reaction and their melting temperatures (T_m).

Primer name	**Primer sequence 5' – 3'**	**T_m / °C**
OEBPM1Fw	TTTGGCCCTTTAGGAGACC	58
OEBPM1R	CCTTGAAATGGGTGCTTCC	58
RHIP F1	CTATTGGGATTGGTGTCGCT	58
RHIP R1	AGAATTGTGCCTCTTCGCTC	58

2. Oligonucleotides for plasmid verification and plant genotyping

Table C2-1 Oligonucleotide sequences for colony PCR plasmid check and plant genotyping together with their melting temperatures (T_m).

Primer name	**Primer sequence 5' – 3'**	**T_m / °C**
attB1AtBPM1	ACAAGTTTGTACAAAAAAGCAGGCTCCATGGGCACAACTAGGGTC	64
AtBPM1attB2a	ACCACTTTGTACAAGAAAGCTGGGTAGTGCAACCGGGGCTTCAC	66
DMS3_BiFC_IF f	CGCCACTAGTGGATCCATGTATCCGACTGGTCAACAGA	79
DMS3_BiFC_IF rev	TACTATCGATGGATCCTCTGGGTGTGTTCATTGGCTG	77
InF_RDM1_fw	ATCACAAGTTTGTACGAATTCATGCAAAGCTCAATGACAATGGAAC	76
InF_RDM1_rev	TGTACAAGAAAGCTGGAATTCTCATTTCTCAGGAAAGATTGGG	76
GUS-dn	GCCAAAAGCCAGACAGAGTC	60
GUS-up2	AACGTATCCACGCCGTATTC	58
M13-rev	GCGGATAACAATTTCACACAGG	60
pCAMBIA-GUSup	GTTTCTACAGGACGGACGAG	58
Kan_FW	ATGGGGATTGAACAAGATGGATTGCACGCAGG	55
Kan_REV	TCAGAAGAACTCGTCAAGAAGGCGATAGAAGGCG	55

3. Oligonucleotides for plasmid sequencing

Table C3-1 Oligonucleotides used for sequencing of generated plasmids. Generated plasmids were checked using plasmid-specific primer thus only original plasmids are written.

Primer name	Primer sequence 5' – 3'	Plasmid sequenced
GAL4AD	TACCACTACAATGGATG	pGAD424
AD_REVERSE	AGATGGTGCACGATGCACAG	pGAD424
GAL4BD	TCATCGGAAGAGAGTAG	pGBT9
GBKR	ATCATAAGAAATTCGCCCGG	pGBT9
EGFP-C	CATGGTCCTGCTGGAGTTCGTG	pB7WGF2
DSRED1-C	AGCTGGACATCACCTCCCACAACG	pH7WGR, pB7WGR2
35S-B	AGTGGAAAAGGAAGGTGGCT	pSPYCE, pSPYNE
EGFP-CR	CGTCCATGCCGAGAGTG	pSPYCE
EGFP-NR	CGTCGCCGTCCAGCTC	pSPYNE
PGEX5	GGCAAGCCACGTTTGGTG	pGEX-4T1
PGEX3	GGAGCTGCATGTGTCAGAGG	pGEX-4T1
M13R	GCGGATAACAATTTCACACAGG	pCambia1301

4. Oligonucleotides for cloning

Table C4-1 Oligonucleotide sequences for generation of domain-omitted BPM1 plasmid constructs and their melting temperature (T_m).

Primer name	Primer sequence 5' – 3'	T_m / °C
MATHdel_fw	GGTGTGGTGAAGTCAGTTACGGAGGG	69
MATHdel_rev	GACTGTTTCTGTGGTAGAGGTCGATACC	68
BTBdel_fw	GGGGTTGCCATAAACACGGTTGCAAC	70
BTBdel_rev	CTGTTGTCCCAAGTTAGAAACTGGCAC	68
BACKdel_fw	CTAAGTGAACACTCTGTTATAGTATCTGG	66
BACKdel_rev	CCCTTCACAGAGTTTTGACTCACAGATT	67

Table C4-2 Oligonucleotide sequences for InFusion cloning of the domain-omitted BPM1 genes into pB7WGF2, pSPYCE and pSPYNE plasmids and their melting temperature (T_m) where applicable*.

Primer name	Primer sequence 5' – 3'	T_m / °C
InF_BPM1_fw	GACGAGCTGTACAAGCCGGAATTCCCGGGGATCCTG	/
InF_BPM1_rev	CAAGAAAGCTGGTCAGTGCAACCGGGGCTTCACTC	/
STOPattB2	TGACCAGCTTTCTTGTACAAAGTGGTG	67
EGFPrev_sdm	CTTGTACAGCTCGTCCATGCC	63
BPM1_BIFC_IFf	CGCCACTAGTGGATCCATGGGCACAACTAGGGTCTGC	/
BPM1_BIFC_IFrev	TACTATCGATGGATCCGTGCAACCGGGGCTTCACTC	/

*STOPattB2 and EGFPrev_sdm primers were used for linearization of pB7WGF2 vector using Q5 Hot Start High-Fidelity DNA polymerase (New England Biolabs) prior InFusion reaction.

Table C4-3 Oligonucleotide sequences for InFusion cloning of the promoter of *FWA* gene (pFWA) into pCambia1301 plasmid and their melting temperature (T_m) where applicable*.

Primer name	Primer sequence 5' – 3'	T_m / °C
Fwa-InF_dn	GTACCCGGGGATCCTAATGAGTATCCCTATATATATATATAT	/
Fwa-InF_up	GGTCAAGAGTCCCCCCTCGTATGAATGTTGAATG	/
pCam1301-InF_dn	GGGGGACTCTTGACCATGGT	63
pCam1301-InF_up	AGGATCCCCGGGTACCGA	61

*pCam1301-InF_dn and pCam1301-InF_up primers were used for linearization of pCambia1301 vector using Q5 Hot Start High-Fidelity DNA polymerase (New England Biolabs) prior InFusion reaction.

5. Oligonucleotides for DNA cassette amplification

Table C5-1 Primers used for DNA cassette amplification prior Biolistic transformation and their melting temperatures (T_m).

Primer name	Primer sequence 5' – 3'	T_m / °C
BiFC_BY2fw	CCCACTGAATCAAAGGCCATG	61
BiFC_BY2rev	GAATTCCCGATCTAGTAACATAGATGACAC	68

Appendix D. Protein extraction and SDS-PAGE

Table D1-1 Protein extraction buffer PEB50

Components	**Concentration**
HEPES pH 7.9	50 mM
KCl	50 mM
$MgCl_2$	2.5 mM
EDTA	1 mM
Triton X-100	0.1%
DTT	1 mM
NaF	1 mM
Roche complete protein inhibitor	1 ×

Table D1-2 Sample loading buffer (SLB)

Components	**Concentration**
Glycerol	32%
SDS	4%
Tris-HCl pH 6.6	125 mM
2-Mercaptoethanol	1.43 M
Bromphenol Blue	0.1%

Table D1-3 Polyacrylamide gel compositions.

Components	**Stacking gel (4%)**	**Resolving gel (12%)**
Tris-HCl pH 8.8	-	375 mM
Tris-HCl pH 6.8	123 mM	-
Acrylamide/Bis-acrylamide	4%	12%
SDS	0.1%	0.1%
APS	0.07%	0.05%
TEMED	0.4%	0.1%

Appendix E. Proteomic analysis

The proteomic analysis was performed with ACQUITY UPLC M-class nano-LC system (Waters, Milford, MA, USA) coupled to Compact™ QqTOF mass spectrometer via CaptiveSpray™ ESI interface supported with nanoBooster™ dopant addition technology (Bruker Daltonik GmbH, Bremen, Germany). Dried peptides were redissolved in 30 µL ultrapure water and 5 µL was injected onto C_{18} Acclaim™ PepMap™ trap column (5 × 0.3 mm, 5 µm, 100 Å, Thermo Fisher Scientific), desalted for three minutes with a 40 µL/min flowrate of 0.1% TFA (*v*/*v*) from the auxiliary pump and diverted to an analytical column. The separation was performed on the HALO C_{18} column (150 × 0.1 mm, 2.7 µm, Advanced Materials Technology, Inc., Wilmington, USA) heated to 30 °C. A linear 90-minute gradient, at a 1 µL/min flowrate, starting from 0% eluent B (0.1% TFA in 80% ACN, *v*/*v*) and 100% eluent A (0.1% TFA, *v*/*v*) and finishing at 80% eluent B, was employed. After separation, the column was equilibrated with 100% eluent A for seven minutes.

The mass spectrometer was operated in a reflectron positive ion mode with line spectra acquisition rate at 5 Hz and in *m*/*z* range 100-3000. ACN-doped nebulizing nitrogen gas was provided at 0.2 bar pressure. Drying gas heated to 150°C was introduced at 4 L/min, and capillary voltage was set to 1.3 kV. Ion transfer time and collision cell RF were stepped up from 70 to 150 µs and from 700 to 2300 Vpp, respectively. The low mass cut-off was set to *m*/*z* 100. The pre-pulse storage time was set to 12 µs. For the auto MS/MS, the three most abundant doubly to quadruply charged precursor ions were subjected to fragmentation with active exclusion after one spectrum. Singly charged ions were excluded from selection. Collision energies were stepped from 50 to 100% (with 50:50% timing) for different *m*/*z* ranges as follows: *m*/*z* 500: 17-21 eV, *m*/*z* 1000: 25-31 eV, *m*/*z* 2000: 33-40 eV. Argon was used as collision gas.

Nano-LC-MS system was operated under otofControl™, MassLynx™ and Compass HyStar™ software.

Appendix F. Results

Chapter F1: BPM1 domains alter its subcellular localization and stability

Table F1-1 Number of fluorescent cells with EGFP fusion proteins (BPM1, BTB-BACK$_{BPM1}$, MATH-BACK$_{BPM1}$, MATH-BTB$_{BPM1}$) 14-16 and 18-20 h after biolistic transformation of tobacco BY-2 cells treated with MG132 (50 μM) and control cells (0.05% DMSO).

EGFP fusion protein	**14-16 h**		**18-20 h**		**Total number of cells**
	control	MG132	control	MG132	
EGFP-BPM1	14	18	5	10	47
EGFP-BTB-BACK$_{BPM1}$	10	15	10	9	44
EGFP-MATH-BACK$_{BPM1}$	10	9	12	11	42
EGFP-MATH-BTB$_{BPM1}$	13	26	6	11	56

Table F1-2 Subcellular localization of BPM1 and its truncated versions missing MATH, BTB or BACK domain in tobacco BY2 cells.

EGFP fusion protein	**Nucleus only**	**Nucleus and nucleolus**	**Nucleus and cytoplasm**	**Nucleus, nucleolus and cytoplasm**	**Total number of cells**
BPM1	1	2	30	17	50
BTB-BACK$_{BPM1}$	55	5	16	0	76
MATH-BACK$_{BPM1}$	16	9	29	1	55
MATH-BTB$_{BPM1}$	1	27	16	15	59

Chapter F2: BTB domain is essential for BPM1 homodimer formations

To determine which BPM1 domain is fundamental for BPM1 homodimerization and in which cell compartment BPM1 forms homodimers, BiFC assay was performed. Non-fluorescent fragments of YFP (N-terminal and C-terminal fragment) were fused to the C-terminus of various BPM1 variants: complete BPM1 and BPM1 lacking MATH (BTB-$BACK_{BPM1}$), BTB (MATH-$BACK_{BPM1}$) or BACK (MATH-BTB_{BPM1}) domain, and plasmids carrying designated fusion proteins under the control of CaMV 35S promoter were agroinfiltrated into *Nicotiana benthamiana* lower leaf epidermis. Signals were observed 48 h after agroinfiltration under the fluorescence microscope. As expected, transformation with complete BPM1 resulted with plenty fluorescent signals confirming that BPM1 forms homodimers (**Figure F2-1**, **Table F2-1**). BPM1 homodimers localized exclusively in nucleus (including nucleolus) in 56% of observed cells (**Figure F2-1 A-C**), in 32% of cells BPM1 homodimers localized in nucleus (including nucleolus) and cytoplasm (**Figure F2-1 D-F**), while in hardly 12% of cells, YFP signal was detected strictly in cytoplasm (**Figure F2-1 G-I**). When using BPM1 variants lacking one of the three domains (MATH, BTB or BACK) it became clear that BTB domain is the one essential for formation of homodimers since no homodimers of MATH-$BACK_{BPM1}$ variant were detected (**Figure F2-2**, **Table F2-1**). BTB-$BACK_{BPM1}$ homodimers localized exclusively in nucleus, but not in nucleolus (**Figure F2-2 A-C**) and only small proportion of cells with observed YFP signal was detected (**Table F2-1**). Contrary, there was suitable number of MATH-BTB_{BPM1} homodimers detected, all with exclusively nuclear localization, 87% of which exhibited nucleolar localization as well (**Figure F2-2 G-I**, **Table F2-1**). In comparison, only 32% of nucleolar localization was observed for intact BPM1 homodimers (**Table F2-1**). Taken all together, BTB domain is crucial for BPM1 homodimer formation, whereas MATH domain promotes the interaction and together with BTB domain stimulates nucleolar localization of protein.

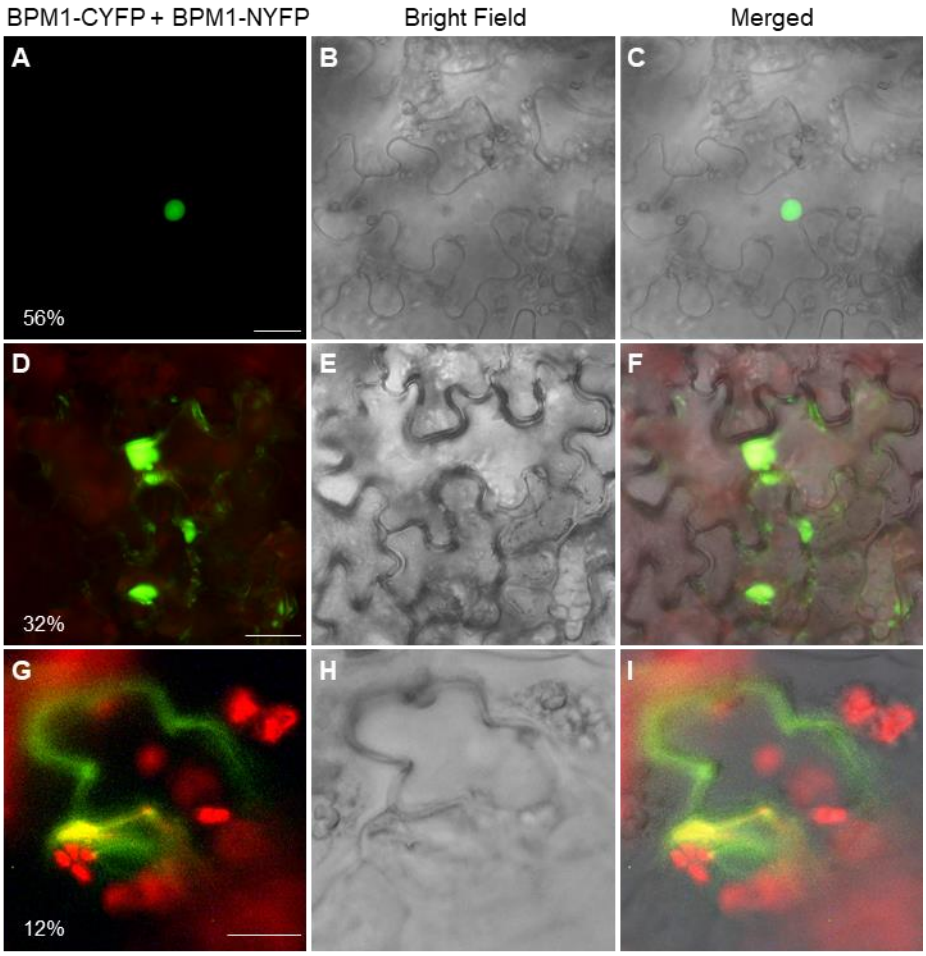

Figure F2-1 Detection of BPM1 homodimers in leaf epidermal cells of *Nicotiana benthamiana* using BiFC. Complete BPM1 protein forms homodimers in nucleus of 56% of cells (**A-C**), in both, nucleus and cytoplasm of 32% of cells (**D-E**), and only in 12% of cells localization was strictly cytoplasmic (**G-I**). Scale bar = 25 μm.

Table F2-1 Number of fluorescent cells with BiFC (formation of BPM1, BTB-BACK$_{BPM1}$, MATH-BACK$_{BPM1}$ and MATH-BTB$_{BPM1}$ homodimers).

Homodimer formation tested	**Subcellular localization**			**Total number of cells**
	Nucleus only (and nucleolus)	**Nucleus and cytoplasm (and nucleolus)**	**Cytoplasm only**	
EGFP-BPM1	19 (3)	11 (8)	4	34
EGFP-BTB-BACK$_{BPM1}$	10 (0)	0 (0)	0	10
EGFP-MATH-BACK$_{BPM1}$	0 (0)	0 (0)	0	0
EGFP-MATH-BTB$_{BPM1}$	23 (20)	0 (0)	0	23

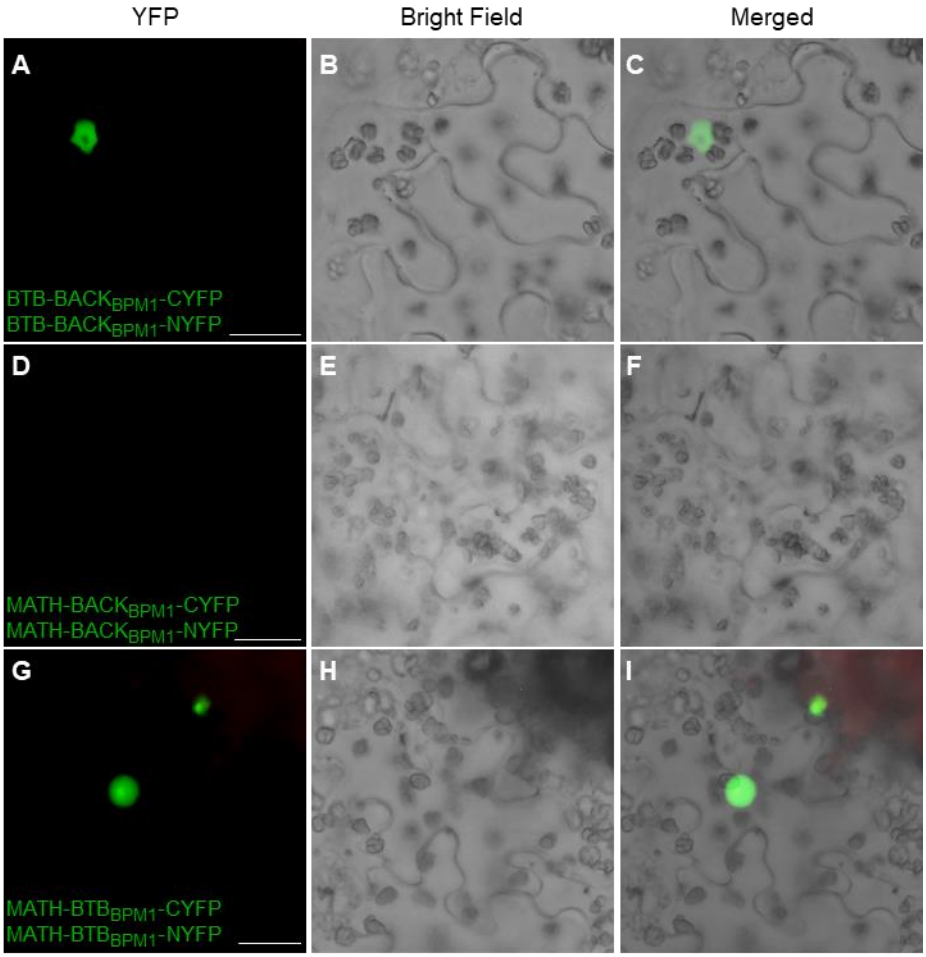

Figure F2-2 BTB domain of BPM1 is essential for homodimer formation in BiFC assay performed in leaf epidermal cells of *Nicotiana benthamiana*. BTB-BACK$_{BPM1}$ forms homodimers exclusively in nucleus (**A-C**), while BPM1 lacking BTB domain (MATH-BACK$_{BPM1}$) is unable to interact with itself (**D-F**). Deletion of BACK domain (MATH-BTB$_{BPM1}$) promotes nuclear and nucleolar localization of homodimers (**G-I**). Scale bar = 25 μm.

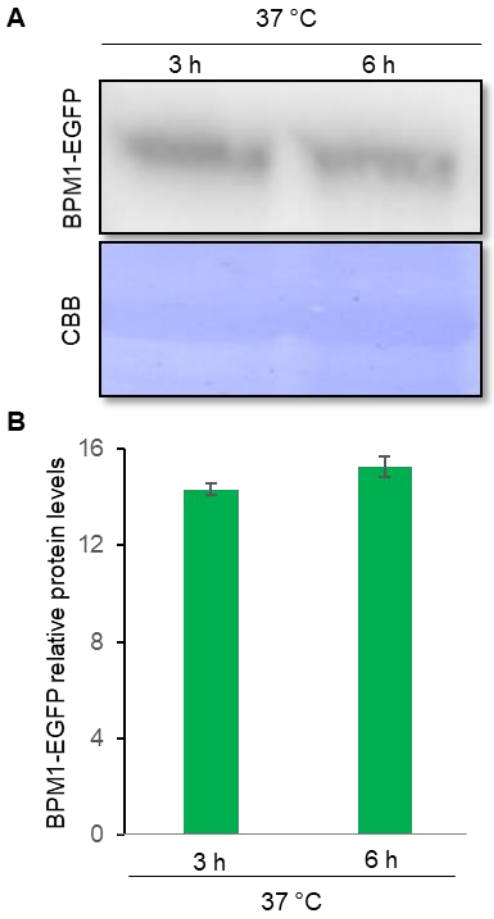

Figure F3-1 There was no difference in protein accumulation of BPM1-EGFP after 3 and 6 h exposure to 37 °C. Seven-day-old seedlings of oeBPM1-EGFP line were sampled after 3 and 6 h incubation at 37 °C. **A**) Whole protein extracts were immunoblotted with anti-GFP monoclonal antibody (upper panel). For loading control, proteins were stained with CBB on PVDF membranes (lower panel). **B**) Relative BPM1-EGFP protein levels were quantified in ImageJ, normalized to CBB bands and calibrated to control conditions (24 °C, 0h) which was taken as 1. Data is presented as means of three individual protein bands per treatment ± SD. No significant difference was observed (Student's t test, $p < 0.05$) between treatments.

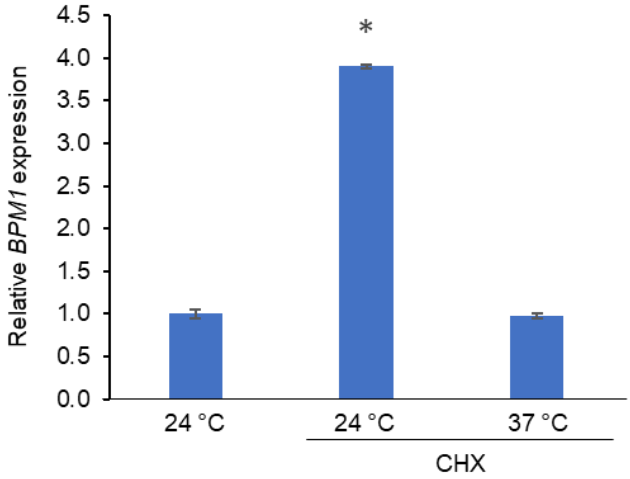

Figure F3-2 Protein synthesis inhibitor cycloheximide (CHX) affects *BPM1* expression.

Figure F3-2 – continued

Native *BPM1* gene expression is stimulated with the addition of the CHX (0.2 mg/mL) at 24 °C, but has no effect after 3 h exposure at 37 °C. Seven-day-old seedlings of WT were sampled before treatment at 24 °C, and after 3 h incubation with CHX at 24 °C and 37°C. *BPM1* expression was analyzed by quantitative RT-qPCR, normalized to *RHIP1* and calibrated to control conditions (24 °C, before treatment) which was taken as 1. Expression values are shown as mean fold change of two biological replicates ± SD. Asterisk indicates statistically significant differences (Duncan t test, $p < 0.05$) between means of sampling conditions.

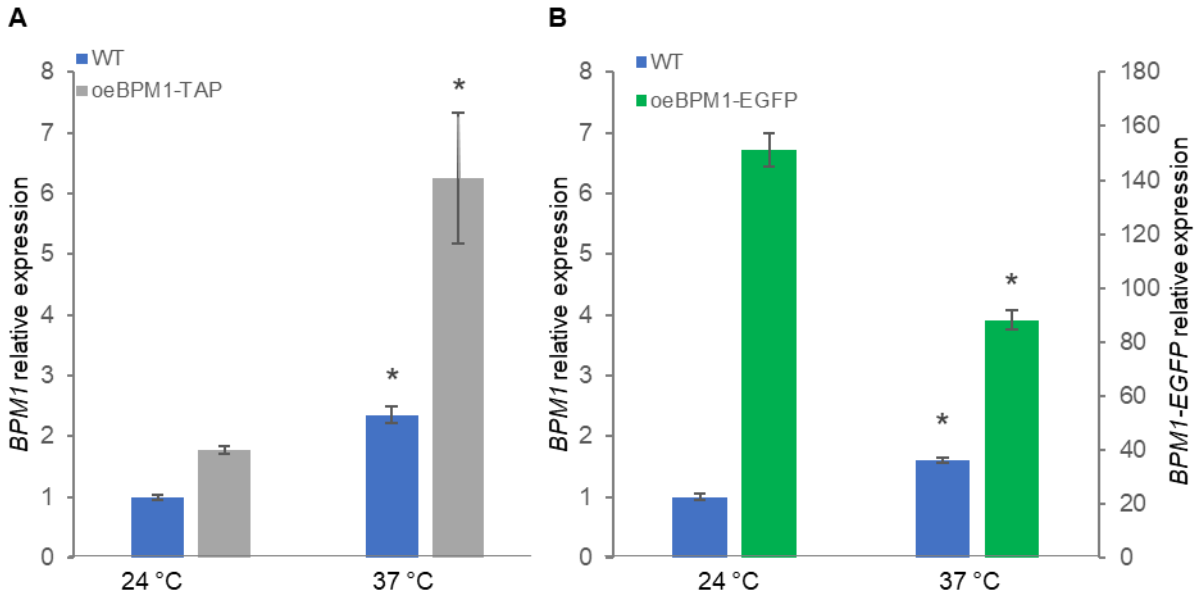

Figure F3-3 Expression of *BPM1* is influenced by exposure to 37 °C. Seven-day-old seedlings of WT (**A** and **B**), oeBPM1-TAP (**A**) and oeBPM1-EGFP (**B**) were sampled before treatment (24 °C) and after 3 h of incubation at 37 °C for 3 h. Endogenous and transgene *BPM1* expression was analyzed by quantitative RT-qPCR, normalized to *RHIP1* and calibrated to WT at control conditions (24 °C), which was taken as 1. Expression values are shown as mean fold change of two biological replicates ± SD. Asterisks indicate statistically significant differences (Student's t test, $p < 0.05$) between means of control and treatment for each used plant line. Similar results were obtained in two independent experiments.

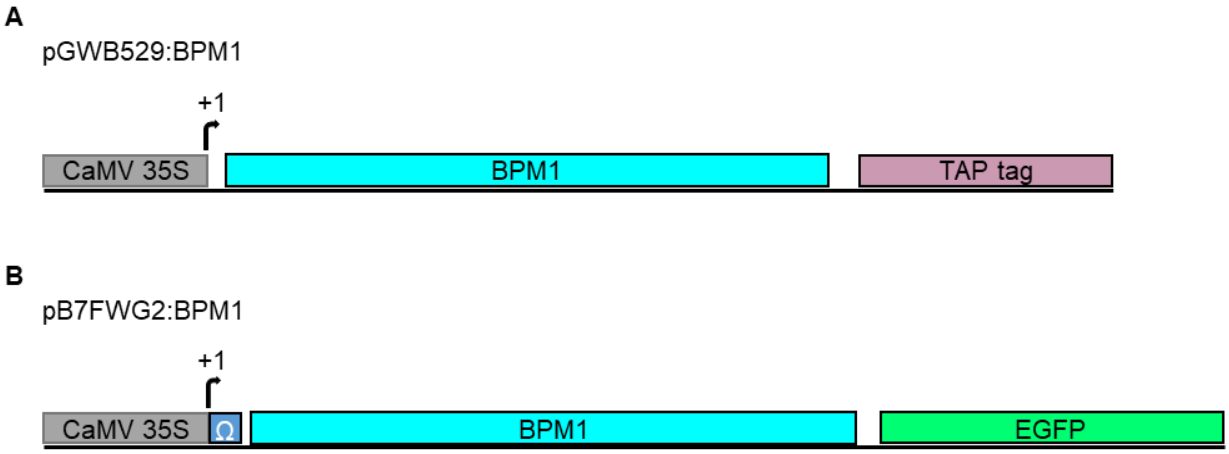

Figure F3-4 Schematic representation of promoter-gene region in binary vectors pGWB529:BPM1 (**A**) and pB7FWG2:BPM1 (**B**). **A**) pGWB529:BPM1 has *BPM1-TAP* under simple CaMV 35S promoter. **B**) Translation of *BPM1-EGFP* from pB7FWG:BPM1 is enhanced by omega (Ω) sequence downstream of the transcription start site (+1) in the 5'UTR.

Table F4-1 Results of mass spectrometry analysis following affinity purification using proteins extracted from 12-day old seedlings of *Arabidopsis thaliana* lines oeBPM1-TAP (**A**) and oeBPM1-EGFP (**B**). From left to right: UniProt IDs, TAIR locus, score, gene, protein description, sequence coverage, sequence length, molecular weight, number of alternative proteins and number of identified unique peptides. Proteins were listed according the score value. Predicted protein function categories are indicated using a color code (**C**).

A

UniProt ID	TAIR gene number	Score	Gene	Protein descriptions	Sequence coverage (%)	Sequence length	Mw	No. of alt. proteins	No. of unique peptides
Q8L765	**AT5G19000**	**323.31**	**BPM1**	**BTB/POZ and MATH domain-containing protein 1**	**14.7**	**407**	**44.729**	**13**	**4**
Q94A79	AT3G49250	234.23	DMS3	DEFECTIVE IN MERISTEM SILENCING 3	36.2	420	46.767	1	12
Q9LUJ3	AT3G22680	182.23	RDM1	RDM1	85.9	163	18.692	1	11
P19366	ATCG00480	113.76	atpB	ATP synthase subunit beta	34.9	498	53.933	1	12
Q9LHA8	AT3G12580	89.87	HSP70-4	Heat shock 70 kDa protein 4	22.5	650	71.101	2	3
P56757	ATCG00120	58.86	atpA	ATP synthase subunit alpha	15.4	507	55.328	1	6
Q9SZJ5	AT4G37930	48.46	SHM1	Serine hydroxymethyltransferase 1	18.8	517	57.4	2	7
P17745	AT4G20360	32.26	TUFA	Elongation factor Tu	8.4	476	51.63	2	3
Q42472	AT1G65960	31.11	GAD2	Glutamate decarboxylase 2	13.8	494	56.14	2	4

Table F4-1 - continued

B

UniProt ID	TAIR gene number	Score	Gene	Protein descriptions	Sequence coverage (%)	Sequence length	Mw	No. of alt. proteins	No. of unique peptides
Q8L765	**AT5G19000**	**172.38**	**BPM1**	**BTB/POZ and MATH domain-containing protein 1**	**53.1**	**407**	**44.729**	**13**	**17**
Q9LUJ3	AT3G22680	21.78	RDM1	RDM1	18.4	163	18.692	1	2
Q94A79	AT3G49250	17.13	DMS3	DEFECTIVE IN MERISTEM SILENCING 3	7.1	420	46.767	1	3
Q9LHA8	AT3G12580	6.33	HSP70-4	Heat shock 70 kDa protein 4	3.1	521	57.236	11	1

C

Function
DNA/chromatin modification
Molecular chaperon
Photosynthesis/chloroplast-related
Other

Chapter F5: DMS3 and RDM1 related subcellular localization of BPM1 and its domain-omitted variants

Table F5-1 Subcellular localization of BPM1 and its truncated versions missing MATH, BTB or BACK domain when co-expressed with DMS3 or RDM1in tobacco BY2 cells.

	In the presence of protein	**Nucleus only**	**Nucleus and nucleolus**	**Nucleus and cytoplasm**	**Nucleus, nucleolus and cytoplasm**	**Total number of cells**
BPM1	DMS3	3	1	39	7	50
BTB-BACK$_{BPM1}$		35	1	14	0	50
MATH-BACK$_{BPM1}$		10	1	32	7	50
MATH-BTB$_{BPM1}$		8	37	8	9	62
BPM1	RDM1	3	2	44	2	51
BTB-BACK$_{BPM1}$		36	2	9	1	48
MATH-BACK$_{BPM1}$		39	5	9	0	53
MATH-BTB$_{BPM1}$		10	31	3	4	48

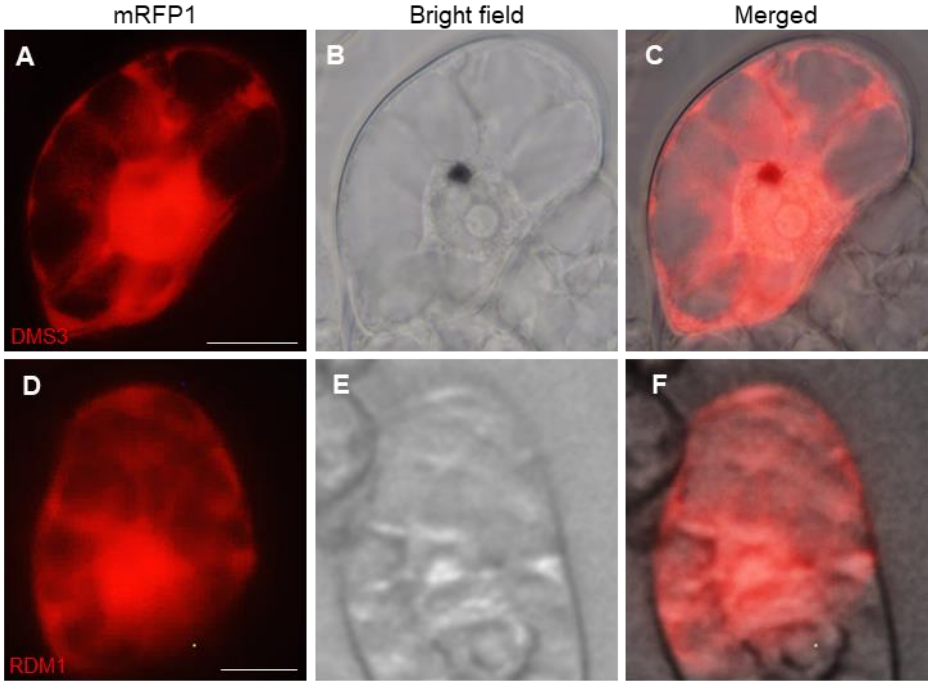

Figure F5-1 DDR complex proteins, DMS3 (**A** – **C**) and RDM1 (**D** – **F**) are found in cytoplasm and nucleus, but not in the nucleolus of tobacco BY-2 cells. Scale bar = 10 μm.

Tobacco BY-2 cells were transiently co-transformed with 35S::EGFP-BPM1 domain-omitted variants (BTB-BACK$_{BPM1}$, MATH-BACK$_{BPM1}$ and MATH-BTB$_{BPM1}$) and 35S::mRFP1-DMS3, and the influence of DMS3 on the subcellular localization of BPM1 domain-omitted variants was observed. Co-expression with DMS3 had almost no influence on BTB-BACK$_{BPM1}$ localization (72% of cells showed strictly nuclear BPM1 localization, **Figure F5-2 A-D**, **M**), when compared to BTB-BACK$_{BPM1}$ protein expressed alone (79% of strictly nuclear localization). On the other side, MATH-BTB$_{BPM1}$ localization was changed to preferentially nuclear (73% vs. 48% strictly nuclear when expressed alone, **Figure F5-2 I-L**, **M**), suggesting a role of BTB in nucleus when DMS3 protein is present. Interestingly, co-transformation of DMS3 with the MATH-BACK$_{BPM1}$ variant decreased the exclusively nuclear localization from 45% when expressed alone to 22% when co-expressed with DMS3 (**Figure F5-2 E-H**, **M**), indicating that the cytoplasmatic localization is preferentially mediated by the affinity of MATH domain in cooperation with BACK domain for targeting potential cytoplasmatic substrates for proteasomal degradation, a known function of MATH-BTB proteins in general. Again, DMS3 localized in nucleus and cytoplasm in all cells (**Figure F5-2 B**, **F**, **J**).

Furthermore, tobacco BY-2 cells were transiently co-transformed with 35S::EGFP-BPM1 domain-omitted variants (BTB-BACK$_{BPM1}$, MATH-BACK$_{BPM1}$ and MATH-BTB$_{BPM1}$) and 35S::mRFP1-RDM1 to see how presence of RDM1 affects subcellular localization of BPM1 domain-omitted variants. All three variants of BPM1 localized mainly in the nucleus (**Figure F5-3**). There was no change in the localization of BTB-BACK$_{BPM1}$ when co-expressed with RDM1 (79% of cells showed strictly nuclear BPM1 localization whether this domain-omitted variant was expressed alone, or with RDM1, **Figure F5-3 A-D**, **M**). Contrary, MATH-BACK$_{BPM1}$ and MATH-BTB$_{BPM1}$ localization was changed to preferentially nuclear (83% of MATH-BACK$_{BPM1}$, **Figure F5-3 E-H**, **M** and 85% of MATH-BTB$_{BPM1}$ **Figure F5-3 I-L**, **M,** vs. 45% of MATH-BACK$_{BPM1}$ expressed alone and 48% of MATH-BTB$_{BPM1}$ when expressed alone). RDM1 localized in nucleus and cytoplasm in all cells (**Figure F5-3 B**, **F**, **J**) and the presence of RDM1 in cells seems to evoke BPM1's strictly nuclear localization regardless of the domains omitted.

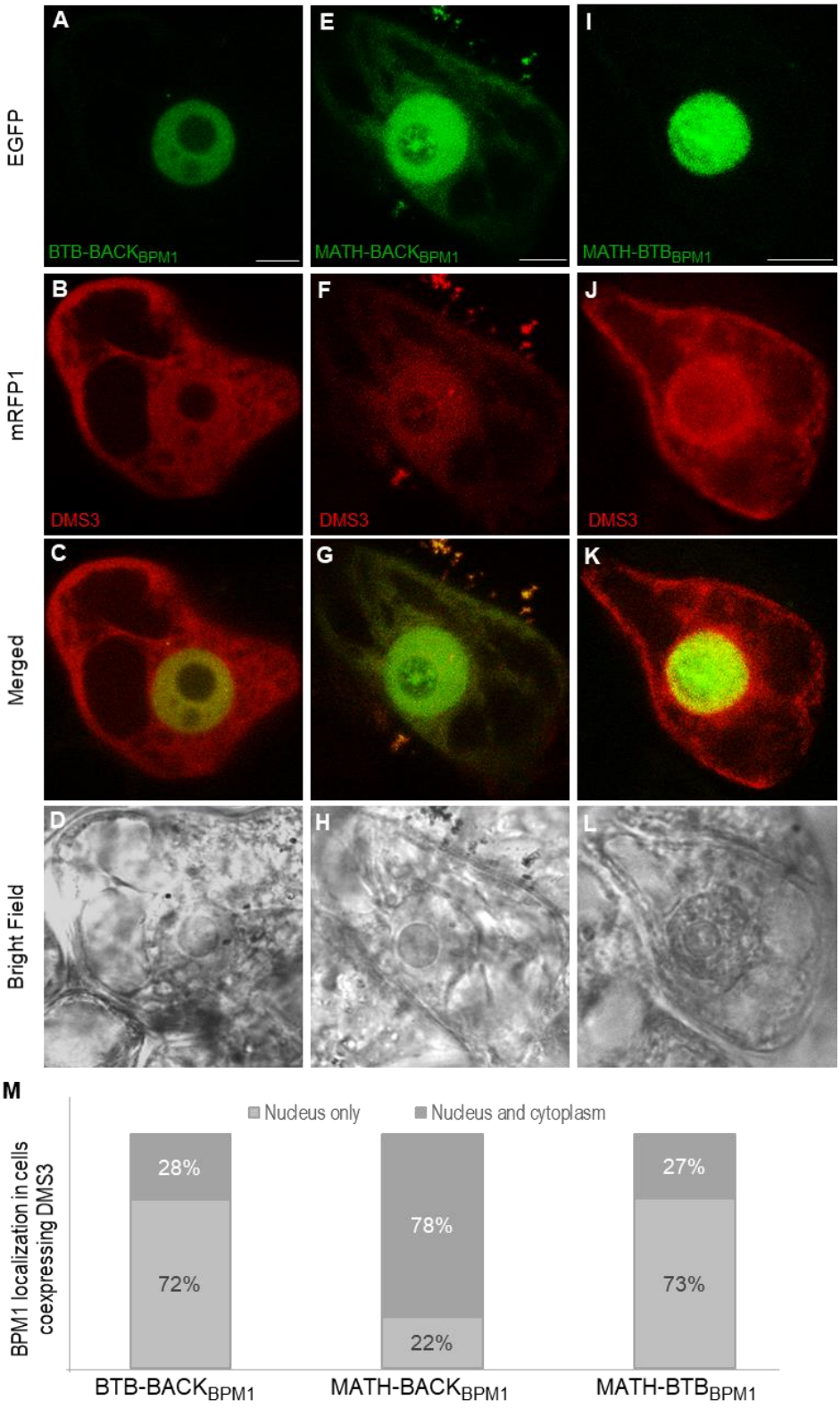

Figure F5-2 Subcellular colocalization of truncated BPM1 variants and DMS3 in tobacco BY-2 cells. Overlap between EGFP-tagged BPM1 variant missing MATH, BTB or BACK domain (green) and mRFP1-DMS3 protein (red) is visible in nucleus between all three variants of BPM1 protein and DMS3 protein: BTB-BACK$_{BPM1}$ and DMS3 (**A-D**), MATH-BACK$_{BPM1}$ and DMS3 (**E-H**), and MATH-BTB$_{BPM1}$ and DMS3 (**I-L**). In MATH-BACK$_{BPM1}$ overlap is also noticed in cytoplasm (**G**). Percentage of BPM1 localization in cytoplasm and nucleus in the presence of DMS3 according to **Appendix F Table F5-1** (**M**). Scale bar = 10 μm.

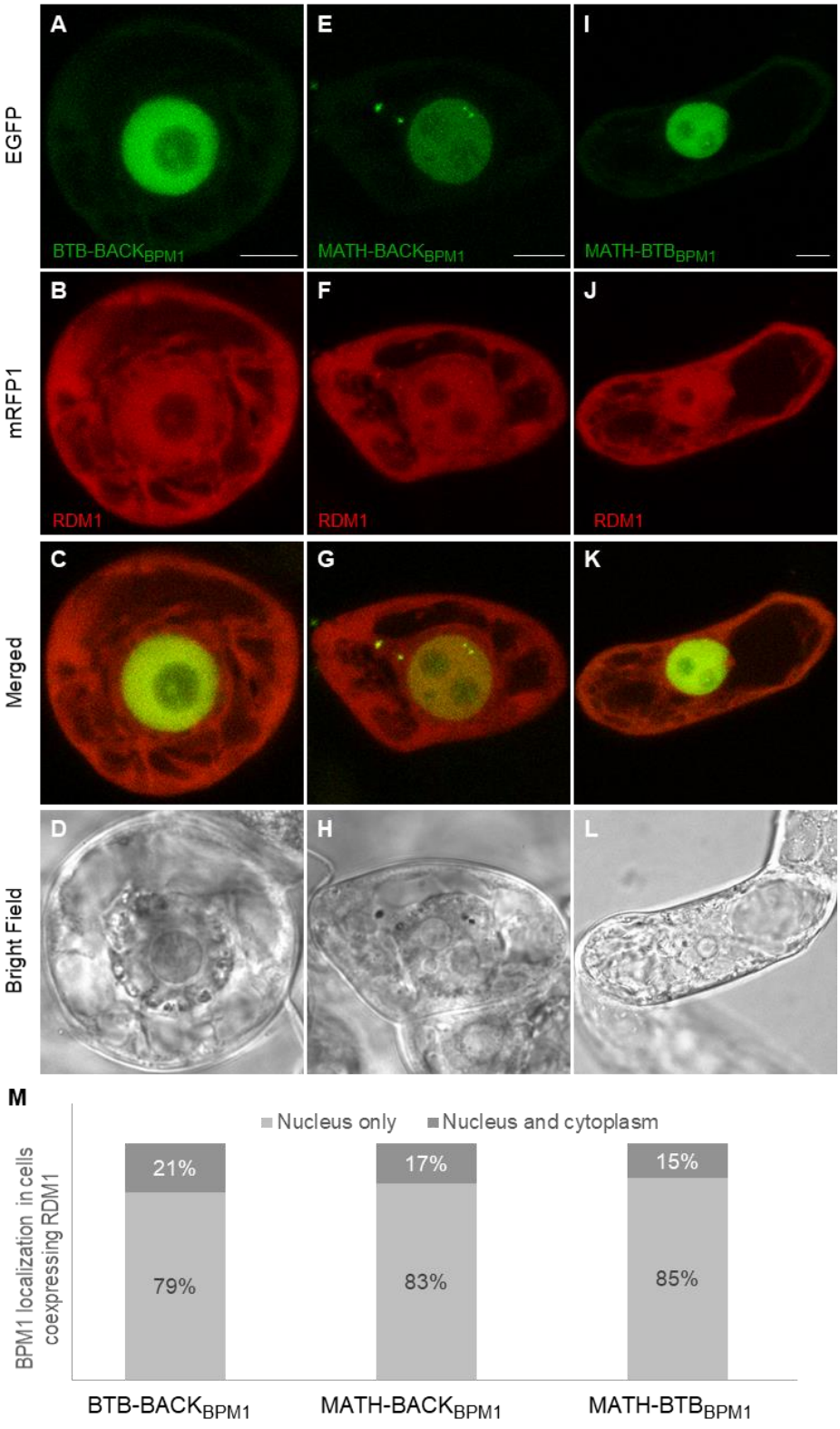

Figure F5-3 Subcellular colocalization of truncated BPM1 variants and RDM1 in tobacco BY-2 cells. Strongest overlap between EGFP-tagged BPM1 variant missing MATH, BTB or BACK domain (green) and mRFP1-RDM1 protein (red) is visible in nucleus between all three variants of BPM1 and RDM1: BTB-BACK$_{BPM1}$ and RDM1 (**A-D**), MATH-BACK$_{BPM1}$ and RDM1 (**E-H**), and MATH-BTB$_{BPM1}$ and RDM1 (**I-L**). Percentage of BPM1 localization in cytoplasm and nucleus in the presence of RDM1 according to **Appendix F Table F5-1** (**M**). Scale bar = 10 μm.

Chapter F6: FRET-FLIM analysis of domain-omitted BPM1 variants interaction with DMS3 and RDM1

Table F6-1 Fraction of fluorescent donor molecules (F) measured in nuclei of *Nicotiana benthamiana* epidermal cells. From left to right: the measured donor/acceptor pair, median fraction of donor molecules that undergo FRET (*F*), interquartile range of the measured F and the significance (p-value) of the measured F compared to the EGFP/mRFP1 control combination (Tukey–Kramer test).

FRET pair	Median	Interquartile range	p-value (vs. EGFP/mRFP1)
EGFP-BTB-BACK$_{BPM1}$/mRFP1-DMS3	0.11	0.05 - 0.13	0.02
EGFP-MATH-BACK$_{BPM1}$/mRFP1- DMS3	0.11	0.09 - 0.18	0.02
EGFP-MATH-BTB$_{BPM1}$/mRFP1-DMS3	0.12	0.09 - 0.15	0.002
EGFP-BTB-BACK$_{BPM1}$/mRFP1-RDM1	0.15	0.12 - 0.23	0.007
EGFP-MATH-BACK$_{BPM1}$/ mRFP1 -RDM1	0.14	0.06 - 0.16	0.02
EGFP-MATH-BTB$_{BPM1}$/mRFP1-RDM1	0.13	0.11 - 0.15	0.0001

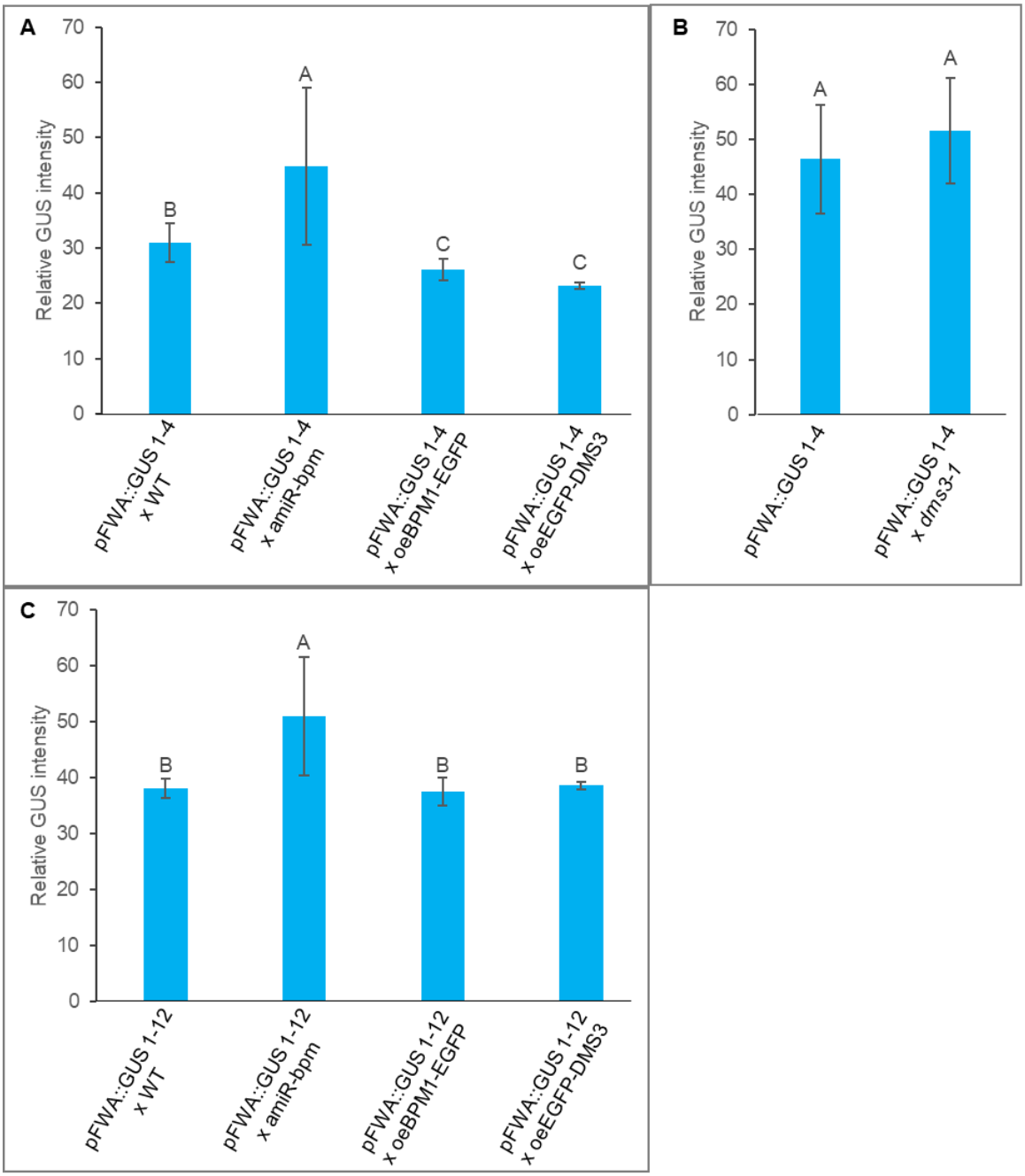

Figure F7-1 Relative GUS intensity quantified after GUS histochemical staining of *pFWA::GUS* in leaves of *Arabidopsis thaliana* crossed lines: **A**) pFWA::GUS 1-4 × WT, pFWA::GUS 1-4 × amiR-bpm, pFWA::GUS 1-4 × oeBPM1-EGFP and pFWA::GUS 1-4 × oeEGFP-DMS3, **B**) pFWA::GUS 1-4 T3 and pFWA::GUS x *dms3-1*, **C**) pFWA::GUS 1-12 × WT, pFWA::GUS 1-12 × amiR-bpm, pFWA::GUS 1-12 × oeBPM1-EGFP and pFWA::GUS 1-12 × oeEGFP-DMS3. Five plants per line represented by 15-20 images were analyzed. Images were converted to HSB and the mean gray value was measured and interpreted as relative GUS intensity. Error bars correspond to standard deviation. Columns marked with different letters indicate a significant difference obtained by Dunn's test (**A** and **C**) or by Student's t test (**B**), $p < 0.05$.

LIST OF ABBREVIATIONS

Genetics and molecular biology

BamHI – *Bacillus amyloliquefaciens* HI, a restriction endonuclease isolated from *B. amyloliquefaciens* strain H

bp – base pair, a fundamental unit of double-stranded nucleic acids

CaMV 35S – cauliflower mosaic virus 35S promoter

DNA – deoxyribonucleic acid

HRP – horseradish peroxidase

Kd – dissociation constant

PCR – polymerase chain reaction

RNA – ribonucleic acid

ss-DNA – single-stranded DNA

T-DNA – transfer DNA

UAS - upstream activating sequences

UTR – untranslated region

Tags

EGFP – enhanced green fluorescent protein

GST – glutathione S-transferase

His-tag – polyhistidine tag

mRFP1 – monomeric red fluorescent protein 1

TAP – tandem affinity purification

YFP – yellow fluorescent protein

Chemicals

2,4-D – 2,4-Dichlorophenoxyacetic acid

3-AT – 3-amino-1,2,4-triazole

DMF – dimethylformamide

DMSO – dimethyl sulfoxide

DTT – dithiothreitol

EDTA – ethylenediaminetetraacetic acid

HEPES – 4-(2-hydroxyethyl)-1-piperazineethanesulfonic acid

IPTG – isopropyl β-D-1-thiogalactopyranoside

ONPG – ortho-Nitrophenyl-β-galactoside

PMSF – phenylmethylsulfonyl fluoride

SDS – sodium dodecyl sulfate

X-gal – 5-bromo-4-chloro-3-indolyl-β-D-galactopyranoside

X-Gluc – 5-bromo-4-chloro-3-indolyl glucuronide

Media and solutions

4xYT – 4 x Yeast Tryptone, microbial growth medium used for the cultivation of *E. coli*

LB – Lysogenia Broth, Luria Broth or Luria-Bertani medium, medium for bacteria cultivation

MS – Murashige and Skoog, plant growth medium used for plant cultivation

SD – synthetic dropout medium, medium used for auxotrophic selection of yeast strains

SOC – Super Optimal broth with Catabolite repression, medium for bacteria cultivation

YPD – Yeast Peptone Dextrose, growth medium for yeast cultivation

Other

× g – times gravity

Abs – absorbance, the amount of light absorbed by the sample

IR – infrared, wavelength from about 700 nm to 1 mm

UV – ultraviolet, wavelength from 10 nm to 400 nm

w/v – weight to volume

v/v – volume to volume

The International System of Units (SI)

°C – degree Celsius

cm – centimeter

g – gram

h – hour

Hz - hertz

L – liter

m – meter

M – molar

mg – milligram

MHz - megahertz

min – minute

mL – milliliter

mM – millimolar

ng – nanogram

nm – nanometer

nM – nanomolar

µg – microgram

µL – microliter

µm – micrometer

µM – micromolar

µmol – micromole

psi - pounds per square inch*

rpm – revolutions per minute**

s – second

* psi is measurement of pressure in the Imperial system of measurement, 1 psi ≈ 6895 Pa

** SI does not recognize rpm as a unit, instead it defines the unit of frequency, Hz ($1\ \text{rpm} = \frac{1}{60}$ Hz).

9. CURRICULUM VITAE

Mateja Jagić was born on May 17th 1990 in Varaždin, Croatia. After graduating from 'Prva gimnazija Varaždin' in 2009 she enrolls in Molecular Biology at the Division of Biology, Faculty of Science, University of Zagreb where she acquires the title of Master in Molecular Biology in December 2014. From 2015 to 2016 she worked as an intern at the Croatian Natural History Museum in Zagreb and after passing the professional exam at Museum Documentation Centre, she has obtained a title of Curator in December 2016. In May 2017 she started a job as a teaching and research assistant at the Division of Molecular Biology, Department of Biology, Faculty of Science, University of Zagreb, where she is involved in teaching practical classes for students of undergraduate and graduate studies of Molecular Biology. In November 2017 she enrolls in Postgraduate doctoral program in Biology within the parent institution and carries out her PhD work under the supervision of Prof. dr. sc. Dunja Leljak-Levanić. She actively participated in three research projects (IP-2016-06-6229 and IP-2019-04-9915 funded by Croatian Science Foundation and PhenoArHeat ID:421 funded by European Plant Phenotyping Network) and has co-authored five original scientific papers, one review paper and 17 congress presentations. She supervised one master thesis as assistant supervisor. During her research work she gained plenty of experience in recombinant vector design and cloning, protein-protein interaction methods, protein purification and analysis, and fluorescence microscopy. She is also well acquainted with the gene expression analysis and induction and manipulation of plant somatic embryos.